1.25 Noble-Gas Chemistry

DS Brock and GJ Schrobilgen, McMaster University, Hamilton, ON, Canada
B Žemva, Jožef Stefan Institute, Ljubljana, Slovenia

© 2013 Elsevier Ltd. All rights reserved.

Copyright © 2013. Elsevier. All rights reserved.
Comprehensive Inorganic Chemistry II - From Elements to Applications, Elsevier, 2013. ProQuest Ebook Central, http://ebookcentral.proquest.com/lib/inflibnet-ebooks/detail.action?docID=1330977.
Created from inflibnet-ebooks on 2021-02-09 22:27:13.

1.25.1 Introduction

1.25.1.1 Discovery of Noble-Gas Reactivity

The joint discovery of argon by Lord Rayleigh (born John William Strutt) and Sir William Ramsay has been described in an essay by John Meuring Thomas.[1] The discovery of argon (lazy) and helium (its presence in the sun had been spectroscopically detected before its discovery on Earth, hence it was named after the Greek god of the Sun, Helios) led Ramsay to conjecture that a new family of chemical elements must exist in the periodic table, which are chemically inert. Ramsey, together with his student, Morris W. Travers, isolated three new elementary gases – neon (new), krypton (hidden), and xenon (strange). With the discovery of radon (named after its original source, radium) some years later, the noble-gas family was complete.

Over the years immediately following their isolation, the chemical reactivities of the noble gases were investigated. Unfortunately, the majority of experiments were performed with argon and krypton because these gases were considerably more accessible than xenon. Even today, the chemistry of argon is limited to matrix-isolation studies, while the krypton compounds that have been isolated in macroscopic quantities are thermodynamically unstable and are therefore challenging to synthesize and to handle. In 1933, Professor Don Yost and his graduate student, Albert Kaye, passed electrical discharges through gaseous mixtures of xenon and fluorine. Up until that time, they came closest to the isolation of a xenon fluoride.[2] At that time, their failure to induce chemical reactivity was taken as proof that the noble gases were indeed inert. This negative finding was in accordance with the current electronic theory of chemical bonding and the octet rule which held that eight electrons in the valence orbital are the most stable electronic configuration. This became a dogma which was espoused in practically all chemistry textbooks of the time and up until 1962.

It was not until 23 March 1962 that this dogma was abandoned. Professor Neil Bartlett, then at the University of British Columbia, reacted xenon, with its complete octet of valence electrons, with the potent oxidant, PtF_6, to give a yellow product which was initially formulated as '$[Xe][PtF_6]$', the first true chemical compound of a noble gas.[3] The discovery, however, was not so straightforward. It began with the attempted purification of PtF_4 which entailed heating PtF_4 in a stream of diluted fluorine in a Pyrex glass apparatus.[4] In this way, Bartlett obtained the salt $[O_2][PtF_6]$.[5] Because his finding was not universally accepted, he searched for the right candidate to prove the extraordinary one-electron affinity of PtF_6 which, according to his calculations, should exceed 7 eV.[6] His subsequent reasoning and the experimental plan were brilliant. He realized that the first ionization potential of Xe (12.129 eV) is marginally higher than the first ionization potential of O_2 (12.075 eV). Because O_2 could be directly oxidized to $[O_2][PtF_6]$ with PtF_6,[5] he proceeded to oxidize xenon gas with PtF_6 and obtained the first compound of a noble-gas element. This experiment has been proclaimed to be among the ten most beautiful chemical experiments performed in the history of chemistry.[7] The product, '$[Xe][PtF_6]$', was amorphous and even today its structure is not fully understood. Details concerning the nature of '$[Xe][PtF_6]$' are discussed in Section 1.25.3.1.4.2 and by Graham et al.[8]

1.25.1.2 Noble-Gas Chemistry Reviews (2000–11)

During the period 2000–11 (inclusive), several reviews have appeared that deal with a broad spectrum of topics in noble-gas chemistry: general noble-gas chemistry;[9] ^{129}Xe nuclear magnetic resonance (NMR) in noble-gas chemistry;[10] syntheses, properties, and chemistry of Xe(II) fluoride;[11] compounds that contain Xe–C bonds;[12] Xe–N-bonded compounds derived from NSF_3;[13] inert matrices for low-temperature isolation and spectroscopy of noble-gas species;[14] krypton chemistry;[15] gold and mercury cations of xenon;[16] calculations to determine the structures of complexes formed by a noble gas and a coinage metal monohalide;[17] XeF_2 as a ligand;[18] xenon NMR spectroscopy, theory and applications;[19] a critical review of experimental and theoretical advances in noble-gas chemistry during the prior 20 years;[20] NMR studies of structure and bonding in xenon and krypton compounds;[21] and a review summarizing the structures of neutral and cationic krypton and xenon-fluoro species.[22] Chapter 9.04, which relates to hypervalent bonding, should also be consulted.

Copyright © 2013. Elsevier. All rights reserved.

Comprehensive Inorganic Chemistry II : From Elements to Applications, Elsevier, 2013. ProQuest Ebook Central, http://ebookcentral.proquest.com/lib/inflibnet-ebooks/detail.action?docID=1330977.
Created from inflibnet-ebooks on 2021-02-09 22:27:13.

1.25.2 Compounds in which the Formal Oxidation Number of Xenon Is Less Than One

1.25.2.1 Polynuclear Xenon Cations

1.25.2.1.1 The Xe_2^+ cation

The Xe_2^+ cation is readily formed in the gas phase by collisions involving excited xenon atoms (eqn [1]).

$$Xe^* + Xe \rightarrow Xe_2^+ + e^- \quad [1]$$

The Xe_2^+ cation was established in the gas phase by mass spectrometry,[23] photoionization,[24–26] and by elastic scattering studies.[27,28] The Xe_2^+ cation was first described in the condensed phase[29] when Xe_2^+ was formed by reaction of $[O_2][SbF_6]$ with xenon gas (500 Torr). It is a bright green intermediate product in the reaction of Xe and $[O_2][SbF_6]$ which gave yellow $[XeF][Sb_2F_{11}]$ as the final product (eqn [2]).[29–31] The cation has only exhibited stability in HF/SbF_5 solutions. A very pale green solution was observed in AsF_5 at low temperature, but there was no indication of Xe_2^+ formation in HSO_3F, BrF_5, or IF_5 solutions.[31]

$$\begin{aligned} 2Xe + 2[O_2][SbF_6] &\rightarrow [Xe_2][SbF_6] + [O_2][SbF_6] + O_2 \\ &\rightarrow [XeF][Sb_2F_{11}] + Xe + 2O_2 \end{aligned} \quad [2]$$

The bright green, paramagnetic Xe_2^+ ion has been characterized by Raman (123 cm^{-1}), ultraviolet (UV)–visible (335 and 710 nm), and electron spin resonance (ESR) spectroscopy.[29,31]

Solutions of Xe_2^+ are stable indefinitely at room temperature under a pressure of xenon gas and can also be prepared by the irreversible reaction of a limited amount of water or other reducing agents (e.g., Pb or Hg) with SbF_5 solutions of $[XeF][Sb_2F_{11}]$ (eqns [3] and [4]).[29,31] The reaction between $[XeF][Sb_2F_{11}]$ and Xe gas in SbF_5 solvent is reversible, with the extent of reaction being influenced by the Xe pressure (eqn [5]).[31,32]

$$\begin{aligned} &4[XeF][Sb_2F_{11}] + 3Pb(6Hg) \rightarrow \\ &2[Xe_2][SbF_6] + 3Pb[SbF_6]_2\left(3[Hg_2][SbF_6]_2\right) \end{aligned} \quad [3]$$

$$\begin{aligned} &8[XeF][Sb_2F_{11}] + 18H_2O \rightarrow \\ &4[Xe_2][SbF_6] + 12[H_3O][SbF_6] + 3O_2 \end{aligned} \quad [4]$$

$$3Xe + [XeF][Sb_2F_{11}] + 2SbF_5 \rightleftharpoons 2[Xe_2][Sb_2F_{11}] \quad [5]$$

Reaction [5] was subsequently repeated and it was shown that the presence of HF and the resulting superacid, HF/SbF_5, is essential for Xe_2^+ formation.[33] A dark green solution of $[Xe_2][Sb_2F_{11}]$, SbF_5, and HF yielded crystalline $[Xe_2][Sb_4F_{21}]$ at −30 °C. The X-ray crystal structure showed that the Xe_2^+ cations and $Sb_4F_{21}^-$ anions were well separated, with Xe···F contacts (>3.22 Å) that are only slightly shorter than or approach the sum of the van der Waals radii of xenon and fluorine (3.63 Å).[34] The Xe–Xe bond (3.087(1) Å) has been cited as the longest bond between main-group elements.[33] The open-chain tetrameric fluoroantimonate (V) anion, which was observed for the first time, has the highest fluoride ion affinity (FIA) among the known $Sb_nF_{n-1}^-$ ($n = 1$–4) anions, which is apparently necessary to overcome the high FIA of the Xe_2^+ cation.[33]

1.25.2.1.2 The Xe_4^+ cation

Green solutions of the Xe_2^+ ion in SbF_5 reversibly convert into dark blue solutions at high pressures of Xe gas (30–50 bar).[35] Under these conditions, the solvent is a homogeneous mixture of SbF_5 and liquid Xe. The reversible color change, from blue to green, was achieved by varying the temperature which, in turn, altered the amount of dissolved xenon. The Xe_3^{2+}, Xe_3^+, and Xe_4^+ cations were considered as possible causes for the blue color. It appears unlikely that single crystals of the blue species can be grown because of the high viscosity of SbF_5, which has been the only appropriate solvent for the generation of this cation, and the high Xe pressures that are required to stabilize the proposed Xe_4^+ cation. The characterization of the blue species was therefore based on spectroscopic data (UV–visible absorption, Raman, infrared (IR), and electron paramagnetic resonance (EPR) spectroscopy) and comparisons with theoretical calculations. It was concluded that the Xe_4^+ ion is likely the origin of the blue color. A linear ($D_{\infty h}$) structure with Xe–Xe bond lengths of 3.529 (terminal bonds) and 3.190 (central bond) Å was calculated as the energy-minimized structure of Xe_4^+.[35]

The possible formation, under different experimental conditions, of higher xenon aggregates such as $Xe_4 \cdot Xe_n^+$ has also been considered.[35] Calculations indicate that 12–18 very loosely bound xenon atoms are needed to stabilize a linear symmetric Xe_4^+ unit, with the outer xenon atoms at ~4.40 Å from the Xe_4^+ core.[36–38] An earlier report suggested that larger Xe_n^+ aggregates underwent photo-decomposition, leaving behind Xe_4^+ ion fragments.[39]

Xenon cations of the type Xe_n^+ ($n \leq 30$) have been detected in molecular beam experiments using mass spectrometry and their structures have been predicted by quantum-chemical calculations.[40] A prominent feature of these clusters is delocalization of their positive charges over their cores, which are comprised of trimeric or tetrameric units held together by covalent bonds. The remaining xenon atoms are polarized and bind to these positively charged cores.[40]

1.25.2.2 Xenon–Gold Cations

There have been indications that metal–xenon bonds can be formed. The complexes $(CO)_5Mo\cdots Xe$, $(CO)_5M\cdots Ng$ (M = Cr, W; Ng = Kr, Xe), $(CO)_5Mn\cdots Xe$, and $(CO)_5Fe^+\cdots Kr$ have been detected in noble-gas matrices.[41–44] Quantum–chemical calculations were reported for $(CO)_5M\cdots Ng$ (M = Cr, Mo, W; Ng = Ar, Kr, Xe).[45] Short-lived transients containing xenon– or krypton–metal bonds have been observed in supercritical Xe and Kr solutions.[46–51] The $AuXe^+$ ion has been detected by mass spectrometry with a calculated bond length of 2.57 Å and a bond energy of 125.60 ± 12.56 kJ mol^{-1},[52] and ArAuCl and KrAuCl have been observed by microwave spectroscopy which yielded Ar–Au and Kr–Au bond lengths of 2.47 and 2.52 Å, respectively.[53]

The reaction between AuF_3 and Xe in HF/SbF_5 solution yielded $[AuXe_4][Sb_2F_{11}]_2$, which was obtained as a dark red, crystalline solid at −78 °C.[54] Removal of Xe at −40 °C yielded $Au[SbF_6]_2$, a rare example of an Au(II) salt. The formation of $AuXe_4^+$ from $Au[SbF_6]_2$ is reversible; thus, for the preparation of $[AuXe_4][Sb_2F_{11}]_2$, a moderately high xenon pressure (10 bar) was required.[54]

Four xenon–gold cations have been isolated as their salts from the $Au^{2+}/HF/SbF_5/Xe$ system with the species depending primarily on the HF solvent acidity (concentration of SbF_5), Xe pressure, and temperature. At a high SbF_5 concentration (0.5 mol of SbF_5 in 1 mol of HF), $[AuXe_4][Sb_2F_{11}]_2$ crystallized

Copyright © 2013. Elsevier. All rights reserved.

Comprehensive Inorganic Chemistry II : From Elements to Applications, Elsevier, 2013. ProQuest Ebook Central, http://ebookcentral.proquest.com/lib/inflibnet-ebooks/detail.action?docID=1330977.
Created from inflibnet-ebooks on 2021-02-09 22:27:13.

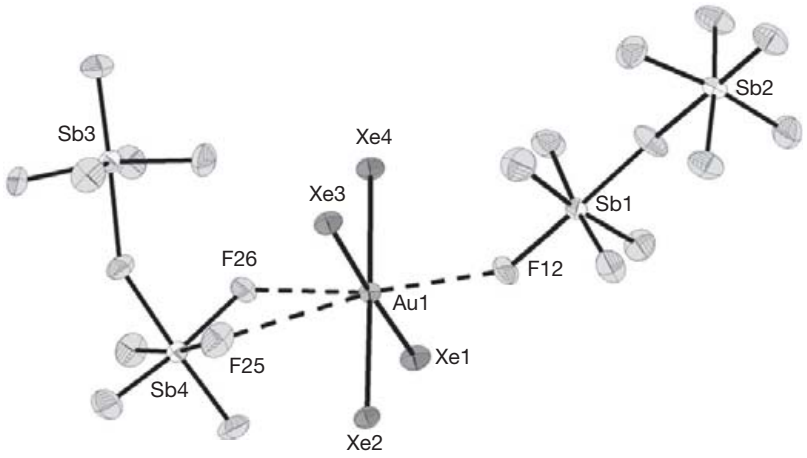

Figure 1 The structural unit in the X-ray crystal structure of the triclinic phase of $[AuXe_4][Sb_2F_{11}]_2$. Data from Ref. 55 were used to draw this figure.

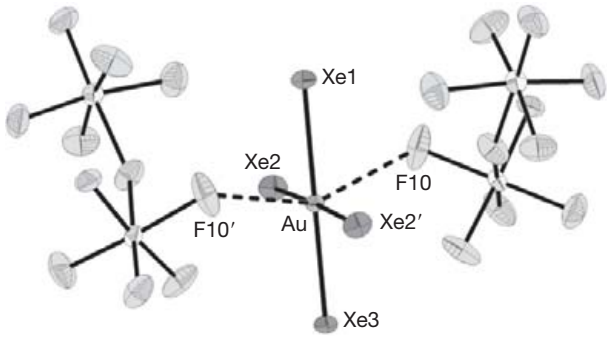

Figure 2 The structural unit in the X-ray crystal structure of the tetragonal phase of $[AuXe_4][Sb_2F_{11}]_2$. Data from Ref. 55 were used to draw this figure.

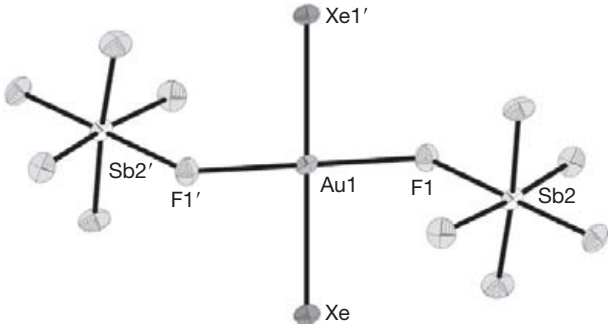

Figure 3 The structural unit in the X-ray crystal structure of *trans*-$[AuXe_2][SbF_6]_2$. Reproduced with permission from Drews, T.; Seidel, S.; Seppelt, K. *Angew. Chem. Int. Ed.* **2002**, *41*, 454–456.

in two crystallographic phases, triclinic (Figure 1) and tetragonal (Figure 2), which only differ with respect to their cation–anion interactions.[55] At lower Xe pressures, which were achieved by pumping on solutions of $[AuXe_4][Sb_2F_{11}]_2$, the $[AuXe_2][Sb_2F_{11}]_2$ salt formed. The effect of acidity was apparent when equimolar amounts of finely divided gold and XeF_2 were reacted with 10–12 bar of Xe in superacid media comprised of ~2:5, 10:7, and 5:1 molar ratios of $HF:SbF_5$, yielding *trans*-$[AuXe_2][SbF_6]$, $[Au_2Xe_2F][SbF_6]_3$, and *trans*-$[AuXe_2F][SbF_6][Sb_2F_{11}]$, respectively.[55] Both $[AuXe_4][Sb_2F_{11}]_2$ phases were stable up to −40 °C. Warming above this temperature resulted in melting accompanied by Xe loss, a color change from dark red to light orange, and formation of $Au[SbF_6]_2$.[54]

The crystal structure of triclinic $[AuXe_4][Sb_2F_{11}]_2$ (Figure 1) consists of discrete $AuXe_4^{2+}$ cations and $Sb_2F_{11}^-$ anions. The Au atom is situated in the middle of a square plane of Xe atoms with the four Au–Xe distances ranging from 2.728(1) to 2.750(1) Å. The three closest Au···F cation–anion contacts are 2.671(5), 2.949(5), and 3.153(5) Å and the $Sb_2F_{11}^-$ anions are bent at their Sb···F···Sb bridges. The triclinic phase has one particularly short Au···F contact (Au···F12, 2.671(5) Å) which, together with the square-planar $AuXe_4^{2+}$ unit, results in a square pyramidal arrangement. The contacts are weaker (Au···F10, 2.927(9) Å) in the tetragonal phase Figure 2.[55]

The Raman spectrum of triclinic $[AuXe_4][Sb_2F_{11}]_2$ showed, in addition to bands attributable to the $Sb_2F_{11}^-$ anion, a very strong band at 129 cm^{-1}. This band was assigned to the totally symmetric stretching vibration of $AuXe_4^{2+}$ based on the frequency predicted by ab initio and density functional theory (DFT) calculations.[54]

The mean thermochemical Au–Xe bond energy for $AuXe_4^{2+}$ in eqn [6] is estimated to be 210 kJ mol^{-1}, which is

$$AuXe_4^{2+} \rightarrow Au^{2+} + 4Xe \qquad [6]$$

in accordance with the thermal stability of $[AuXe_4][Sb_2F_{11}]_2$. Because gold is the most electronegative transition metal, a large charge transfer from xenon to gold occurs in $AuXe_4^{2+}$, which is reflected in the calculated charge distribution of the cation, where most of the positive charge is located on the Xe atoms.[54]

Reduction of Au^{3+} to Au^{2+} and its complexation with xenon only occur in the superacid medium, HF/SbF_5. The overall reaction emphasizes, yet again, the role of 'protons' (H_2F^+) and HF elimination in Au–Xe bond formation (eqn [7]).[54] Crystals of green $[Xe_2][Sb_4F_{21}]$[33] were also identified in the solid reaction mixture at −60 °C.

$$AuF_3 + 6Xe + 3H^+ \rightarrow AuXe_4^{2+} + Xe_2^+ + 3HF \qquad [7]$$

Thermally unstable, violet-black *cis*-$[AuXe_2][Sb_2F_{11}]_2$ and thermally very unstable, ochre-colored *trans*-$[AuXe_2][SbF_6]_2$ (Figure 3) crystals were isolated.[55] In the case of the

Copyright © 2013. Elsevier. All rights reserved.

Comprehensive Inorganic Chemistry II : From Elements to Applications, Elsevier, 2013. ProQuest Ebook Central, http://ebookcentral.proquest.com/lib/inflibnet-ebooks/detail.action?docID=1330977.
Created from inflibnet-ebooks on 2021-02-09 22:27:13.

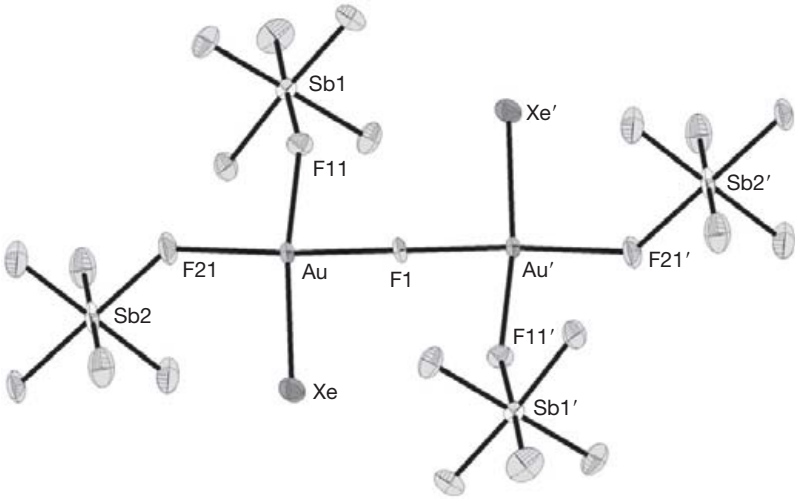

Figure 4 The structural unit in the X-ray crystal structure of $[Au_2Xe_2F][SbF_6]_3$. Reproduced with permission from Drews, T.; Seidel, S.; Seppelt, K. *Angew. Chem. Int. Ed.* **2002**, *41*, 454–456.

cis-isomer, the Au atom is in a square-planar environment consisting of two Xe atoms that are cis to one another (2.658(1), 2.671(1) Å) and two bridging cis-F atoms (2.181(4), 2.238(4) Å) from two $Sb_2F_{11}^-$ anions. The Au atom in the trans-isomer is also in a square-planar environment and is coordinated to two Xe atoms (2.709(1) Å) that are trans to one another and two bridging F atoms (2.159(6) Å) from different SbF_6^- anions.[55]

Green crystals of $[Au_2Xe_2F][SbF_6]_3$ were shown to be stable up to nearly room temperature. The crystal structure of $[Au_2Xe_2F][SbF_6]_3$ is shown in Figure 4. Both Au atoms are in square-planar environments comprised of one Xe atom and three bridging F atoms. The bridging F atom (F1) distance to Au is very short (2.045(2) Å) relative to the Au···F distance in triclinic $[AuXe_4][Sb_2F_{11}]_2$ (2.671(5) Å).[55]

The only known Au^{3+} complex is *trans*-$[AuXe_2F][SbF_6][Sb_2F_{11}]$. The compound was isolated from an HF/SbF_5 mixture having a lower acidity ($HF/SbF_5 \sim 5{:}1$). The compound was surprisingly stable when the reaction was carried out at −10 °C, with ochre-colored crystals forming at −35 °C. The Au atom is in a square-planar environment where it is surrounded by two trans-Xe atoms and two trans-F atoms, one terminal and one bridged to Sb1 (Figure 5).

The Au(III)−Xe bonds (2.593(1) and 2.619(1) Å) are shorter than the Au(II)−Xe bonds in triclinic and tetragonal $[AuXe_4][Sb_2F_{11}]_2$, *cis*-$[AuXe_2][Sb_2F_{11}]_2$, and *trans*-$[AuXe_2][SbF_6]_2$.[55] The Au−F bond lengths (1.881(4) and 1.983(4) Å) are typical for Au, for example, AuF_3 (1.91(4), 2.04(3) Å).[56]

The only xenon cation that contains Au(I) has been synthesized and isolated as the salt, $[(F_3As)AuXe][Sb_2F_{11}]$.[57] The synthetic strategy leading to this cation entailed exchange of the weakly basic SbF_6^- anion in $[(F_3As)Au][SbF_6]$ for the more weakly basic $Sb_2F_{11}^-$ anion.[58] The reaction was carried out in a 5:1 molar ratio of $HF:SbF_5$ in the presence of excess xenon (7:1 molar ratio relative to $[(F_3As)AuXe][Sb_2F_{11}]$). The compound, $[(F_3As)AuXe][Sb_2F_{11}]$, crystallizes as colorless needles which are stable at room temperature. The interactions between $(F_3As)AuXe^+$ and $Sb_2F_{11}^-$ are weak, with the shortest Au···F distance at 2.848 Å. The As–Au–Xe unit is nearly

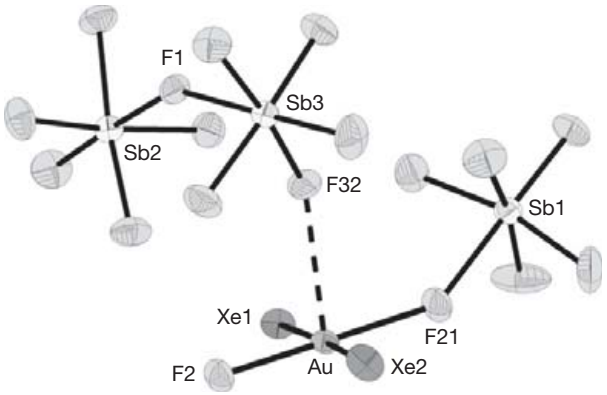

Figure 5 The structural unit in the X-ray crystal structure of *trans*-$[AuXe_2F][SbF_6][Sb_2F_{11}]$. Reproduced with permission from Drews, T.; Seidel, S.; Seppelt, K. *Angew. Chem., Int. Ed.* **2002**, *41*, 454–456.

linear, and the Au(I)−Xe bond (2.6072(6) Å) is as short as the Au(III)−Xe bond in $[AuXe_2F][SbF_6][Sb_2F_{11}]$ and significantly shorter than Au(II)−Xe bonds.[57]

Reactions of the type $AuXe_n^{2+} + n\text{Kr} \rightarrow AuKr_n^{2+} + n\text{Xe}$ are thermodynamically unfavorable, requiring about 42 kJ mol^{-1} per Xe/Kr substitution.[16] Because gold–xenon complexes seem to be at the border of thermodynamic stability, the outlook for the syntheses of gold–krypton complexes is not promising.

1.25.2.3 Prospects for Xenon–M(Pt,Pd,Ag) Bonds and the $HgXe^+$ Cation

When gold is substituted by neighboring heavy metals such as Pt, Pd, Ag, or Hg, quantum-chemical calculations consistently predict that complexes of the type MXe_n^{x+} will have reasonable bond energies. It may be difficult, however, to compare the numerical values of the mean bond energies of different complexes with those of different metal atoms because the economical use of core potentials and basis sets makes such energy comparisons unreliable. Experimental attempts to isolate $AgXe_n^{2+}$ and $CuXe_n^{2+}$ have failed.[16] The theoretical calculations favor the formation of the $PtXe_n^{2+}$ cations which

Copyright © 2013. Elsevier. All rights reserved.

Comprehensive Inorganic Chemistry II : From Elements to Applications, Elsevier, 2013. ProQuest Ebook Central, http://ebookcentral.proquest.com/lib/inflibnet-ebooks/detail.action?docID=1330977.
Created from inflibnet-ebooks on 2021-02-09 22:27:13.

are predicted to be more stable than the corresponding $AuXe_n^{2+}$ complexes.[16] The problem is a source of naked Pt^{2+}. Although Pd^{2+} exists as a cationic species in HF/SbF_5 solution,[59] it does not add xenon.

The colorless $HgXe^{+}$ salt, $[HgXe][SbF_6][Sb_2F_{11}]$, has been obtained[57] (**Figure 6**) by reaction of HgF_2 and Xe in SbF_5 solvent at 80 °C. The Hg–Xe distance is 2.76 Å. When HF was present, xenon was replaced by HF and $[HgHF][SbF_6][Sb_2F_{11}]$ was formed.

1.25.2.4 Computational Treatment of Gold Complexes

Following experimental confirmation of the existence of the $AuXe_4^{2+}$ cation[54] in the crystal structure of $[AuXe_4][Sb_2F_{11}]_2$ and the discovery of the matrix-isolated NgAuCl (Ng = Ar, Kr) molecules,[53] a computational study of the $AuNg_4^{2+}$ (Ng = Ar, Kr, and Xe) cation series was undertaken[60] which consisted of topological analyses of the electron localization function (ELF) and the electron densities (atoms in molecules, AIM). The ELF analyses of the $AuNg_4^{2+}$ cations (Ng = Ar, Kr, and Xe) indicated that the Au–Ng bonding is dominated by electrostatic interactions and is of a 'closed shell' nature. The AIM method revealed similar results. The bond critical point of the Au–Ng bond was calculated to have a positive value for the Laplacian of the electron density that decreases from 0.163 ($AuAr_4^{2+}$) to 0.087 ($AuXe_4^{2+}$). The atomic charge separations, $Au^{+1.30}Ar_4^{+0.18}$, $Au^{+1.19}Kr_4^{+0.20}$, and $Au^{+0.29}Xe_4^{+0.43}$, show a decrease of the positive charge on the gold atom and, correspondingly, increases on the noble-gas atoms. Paired electron densities were found to accumulate inside topological bonding regions while unpaired electron density concentrations occurred outside. The integrated spin densities increased from 0.16 e for $AuXe_4^{2+}$ to 0.28 e for $AuAr_4^{2+}$.[60]

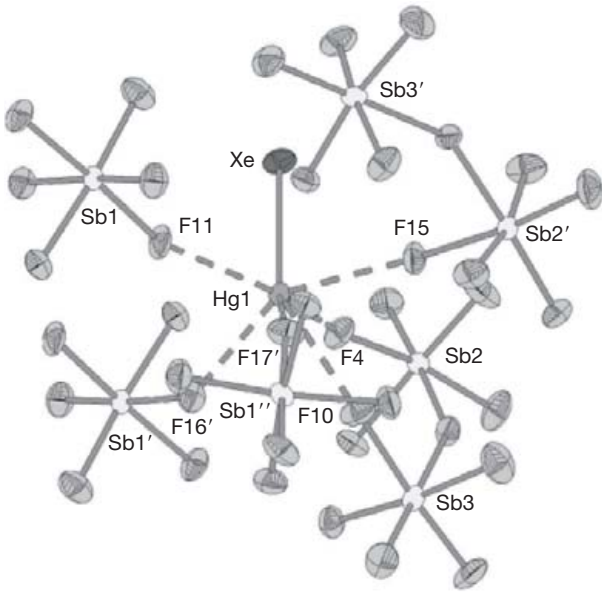

Figure 6 The Hg(II) coordination sphere in the X-ray crystal structure of $[HgXe][SbF_6][Sb_2F_{11}]$. Reproduced with permission from Hwang, I. C.; Seidel, S.; Seppelt, K. *Angew. Chem., Int. Ed.* **2003**, *42*, 4392–4395.

1.25.3 Xe(II) Compounds

1.25.3.1 Cationic Species

1.25.3.1.1 Xenon(II)–carbon bonded cations

Two reviews relating to the syntheses, structures, and reactivities of [RXe][Y] salts and the neutral compound series, RXeX and RXeR′ (R and R′ are organic groups), have been published.[12,61] The first xenon–carbon bonded species, $C_6F_5Xe^{+}$, was synthesized as the $C_6F_5BF_3^{-}$ [62] and $(C_6F_5)_3BF^{-}$ [63] salts with the anion depending on whether XeF_2 or $B(C_6F_5)_3$ is in excess (eqns [8] and [9]). High-yield syntheses have since been achieved for $[C_6F_5Xe][BF_4]$ salts as well as for the BF_4^{-} salts of 2,3,4,5-$C_6HF_4Xe^{+}$, 3,4,5-$C_6H_2F_3Xe^{+}$, and 3,5-$C_6H_3F_2Xe^{+}$ by the reaction of the appropriate aryldifluoroborane with XeF_2 in CH_2Cl_2 (eqn [10]).[64]

$$XeF_{2(excess)} + B(C_6F_5)_3 \xrightarrow[-30\ ^\circ C]{CH_2Cl_2} [C_6F_5Xe][C_6F_5BF_3] \quad [8]$$

$$XeF_2 + B(C_6F_5)_{3(excess)} \xrightarrow[0\ ^\circ C]{CH_3CN} [C_6F_5Xe][(C_6F_5)_3BF] \quad [9]$$

$$K[RBF_3] \xrightarrow{BF_3} RBF_2 \xrightarrow{XeF_2} [RXe][BF_4] \quad [10]$$

1.25.3.1.1.1 Stabilities and reactivities of salts containing the $C_6F_5Xe^{+}$ cation

When the reaction of $C_6F_5BF_2$ or $K[C_6F_5BF_3]$ with XeF_2 is carried out in aHF at −30 °C, two competing reactions occur: xenodeborylation (formation of $C_6F_5Xe^{+}$) and fluorine addition to the aryl group.[65] The products were confirmed by ^{19}F NMR spectroscopy and were the same products observed when $[C_6F_5Xe][BF_4]$ was dissolved in aHF. In the case of $C_6F_5BF_2$, the reaction products are given in **Scheme 1**.[65] In contrast, the reaction between $K[C_6F_5BF_3]$ and XeF_2 gave predominantly $[C_6F_5Xe][BF_4]$ with minor oxidative fluorination of the $C_6F_5BF_3^{-}$ anion to $C_6F_7BF_3^{-}$.

The reaction of XeF_2 with the analogous perfluoroalk-1-enyldifluoroboranes, R_FBF_2, and potassium perfluoroalk-1-enyltrifluoroborates, $K[R_FBF_3]$ (R_F = *cis*-$C_2F_5CF{=}CF$, *trans*-$C_4F_9CF{=}CF$), resulted in fluorine addition across the C=C double bond in aHF, with no evidence for organoxenon cation formation.[65] However, $K[C_6F_{13}BF_3]$ did not react with XeF_2 in aHF. The oxidative addition of fluorine by XeF_2 was attributed to a dramatic increase in the oxidation potential of XeF_2 as a result of the highly acidic solvent medium and the greater reducing potentials of fluoroalkenyl and aryl groups in organotrifluoroborate anions relative to those of the neutral organodifluoroboranes.

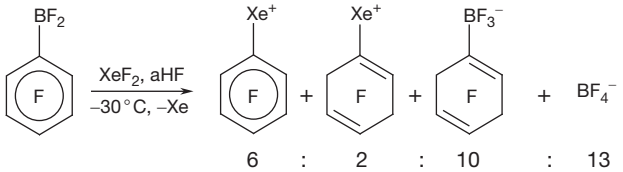

Scheme 1 Products arising from the reaction of $C_6F_5BF_2$ with XeF_2 in aHF at −30 °C. The molar ratio is given beneath each product. Redrawn from Ref. 65.

Copyright © 2013. Elsevier. All rights reserved.

Comprehensive Inorganic Chemistry II : From Elements to Applications, Elsevier, 2013. ProQuest Ebook Central, http://ebookcentral.proquest.com/lib/inflibnet-ebooks/detail.action?docID=1330977.
Created from inflibnet-ebooks on 2021-02-09 22:27:13.

Further examples of $C_6F_5Xe^+$ salts that have been synthesized include those of the weakly coordinating BY_4^- (Y = CF_3, C_6F_5, CN, or $OTeF_5$) anions.[66] The latter were obtained by salt metatheses of $[C_6F_5Xe][BF_4]$ and $M[BY_4]$ (M = K, Cs). The $[C_6F_5Xe][BY_4]$ salts showed no direct correlation between the nucleophilicity of the anion and the temperatures at which they decomposed in the solid state or in solution. The $C_6F_5Xe^+$ salt exhibiting the lowest stability in the solid state and in solution (weakly coordinating CH_2Cl_2 and strongly coordinating CH_3CN) was $[C_6F_5XeNCCH_3][B(C_6F_5)_4]$.[66] All salts of the series decompose to C_6F_5H in CH_3CN. In the case of $[C_6F_5XeNCCH_3][B(C_6F_5)_4]$, the decomposition also proceeded through a second pathway where the cation attacked the nucleophilic *ipso*-carbon of the anion, resulting in significant amounts of $(C_6F_5)_2$. By contrast, the decompositions of $[C_6F_5Xe][BY_4]$ (Y = CF_3 or $OTeF_5$) in CH_2Cl_2 resulted in hydrogen and chlorine abstraction by the $C_6F_5\cdot$ radical to produce C_6F_5H and C_6F_5Cl, whereas $[C_6F_5XeNCCH_3][B(C_6F_5)_4]$ also formed significant amounts of $(C_6F_5)_2$.[66]

The reactions of $[C_6F_5Xe][BY_4]$ (Y = CF_3, C_6F_5, CN, or $OTeF_5$) with the π nucleophile, C_6H_5F, were carried out in CH_3CN and CH_2Cl_2 solvents.[66] These weakly ion-paired $[C_6F_5Xe][BY_4]$ salts exhibited a range of stabilities that were not drastically influenced by CH_3CN coordination. However, it was shown that the reactivities of $[C_6F_5Xe][BY_4]$ with excess C_6H_5F differed in CH_3CN. The reactions between $[C_6F_5Xe][BY_4]$ and C_6H_5F proceeded significantly faster than their decompositions in the solvent alone; however, the rates of reaction and product distributions were dependent upon the anion substituents, Y, the solvent, and the presence of additional molecular or anionic (e.g., H_2O or F^-) nucleophiles. In each case, the major products were isomeric mixtures of hexafluorobiphenyls, $F_5C_6–C_6H_4F$, with the rate of formation occurring more rapidly in weakly coordinating CH_2Cl_2 than in strongly coordinating CH_3CN. The aforementioned description of factors influencing the rates of pentafluorophenylation and product distributions is consistent with the intermediate coordination of C_6H_5F at $C_6F_5Xe^+$ and the subsequent radical attack of C_6H_5F by $C_6F_5\cdot$.

The relative degrees of cation–solvent interactions for the $C_6F_5Xe^+$ cation in $[C_6F_5Xe][BY_4]$ (Y = CF_3, C_6F_5, CN, or $OTeF_5$) are also reflected in the ^{19}F NMR parameters.[66] The ^{19}F NMR resonances of $C_6F_5Xe^+$ in CH_2Cl_2 and $CF_3CH_2CF_2CH_3$ (PFB) are shifted to high frequency relative to those obtained for $C_6F_5Xe^+$ in CH_3CN and are consistent with a more weakly coordinated $C_6F_5Xe^+$ cation and significant polarization of the C_6F_5 group by Xe(II) in CH_2Cl_2 and PFB. The enhanced shielding and narrow chemical shift range found in CH_3CN solutions are consistent with $C_6F_5XeNCCH_3^+$ formation. The similarity between the ^{19}F chemical shifts of $[C_6F_5Xe][BF_4]$ in aHF and those obtained for $[C_6F_5Xe][B(CF_3)_4]$ in a PFB solution are indicative of a weakly coordinated $C_6F_5Xe^+$ cation. To account for this observation, it was proposed that HF solvates the anion, thereby resulting in the much larger $BF_4\cdot(HF)_n^-$ anion, which disperses the negative charge over more than four fluorine atoms, rendering the anion less basic.

Simulations of the ^{19}F and ^{129}Xe NMR spectra of $C_6F_5Xe^+$ have provided the complete set of aryl $^{19}F–^{19}F$ and $^{129}Xe–^{19}F$ coupling constants and their relative signs,[66] which are in accord with those of isoelectronic C_6F_5I.

1.25.3.1.1.2 Solid-state characterization of salts of the $C_6F_5Xe^+$ and $C_6F_5XeNCCH_3^+$ cations

The $C_6F_5Xe^+$ and $C_6F_5XeNCCH_3^+$ cations have been structurally characterized in the solid state as the $[C_6F_5Xe][B(CF_3)_4]$, $[C_6F_5XeNCCH_3][B(CF_3)_4]$, $[C_6F_5Xe][B(CN)_4]$, and $[C_6F_5XeNCCH_3][B(C_6F_5)_4]$ salts, providing a number of insights into the coordination behavior of the $[C_6F_5Xe]^+$ cation in weakly coordinating anion salts.[67]

Raman spectroscopic results indicated that there are negligible effects upon anion substitution or upon CH_3CN coordination, with the cation bands remaining unshifted. In particular, $\nu(Xe–C)_{ip}$, which in-phase couples with $\delta(CCF)_{ip}$, was observed at 201 and 205 cm^{-1} for $[C_6F_5Xe][B(CN)_4]$ and $[C_6F_5Xe][BF_4]$, respectively, and at 202 and 203 cm^{-1} for $[C_6F_5XeNCCH_3][B(CF_3)_4]$ and $[C_6F_5XeNCCH_3][B(C_6F_5)_4]$, respectively.[67] The weak donor–acceptor interaction with CH_3CN is also reflected in the C–N stretch, which shifts by only 25 and 30 cm^{-1} for $[C_6F_5XeNCCH_3][B(C_6F_5)_4]$ and $[C_6F_5XeNCCH_3][B(CF_3)_4]$, respectively, relative to CH_3CN. Furthermore, ν(Xe---N), which occurs at 144 cm^{-1}, is significantly lower than for the more covalent donor–acceptor Xe–N bonds, that is, $FXeNCH^+$, 330 cm^{-1};[68,69] $FXeNCCH_3^+$, 268, 284, 288 cm^{-1};[70] and $FXeNSF_3^+$, 194 cm^{-1}.[71]

The aforementioned weak donor–acceptor interactions are also manifested in the X-ray crystal structures (**Figures 7–10**).[67] In each structure, the C–C and C–F bond lengths are within ±3σ as are the Xe–C bond lengths ($[C_6F_5Xe][B(CN)_4]$, 2.081(3) Å; $[C_6F_5Xe][B(CF_3)_4]$, 2.104(5) Å; $[C_6F_5XeNCCH_3][B(CF_3)_4]$, 2.100(6) Å; and $[C_6F_5XeNCCH_3][B(C_6F_5)_4]$, 2.100(10) Å). The Xe---N bond lengths ($[C_6F_5XeNCCH_3][B(CF_3)_4]$, 2.640(6) Å; $[C_6F_5XeNCCH_3][B(C_6F_5)_4]$, 2.610(10) Å) are indicative of weak adduct formation as are the C–N bond lengths ($[C_6F_5XeNCCH_3][B(CF_3)_4]$, 1.096(9) Å; $[C_6F_5XeNCCH_3]$

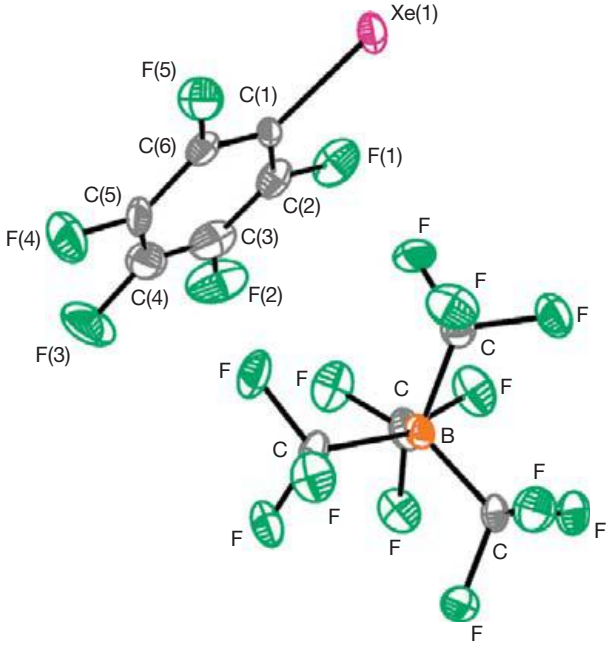

Figure 7 The structural unit in the X-ray crystal structure of $[C_6F_5Xe][B(CF_3)_4]$. Reproduced with permission from Koppe, K.; Frohn, H.-J.; Mercier, H. P. A.; Schrobilgen, G. J. *Inorg. Chem.* **2008**, *47*, 3205–3217.

Copyright © 2013. Elsevier. All rights reserved.

Comprehensive Inorganic Chemistry II : From Elements to Applications, Elsevier, 2013. ProQuest Ebook Central, http://ebookcentral.proquest.com/lib/inflibnet-ebooks/detail.action?docID=1330977.
Created from inflibnet-ebooks on 2021-02-09 22:27:13.

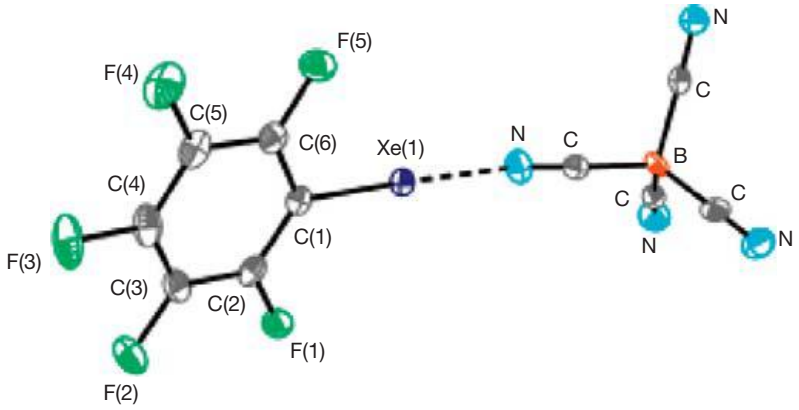

Figure 8 The structural unit in the X-ray crystal structure of $[C_6F_5Xe][B(CN)_4]$. Reproduced with permission from Koppe, K.; Frohn, H.-J.; Mercier, H. P. A.; Schrobilgen, G. J. *Inorg. Chem.* **2008**, *47*, 3205–3217.

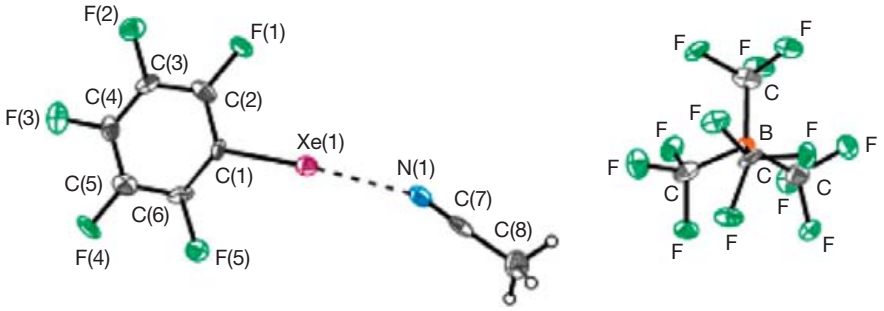

Figure 9 The structural unit in the X-ray crystal structure of $[C_6F_5XeNCCH_3][B(CF_3)_4]$. Reproduced with permission from Koppe, K.; Frohn, H.-J.; Mercier, H. P. A.; Schrobilgen, G. J. *Inorg. Chem.* **2008**, *47*, 3205–3217.

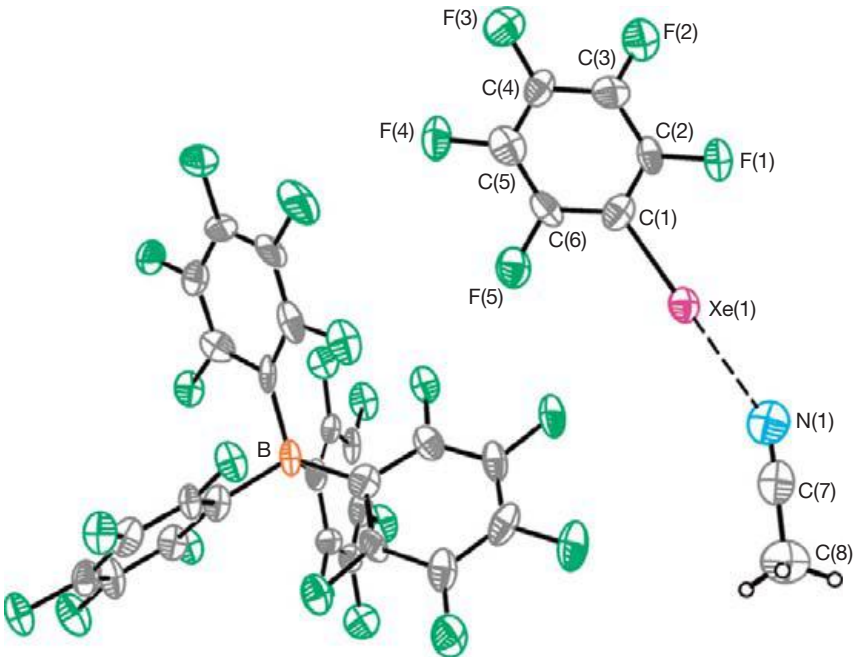

Figure 10 The structural unit in the X-ray crystal structure of $[C_6F_5XeNCCH_3][B(C_6F_5)_4]$. Reproduced with permission from Koppe, K.; Frohn, H.-J.; Mercier, H. P. A.; Schrobilgen, G. J. *Inorg. Chem.* **2008**, *47*, 3205–3217.

Copyright © 2013. Elsevier. All rights reserved.

Comprehensive Inorganic Chemistry II : From Elements to Applications, Elsevier, 2013. ProQuest Ebook Central, http://ebookcentral.proquest.com/lib/inflibnet-ebooks/detail.action?docID=1330977.
Created from inflibnet-ebooks on 2021-02-09 22:27:13.

$[B(C_6F_5)_4]$, 1.157(19) Å), which are essentially the same as in CH_3CN[72] (1.141(2) Å). In both cases, the Xe···N—C bond angles associated with coordinated CH_3CN are slightly bent for the $B(CF_3)_4^-$ (174.8(2)°) and $B(CN)_4^-$ salts (177.1(4)°), and are attributed to crystal packing. The trends in Raman frequencies and bond lengths are also reproduced by quantum-chemical calculations, which reveal that the geometrical parameters of $C_6F_5Xe^+$ are rather insensitive to CH_3CN coordination. The $B(CF_3)_4^-$ salt displays the weakest cation–anion interaction in its crystal structure (2.913(4) Å; cf. van der Waals sum for N and Xe of 3.63 Å[34]) providing the closer approximation to gas-phase $C_6F_5Xe^+$ for the two unsolvated $C_6F_5Xe^+$ salts examined in this study.[67] The ability of CH_3CN to compete effectively with the weakly coordinating $B(C_6F_5)_4^-$ and $B(CF_3)_4^-$ anions for the Lewis acidic xenon center of the cation is demonstrated by formation of their $C_6F_5XeNCCH_3^+$ salts. By contrast, the anion–cation interaction (2.716(3) Å) is apparently sufficiently strong to prevent CH_3CN coordination in the $B(CN)_4^-$ salt. Coordination of a single CN ligand of the anion to xenon is apparent from the C–N stretching region of $B(CN)_4^-$ in the Raman spectrum, where symmetry lowering of the anion results in four bands instead of the two bands ($\nu_1(A_1)$ and $\nu_6(T_2)$) expected for a tetrahedral (T_d) anion. The distortion, however, is not apparent, within $\pm 3\sigma$, from the geometric parameters of the $B(CN)_4^-$ anion.

1.25.3.1.1.3 Syntheses and NMR characterizations of alkenyl derivatives of Xe(II) cations

Prior to 2000, the only alkenyl derivative of Xe(II) was reported in a preliminary communication dealing with the NMR spectroscopic observation of the $F_2C{=}CFXe^+$ cation.[73] Following the successful synthetic methodologies used to form arylxenon(II) cations (see Section 1.25.3.1.1), and the syntheses of $K[RBF_3]$ salts (eqns [11–14]), reactions analogous to eqn [10] have enabled the syntheses of several $XCF{=}CFBF_2$ (X = F, *trans*-H, *cis*-Cl, *trans*-Cl, *cis*-CF_3, *cis*-C_2F_5) derivatives that were subsequently reacted with XeF_2 to prepare new alkenylxenon(II) and 2-X-1,2-difluoroalk-1-enylxenon(II) salts.[74]

$$XCF{=}CFLi + B(OMe)_3 \rightarrow Li[XCF{=}CFB(OMe)_3] \xrightarrow[-LiF,\ MeOH]{K[HF_2],\ aq\ HF} K[XCF{=}CFBF_3] \quad [11]$$

$$trans\text{-}Et_3SiCF{=}CFH \xrightarrow[2.B(OMe)_3]{1.BuLi} Li[trans\text{-}Et_3SiCF{=}CFB(OMe)_3] \xrightarrow[-LiF,\ MeOH]{K[HF_2],\ aq\ HF} K[trans\text{-}Et_3SiCF{=}CFBF_3] \quad [12]$$

$$K[trans\text{-}Et_3SiCF{=}CFBF_3] + HF + H_2O \xrightarrow[100\,^\circ C,\ 94\,h,\ -FSiEt_3]{DMSO} K[trans\text{-}HCF{=}CFBF_3] \quad [13]$$

$$Li[CF_3CF{=}CFB(OMe)_3] + K[HF_2] \xrightarrow[-LiF,\ MeOH]{aHF} K[cis\text{- and }trans\text{-}CF_3CF{=}CFBF_3] \quad [14]$$

It is noteworthy that no organoxenon(II) cations were obtained when the *trans*-$XCF{=}CFBF_2$ (X = CF_3, C_4F_9, C_4H_9, Et_3Si) precursors were used under similar conditions. It was consequently surmised that reactions leading to alkenylxenon(II) salts proceed according to Scheme 2, which also accounted for the formation of traces of organotrifluoroborate anions and moderate to equimolar amounts of alkyltrifluoroborate anions. When the Xe–C(1) distance was sufficiently short in the transition state for successful Xe–C bond formation, xenodeborylation occurred and the $[XCF{=}CFXe][BF_4]$ salt formed according to Scheme 2, reaction [1].[74] However, when the ligand was too bulky, preventing interaction between C(1) and Xe, a more complex series of reactions had to be proposed to account for the sole observation of organotrifluoroborate and alkyltrifluoroborate anions. The alkenylxenon(II) salts and reaction products were unambiguously characterized by ^{19}F, ^{13}C, and ^{129}Xe NMR spectroscopy.[74]

Using reaction conditions analogous to those used for the syntheses of the 2-X-1,2-difluoroalk-1-enylxenon(II) salts, the $[CF_2{=}CXXe][BF_4]$ (X = H, Cl, CF_3) salts were prepared by the reaction of XeF_2 with the corresponding alkenyldifluoroborane, $CF_2{=}CXBF_2$, in 1,1,1,3,3-pentafluoropropane (PFP) at −60 °C.[75] The alkenylxenon(II) salts were characterized by multi-NMR spectroscopy. It was noted that, although all three salts were synthesized, $[CF_2{=}C(CF_3)Xe][BF_4]$ was obtained in highest yield (77%), and was the only salt that was stable in aHF at −60 °C. The yields of the remaining salts were $[CF_2{=}CHXe][BF_4]$ (60%) and $[CF_2{=}CClXe][BF_4]$ (19%). The latter decomposed under the stated reaction conditions, yielding $CF_2{=}CFCl$, CF_3CF_2Cl, and BF_3, and upon dissolution

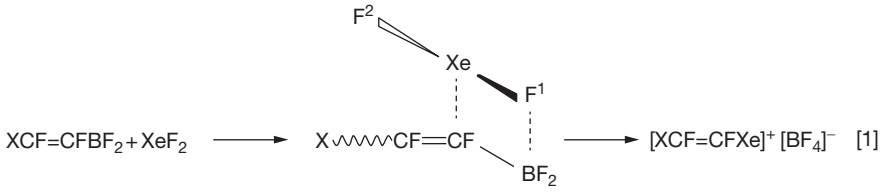

$$XCF{=}CFBF_2 + [BF_4]^- \rightleftharpoons [XCF{=}CFBF_3]^- + BF_3 \quad [2]$$

$$[XCF{=}CFBF_3]^- + FXe^{\delta+}\cdots{}^{\delta-}FB{\equiv} \rightarrow [XCF_2CF_2BF_3]^- + Xe^0 + B{\equiv} \quad [3]$$

Scheme 2 Proposed reaction mechanism for xenodeborylation. Redrawn from Ref. 74.

Copyright © 2013. Elsevier. All rights reserved.

Comprehensive Inorganic Chemistry II : From Elements to Applications, Elsevier, 2013. ProQuest Ebook Central, http://ebookcentral.proquest.com/lib/inflibnet-ebooks/detail.action?docID=1330977.
Created from inflibnet-ebooks on 2021-02-09 22:27:13.

in aHF, the $CF_3CFClBF_3^-$ anion was also formed. With the exception of the $CF_3CFHBF_3^-$ anion, which was not observed, $[CF_2{=}CHXe][BF_4]$ showed analogous decomposition products under the stated reaction conditions. Replacement of the α-fluorine atom of $CF_2{=}CFBF_2$ by the less electron-withdrawing H and Cl atoms or by the trifluoromethyl group had no effect on the substitution of the difluoroboryl group by Xe(II), but did affect the stabilities of the salts when suspended in PFP or dissolved in aHF.[75]

1.25.3.1.1.4 Syntheses and NMR characterizations of alkynyl derivatives of Xe(II) cations

A communication was published in 1992[76] describing the reaction of Li[*t*-BuC≡CBF_3] with XeF_2 in CH_2Cl_2 and the detection of [*t*-BuC≡CXe][BF_4]. However, as a result of its thermal instability (decomposition at −30 °C), the salt was not isolated, but the structure was established by ^{1}H, ^{11}B, ^{13}C, ^{19}F, and ^{129}Xe NMR spectroscopy (at −40 °C), IR spectroscopy (at 0 °C), and by alkynylation of PPh_3 to form [*t*-BuC≡$CPPh_3$][BF_4] (−78 °C). Further attempts to prepare other alkynyl derivatives of Xe(II) by analogous reactions and by reactions of alkynyltrimethylsilane in combination with $BF_3 \cdot OEt_2$ and XeF_2 were unsuccessful.

An alkynylxenon(II) salt was subsequently isolated in satisfactory to good yields by adding XeF_2 to a cold (−47 °C) solution of $CF_3C{\equiv}CBF_2$ in PFP.[77] The product, [$CF_3C{\equiv}CXe$][BF_4], was isolated as a white solid that was stable at 20 °C for at least 2–3 h. The salt was soluble in aHF where it was remarkably stable, showing a 30% conversion to a mixture of *cis*- and *trans*-$CF_3CH{=}CHF$ after 24 h at 20 °C. The alkynylxenon(II) salt was characterized by ^{13}C, ^{19}F, and ^{129}Xe NMR spectroscopy and displayed $^1J(^{13}C\text{-}1-^{129}Xe)$ and $^2J(^{13}C\text{-}2-^{129}Xe)$ couplings of 343 and 69 Hz, respectively (the $^3J(^{13}C\text{-}3-^{129}Xe)$ coupling was not observed). These were the largest $J(^{13}C-^{129}Xe)$ couplings observed in Xe−C compounds up until that time.

The range of alkynylxenon(II) salts has been extended to [$R_FC{\equiv}CXe$][BF_4] [$R_F = CF_3$, C_3F_7, $(CF_3)_2CF$, *cis*-, *trans*-$CF_3CF{=}CF$, C_6F_5] by the reaction of XeF_2 with the corresponding perfluoroorganoethynyldifluoroboranes, $R_FC{\equiv}CBF_2$, in PFP or CH_2Cl_2 at −60 to −40 °C, and were isolated in 30–98% yields.[78] In contrast with the reaction of alk-1-enyldifluoroboranes, $RCF{=}CFBF_2$, with XeF_2,[75] neither the alk-1-enyltrifluoroborate anions, $R_FCF{=}CFBF_3^-$, nor their fluorination products, XBF_3^- (X = RCF=CF, RCF_2CF_2), were observed.[78] Similar methods were used to synthesize the nonfluorinated organoethynylxenon (II) salts, [$C_4H_9C{\equiv}CXe$][BF_4] and [$(CH_3)_3CC{\equiv}CXe$][BF_4], which were obtained in 20–40% yields. All salts were soluble in aHF with the [$C_4H_9C{\equiv}CXe$][BF_4] and [$(CH_3)_3CC{\equiv}CXe$][BF_4] salts also having good solubilities in the weakly coordinating solvents, CH_2Cl_2 and PFP.

The aforementioned salts have been characterized in aHF by ^{1}H, ^{11}B, ^{13}C, ^{19}F, and ^{129}Xe NMR spectroscopy.[78] The ^{129}Xe resonances of alkynylxenonium salts range from −3601 ([$(CF_3)_2CFC{\equiv}CXe$][BF_4]) to −3781 ppm ([$(CH_3)_3CC{\equiv}CXe$][BF_4]) with the most shielded ^{129}Xe resonances occurring at −3775 and −3781 ppm for [$C_4H_9C{\equiv}CXe$][BF_4] and [$(CH_3)_3CC{\equiv}CXe$][BF_4], respectively, in aHF (−60 °C). The C-1 resonances in the ^{13}C spectra were unusually shielded (between 8 and −24 ppm relative to TMS). Xenon-129 satellites were observed for C-1 of the $R_FC{\equiv}CXe^+$ cations which arose from the $^1J(^{13}C\text{-}1-^{129}Xe)$ coupling and which increased in the order 264, 267 Hz [$R_F = C_4H_9$, $(CH_3)_3C$], 308 Hz ($R_F = C_6F_5$), and 332–349 Hz (R_F = perfluoroalkyl). By contrast, the opposite ordering was found for $^2J(^{13}C\text{-}2-^{129}Xe)$, that is, ranges of 69–76 Hz for the alkyl groups and 64–70 Hz for the perfluoroalkyl groups.[78]

1.25.3.1.1.5 Reactivities of xenon(II)–carbon bonded cations

The substitution of xenon in reactions of [*cis*-$C_nF_{2n+1}CF{=}CFXe$][Y] ($n = 0, 1, 2$) with C_6H_6, I^-, and Br^- in propionitrile solution has been studied.[79] To initially establish the stabilities of the salts in propionitrile, solutions containing [*cis*-$CF_3CF{=}CFXe$][$C_3F_7BF_3$] and [*cis*-$C_2F_5CF{=}CFXe$][AsF_6] were studied at −50 to −60 °C where the salts were stable for 2–5 h, but at −40 °C, 80% of the [*cis*-$C_2F_5CF{=}CFXe$][AsF_6] was converted into *cis*-$C_2F_5CF{=}CFH$ within 1 h. In contrast, [*cis*-$CF_3CF{=}CFXe$][$C_3F_7BF_3$] was stable at −40 °C. Reaction of the aforementioned salts with [Me_4N]Br and [Me_4N]I resulted in stereospecific substitution of xenon by bromine and iodine. In the case of I^-, a quantitative yield was obtained when a solution of [*cis*-$CF_3CF{=}CFXe$][$C_3F_7BF_3$] was added to a suspension of [Me_4N]I in propionitrile and warmed from −50 to 20 °C. However, when [*cis*-$C_2F_5CF{=}CFXe$][AsF_6] was allowed to react with [Bu_4N]Br for 2 h at −50 °C, a mixture of *cis*-$C_2F_5CF{=}CFBr$, [Bu_4N][AsF_6], *cis*-$C_2F_5CF{=}CFH$ (∼15 %), and Xe^0 formed. The reaction of [*cis*-$CF_3CF{=}CFXe$][$C_3F_7BF_3$] and [*cis*-$C_2F_5CF{=}CFXe$][AsF_6] with C_6H_6 resulted in the substitution of xenon by the phenyl group, producing the stereospecific products, *cis*-$CF_3CF{=}CFC_6H_5$ and *cis*-$C_2F_5CF{=}CFC_6H_5$, respectively. Mechanisms for each set of reactions have been proposed and discussed in the context of the observed products.

A similar reactivity study was carried out for alkenylxenonium(II) salts and alkynylxenonium(II) salts in aHF.[80] The stabilities of the alkynylxenonium(II) salts, [$R_FC{\equiv}CXe$][BF_4] ($R_F = CF_3$, C_3F_7, $(CF_3)_2CF$, *cis*- and *trans*-$CF_3CF{=}CF$, C_6F_5), in aHF were largely dependent on the substituent, R_F, with the perfluorinated alkyl salts, $R_F = CF_3$, C_3F_7, $(CF_3)_2CF$, showing no solvolysis or decomposition for 20–24 h at 20 °C, but salts with $R_F = CF_3CF{=}CF$ and C_6F_5 decomposed rapidly (R_F = *cis*- and *trans*-$CF_3CF{=}CF$, total decomposition at 24 °C within 4 h; $R_F = C_6F_5$, total decomposition at −40 °C within 1 h). A similar dependence on the R-substituent (R = $CF_2{=}CF$, *trans*-$HCF{=}CF$, *cis*-$C_2F_5CF{=}CF$) was noted for alkenylxenonium(II) salts.

Reactions of the stable alkenylxenonium(II) salts, [$RCF{=}CFXe$]Y (R = *cis*-C_2F_5, *trans*-H), and alkynylxenonium(II) salt, [$C_3F_7C{\equiv}CXe$][BF_4], with NaI in aHF resulted in stereospecific xenon replacement by iodine or hydrogen.[80] At −60 °C, the substitution of xenon by bromine in the perfluorinated salts [*cis*-$CF_3CF{=}CFXe$]Y and [*trans*-$C_4F_9CF{=}CFXe$]Y proceeded regio- and stereospecifically with NaBr in aHF, but after 10–30 min at −25 to −30 °C, the reaction of [*cis*-$C_2F_5CF{=}CFXe$]Y with NaBr, KBr, or [Bu_4N]Br in aHF gave mixtures of *cis*- and *trans*-perfluorobut-1-enyl bromides. The reaction of [$C_3F_7C{\equiv}CXe$][BF_4] with NaBr in aHF at −65 °C gave a 48% yield of $C_3F_7C{\equiv}CBr$ and was accompanied by a mixture of olefins that included $C_3F_7C{\equiv}CH$, $C_3F_7CBr{=}CBr_2$, $C_3F_7CBr{=}CHBr$, and $C_3F_7CBr{=}CHF$. Reaction pathways leading to the main products have also been considered in these studies.

Copyright © 2013. Elsevier. All rights reserved.

Comprehensive Inorganic Chemistry II : From Elements to Applications, Elsevier, 2013. ProQuest Ebook Central, http://ebookcentral.proquest.com/lib/inflibnet-ebooks/detail.action?docID=1330977.
Created from inflibnet-ebooks on 2021-02-09 22:27:13.

1.25.3.1.1.6 Attempts to form a Xe-(4-C_5F_4N) cation and calculated gas-phase F^- affinities of selected fluoroorganodifluoroboranes, R_FBF_2

As discussed in Section 1.25.3.1.1, organodifluoroboranes, RBF_2, are generally suitable reagents to transform XeF_2 into the corresponding xenonium tetrafluoridoborate salts, [RXe][BF_4].[64,65,75,77,78] However, an attempt to react (4-C_5F_4N)BF_2, a borane of high acidity, with XeF_2 to form a Xe−C bonded xenonium salt proved to be unsuccessful.[81] Instead, the reaction of (4-C_5F_4N)BF_2 with XeF_2 resulted in a XeF_2–borane adduct. Interestingly, the reaction of C_6F_5XeF with Cd(4-C_5F_4N)$_2$ was successful and produced C_6F_5Xe(4-C_5F_4N), which is discussed in Section 1.25.3.2.1.2. The gas-phase fluoride ion affinities of selected fluoro-organodifluoroboranes, R_FBF_2, and their hydrocarbon analogs have been calculated at the B3LYP/6-31+G* level of theory and have been discussed with respect to their potential use as R_F transfer reagents for Xe−C bond formation in reactions with XeF_2.

1.25.3.1.2 Xenon derivatives of the $OTeF_5$ and $OSeF_5$ groups

1.25.3.1.2.1 [$XeOTeF_5$][$Sb(OTeF_5)_6$]·SO_2ClF

The strong oxidant salt, [$XeOTeF_5$][$Sb(OTeF_5)_6$], has been formed by the stoichiometric reaction of $Xe(OTeF_5)_2$ and $Sb(OTeF_5)_3$ in SO_2ClF solvent at −20 °C (eqn [15]), yielding bright yellow to yellow–orange solutions.[82] The synthesis and crystal structure of [$XeOTeF_5$][$Sb(OTeF_5)_6$] also appear in another publication;[83] the findings reviewed below refer to Mercier et al.[82]

$$2Xe(OTeF_5)_2 + Sb(OTeF_5)_3 \rightarrow [XeOTeF_5][Sb(OTeF_5)_6] + Xe \quad [15]$$

The solubility of [$XeOTeF_5$][$Sb(OTeF_5)_6$] in SO_2ClF at −78 °C is high, exceeding 2 M, whereas the fluorine analog, [XeF][SbF_6], is insoluble in SO_2ClF at room temperature. Solutions of [$XeOTeF_5$][$Sb(OTeF_5)_6$] in SO_2ClF show significant decomposition after 30 min to 1 h at −10 °C. The salt was isolated as a pale yellow solvate, [$XeOTeF_5$][$Sb(OTeF_5)_6$]·SO_2ClF, after pumping a SO_2ClF solution for several hours at −78 to 0 °C. The solvate was stable to pumping at 0 °C for at least 4–5 h. The solid decomposes above 10 °C over a period of 4–6 h, in marked contrast with [$XeOTeF_5$][AsF_6][84–86] and [XeF][SbF_6],[87] which are room-temperature stable.

The strong oxidant properties of [$XeOTeF_5$][$Sb(OTeF_5)_6$] are, to a large extent, attributable to the weakly coordinating nature of the anion which renders the weak Lewis acid–base pair, $F_5TeOXe^+\cdots OSOClF$ (*vide infra*), a potent electrophile for the syntheses of salts of trihalomethyl cations in SO_2ClF solvent.[88] The syntheses were accomplished by the low-temperature oxidation of a halide ligand of the corresponding tetrahalomethane[88] in SO_2ClF solvent. Among the trihalomethyl cations that have been synthesized are CCl_3^+, CBr_3^+ (eqns [16] and [17]), $CFCl_2^+$, and $CFBr_2^+$, as well as $C(OTeF_5)_3^+$ (eqn [17]).[88–90] The carbocations have been stabilized as salts of the preformed, oxidatively resistant, and weakly coordinating $Sb(OTeF_5)_6^-$ anion, thus avoiding the use of more strongly coordinating anions derived from strong Lewis acid ligand acceptors such as SbF_5.

$$[XeOTeF_5][Sb(OTeF_5)_6] + CCl_4 \rightarrow [CCl_3][Sb(OTeF_5)_6] + ClOTeF_5 + Xe \quad [16]$$

$$3[XeOTeF_5][Sb(OTeF_5)_6] + 3CBr_4 \rightarrow 2[CBr_3][Sb(OTeF_5)_6] + [C(OTeF_5)_3][Sb(OTeF_5)_6] + 3Br_2 + 3Xe \quad [17]$$

The ^{19}F, ^{121}Sb, ^{125}Te, and ^{129}Xe NMR spectra of [$XeOTeF_5$][$Sb(OTeF_5)_6$] have been recorded at −50 °C in SO_2ClF.[82] The ^{17}O NMR spectrum was recorded for an enriched [$^{17,18}O$]-[$XeOTeF_5$][$Sb(OTeF_5)_6$] sample at −15 °C. The NMR parameters are summarized in Table 1 and are in accordance with the NMR spectra of $XeOTeF_5^+$ recorded in SbF_5 solution[91] and of $Sb(OTeF_5)_6^-$ recorded in CH_3CN solution.[92] Although Raman spectroscopy and the X-ray crystal structure of [$XeOTeF_5$][$Sb(OTeF_5)_6$]·SO_2ClF show that SO_2ClF is coordinated through an oxygen atom to the xenon atom of the $XeOTeF_5^+$ cation (*vide infra*), the ^{19}F NMR spectrum provides no direct evidence for coordinated SO_2ClF. This is attributed to the lability of the Xe---O donor–acceptor bond in solution which results in rapid chemical exchange between bulk SO_2ClF solvent molecules and coordinated SO_2ClF molecules at temperatures as low as −80 °C.

The salt crystallizes at −20 °C from SO_2ClF as [$XeOTeF_5$][$Sb(OTeF_5)_6$]·SO_2ClF. The crystal structure consists of well-separated $XeOTeF_5^+$ cations and $Sb(OTeF_5)_6^-$ anions in which each $XeOTeF_5^+$ cation is oxygen-coordinated to a SO_2ClF molecule (Figure 11). Unlike MF_6^- in [XeF][MF_6] (e.g., M = As, Sb, Bi)[93] and [$XeOTeF_5$][AsF_6],[86] the $Sb(OTeF_5)_6^-$ anion is significantly less fluorobasic and does not interact with the coordinately unsaturated $XeOTeF_5^+$ cation. Rather, the $XeOTeF_5^+$ cation and weak Lewis base, SO_2ClF, interact by coordination of an oxygen atom of SO_2ClF to xenon (Xe---O, 2.471(5) Å). By analogy with XeF^+ salt formation from XeF_2, which leads to a shortened terminal Xe−F bond relative to that of XeF_2,[93,94] the Xe–O(7) distance (1.969(4) Å) is shorter than in neutral $Xe(OTeF_5)_2$ (2.119(11) Å).[86] The Te−O(7) bond distance (1.938(5) Å) in $XeOTeF_5^+$ is significantly longer than in $Xe(OTeF_5)_2$ (1.843(11) Å),[86] consistent with the increased

Table 1 The ^{19}F, ^{125}Te, ^{129}Xe, ^{17}O, and ^{121}Sb NMR parameters for [$XeOTeF_5$][$Sb(OTeF_5)_6$][a]

	Chem shift (δ) (ppm)					*Coupling constant (Hz)*		
Species	^{19}F[b]	^{125}Te	^{129}Xe	^{17}O[c]	^{121}Sb	$^2J(^{19}F_A–^{19}F_X)$[b]	$^1J(^{19}F–^{125}Te)$[b]	$^1J(^{19}F–^{123}Te)$
$XeOTeF_5^+$	−51.7 (F_A)	579.9	−1459.5	133		175	3776 (F_A)	
	−40.3 (F_X)						3810 (F_X)	
$Sb(OTeF_5)_6^-$	−42.4 ($F_A \approx F_B$)	548.4		107	−13		3553	2950

[a]Reproduced with permission from Ref. 82. All NMR spectra were recorded in SO_2ClF solvent at −50 °C except the ^{17}O spectrum, which was recorded at −15 °C.
[b]The subscripts A and B/X denote axial and equatorial fluorine atoms, respectively.
[c]The ^{17}O NMR parameters for SO_2ClF solvent were also determined at natural abundance: doublet at δ(^{17}O), 227.0 ppm; $^2J(^{17}O–^{19}F)$, 27.9 Hz.

Copyright © 2013. Elsevier. All rights reserved.

Comprehensive Inorganic Chemistry II : From Elements to Applications, Elsevier, 2013. ProQuest Ebook Central, http://ebookcentral.proquest.com/lib/inflibnet-ebooks/detail.action?docID=1330977.
Created from inflibnet-ebooks on 2021-02-09 22:27:13.

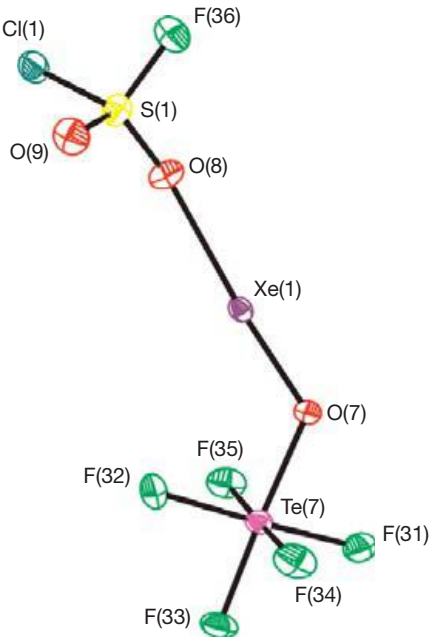

Figure 11 The structural unit in the X-ray crystal structure of $[XeOTeF_5][Sb(OTeF_5)_6]\cdot SO_2ClF$; thermal ellipsoids are shown at the 50% probability level. Reproduced with permission from Mercier, H. P. A.; Moran, M. D.; Sanders, J. C. P.; Schrobilgen, G. J.; Suontamo, R. J. *Inorg. Chem.* **2005**, *44*, 49–60.

bond order and decreased bond length of the Xe–O(7) bond trans to it. The Te–F bond lengths of the cation and the anion are similar to those found in other $OTeF_5$ compounds,[88,95,96] $[N(CH_2CH_3)_4][Sb(OTeF_5)_6]$ and $[N(CH_3)_4][Sb(OTeF_5)_6]$.[92]

1.25.3.1.2.2 $[XeOChF_5][AsF_6]$ and $Xe(OChF_5)_2$

The salt, $[XeOSeF_5][AsF_6]$, has been synthesized[86] by analogy with $[XeOTeF_5][AsF_6]$[84] according to eqn [18].

$$FXeOSeF_5 + AsF_5 \rightarrow [XeOSeF_5][AsF_6] \qquad [18]$$

Like the tellurium analog, this salt is a stable yellow solid at room temperature which sublimes under dynamic vacuum at 45 °C. The $XeOSeF_5^+$ cation resists solvent attack in BrF_5 at −51 °C. The $XeOTeF_5^+$ cation has been shown to undergo rapid solvolysis in BrF_5 at room temperature to form TeF_6 and $[BrOF_2][AsF_6]\cdot XeF_2$.[91]

The ^{19}F NMR spectrum of $[XeOSeF_5][AsF_6]$ in SbF_5 solvent at 28 °C [BrF_5 solvent, −51 °C] consists of a first-order AX_4 spectrum which is accompanied by ^{77}Se ($I = ½$, 7.58%) satellites: $\delta(F_A)$, 57.1 [62.2] ppm; $\delta(F_X)$, 74.9 [73.3] ppm; $^2J(^{19}F_A-^{19}F_X)$, 216 [219] Hz; $^1J(^{19}F_A-^{77}Se)$, 1459 Hz (not resolved owing to increased line broadening in BrF_5); and $^1J(^{19}F_X-^{77}Se)$, 1415 [1398] Hz. The ^{77}Se NMR spectrum (SbF_5 solvent, 29 °C) is a single ^{77}Se environment at 627.5 ppm comprised of a binomial doublet of quintets resulting from the spin–spin couplings $^1J(^{19}F_A-^{77}Se) = 1460$ Hz and $^1J(^{19}F_X-^{77}Se) = 1415$ Hz. The ^{129}Xe spectrum in SbF_5 solvent at 25 °C [BrF_5 solvent, −56 °C] consists of a single resonance at −1349.0 [−1438] ppm in the Xe(II) region of the spectrum.[86]

The $[XeOChF_5][AsF_6]$ salts are isotypic and present the same fourfold orientational disorder of the fluorine and oxygen atoms. The AsF_6^- anion is fluorine-bridged to $XeOChF_5^+$ through short Xe···F contacts ($[XeOTeF_5][AsF_6]$, 2.24(3) Å; $[XeOSeF_5][AsF_6]$, 2.31(4) Å) that are comparable to that observed in the fluorine analog, $[XeF][AsF_6]$ (2.208(3) Å),[93] but significantly shorter than that in the isovalent $[F_5TeN(H)Xe][AsF_6]$ (2.580(3) Å) salt.[97] As in the cases of the XeF^+ salts[93] and the neutral parent molecule, XeF_2,[93] the Xe–O bonds in $[XeOChF_5][AsF_6]$ (Te, 1.96(4) Å; Se, 2.04(4) Å), when compared with those in neutral $Xe(OChF_5)_2$ (Te, 2.119(11) and 2.112(12) Å; Se, 2.16(3) Å) and $FXeOSO_2F$ (2.155(8) Å),[98] are shorter.

Both $Xe(OChF_5)_2$ compounds were previously known,[84,99] but single-crystal X-ray structures of good precision were lacking. While the structure of $Xe(OTeF_5)_2$ (−127 °C) is ordered,[86] the fluorine and oxygen atoms are orientationally threefold disordered in the selenium analog. The $OChF_5$ groups in $Xe(OChF_5)_2$ and the $OChF_5$ group and AsF_6^- anion in $[XeOChF_5][AsF_6]$ are arranged trans to each other and have Xe–O–Ch and Xe---F–As angles that are significantly less than 180° [(As–F–Xe: $[XeOTeF_5][AsF_6]$, 135(1)°; $[XeOSeF_5][AsF_6]$, 129(2)°), (Xe–O–M: $[XeOTeF_5][AsF_6]$, 128(2)°; $[XeOSeF_5][AsF_6]$, 120(3)°; $Xe(OTeF_5)_2$, 122.3(5)° and 121.2(6)°; $Xe(OSeF_5)_2$, 123.9(13)°)]. The bent arrangements about the bridging fluorine and oxygen atoms are in accordance with AX_2E_2 valence shell electron pair repulsion (VSEPR) arrangements.[100] In all structures, the geometries around the chalcogen atoms are pseudo-octahedral with *cis*-F–Ch–F and *cis*-F–Ch–O angles deviating significantly from 90° in $[XeOTeF_5][AsF_6]$, $[XeOSeF_5][AsF_6]$, and $Xe(OSeF_5)_2$ because of the disorders. The F–Te–F and F–Te–O bond angles in the ordered structure of $Xe(OTeF_5)_2$ are all equal to 90° within experimental error. Although the Se–O (1.58(3) Å) and Se–F (1.65(3)–1.81(2) Å) bond lengths in $Xe(OSeF_5)_2$ are significantly affected by disorder, the Te–O ($[XeOTeF_5][AsF_6]$, 1.85(3) Å; $Xe(OTeF_5)_2$, 1.843(11) and 1.842(11) Å), Te–F ($[XeOTeF_5][AsF_6]$, 1.79(3)–1.84(2) Å; $Xe(OTeF_5)_2$, 1.823(9)–1.855(11) Å), Se–O ($[XeOSeF_5][AsF_6]$, 1.74(4) Å), and Se–F ($[XeOSeF_5][AsF_6]$, 1.70(1) Å) bond lengths in $[XeOChF_5][AsF_6]$ and $Xe(OTeF_5)_2$ are in good agreement with values previously reported for $OSeF_5$ and $OTeF_5$ compounds.[92,101–104]

1.25.3.1.3 Xenon–nitrogen bonded cations

The fields of noble-gas chemistry and sulfur–nitrogen–fluorine chemistry have been significantly extended by the syntheses and characterizations of four Xe–N-bonded cations derived from $N{\equiv}SF_3$.[13,71,105–107] The reaction of the Lewis-acidic XeF^+ cation with $N{\equiv}SF_3$ has added a further example, $F_3S{\equiv}NXeF^+$,[71] to the large number of nitrogen base–XeF^+ adducts that were already known.[68,69,108,109] It was subsequently shown that the adduct-cation, $F_3S{\equiv}NXeF^+$, provides an entry point into a significant new chemistry through HF solvolysis of the coordinated $N{\equiv}SF_3$ ligand and through its HF-catalyzed and solid-state rearrangements.[105–107]

1.25.3.1.3.1 $[F_3S{\equiv}NXeF][AsF_6]$

The salt, $[F_3S{\equiv}NXeF][AsF_6]$, has been synthesized by the reaction of $[XeF][AsF_6]$ with liquid $N{\equiv}SF_3$ (eqn [19]) and represents the first example of xenon bound to an inorganic nitrogen base in which nitrogen is formally sp-hybridized.[71]

Copyright © 2013. Elsevier. All rights reserved.

Comprehensive Inorganic Chemistry II : From Elements to Applications, Elsevier, 2013. ProQuest Ebook Central, http://ebookcentral.proquest.com/lib/inflibnet-ebooks/detail.action?docID=1330977.
Created from inflibnet-ebooks on 2021-02-09 22:27:13.

The $F_3S{\equiv}NXeF^+$ cation was characterized in the solid state by low-temperature Raman spectroscopy and by single-crystal X-ray diffraction.

$$N{\equiv}SF_3 + [XeF][AsF_6] \xrightarrow[-25\ \text{to}-15\ ^\circ\text{C}]{N{\equiv}SF_3} [F_3S{\equiv}NXeF][AsF_6] \qquad [19]$$

The solution characterization of $[F_3S{\equiv}NXeF][AsF_6]$ by ^{14}N, ^{19}F, and ^{129}Xe NMR spectroscopy[71] (Figures 12 and 13) has provided unambiguous characterizations of $F_3S{\equiv}NXeF^+$ in aHF (−20 °C) and BrF_5 (−60 °C, given in parentheses) solvents (NMR parameters are provided in Table 2). The ^{129}Xe spectrum (Figure 13) was a doublet of 1:1:1 triplets in aHF. The outer triplet transitions were broader than the central transition owing to partial quadrupolar relaxation of ^{14}N ($I=1$) which resulted from the small electric field gradient at ^{14}N in this axially symmetric cation. The ^{129}Xe NMR chemical shift (−1652 (−1661) ppm) was consistent with that expected for a Xe–F moiety bound to an sp-hybridized nitrogen (cf. $HC{\equiv}NXeF^+$, $\delta(^{129}Xe) = 1552$ (−1570) ppm in aHF (BrF_5) solvent at −10 (−50) °C).[69] When the ^{129}Xe NMR spectrum of $F_3S{\equiv}NXeF^+$ was recorded in BrF_5 solvent, the $^1J(^{129}Xe-^{14}N)$ coupling was collapsed to a doublet corresponding to $^1J(^{129}Xe-^{19}F)$ due to fast quadrupolar relaxation of ^{14}N that mainly resulted from the high viscosity of BrF_5 at −60 °C. The ^{14}N spectrum of $F_3S{\equiv}NXeF^+$, recorded in aHF at −20 °C, consisted of a quadrupole broadened resonance ($\Delta\nu_{1/2} = 750$ Hz) at −278.0 ppm. Consequently, the expected natural abundance ^{129}Xe satellites were obscured. The line broadenings of the ^{19}F resonances in HF solvent have provided indirect evidence for slow chemical exchange between HF and $F_3S{\equiv}NXeF^+$ (eqn [20]). The fluorine exchange rate was diminished in BrF_5 as evidenced by the narrowing of the ^{19}F resonances:[110]

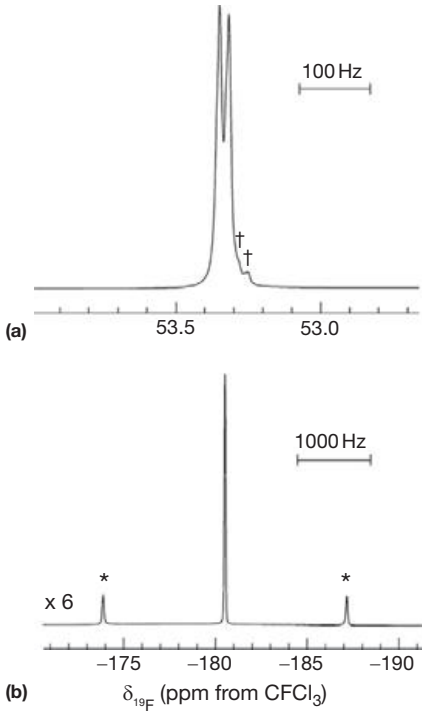

Figure 12 The ^{19}F NMR spectrum (470.592 MHz) of $[F_3S{\equiv}NXeF][AsF_6]$ in BrF_5 solvent at −60 °C showing the cation resonances: (a) the F-on-S environment; daggers (†) denote the $^1\Delta^{19}F_S(^{34/32}S)$ secondary isotope shift and (b) the F-on-Xe environment; asterisks (*) denote ^{129}Xe satellites. Reproduced with permission from Smith, G. L.; Mercier, H. P. A.; Schrobilgen, G. J. *Inorg. Chem.* **2007**, *46*, 1369–1378.

$$F_3S{\equiv}NXeF^+ + 2HF \rightleftharpoons XeF_2 + N{\equiv}SF_3 + H_2F^+ \qquad [20]$$

Colorless $[F_3S{\equiv}NXeF][AsF_6]$ was crystallized from aHF at −45 °C and its low-temperature X-ray crystal structure was determined (Figure 14). The Xe–N bond is among the longest Xe–N bonds known (2.236(4) Å),[97,105–107,111–115] whereas the Xe–F bond length (1.938(3) Å) is significantly shorter than that of XeF_2, but longer than in XeF^+ salts (see Section 1.25.3.1.4.1). The Xe–F and Xe–N bond lengths are similar to those of $HC{\equiv}NXeF^+$ (1.936(2) and 2.235(3) Å),[70] placing $F_3S{\equiv}NXeF^+$ among the most ionic Xe–N bonds known. The nonlinear Xe–N–S angle (142.6(3)°) contrasts with the linear angle obtained for the energy-minimized geometry and was attributed to N···F contacts within the crystallographic unit cell.

Quantum-chemical calculations at the MP2 and DFT levels of theory were used to calculate the gas-phase geometries, charges, bond orders, and valencies of $F_3S{\equiv}NXeF^+$ and to

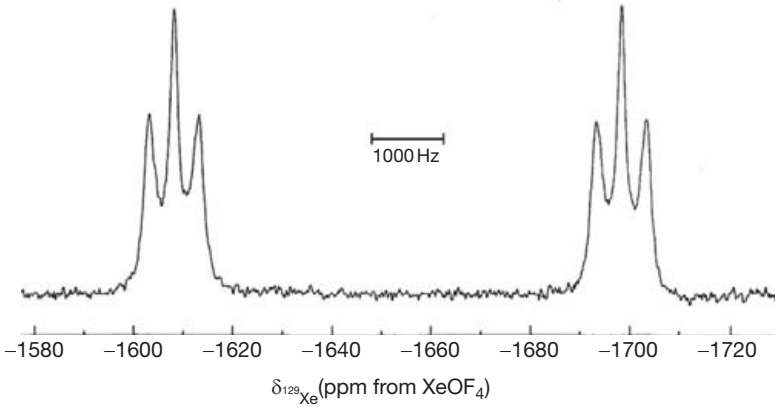

Figure 13 The ^{129}Xe NMR spectrum (138.086 MHz) of $[F_3S{\equiv}NXeF][AsF_6]$ in aHF solvent at −20 °C. Reproduced with permission from Smith, G. L.; Mercier, H. P. A.; Schrobilgen, G. J. *Inorg. Chem.* **2007**, *46*, 1369–1378.

Copyright © 2013. Elsevier. All rights reserved.

Comprehensive Inorganic Chemistry II : From Elements to Applications, Elsevier, 2013. ProQuest Ebook Central, http://ebookcentral.proquest.com/lib/inflibnet-ebooks/detail.action?docID=1330977.
Created from inflibnet-ebooks on 2021-02-09 22:27:13.

Table 2 NMR chemical shifts and spin–spin coupling constants for $[F_3S{\equiv}NXeF][AsF_6]$,[a] $[F_4S{=}NXe][AsF_6]$,[a,b] $[F_5TeN(H)Xe][AsF_6]$,[a] and $[F_5SN(H)Xe][AsF_6]$[a]

$F_3S{\equiv}NXeF^+$ [c]					*$F_4S{=}NXe^+$* [d]				
Chem. shifts (ppm)		T (°C)	*Coupling constants (Hz)*		*Chem. shifts (ppm)*		T (°C)	*Coupling constants (Hz)*	
$\delta(^{129}Xe)$	−1652 (−1661)	−20 (−60)	$^1J(^{129}Xe-^{19}F_{Xe})$	6265 (6248)	$\delta(^{129}Xe)$	−2674 (−2588) [−2510]	−20 (−60) [0]		
			$^1J(^{129}Xe-^{14}N)$	350					
$\delta(^{19}F_{Xe})$	−185.5 (−180.5)				$\delta(^{19}F_A)$	53.6 (55.1) [58.6]	−20 (−60) [0]	$^2J(^{19}F_A-^{19}F_B)$	206.8 (212.3) [206.3]
								$^2J(^{19}F_A-^{19}F_X)$	206.5 (210.2) [209.6]
$\delta(^{19}F_S)$	51.2 (53.3)		$^nJ(^{19}F-^{19}F)$	(15.1), $n=4$	$\delta(^{19}F_B)$	63.8 (64.7) [e]	−20 (−60)	$^2J(^{19}F_B-^{19}F_X)$	18.2 (18.0) [21.6]
								$^3J(^{129}Xe-^{19}F_B)$	203.6 (208.7) [208.9]
					$\delta(^{19}F_X)$	110.2 (113.3) [110.6]	−20 (−60) [0]	$^3J(^{129}Xe-^{19}F_X)$	129.7 (126.7) [102.0]
$\delta(^{14}N)$	−278.0								

$[F_5TeN(H)Xe][AsF_6]$ [f]					*$[F_5SN(H)Xe][AsF_6]$* [h]				
Chem. shifts (ppm)		T (°C)	*Coupling constants (Hz)*		*Chem. shifts (ppm)*		T (°C)	*Coupling constants (Hz)*	
$\delta(^{129}Xe)$	−2841 (−2902)[g]	−39 (−45)[g]	$^1J(^{129}Xe-^{15}N)$	138 (142)[g]	$\delta(^{129}Xe)$	−2897 (−2956)			
			$^2J(^{129}Xe-^{1}H)$	240					
			$^3J(^{129}Xe-^{19}F_e)$	6					
$\delta(^{125}Te)$	598[g]	−34[g]	$^1J(^{125}Te-^{19}F_a)$	3578[g]					
			$^1J(^{125}Te-^{19}F_e)$	3766[g]					
			$^1J(^{123}Te-^{19}F_e)$	(3113)					
$\delta(^{19}F_a)$	−51.6 (−51.9)	−31 (−44)	$J(^{19}F_a-^{19}F_e)$	166	$\delta(^{19}F_a)$	59.0 (59.6)	−20 °C (−70 °C)	$^2J(^{19}F_a-^{19}F_e)$	152.9 (154.7)
$\delta(^{19}F_e)$	−43.4 (−43.2)				$\delta(^{19}F_e)$	71.3 (73.0)			
$\delta(^{15}N)$	−268.0[g] (−266.3)[g]	−40[g] (−45)[g]	$^1J(^{125}Te-^{15}N)$	333[g]					
$\delta(^{1}H)$	(6.90)	(−44)	$^1J(^{15}N-^{1}H)$	62[g] (62)[g]	$\delta(^{1}H)$	(9.57)			
			$^2J(^{125}Te-^{1}H)$	46[g] (46)					

[a]The values in parentheses have been measured in BrF_5 solvent; except for $F_4S{=}NXe^+$, which was measured in HF/BrF_5 solvent; all other values have been measured in aHF solvent.
[b]The values in square brackets were measured in $N{\equiv}SF_3$ solvent.
[c]The secondary isotope effect of $^{32/34}S$ on ^{19}F, $^1\Delta^{19}F(^{34/32}S) = -0.066$ ppm, was observed in both HF and BrF_5 solvents. The fluorines bonded to Xe and S are denoted by F_{Xe} and F_S, respectively. The ^{14}N spectrum consisted of a quadrupole broadened resonance ($\Delta\nu_{1/2} = 750$ Hz).
[d]Secondary isotope effects were observed for $F_4S{=}NXe^+$ in aHF solvent; $^1\Delta^{19}F_A(^{34/32}S) = -0.064$ ppm, $^1\Delta^{19}F_B(^{34/32}S) = -0.055$ ppm, and $^1\Delta^{19}F_X(^{34/32}S) = -0.055$ ppm. All coupling constants have positive signs based on the spectral simulations. The $^3J(^{129}Xe-^{19}F_A)$ coupling constant of $F_4S{=}NXe^+$ was too small to be resolved in all solvents.
[e]The $^{19}F_B$ resonance in $N{\equiv}SF_3$ solvent was not observed because of overlap with the solvent.
[f]The axial and equatorial fluorines of the TeF_5 groups are denoted by F_a and F_e, respectively.
[g]Obtained from a 99.5% ^{15}N-enriched sample of $[F_5TeN(H)Xe][AsF_6]$.
[h]The axial and equatorial fluorines are denoted by F_a and F_e, respectively. The secondary isotope shift arising from $^{32/34}S$ was measured in the ^{19}F NMR spectrum in aHF solvent, $^1\Delta^{19}F_e(^{34/32}S) = -0.056$ ppm and $^1\Delta^{19}F_a(^{34/32}S) = -0.060$ ppm.

assign vibrational frequencies.[71] The small calculated energy difference (7.9 kJ mol^{-1}) between bent and linear Xe–N–S angles indicates that the bent geometry is likely the result of crystal packing. The structural studies, natural bond orbital analyses, and calculated gas-phase dissociation enthalpies reveal that $F_3S{\equiv}NXeF^+$ is among the weakest donor–acceptor adducts of XeF^+ with a Xe−N donor–acceptor bond energy that is very similar to that of $HC{\equiv}NXeF^+$, but considerably

Copyright © 2013. Elsevier. All rights reserved.

Comprehensive Inorganic Chemistry II : From Elements to Applications, Elsevier, 2013. ProQuest Ebook Central, http://ebookcentral.proquest.com/lib/inflibnet-ebooks/detail.action?docID=1330977.
Created from inflibnet-ebooks on 2021-02-09 22:27:13.

stronger than that of $F_3S{\equiv}NAsF_5$. Despite the low dissociation enthalpy of the $F_3S{\equiv}NXeF^+$ donor–acceptor bond, the observation of ^{19}F, ^{14}N, and ^{129}Xe couplings between the XeF and $N{\equiv}SF_3$ moieties of the cation shows that the Xe−N bond is not labile in aHF or BrF_5 under the conditions at which the ^{129}Xe, ^{19}F, and ^{14}N NMR spectra were recorded.[13,71]

1.25.3.1.3.2 $[F_4S{=}NXe][AsF_6]$ and $[F_4S{=}NXe{---}N{\equiv}SF_3][AsF_6]$

The $F_4S{=}NXe^+$ and $F_4S{=}NXe{---}N{\equiv}SF_3^+$ cations provide the first examples of a noble gas bonded to an imido-nitrogen.[13,105,107] The $F_4S{=}NXe^+$ and $F_4S{=}NH_2^+$ cations are intermediates in the HF solvolysis pathways of $F_3S{\equiv}NXeF^+$ and provide a significant extension of the chemistry of the $F_4S{=}N-$ group.

The salt, $[F_4S{=}NXe][AsF_6]$, is derived directly from $[F_3S{\equiv}NXeF][AsF_6]$ by HF-catalyzed rearrangements in aHF, HF/BrF_5, and $N{\equiv}SF_3$ (**Scheme 3**).[105] The $F_4S{=}NXe^+$ cation undergoes HF displacement to form the novel $F_4S{=}NH_2^+$ cation and XeF_2, as well as HF addition to the S=N bond to form $F_5SN(H)Xe^+$ (*vide infra*). The latter cations undergo further HF solvolyses to form $F_5SNH_3^+$, SF_6, and NH_4^+. The solvolysis products of $F_4S{=}NXe^+$ and $F_5SN(H)Xe^+$ (**Scheme 4**) have also been characterized by ^{129}Xe, ^{19}F, ^{14}N, and ^1H NMR spectroscopy in aHF and HF/BrF_5.

The $F_4S{=}NXe^+$ cation has been characterized in solution by ^{19}F and ^{129}Xe NMR spectroscopy (**Figures 15** and **16**, **Table 2**). Spectral simulation reproduced the fine structure and asymmetries observed in the ^{19}F spectrum.[105] The ^{19}F NMR spectrum of $F_4S{=}NXe^+$ was interpreted in terms of the superimposition of an A_2BX spin–spin coupling pattern, which arises from the $F_4S{=}N-$ group (C_s symmetry), and satellite spectra arising from an $A_2BX\Omega$ spin system that results from coupling to natural abundance ^{129}Xe (indicated by Ω).

The ^{129}Xe NMR chemical shift is consistent with that expected for xenon bound to a sp^2-hybridized nitrogen, but is considerably more shielded than the ^{129}Xe resonances of $Xe[N(SO_2CF_3)_2]_2$ (−2444 ppm in SO_2ClF at 8 °C),[114] $Xe[N(SO_2F)_2]_2$ (−2257 ppm in SO_2ClF at −40 °C),[114] $FXeN(SO_2F)_2$ (−2009 ppm in SO_2ClF at −40 °C),[114] $XeN(SO_2F)_2^+$ (−1943 ppm in SbF_5 at 25 °C),[115] and $F[XeN(SO_2F)_2]_2^+$ (−1933 ppm in BrF_5 at −5 °C).[112] The relatively high ^{129}Xe shielding of $F_4S{=}NXe^+$ is in accordance with a Xe−N bond that is significantly more covalent than those of the aforementioned species,[10] with a ^{129}Xe chemical shift that is most similar to those of xenon bound to sp^3-hybridized nitrogen in $F_5SN(H)Xe^+$ (−2897 ppm in HF at −20 °C)[106] and $F_5TeN(H)Xe^+$ (−2841 ppm in HF at −45 °C).[97]

The solid-state rearrangement of $[F_3S{\equiv}NXeF][AsF_6]$ at 22 °C yielded bright yellow $[F_4S{=}NXe][AsF_6]$, which was characterized by Raman spectroscopy.[105] Low-temperature recrystallization of the thermally rearranged product from aHF at −50 to −67 °C afforded single crystals for a structure determination.

The $F_4S{=}NXe^+$ cation and the AsF_6^- anion form an ion pair by interaction through a Xe---F–As fluorine bridge (**Figure 17**).[105] The Xe−N bond is among the shortest Xe−N bonds presently known (2.084(3) Å), and the Xe---F distance of the Xe---F–As bridge is 2.618(2) Å, which is significantly less than the sum of the Xe and F van der Waals radii

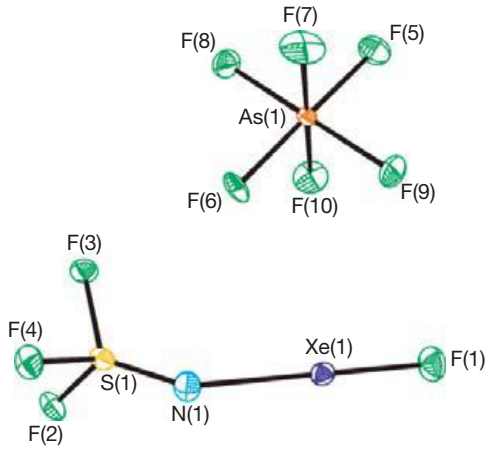

Figure 14 The structural unit in the X-ray crystal structure of $[F_3S{\equiv}NXeF][AsF_6]$ at −173 °C; thermal ellipsoids are shown at the 50% probability level. Reproduced with permission from Smith, G. L.; Mercier, H. P. A.; Schrobilgen, G. J. *Inorg. Chem.* **2007**, *46*, 1369–1378.

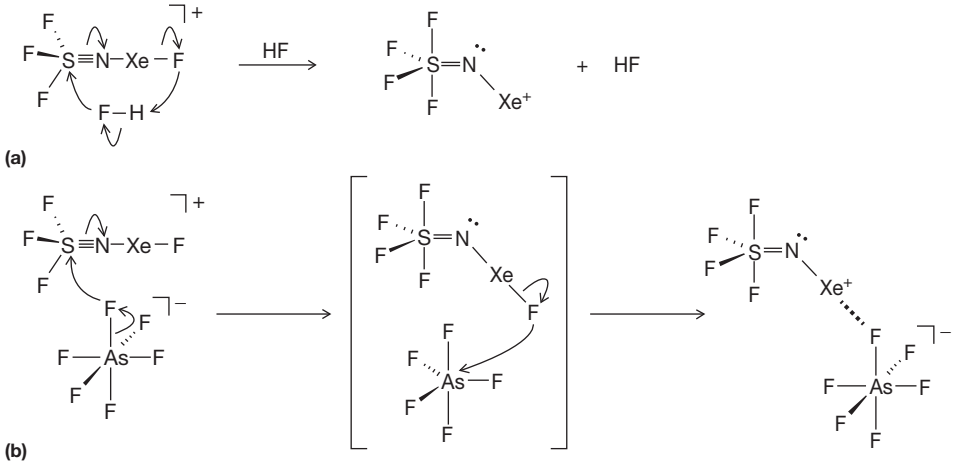

Scheme 3 Proposed (a) solution and (b) solid-state rearrangements of $F_3S{\equiv}NXeF^+$ leading to $F_4S{=}NXe^+$. Reproduced with permission from Smith, G. L.; Mercier, H. P. A.; Schrobilgen, G. J. *J. Am. Chem. Soc.* **2009**, *131*, 7272–7286.

Copyright © 2013. Elsevier. All rights reserved.

Comprehensive Inorganic Chemistry II : From Elements to Applications, Elsevier, 2013. ProQuest Ebook Central, http://ebookcentral.proquest.com/lib/inflibnet-ebooks/detail.action?docID=1330977.
Created from inflibnet-ebooks on 2021-02-09 22:27:13.

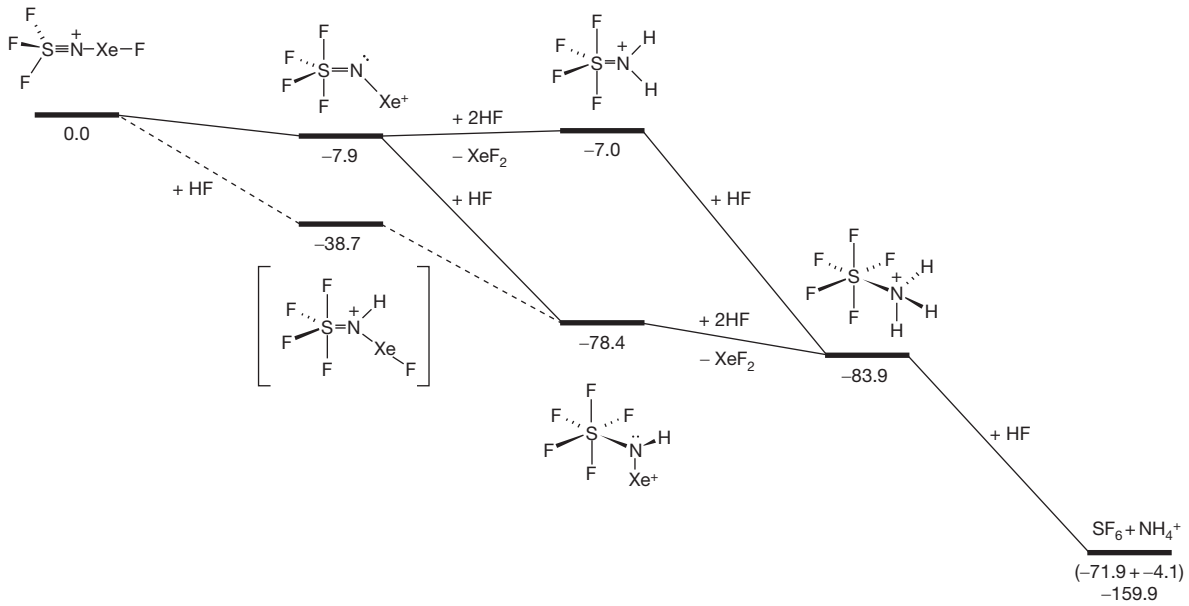

Scheme 4 Calculated relative gas-phase energies of products resulting from the HF-catalyzed rearrangement of $F_3S{\equiv}NXeF^+$ and HF solvolysis of $F_4S{=}NXe^+$ (kJ mol^{-1}; MP2/aug-cc-pVTZ(−PP)). Reproduced with permission from Smith, G. L.; Mercier, H. P. A.; Schrobilgen, G. J. *J. Am. Chem. Soc.* **2009**, *131*, 7272–7286.

(3.63 Å).[34] The Xe−N bond length is similar to that of $[F_5SN(H)Xe][AsF_6]$ (2.069(4) Å) (*vide infra*)[106] and is only slightly longer than the Xe−N bond in $[F_5TeN(H)Xe][AsF_6]$ (2.044(4) Å) (*vide infra*).[97] The xenon atom lies in the N(1), S(1), F(1), F(4)-plane and the nonlinear S−N−Xe angle is attributed to the stereochemically active valence electron lone pair of nitrogen.

The rearrangement of $[F_3S{\equiv}NXeF][AsF_6]$ in a large excess of liquid $N{\equiv}SF_3$ at 0 °C was monitored by Raman spectroscopy and yielded $[F_4S{=}NXe{---}N{\equiv}SF_3][AsF_6]$, which represents the first compound containing a N−Xe−N unit to have been characterized crystallographically.[107]

Thiazyl trifluoride solvent likely induces the rearrangement of $F_3S{\equiv}NXeF^+$ by means of an S_N2 displacement of fluoride ion from the Xe−F group, and concomitant fluoride ion coordination to sulfur (**Scheme 5**). An alternative mechanism in which $N{\equiv}SF_3$ accepts fluoride ion from the Xe−F group of $F_3S{\equiv}NXeF^+$ to form $F_4S{=}N^-$ as an intermediate may be less likely because this anion has not been experimentally observed when F^- is directly reacted with $N{\equiv}SF_3$.[116] A competing redox decomposition of $[F_4S{=}NXe{---}N{\equiv}SF_3][AsF_6]$ also occurs in $N{\equiv}SF_3$ at 0 °C which generates Xe, *cis*-N_2F_2, and $[F_3S(N{\equiv}SF_3)_2][AsF_6]$ according to eqn [21].

$$[F_4S{=}NXe{---}N{\equiv}SF_3][AsF_6] + N{\equiv}SF_3 \xrightarrow[0\,^\circ C]{N{\equiv}SF_3} [F_3S(N{\equiv}SF_3)_2][AsF_6] + Xe + \tfrac{1}{2}cis{-}N_2F_2 \quad [21]$$

The crystal structure of $[F_4S{=}NXe{---}N{\equiv}SF_3][AsF_6]$ consists of well-separated $F_4S{=}NXe{---}N{\equiv}SF_3^+$ cations and AsF_6^- anions (**Figure 18**),[107] with closest cation–anion F···F contacts that are only somewhat less than the sum of the fluorine van der Waals radii (2.94 Å).[34] Consequently, the AsF_6^- anion shows little distortion from O_h geometry.

The ligand arrangement around the sulfur atom of the cation is distorted trigonal bipyramidal, with the nitrogen and two fluorine atoms occupying the equatorial plane and two axial fluorine atoms essentially perpendicular to that plane. The xenon atom is coplanar with the orthogonal plane defined by the N, S, and axial F atoms, and the Xe−N−S angle is bent as a result of the electron lone pair on nitrogen. The Xe(1)−N(1) bond length (2.079(3) Å) is equal, within ±3σ, to those of $[F_4S{=}NXe][AsF_6]$[105] and $[F_5SN(H)Xe][AsF_6]$,[106] somewhat longer than the Xe−N bond of $[F_5TeN(H)Xe][AsF_6]$.[97] The S(1)–N(1) bond length (1.53993) Å) of $F_4S{=}N{-}Xe{---}N{\equiv}SF_3^+$ is also equal, within experimental error, to that of $[F_4S{=}NXe][AsF_6]$.[105] All SF_4 bond lengths in $F_4S{=}N{-}Xe{---}N{\equiv}SF_3^+$ are the same, within ±3σ, as those of $[F_4S{=}NXe][AsF_6]$.[105] The Xe(1)–N(1)–S(1) and N(1)–S(1)–F(1) angles of $F_4S{=}N{-}Xe{---}N{\equiv}SF_3^+$ are slightly greater than those of $[F_4S{=}NXe][AsF_6]$.[105] All other angles that are in common with the two structures are equal to within ±0.9°.

The short Xe(1)---N(2) contact (2.583(3) Å) is well within the sum of the nitrogen and xenon van der Waals radii (3.71 Å)[34] but considerably longer than the Xe−N bond length of $[F_3S{\equiv}NXeF][AsF_6]$ (2.236(4) Å).[71] The donor–acceptor bond length trends are in accordance with the gas-phase donor–acceptor dissociation energies calculated for $F_3S{\equiv}NXeF^+$, $HC{\equiv}NXeF^+$, $F_4S{=}NXe{---}N{\equiv}SF_3^+$, and $F_3S{\equiv}NAsF_5$.[107]

The deviation of the Xe(1)---N(2)–S(2) angle (148.0(2)°) from linearity is similar to that observed for the corresponding angle in $[F_3S{\equiv}NXeF][AsF_6]$ (142.6(3)°)[71] and is likewise attributable to crystal packing. The N(1)−Xe(1)---N(2) angle (168.4(1)°) deviates less from linearity. The S(2)−N(2) (1.398(3) Å) and average S−F bond lengths of adducted $N{\equiv}SF_3$ (average 1.524(4) Å) in $F_4S{=}NXe{---}N{\equiv}SF_3^+$ are shorter than those in gaseous $N{\equiv}SF_3$ (S–N, 1.416(3) and S–F, 1.552(6) Å).[117] Similar S≡N and S–F bond length contractions have been observed in $F_3S{\equiv}NAsF_5$ (1.383 and 1.439 Å)[116] and $[F_3S{\equiv}NXeF][AsF_6]$ (1.397(5) and 1.503(3) Å).[71]

Copyright © 2013. Elsevier. All rights reserved.

Comprehensive Inorganic Chemistry II : From Elements to Applications, Elsevier, 2013. ProQuest Ebook Central, http://ebookcentral.proquest.com/lib/inflibnet-ebooks/detail.action?docID=1330977.
Created from inflibnet-ebooks on 2021-02-09 22:27:13.

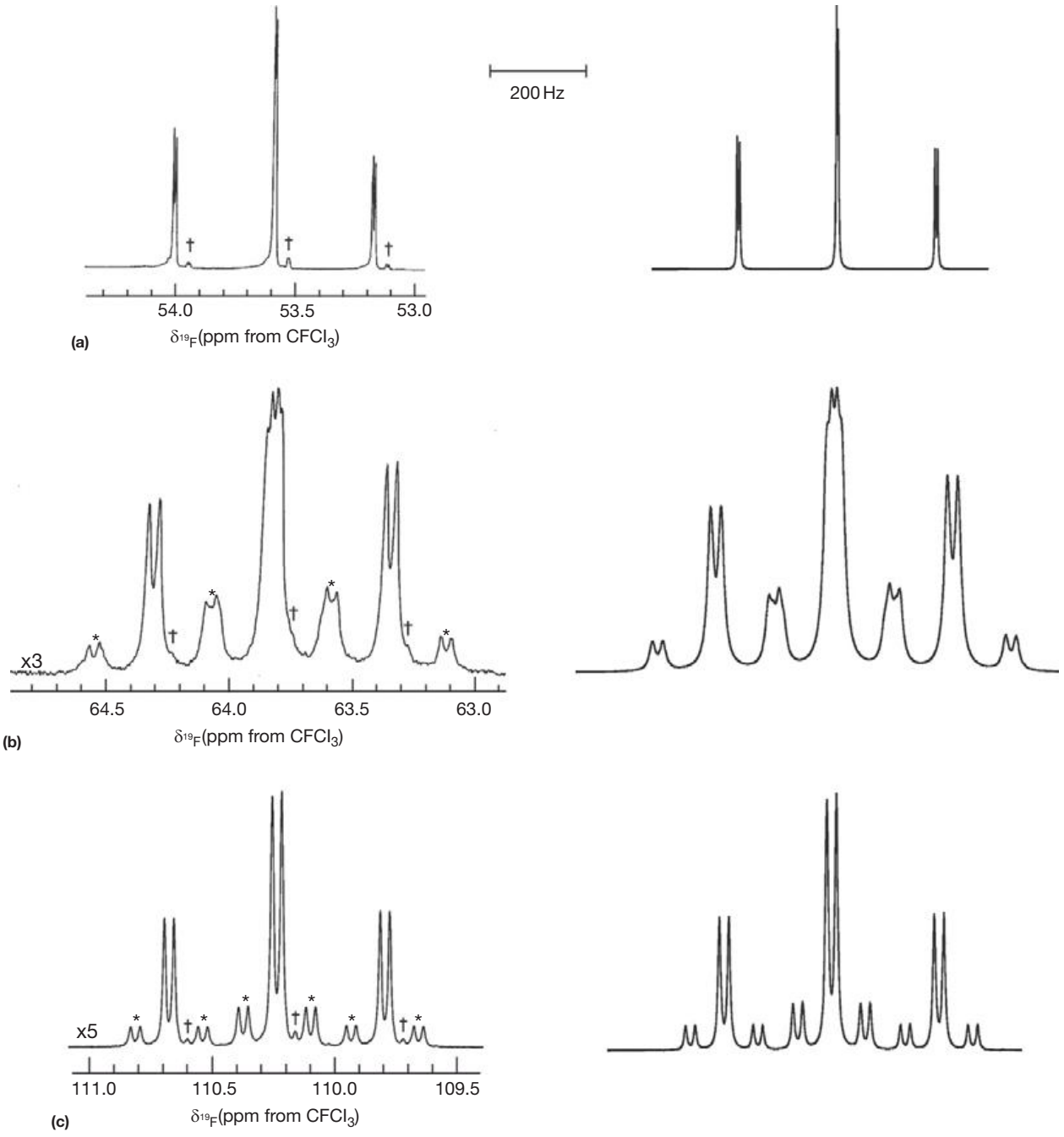

Figure 15 The ^{19}F NMR spectrum (470.592 MHz) of $F_4S{=}NXe^+$ in aHF solvent at −20 °C (left-hand traces) and simulated spectrum (right-hand traces) depicting (a) F_A, (b) F_B, and (c) F_X; symbols denote the $^1\Delta^{19}F(^{34/32}S)$ secondary isotope shifts (†) and ^{129}Xe satellites (*) in the experimental spectrum. Reproduced with permission from Smith, G. L.; Mercier, H. P. A.; Schrobilgen, G. J. *J. Am. Chem. Soc.* **2009**, *131*, 7272–7286.

The N−S−F and F−S−F angles in the adducted $N{\equiv}SF_3$ molecule average 121.4(2)° and 95.4(2)°, respectively, comprising a distorted tetrahedral arrangement about sulfur that is similar to those of $N{\equiv}SF_3$ [117,118] and its adducts.[71,116,119,120]

1.25.3.1.3.3 $[F_5TeN(H)Xe][AsF_6]$

Prior to the synthesis of $[F_5SN(H)Xe][AsF_6]$ (*vide infra*), $[F_5TeN(H)Xe][AsF_6]$ had been synthesized as the natural abundance and 99.5% ^{15}N-enriched compounds.[97] The $F_5TeN(H)Xe^+$ cation was obtained as the product of the reactions of $[F_5TeNH_3][AsF_6]$ with XeF_2 (HF and BrF_5 solvents) and F_5TeNH_2 with $[XeF][AsF_6]$ (HF solvent) (eqns [22]–[25]) and characterized in solution by ^{129}Xe, ^{19}F, ^{125}Te, ^1H, and ^{15}N NMR spectroscopy at −60 to −30 °C (see **Table 2** for NMR parameters). The ^{19}F NMR spectra of $F_5TeN(H)Xe^+$ in aHF (−31 °C) and in BrF_5 (−44 °C) consisted of AX_4 spin–spin coupling patterns that arose from the pseudo-octahedral F_5TeN-group.[97]

Copyright © 2013. Elsevier. All rights reserved.

Comprehensive Inorganic Chemistry II : From Elements to Applications, Elsevier, 2013. ProQuest Ebook Central, http://ebookcentral.proquest.com/lib/inflibnet-ebooks/detail.action?docID=1330977.
Created from inflibnet-ebooks on 2021-02-09 22:27:13.

$$[XeF][AsF_6] + 2HF \rightleftharpoons XeF_2 + [H_2F][AsF_6] \quad [22]$$

$$F_5TeNH_2 + [H_2F][AsF_6] \rightarrow [F_5TeNH_3][AsF_6] + HF \quad [23]$$

$$F_5TeNH_2 + (n+2)HF \rightarrow [F_5TeNH_3][HF_2{\cdot}nHF] \quad [24]$$

$$[F_5TeNH_3][AsF_6] + XeF_2 \rightleftharpoons [F_5TeN(H)Xe][AsF_6] + 2HF \quad [25]$$

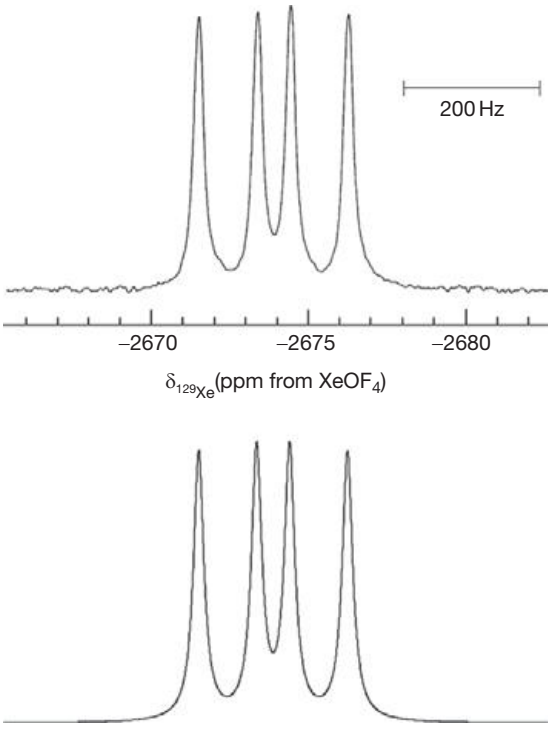

Figure 16 The ^{129}Xe NMR spectrum (138.086 MHz) of $F_4S{=}NXe^+$ in HF solvent at −20 °C (upper trace) and simulated spectrum (lower trace). Reproduced with permission from Smith, G. L.; Mercier, H. P. A.; Schrobilgen, G. J. *J. Am. Chem. Soc.* **2009**, *131*, 7272–7286.

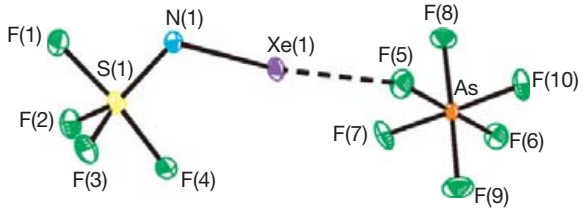

Figure 17 The structural unit in the X-ray crystal structure of $[F_4S{=}NXe][AsF_6]$; thermal ellipsoids are shown at the 50% probability level. Modified from Smith, G. L.; Mercier, H. P. A.; Schrobilgen, G. J. *J. Am. Chem. Soc.* **2009**, *131*, 7272–7286.

The $F_5TeN(H)Xe^+$ cation is markedly less stable than the isoelectronic F_5TeOXe^+ cation and is among the least stable Xe–N-bonded species reported to date. Its relative instability is attributed to the lower electronegativity of the $F_5TeN(H)$ ligand, which is reflected in the high shielding of the ^{129}Xe NMR resonance of $F_5TeN(H)Xe^+$ (*vide infra*) relative to that of F_5TeOXe^+, and is consistent with the Xe−N bond in this cation being one of the most covalent Xe−N bonds known. The decomposition of $F_5TeN(H)Xe^+$ in HF and BrF_5 solutions at −33 °C was monitored by ^{129}Xe, ^{19}F, ^{1}H, and ^{15}N NMR spectroscopy and is consistent with eqns [22]–[25] and [26], with resonances arising from the $F_5TeNH_3^+$ cation, XeF_2, TeF_6 (aHF solvent), and trace amounts of F_5TeNF_2 (*vide infra*).

$$[F_5TeNH_3][AsF_6]/[HF_2{\cdot}nHF] + HF \rightarrow TeF_6 + [NH_4][AsF_6]/[HF_2{\cdot}nHF] \quad [26]$$

At initial XeF_2 and $[F_5TeNH_3][AsF_6]$ concentrations of 0.38 and 0.36 M, respectively, in BrF_5 at −60 °C, the relative concentrations, $[F_5TeNH_3^+]$:$[F_5TeN(H)Xe^+]$, were 1.0:1.2 based on integration of the ^{19}F NMR spectrum after warming the initial sample mixture to −40 °C for 10 min. The equilibrium ratio, $[F_5TeNH_3^+]$:$[F_5TeN(H)Xe^+]$, was 1.0:0.3 when initial $[XeF][AsF_6]$ and F_5TeNH_2 concentrations of 0.71 M in aHF at −33 °C were used. The lower concentration of $F_5TeN(H)Xe^+$ in aHF is attributed to suppression of the HF elimination reaction (eqn [25]). The observation of XeF_2 in the ^{19}F and ^{129}Xe NMR spectra is also in accordance with eqn [25]. The XeF_2 resonance in the ^{19}F NMR spectrum in BrF_5 was observed at −184.1 ppm [$^1J(^{129}Xe{-}^{19}F) = 5621$ Hz] along with a doublet assigned to HF at −192.8 ppm [$^1J(^{19}F{-}^1H) = 527$ Hz].

The ^{129}Xe chemical shift of $F_5TeN(H)Xe^+$ (−2841 ppm, HF solvent, −39 °C) is similar to those of $F_5SN(H)Xe^+$ (−2886 ppm, HF solvent, −20 °C) and $F_4S{=}NXe^+$ (−2672 ppm, HF, −20 °C) and is considerably more shielded than in $(FSO_2)_2NXe^+$ (−1943 ppm, SbF_5 solvent, 25 °C)[115] and isoelectronic F_5TeOXe^+ (−1472 ppm, SbF_5 solvent, 5 °C).[91]

Orange $[F_5TeN(H)Xe][AsF_6]$ and colorless $[F_5TeNH_3][AsF_6]$ were crystallized as a mixture from aHF (−35 °C) and were characterized by Raman spectroscopy (−165 °C) and by X-ray crystallography (−109 °C).[97] The $F_5TeN(H)Xe^+$ cation and the AsF_6^- anion form an ion pair by interaction through a Xe---F−As fluorine bridge (**Figure 19**). The Xe–N bond length (2.044(4) Å) is comparable to that observed in $[XeN(SO_2F)_2][Sb_3F_{16}]$ (2.02(1) Å),[116] but is significantly shorter than that in $FXeN(SO_2F)_2$ (2.200(3) Å).[113] The Xe---F bridge bond (2.580(3) Å) is approximately 1.0 Å shorter than the sum of the xenon and fluorine van der Waals radii [34] but is significantly longer than the terminal Xe−F bond in $FXeN(SO_2F)_2$ (1.967(3) Å)[113] and the bridging Xe---F bond distances in $[XeN(SO_2F)_2][Sb_3F_{16}]$ (2.457(8) Å)[116] and $[XeF][AsF_6]$ (2.208(3) Å).[93]

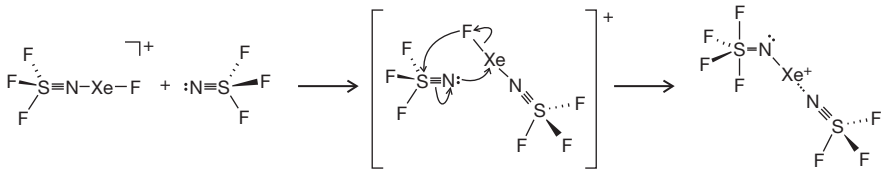

Scheme 5 Proposed mechanism for the $N{\equiv}SF_3$ promoted rearrangement of $F_3S{\equiv}NXeF^+$. Reproduced with permission from Smith, G. L.; Schrobilgen, G. J. *Inorg. Chem.* **2009**, *48*, 7714–7728.

Copyright © 2013. Elsevier. All rights reserved.

Comprehensive Inorganic Chemistry II : From Elements to Applications, Elsevier, 2013. ProQuest Ebook Central, http://ebookcentral.proquest.com/lib/inflibnet-ebooks/detail.action?docID=1330977.
Created from inflibnet-ebooks on 2021-02-09 22:27:13.

The Xe, Te, and H atoms in $[F_5TeN(H)Xe][AsF_6]$ form a near-tetrahedral (sp^3-hybridized) arrangement about nitrogen having a bond angle sum (331.1(3)°) that is only slightly larger than the sum of the ideal tetrahedral angles ($3 \times 109.5° = 328.5°$), whereas the $XeNS_2$ arrangements in $FXeN(SO_2F)_2$[113] and $[XeN(SO_2F)_2][Sb_3F_{16}]$[116] are planar ($sp^2$-hybridized) having bond angle sums of 359.9 and 359.6°, respectively. The N–Xe---F angle (171.6(2)°) in $[F_5TeN(H)Xe][AsF_6]$ is significantly less than that of $[XeN(SO_2F)_2][Sb_3F_{16}]$ (178.3(3)°).[116] The distortion from linearity appears to be inconsistent with a linear AX_2E_3 VSEPR arrangement and may result from several fluorine contacts which are within the sum of fluorine and xenon van der Waals radii and avoid the electron lone pairs of xenon. Similar deviations from linearity were also obtained for the energy-minimized gas-phase geometries and therefore are unlikely to be attributable to packing effects alone.

1.25.3.1.3.4 $[F_5SN(H)Xe][AsF_6]$

Solvolysis of $[F_3S{\equiv}NXeF][AsF_6]$ in aHF (~4 h at −20 °C) led to $[F_5SN(H)Xe][AsF_6]$ formation (eqn [27]).[106] The salt, obtained as transparent yellow plates, was characterized by Raman spectroscopy (−45 °C). The $F_5SN(H)Xe^+$ cation was also formed by reaction of $[F_5SNH_3][AsF_6]$ with XeF_2 in aHF and BrF_5 (−30 °C, ca. 30 min) (eqn [28]) and was

$$[F_3S{\equiv}NXeF][AsF_6] + HF \xrightarrow[HF]{-20\,^\circ C} [F_5SN(H)Xe][AsF_6] \qquad [27]$$

$$[F_5SNH_3][AsF_6] + XeF_2 \underset{BrF_5}{\overset{HF\ or}{\rightleftharpoons}} [F_5SN(H)Xe][AsF_6] + 2HF \qquad [28]$$

characterized by ^{19}F NMR spectroscopy (at −20 °C and supercooled to −70 °C, respectively). In both syntheses, $F_5SNH_3^+$ and $F_5SN(H)Xe^+$ were observed in equilibrium with XeF_2 and HF. In BrF_5 and aHF solutions below −20 °C, equilibrium [28] exists, but in aHF above −20 °C, no $F_5SN(H)Xe^+$ was observed. Analogous equilibria have been noted for $F_5TeNH_3^+$ and $F_5TeN(H)Xe^+$ (*vide supra*).

The NMR spectra are consistent with eqns [27] and [28] and Scheme 4 in which resonances arising from $F_5SNH_3^+$, SF_6, and NH_4^+ were also observed. The ^{19}F NMR spectrum of the $F_5SN(H)Xe^+$ cation was an AB_4 spin–spin coupling pattern that arose from the square-pyramidal F_5S group (Table 2).[106] The ^{129}Xe NMR spectrum consisted of a singlet at −2897 (aHF) (−2956, BrF_5) ppm.[106] The high ^{129}Xe shielding places the Xe–N bond among the most covalent Xe–N bonds formed by xenon and is very similar to that of $F_5TeN(H)Xe^+$ (*vide infra*).

The decompositions of $[F_5SNH_3][AsF_6]$ and $[F_5SN(H)Xe][AsF_6]$, monitored in aHF at 0 °C by ^{19}F NMR spectroscopy, were consistent with Scheme 4. The $F_5SN(H)Xe^+$ cation underwent solvolysis to form $F_5SNH_3^+$ and XeF_2 according to the reverse of eqn [28]. Solvolysis of the $F_5SNH_3^+$ cation (eqn [29]) led to SF_6 and NH_4^+.

$$[F_5SNH_3][AsF_6] + HF \xrightarrow[HF]{-20\ to\ 0\,^\circ C} SF_6 + [NH_4][AsF_6] \qquad [29]$$

Small amounts of F_5SNF_2 also formed in the course of $F_5SN(H)Xe^+$ decompositions in BrF_5 and aHF. The formation of F_5SNF_2 likely resulted from a series of reactions analogous to those that led to minor amounts of F_5TeNF_2 encountered in the decomposition of the $F_5TeN(H)Xe^+$ cation.[97]

The $F_5SN(H)Xe^+$ cation and the AsF_6^- anion form an ion pair similar to that of the tellurium analog[97] by interaction through a Xe---F–As fluorine bridge (Figure 20).[106] The crystal structures of $[F_5SN(H)Xe][AsF_6]$ (Figure 20)[106] and $[F_5TeN(H)Xe][AsF_6]$ (Figure 19)[97] are isotypes. The Xe–N (2.069(4) Å) and Xe–F(6) (2.634(4) Å) bond lengths of $[F_5SN(H)Xe][AsF_6]$ are somewhat longer than their counterparts in the tellurium analog (2.044(4) and 2.580(3), respectively), while the Xe–N–H, N–Xe---F(6) and S/Te–N–Xe angles are all equal within

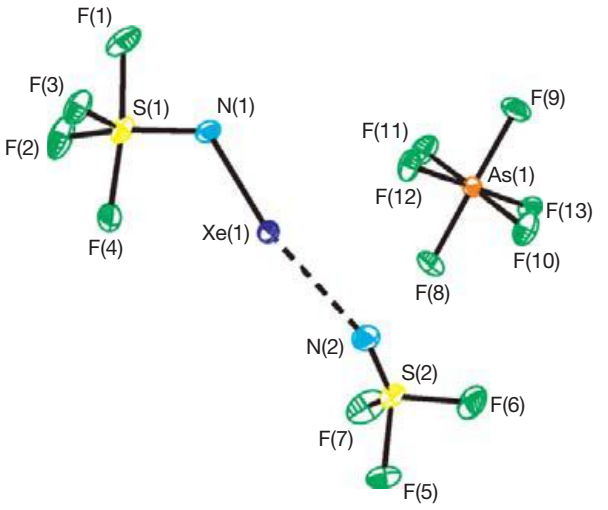

Figure 18 The structural unit in the X-ray crystal structure of $[F_4S{=}NXe{---}N{\equiv}SF_3][AsF_6]$. Thermal ellipsoids are shown at the 50% probability level. Modified from Smith, G. L.; Schrobilgen, G. J. *Inorg. Chem.* **2009**, *48*, 7714–7728.

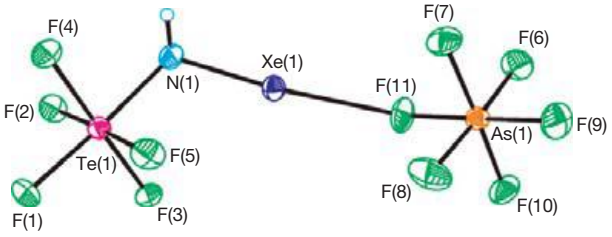

Figure 19 The structural unit in the X-ray crystal structure of $[F_5TeN(H)Xe][AsF_6]$; thermal ellipsoids are shown at the 50% probability level. Reproduced with permission from Fir, B.; Whalen, J. M.; Mercier, H. P. A.; Dixon, D. A.; Schrobilgen, G. J. *Inorg. Chem.* **2006**, *45*, 1978–1996.

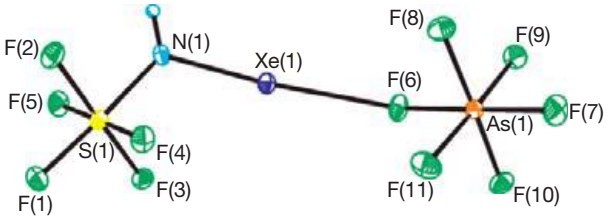

Figure 20 The structural unit in the X-ray crystal structure of $[F_5SN(H)Xe][AsF_6]$; thermal ellipsoids are shown at the 50% probability level. Reproduced with permission from Smith, G. L.; Mercier, H. P. A.; Schrobilgen, G. J. *Inorg. Chem.* **2008**, *47*, 4173–4184.

Copyright © 2013. Elsevier. All rights reserved.

Comprehensive Inorganic Chemistry II : From Elements to Applications, Elsevier, 2013. ProQuest Ebook Central, http://ebookcentral.proquest.com/lib/inflibnet-ebooks/detail.action?docID=1330977.
Created from inflibnet-ebooks on 2021-02-09 22:27:13.

experimental error. As expected, the S–N (1.761(4) Å), S–F_{ax} (1.559(3) Å), and average S–F_{eq} (1.573(4) Å) bond lengths are shorter when compared with the Te–N (1.982(5) Å), Te–F_{ax} (1.791(4) Å), and average Te–F_{eq} (1.811(5) Å) bond lengths of $[F_5TeN(H)Xe][AsF_6]$.

1.25.3.1.4 Xenon halides and oxide fluorides

1.25.3.1.4.1 XeX^+ (X = F, Cl) salts

The fluoride ion donor properties of XeF_2 toward the strong Lewis acids AsF_5,[121,122] SbF_5,[122–124] and BiF_5 [125] are well established. The crystal structures of $[XeF][SbF_6]$, $[XeF][BiF_6]$, and $[XeF][Bi_2F_{11}]$ were determined for the first time and those of XeF_2, $[XeF][AsF_6]$, $[XeF][Sb_2F_{11}]$, and $[XeF_3][Sb_2F_{11}]$ were redetermined with greater precision.[93] The $[XeF][MF_6]$ (M = As, Sb, Bi) salts were prepared by dissolution of 1:1 molar ratios of XeF_2 and MF_5 in aHF. Crystals of these salts were obtained by slowly cooling their aHF solutions, followed by the removal of the solvent as previously described.[126,127]

The $[XeF][Sb_2F_{11}]$ salt was prepared by the direct reaction of XeF_2 with excess liquid SbF_5.[93,128] Single crystals were obtained by allowing a SbF_5 solution of the salt to cool from 45 °C to ambient temperature over the course of several days. The $[XeF][Bi_2F_{11}]$ salt was prepared by allowing a 1:2 molar ratio of XeF_2 and BiF_5 to react in aHF.[93,125] Crystals suitable for X-ray structure determination were obtained by slow removal of the solvent under vacuum at −48 °C.[93] The attempted isolation of crystalline $[XeF][Bi_2F_{11}]$ by slowly cooling a dilute HF solution containing a 2:1 molar ratio of BiF_5/XeF_2 resulted in the crystallization of $[XeF][BiF_6]$, which is consistent with an equilibrium between $Bi_2F_{11}^-$ and BiF_5/BiF_6^- (eqn [30]) that shifts to the right when the solution concentration is low.

$$Bi_2F_{11}^- \rightleftharpoons BiF_5 + BiF_6^- \qquad [30]$$

Isolation of $[XeF][BiF_6]$ under dilute conditions is also expected to be favored by its lower solubility relative to that of $[XeF][Bi_2F_{11}]$. The greater lattice energy calculated for $[XeF][BiF_6]$ (536 kJ mol^{-1}) compared to that of $[XeF][Bi_2F_{11}]$ (471 kJ mol^{-1}) (*vide infra*) likely also contributes to the lower solubility of $[XeF][BiF_6]$ and its preferential crystallization. Attempts to prepare $[XeF][As_2F_{11}]$ by the reaction of $[XeF][AsF_6]$ with a 15-fold molar excess of liquid AsF_5 at −30 and −78 °C and by the reaction of a 15-fold molar excess of AsF_5 dissolved in aHF (50/50 v/v) at −40 °C were unsuccessful and led to the recovery of only $[XeF][AsF_6]$.[93] Failure to isolate $[XeF][As_2F_{11}]$ under these conditions is consistent with volume-based thermodynamic calculations (see **Section 1.25.8**).[93]

The X-ray crystal structures of XeF_2, $[XeF][MF_6]$ (M = As, Sb, Bi), and $[XeF][M_2F_{11}]$ (M = Sb, Bi) were determined at −173 °C.[93] Although the crystal structure of XeF_2 had been previously reported,[129–131] a higher precision crystal structure was obtained in order to provide a more accurate Xe–F bond length (1.999(4) Å).[93] The geometrical parameters for $[XeF][MF_6]$ (M = As, Sb, Bi) and $[XeF][M_2F_{11}]$ (M = Sb, Bi) are summarized in **Figures 21** and **22** and have been compared with the high-precision crystal structure of XeF_2 [93] and the previously reported structures of $[XeF][RuF_6]$,[132] $[XeF][AsF_6]$,[121] and $[XeF][Sb_2F_{11}]$.[123,124]

The XeF^+ cations in $[XeF][MF_6]$ (M = As, Sb, Bi) and $[XeF][M_2F_{11}]$ (M = Sb, Bi) are strongly coordinated to their MF_6^- and $M_2F_{11}^-$ counteranions through fluorine bridges.[93] The Xe–F_t (F_t, terminal fluorine) bond lengths in $[XeF][AsF_6]$ (1.888(3) Å), $[XeF][SbF_6]$ (1.885(2) Å), and $[XeF][Sb_2F_{11}]$ (1.888(4) Å) are not significantly different, within ±3σ, but are shorter than those of $[XeF][BiF_6]$ (1.913(7) Å) and $[XeF][Bi_2F_{11}]$ (1.909(6) Å). Overall, the Xe–F_t bond lengths are shorter than those of crystalline[93] and gaseous XeF_2.[133,134] This trend has also been noted for the Kr–F_t bond lengths of $[KrF][MF_6]$ (M = As, Sb, Bi, Au) relative to the Kr–F bond length of α-KrF_2 [126] (see **Section 1.25.7.2**) and is consistent with three-center–four-electron M.O. descriptions for NgF_2 [135] and resonance structures I and II which predict formal Ng–F bond orders of one-half for NgF_2 and one for the free NgF^+ cations:

$$\underset{\text{I}}{F^- {}^+Ng - F} \quad \leftrightarrow \quad \underset{\text{II}}{F - Ng^+F^-}$$

The Xe---F_b and M---F_b (F_b, bridging fluorine) bond lengths are longer than those of XeF_2 and the terminal M—F bond lengths of their counteranions. While the Xe---F_b bond lengths differ little among $[XeF][AsF_6]$ (2.208(3) Å), $[XeF][BiF_6]$ (2.204(7) Å), and $[XeF][RuF_6]$ (2.182(15) Å),[132] this bond is significantly longer in $[XeF][SbF_6]$ (2.278(2) Å). The M---F_b

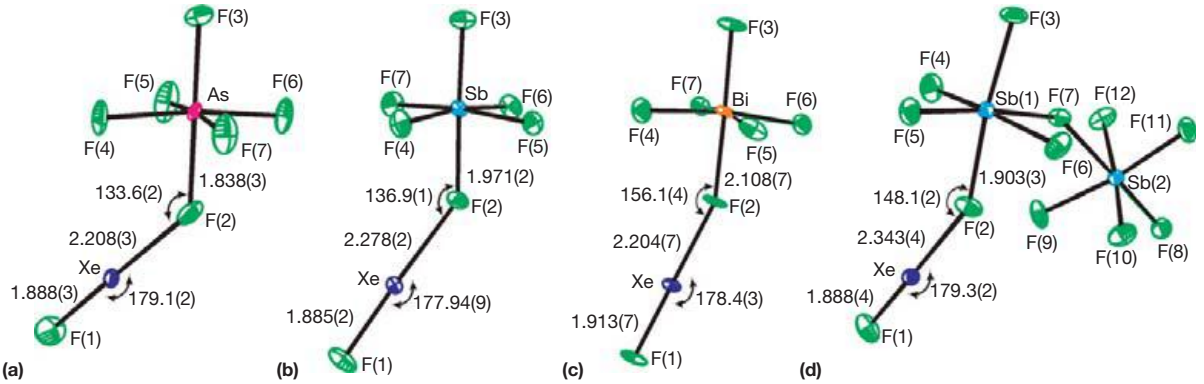

Figure 21 The structural units in the X-ray crystal structures of the (a) $[XeF][AsF_6]$, (b) $[XeF][SbF_6]$, (c) $[XeF][BiF_6]$, and (d) $[XeF][Sb_2F_{11}]$ salts with thermal ellipsoids drawn at the 50% probability level. Reproduced with permission from Elliott, H. St. A.; Lehmann, J.; Mercier, H.P.A.; Jenkins, H. D.; Schrobilgen, G. J. *Inorg. Chem.* **2010**, 49, 8504–8523.

Copyright © 2013. Elsevier. All rights reserved.

Comprehensive Inorganic Chemistry II : From Elements to Applications, Elsevier, 2013. ProQuest Ebook Central, http://ebookcentral.proquest.com/lib/inflibnet-ebooks/detail.action?docID=1330977.
Created from inflibnet-ebooks on 2021-02-09 22:27:13.

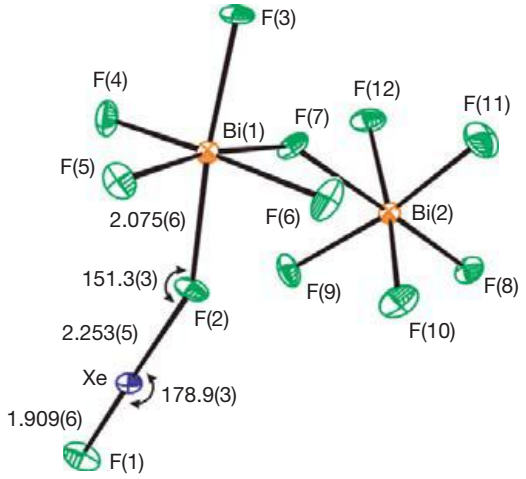

Figure 22 The structural unit in the X-ray crystal structure of [XeF][Bi_2F_{11}], with thermal ellipsoids drawn at the 50% probability level. Reproduced with permission from Elliott, H. St. A.; Lehmann, J.; Mercier, H. P.A.; Jenkins, H. D.; Schrobilgen, G. J. *Inorg. Chem.* **2010**, 49, 8504–8523.

bond lengths – [XeF][AsF_6] (1.838(3) Å), [XeF][SbF_6] (1.971(2) Å), [XeF][BiF_6] (2.108(7) Å), [XeF][Sb_2F_{11}] (1.930(3) Å), and [XeF][Bi_2F_{11}] (2.075(6) Å) – are longer than the average terminal M–F bond lengths of the anions (1.697(7), 1.863(4), 1.960(15), 1.855(10), and 1.952(17) Å, respectively).

The Xe---F_b---M angles are bent and are consistent with AX_2YE_2 VSEPR arrangements at their respective fluorine bridge atoms. Because of the high ionic characters of these bonds, these angles are significantly more open than the ideal tetrahedral angle. The F_t–Xe---F_b angles are highly deformable, and are likely influenced by crystal packing. The F–Xe---F_b bond angles, which are predicted to be linear (AX_2E_3 VSEPR arrangements), are slightly bent, within $\pm 3\sigma$, in the structures of [XeF][SbF_6] (177.94(9)°), [XeF][AsF_6] (179.1(2)°), [XeF][BiF_6] (178.4(3)°), [XeF][Sb_2F_{11}] (179.3(2)°), and [XeF][Bi_2F_{11}] (178.9(3)°). Similar F–Kr---F_b angles have been noted for the [KrF][MF_6] salts.[126] These angles are reproduced in the calculated gas-phase structures of the [NgF][MF_6] (Ng = Kr, Xe; M = As, Sb, Bi) ion pairs.

The salt, [XeF][Bi_2F_{11}], has provided the first crystallographic characterization of the $Bi_2F_{11}^-$ anion. Like its lighter arsenic and antimony analogs, the $Bi_2F_{11}^-$ anion is comprised of two pseudo-octahedrally coordinated pnictogen atoms bridged by a fluorine atom (F_b') (**Figure 22**). The Bi---F_b'---Bi bond angle (145.3(3)°) is similar to the Sb---F_b'---Sb (146.0(2)°) bond angle in [XeF][Sb_2F_{11}]. Although [XeF][As_2F_{11}] remains unknown, similar bond angles have been reported for $As_2F_{11}^-$.[136–138]

The calculated gas-phase geometries of the [NgF][MF_6] (Ng = Kr, Xe) ion pairs have been compared with their crystal structures[93] (also see Lehmann et al. [126] for the [KrF][MF_6] structures). The optimized geometries of the [NgF][MF_6] ion pairs have staggered conformations, with the exception of [XeF][AsF_6] which displays a staggered geometry in its crystal structure. The vibrational spectra obtained from these energy-minimized structures have been used to assign the Raman spectra of the [NgF][MF_6] (M = As, Sb, Bi) salts in greater detail. Reasonable agreement was obtained for the Ng–F_t stretching frequencies; however, the calculations showed that the Ng---F_b and M---F_b stretches are in-phase and out-of-phase coupled. The natural bond orbital (NBO) analyses of calculated structures indicate that the [XeF][MF_6] salts are more ionic than the [KrF][MF_6] salts, attesting to the greater fluoride ion donor strength of XeF_2 relative to that of KrF_2.[93]

1.25.3.1.4.2 The nature of '[Xe][PtF_6]' and its relationship to XeF^+ salts

The reaction which provided the first example of a noble-gas compound has been critically reexamined by Neil Bartlett,[8] the discoverer of noble-gas reactivity. His original reaction[3] involved the interaction of PtF_6 vapor with a large stoichiometric excess of Xe gas, yielding a mustard-yellow solid which approached a 1:1 stoichiometry and was initially formulated as [Xe][PtF_6]. When the amount of PtF_6 exceeded the stoichiometric amount of Xe, the product was a sticky, deep red solid which approached the composition $Xe(PtF_6)_2$. In the latter case, and whenever the stoichiometry was significantly greater than 1:1, X-ray powder diffraction (XRPD) revealed the presence of [XeF][PtF_6].[139] It was concluded that the initial product of the oxidation of Xe by PtF_6 interacts with additional PtF_6 to give [XeF][PtF_6] and PtF_5 (eqn [31]).[8] Further warming of the mixture at <60 °C converted it to a red–orange, friable solid, [XeF][Pt_2F_{11}], according to eqn [32].

$$[Xe][PtF_6] + PtF_6 \rightarrow [XeF][PtF_6] + PtF_5 \quad [31]$$

$$[XeF][PtF_6] + PtF_5 \rightarrow [XeF][Pt_2F_{11}] \quad [32]$$

Mixing PtF_6 vapor (diluted with SF_6 gas) with a large excess of Xe gas also gave a mustard-yellow solid having the composition, $XePtF_6$, which did not give an XRPD pattern.[8] Dissolution of PtF_4, along with a large excess of XeF_2 in aHF, yielded a yellow solution which showed the presence of PtF_6^{2-} in the ^{19}F NMR spectrum. A diamagnetic, amorphous, aHF-insoluble solid of composition $XePtF_6$ obtained from that solution is probably a XeF^+ salt of polymeric $(PtF_5^-)_n$ and the 1:1 product of Xe + PtF_6 is also likely to have this formulation.

1.25.3.1.4.3 $Xe_2F_3^+$ salts

X-ray crystal structures have been obtained for monoclinic [Xe_2F_3][AsF_6], monoclinic *C*-centered [Xe_2F_3][SbF_6],[140] and triclinic [Xe_2F_3][AsF_6].[140] The $Xe_2F_3^+$ cations are planar, V-shaped, and symmetrical about the bridging F_b atom with essentially undistorted AsF_6^- anions.

The crystal structure of monoclinic [Xe_2F_3][AsF_6] has been redetermined at higher precision. As in the earlier structure,[141] two crystallographically nonequivalent $Xe_2F_3^+$ cations and two AsF_6^- anions were found in the asymmetric unit, whereas only one $Xe_2F_3^+$ cation and one SbF_6^- anion are defined in the asymmetric unit of monoclinic [Xe_2F_3][SbF_6]. A lower *R*-factor for the more recent structure of [Xe_2F_3][AsF_6] resulted, in part, from the refinement of a twofold orientationally disordered AsF_6^- anion which was not resolved in the earlier study. The terminal Xe–F_t (As: 1.929(6), 1.908(7), 1.908(6) Å; Sb: 1.922(9), 1.918(9) Å) and bridging Xe---F_b (As: 2.157(3), 2.142(7), 2.148(7) Å; Sb: 2.141(8), 2.146(8) Å) bond distances are comparable in both salts, but the bridge Xe---F_b---Xe angles (As: 149.5(4) and 148.6(4)°; Sb: 160.3(3)°) and terminal F_t–Xe---F_b (As: 177.6(3), 177.3(4), 177.7(3)°; Sb: 148.6(4)°, 149.5(4)°) moieties are significantly more open in the

Copyright © 2013. Elsevier. All rights reserved.

Comprehensive Inorganic Chemistry II : From Elements to Applications, Elsevier, 2013. ProQuest Ebook Central, http://ebookcentral.proquest.com/lib/inflibnet-ebooks/detail.action?docID=1330977.
Created from inflibnet-ebooks on 2021-02-09 22:27:13.

AsF_6^- salt than in the SbF_6^- salt. The $Xe_2F_3^+$ cation in triclinic $[Xe_2F_3][AsF_6]$ is twofold disordered in the triclinic phase, and only allowed the accurate determination of the Xe---F_b---Xe angle (139.8(8)°), which is significantly more closed than in the monoclinic phase.[140]

Quantum-chemical calculations of the vibrational frequencies of $Xe_2F_3^+$ have also been carried out and give a very low frequency for the bending mode of the Xe---F_b---Xe bridge that is indicative of the deformability of this angle. The X-ray crystal structures also demonstrate the deformability of the Xe---F---Xe bridge angle and its strong dependence on the crystal packing and on the nature of the counter anion.

1.25.3.1.4.4 $[XeCl][Sb_2F_{11}]$

Prior examples of Xe–Cl bonds include $XeCl_2$ which has been produced in a matrix.[142–145] The X-ray crystal structures of 2.25 $MCl \cdot XeO_3$ (M = Rb, Cs) feature infinite chains of XeO_3Cl^- anions linked by nearly linear chlorine bridges in which Xe···Cl distances range from 2.75(5) to 2.97(1) Å.[146] More recently, $(C_6F_5Xe)_2Cl^+$ was prepared from $C_6F_5Xe^+$ and $(CH_3)_3SiCl$.[147] The distances between Xe and Cl in the X-ray crystal structure are 2.847(1) and 2.784(2) Å with a Xe---Cl---Xe bond angle of 116.96(8)°. The neutral chloride, C_6F_5XeCl, has been isolated starting from $C_6F_5Xe^+$ and 4-$ClC_5H_4N \cdot HCl$. Because of the instability of C_6F_5XeCl in solution, no detailed structural information is available, but it can be assumed that it contains a Xe–Cl bond.[147]

Because the bond of XeF^+ is stronger than in XeF_2, the $XeCl^+$ ion may be expected to be the most stable xenon–chlorine-bonded species. The $XeCl^+$ cation has been obtained as its $Sb_2F_{11}^-$ salt by reaction of $[XeF][SbF_6]$ in HF/SbF_5 solution with small amounts of $SbCl_5$.[148] Besides nucleophilic Cl/F metathesis (eqn [33]), oxidation of Cl^- also occurs, leading to an intermediate blue solution which is stable for some time at room temperature. The blue solution is suspected to contain Cl_4^+.[149] Solution decomposition of Cl_4^+ to Cl_3^+[149] resulted in a color change from blue to green and finally to orange, from which orange crystals (melting at ca.−20 °C with partial decomposition) were obtained on slow cooling of the solution to −30 °C. Solid $[XeCl][Sb_2F_{11}]$ obtained in this manner decomposed at room temperature according to eqn [34].

$$XeF^+(\text{yellow}) + Cl^- \rightarrow XeCl^+(\text{orange}) + F^- \qquad [33]$$

$$2[XeCl][Sb_2F_{11}] \rightarrow Xe + Cl_2 + [XeF][Sb_2F_{11}] + 2SbF_5 \qquad [34]$$

The crystallographic unit cell contained two distinct, but very similar, $[XeCl][Sb_2F_{11}]$ units (Figure 23). The Xe–Cl distances were marginally shorter (2.309(2) and 2.304(2) Å) than any Xe–Cl distances measured to date and corresponded to Xe–Cl single bonds, as predicted by ab initio calculations (2.301 Å). For comparison, isoelectronic ICl has an I–Cl bond length of 2.303 Å in the gaseous state and 2.351 Å in the solid state.[150,151] Similar to the salts of the XeF^+ [93] and KrF^+ [126] cations, a contact was observed between the $XeCl^+$ ion and a F atom of the $Sb_2F_{11}^-$ ion of each structural unit, which resulted in almost linear Cl–Xe---F arrangements (174.6(1) and 175.2(1)°) and Xe---F distances of 2.644(4) and 2.612(4) Å. These Xe---F distances are shorter than the Xe---Cl bond lengths observed in the $(C_6F_5Xe)_2Cl^+$ cation (2.847(2) and 2.784(2) Å) which has a Xe---Cl---Xe bond angle of 116.96(8)°.[147]

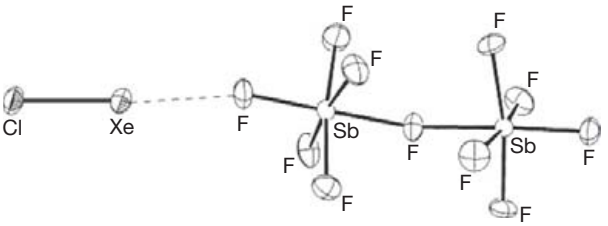

Figure 23 One of the structural units in the X-ray crystal structure of $[XeCl][Sb_2F_{11}]$ with thermal ellipsoids drawn at the 50% probability level. Reproduced with permission from Siedel, S.; Seppelt, K. *Angew. Chem., Int. Ed.* **2001**, *40*, 4225–4227.

The ^{129}Xe NMR spectrum of $XeCl^+$ in HF/SbF_5 solvent consisted of a very broad saddle-shaped resonance. The saddle shape arose from the partially quadrupole-collapsed pair of overlapping 1:1:1:1 quartets that result from spin–spin couplings between $^{35/37}Cl$ ($I = {}^3/_2$) and ^{129}Xe. The Raman spectrum is also in accord with $[XeCl][Sb_2F_{11}]$ salt formulation, with a Raman band at 391 cm^{-1} (calculated 390.2 cm^{-1}) assigned to the Xe–Cl stretching frequency, with the remaining bands being typical of the $Sb_2F_{11}^-$ ion.[152]

1.25.3.1.4.5 $Xe_3OF_3^+$ salts and $H_3O^+ \cdot XeF_2$

A report of the synthesis of the H_2OF^+ cation by oxidative fluorination of H_2O by $[XeF][PnF_6]$ (Pn = As, Sb)[153] in aHF solution was reinvestigated and shown to exhibit a more complex chemistry than had been previously indicated.[154] Two new Xe(II) compounds, $[Xe_3OF_3][PnF_6]$ and $[H_3O][PnF_6] \cdot 2XeF_2$ (Pn = As, Sb), were discovered with no evidence for the H_2OF^+ cation (eqns [35] and [36]).[154]

$$3XeF_2 + [H_3O][PnF_6] \rightarrow [Xe_3OF_3][PnF_6] + 3HF \qquad [35]$$

$$[H_3O][AsF_6] + 2XeF_2 \rightarrow [H_3O][AsF_6] \cdot 2XeF_2 \qquad [36]$$

The compounds were isolated and characterized by vibrational spectroscopy and single-crystal X-ray diffraction. The X-ray crystal structures of the $[Xe_3OF_3][PnF_6]$ salts (Figure 24 (a), only the SbF_6^- salt is shown) represent the first examples of an isolated and structurally characterized Xe(II) oxide fluoride. The bridging oxygen and fluorine atoms are positionally disordered, leading to equal splitting of the Xe(2) positions between a longer Xe(2)–F/O (As: 2.502(10) Å; Sb: 2.513(6) Å) and a shorter Xe(2)–O/F (As: 1.919(9) Å; Sb: 1.908(6) Å) bond in the *Z*-shaped $FXeOXeFXeF^+$ cations. The terminal Xe–F bond lengths (As: 1.992(6) and 1.977(6) Å; Sb: 1.975(6) Å) and the F–Xe(1)–F/O bond angles (As: 177.4(5) and 178.2(5)°; Sb: 178.6(3)°) were unaffected by the disorder. The cation was therefore shown to contain three xenon atoms, two terminal fluorine atoms, one bridging fluorine atom, and one bridging oxygen atom. The presence of oxygen in the cation was confirmed by ^{18}O substitution and $^{16/18}O$ isotopic shifts in the Raman spectra. The geometry of $Xe_3OF_3^+$ was confirmed by quantum-chemical calculations (Figure 24 (b)) and showed that the distances observed in the disordered structures are consistent with the energy-minimized structure (F_1–Xe_1, 1.958 Å; Xe_1–O_1, 2.151 Å; O_1–Xe_2, 1.952 Å; Xe_2---F_2, 2.378 Å; F_2–Xe_3, 2.111 Å; Xe_3–F_3, 1.925 Å;

Copyright © 2013. Elsevier. All rights reserved.

Comprehensive Inorganic Chemistry II : From Elements to Applications, Elsevier, 2013. ProQuest Ebook Central, http://ebookcentral.proquest.com/lib/inflibnet-ebooks/detail.action?docID=1330977.
Created from inflibnet-ebooks on 2021-02-09 22:27:13.

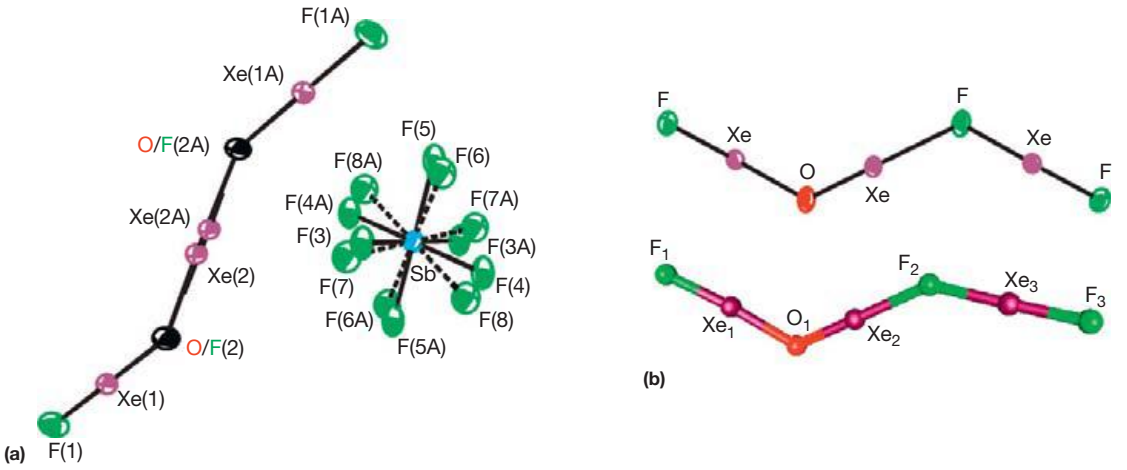

Figure 24 (a) The disordered structural unit in the X-ray crystal structure of $[Xe_3OF_3][SbF_6]$. Thermal ellipsoids are given at the 50% probability level. (b) One of the two orientations obtained from the experimental crystal structure (upper structure) and the calculated geometry (MP2/aug-cc-pVTZ (−PP)) (lower structure) for the $Xe_3OF_3^+$ cation. Reproduced with permission from Gerken, M.; Moran, M. D.; Mercier, H. P. A.; Pointner, B. E.; Schrobilgen, G. J.; Hoge, B.; Christe, K. O.; Boatz, J. A. *J. Am. Chem. Soc.* **2009**, *131*, 13474–13489.

$F_1-Xe_1-O_1$, 176.5°; $F_2-Xe_3-F_3$, 179.9° at the MP2 level). The vibrational assignments for $Xe_3OF_3^+$ were made with the aid of quantum-chemical calculations showing good overall agreement with experiment.[154] The majority of the vibrational modes assigned to $Xe_3OF_3^+$ are strongly coupled but the predominant components of the calculated mode descriptions remained the same at all levels of theory that were examined.

The crystal structure of $[H_3O][AsF_6]\cdot 2XeF_2$ was determined and contained XeF_2 molecules that interact with the H_3O^+ cations (Figure 25). The vibrational assignments for $[H_3O][AsF_6]\cdot 2XeF_2$ were made with the aid of quantum-chemical calculations and were confirmed by ^2H- and ^{18}O-enrichment studies. Although not disordered, the high symmetry imposed by the crystal structure gave two equivalent fluorine atoms with Xe−F bond lengths (1.984(3) Å) comparable to that of free XeF_2 (1.999(4) Å).[93] This prevented the observation of an asymmetric XeF_2 molecule as indicated by the presence of two bands at 470 and 552 cm^{-1} in the Raman spectrum, which are indicative of a terminally coordinated XeF_2 ligand (see Section 1.25.3.2.3). The X-ray crystal structure refinement and vibrational assignments for $[H_3O][AsF_6]\cdot 2XeF_2$ were also supported by the calculated structures and frequencies of the $H_3O^+\cdot nXeF_2$ ($n = 1–4$) adducts.[154]

Energy-minimized geometries and calculated vibrational frequencies for HOF and H_2OF^+ [154] further disproved the original report of the H_2OF^+ cation.[153] Quantum-chemical calculations also indicated that both FXeOH and $FXeOH_2^+$ are viable intermediates in the proposed equilibria between XeF^+ and H_2O that lead to the $Xe_3OF_3^+$ cation (Scheme 6).[154]

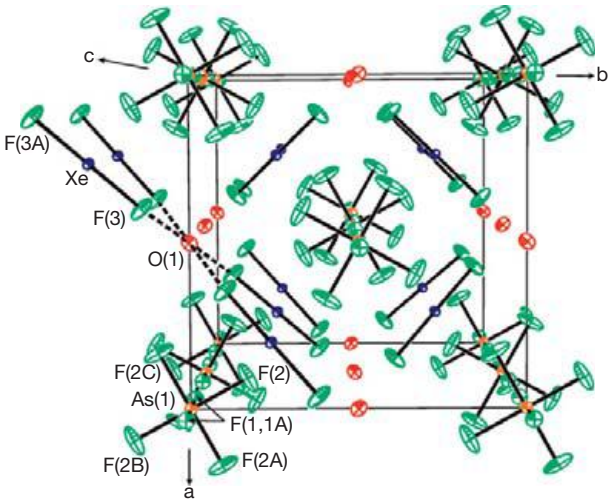

Figure 25 The packing diagram for $[H_3O][AsF_6]\cdot 2XeF_2$ viewed along the *c*-axis showing four O···F contacts. Thermal ellipsoids are drawn at the 50% probability level. Reproduced with permission from Gerken, M.; Moran, M. D.; Mercier, H. P. A.; Pointner, B. E.; Schrobilgen, G. J.; Hoge, B.; Christe, K. O.; Boatz, J. A. *J. Am. Chem. Soc.* **2009**, *131*, 13474–13489.

1.25.3.2 Neutral Xenon(II) Species

1.25.3.2.1 Xenon(II)–carbon bonded species

Although the first xenon(II)–carbon bonded species, $Xe(C_6F_5)^+$, was synthesized in 1989 (see Section 1.25.3.1.1),[62,63] and several species containing Xe−C bonds and a second covalent Xe−E (E = O, Cl) bond were subsequently synthesized (C_6F_5XeCl,[147] $[(C_6F_5Xe)_2Cl][AsF_6]$,[147] and $C_6F_5XeOCOC_6F_5$ [155]), it was not until 2000 that the first derivatives containing a C−Xe−C linkage were reported.

1.25.3.2.1.1 $Xe(C_6F_5)_2$, C_6F_5XeF, and C_6F_5XeCN

Both $Xe(C_6F_5)_2$[156,157] and C_6F_5XeCN[156] share the same precursor, C_6F_5XeF. In the case of the cyano derivative, the $[C_6F_5Xe][Y]$ salts (Y = AsF_6, BF_4) were reacted with $[N(CH_3)_4][F]$ in CH_2Cl_2 (eqn [37]).[156] The reaction of C_6F_5XeF with $(CH_3)_3SiCN$ produced C_6F_5XeCN (eqn [38]), but C_6F_5XeF did not react with $(CH_3)_3SiC_6F_5$ to form $Xe(C_6F_5)_2$.

Copyright © 2013. Elsevier. All rights reserved.

Comprehensive Inorganic Chemistry II : From Elements to Applications, Elsevier, 2013. ProQuest Ebook Central, http://ebookcentral.proquest.com/lib/inflibnet-ebooks/detail.action?docID=1330977.
Created from inflibnet-ebooks on 2021-02-09 22:27:13.

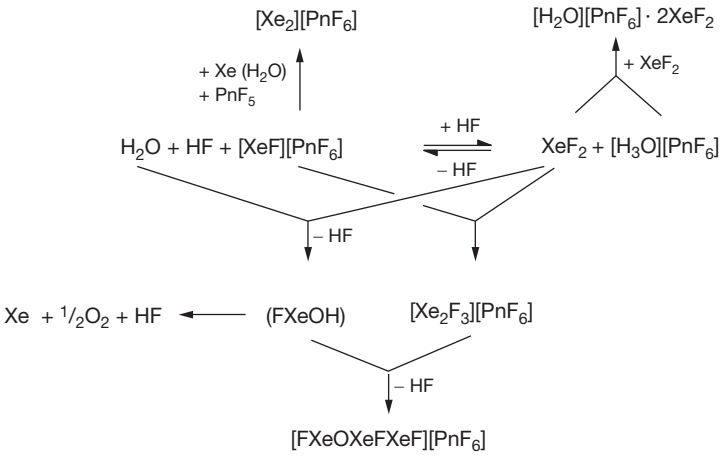

Scheme 6 Products resulting from the equilibrium between XeF^+/H_2O and XeF_2/H_3O^+. Reproduced with permission from Gerken, M.; Moran, M. D.; Mercier, H. P. A.; Pointner, B. E.; Schrobilgen, G. J.; Hoge, B.; Christe, K. O.; Boatz, J. A. *J. Am. Chem. Soc.* **2009**, *131*, 13474–13489.

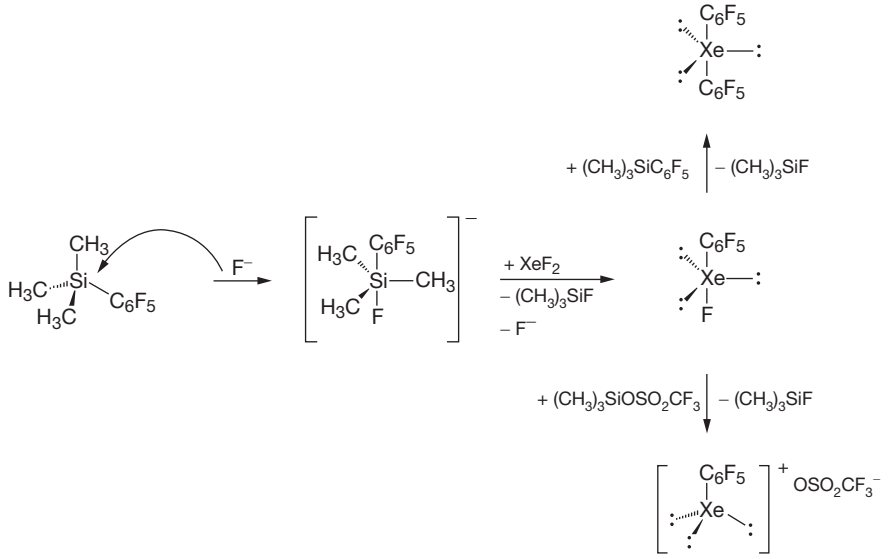

Scheme 7 The synthesis and reactions of C_6F_5XeF. Reproduced with permission from Maggiarosa, N.; Naumann, D.; Tyrra, W. *Angew. Chem., Int. Ed.* **2000**, *39*, 4588–4591.

$$[C_6F_5Xe][Y] + [N(CH_3)_4][F] \xrightarrow[-78\ ^\circ C,\ slow]{CH_2Cl_2} C_6F_5XeF + [N(CH_3)_4][Y]\downarrow \quad [37]$$

$$C_6F_5XeF + (CH_3)_3SiCN \xrightarrow[-78\ ^\circ C,\ slow]{CH_2Cl_2} C_6F_5XeCN + (CH_3)_3SiF \quad [38]$$

The difference in reactivities was attributed to differences in Lewis acidities rather than to steric effects. Instead, the reaction of $Cd(C_6F_5)_2$ with C_6F_5XeF was used to synthesize $Xe(C_6F_5)_2$ (eqn [39]). The reaction of $Cd(C_6F_5)_2$ with XeF_2 did not introduce the C_6F_5 group because its nucleophilicity is insufficient to displace the more strongly bound fluorine ligand of XeF_2.

$$2C_6F_5XeF + Cd(C_6F_5)_2 \xrightarrow[-78\ ^\circ C,\ fast]{CH_2Cl_2} 2Xe(C_6F_5)_2 + CdF_2 \quad [39]$$

The reaction of $(CH_3)_3SiC_6F_5$ with XeF_2 proved successful in a variety of solvents when C_6F_5-group transfer was activated by the introduction of $[N(CH_3)_4][F]$ (Scheme 7).[157] The basicity of the F ligand of XeF_2 is presumably sufficient to allow displacement of F^- from XeF_2 by the C_6F_5 group to generate C_6F_5XeF *in situ* enroute to $Xe(C_6F_5)_2$ formation.

It was subsequently determined that $(CH_3)_3SiC_6F_5$ was consumed without conversion to C_6F_5XeF at $[N(CH_3)_4][F]$ concentrations less than 0.03 M, producing only $(CH_3)_3SiF$ and C_6HF_5, whereas $[N(CH_3)_4][F]$ concentrations greater than 0.05 M enabled the reaction to proceed to $Xe(C_6F_5)_2$.[158] Further studies showed that $Xe(C_6F_5)_2$ was synthesized using the stronger Lewis acid, $C_6F_5SiF_3$ (eqn [40]). However, the use of an even more acidic center, $C_6F_5BF_2$, resulted in fluoride ion abstraction (eqn [41]).

$$C_6F_5XeF + C_6F_5SiF_3 \xrightarrow[-78\ ^\circ C,\ fast]{CH_2Cl_2} Xe(C_6F_5)_2 + SiF_4 \quad [40]$$

Copyright © 2013. Elsevier. All rights reserved.

Comprehensive Inorganic Chemistry II : From Elements to Applications, Elsevier, 2013. ProQuest Ebook Central, http://ebookcentral.proquest.com/lib/inflibnet-ebooks/detail.action?docID=1330977.
Created from inflibnet-ebooks on 2021-02-09 22:27:13.

$$C_6F_5XeF + C_6F_5BF_2 \xrightarrow[-78\ ^\circ C,\ fast]{CH_2Cl_2} [XeC_6F_5][C_6F_5BF_3] \qquad [41]$$

The compounds $Xe(C_6F_5)_2$, C_6F_5XeCN, and C_6F_5XeF are unstable at room temperature. Methylene chloride solutions of each compound decomposed within several weeks at −78 °C.[156] It has been proposed that the decomposition products arise from homolytic cleavage of the Xe−C and Xe−F bonds followed by radical recombinations and radical attack on the solvent. Acetonitrile solutions of $Xe(C_6F_5)_2$ are unstable at −40 °C, and solutions in CH_3CH_2CN, CH_2Cl_2, [D_6]acetone, or in a CH_3CH_2CN/CH_3CN mixture decompose above −45 °C to produce $(C_6F_5)_2$, C_6F_5H, and C_6F_5D.[157] The solubility of $Xe(C_6F_5)_2$ was significantly higher in CH_3CN and CD_3CN than in CH_3CH_2CN, CH_2Cl_2, or acetone.

The series, $Xe(C_6F_5)_2$, C_6F_5XeCN, and C_6F_5XeF, was characterized by ^{19}F, ^{129}Xe, ^{13}C, and ^{15}N NMR spectroscopy in CD_2Cl_2[156] and $Xe(C_6F_5)_2$ was also characterized by ^{129}Xe NMR spectroscopy in [D_6]acetone.[157] The ^{129}Xe chemical shift and the $^3J(^{129}Xe-^{19}F)$, $^4J(^{129}Xe-^{19}F)$, and $^5J(^{129}Xe-^{19}F)$ couplings of $Xe(C_6F_5)_2$ in [D_6]acetone were −4198 ppm and 45.1, 34.7, and 9.5 Hz, respectively.[157] Similar results were obtained in CH_2Cl_2 solvent where the ^{129}Xe chemical shift was −4152 ppm and $^3J(^{129}Xe-^{19}F)$ was 43 Hz.[156] These are among the most shielded ^{129}Xe chemical shifts presently known. The ^{129}Xe NMR chemical shift of C_6F_5XeCN was less shielded (−3883.2 ppm and $^3J(^{129}Xe-^{19}F) = 86$ Hz).[156] It was also noted that the *p*-fluorine shifted to significantly higher frequency with increasing covalency of the Xe−C bond.[157]

The reactivity of $Xe(C_6F_5)_2$ with Hg metal in CH_3CN between −40 °C and room temperature gave $Hg(C_6F_5)_2$, $(C_6F_5)_2$, and traces of C_6F_5H.[157] Solvolysis of $Xe(C_6F_5)_2$ in aHF resulted in the quantitative removal of an aryl group to produce $[C_6F_5Xe][F(HF)_n]$ and C_6F_5H, and reaction of $Xe(C_6F_5)_2$ with I_2 in CH_2Cl_2 resulted in C_6F_5I and Xe.[156] When C_6F_5XeCN reacted with I_2 or HF, the products, C_6F_5I, C_6F_5H, and C_6F_5CN, were obtained in a 5:3:1 molar ratio, respectively, or $C_6F_5Xe^+$, C_6F_5H, and C_6F_5CN were obtained in a 4:1:3 molar ratio, respectively.

Although $Xe(C_6F_5)_2$ decomposes explosively above −20 °C and single crystals could not be obtained, the structure was determined at −223 °C by powder diffraction using the Rietveld method (**Figure 26**).[159] The Xe−C bond lengths (2.394(9) and 2.35(1) Å) are 0.3 Å longer than in the $[C_6F_5Xe]^+$ cation.[67] The aryl rings are twisted with respect to each other with a dihedral angle of 72.5° between the planes of the rings. The dihedral angle is comparable to that of the isoelectronic $I(C_6F_5)_2^-$ ion[160] (69.54°). The C_6F_5 rings stack with interplanar distances of 3.57 and 3.73 Å, which are comparable to those of graphite (3.40 Å)[161] and are indicative of weak π-stacking interactions.[159]

1.25.3.2.1.2 C–Xe–C bonded molecules

As noted in **Section 1.25.3.2.1.1**, molecules having the general formula RXeF possess more polar Xe–F bonds than XeF_2, making them versatile starting materials for substitution reactions. Substitutions with CdR_2 (R = C_6F_5, 2,4,6-$C_6H_2F_3$, 4-C_5F_4N), $C_6F_5Si(CH_3)_3/F^-$, and $C_6F_5SiF_3$ formed symmetric and/or asymmetric diarylxenon compounds where the primary driving force was the lattice energy of CdF_2 (eqn [42]).[158] More specifically, when C_6F_5XeF reacted with $Cd(2,4,6\text{-}C_6H_2F_3)_2$, the main product was 2,4,6-$C_6H_2F_3XeC_6F_5$ (eqn [42]); however, $Xe(C_6F_5)_2$ and $Xe(2,4,6\text{-}C_6H_2F_3)_2$ also formed as minor products.

$$\begin{aligned} &2C_6F_5XeF + Cd(2,4,6\text{-}C_6H_2F_3)_2 \xrightarrow{CH_2Cl_2} \\ &2(2,4,6\text{-}C_6H_2F_3XeC_6F_5) + CdF_2\downarrow + \\ &\text{minor products}\left[Xe(C_6F_5)_2 + Xe(2,4,6\text{-}C_6H_2F_3)_2\right] \end{aligned} \qquad [42]$$

This type of dismutation was previously unknown in xenon–carbon chemistry. Further experiments showed that C_6F_5XeF and CdF_2 do not interact and do not form $Xe(C_6F_5)_2$. In addition, 2,4,6-$C_6H_2F_3XeC_6F_5$ did not form C_6F_5XeF or 2,4,6-$C_6H_2F_3XeF$ when reacted with $[N(CH_3)_4]F$. Accordingly, it was concluded that the permanent dipole moment of 2,4,6-$C_6H_2F_3XeC_6F_5$ leads to an intermolecular interaction with the fluorine atom bonded to xenon in C_6F_5XeF (**Scheme 8**). The compounds were characterized by ^1H, ^{13}C, ^{19}F, and ^{129}Xe NMR spectroscopy and by quantum-chemical calculations. The ^{129}Xe environment of 2,4,6-$C_6H_2F_3XeC_6F_5$ (−4176 ppm) and $Xe(2,4,6\text{-}C_6H_2F_3)_2$ (−4209 ppm) was slightly more shielded than $Xe(C_6F_5)_2$ (−4152 ppm). In addition, the relative charge on the polyfluoroaryl group could be assessed by the ^{19}F NMR chemical shift of the *p*-F resonance.

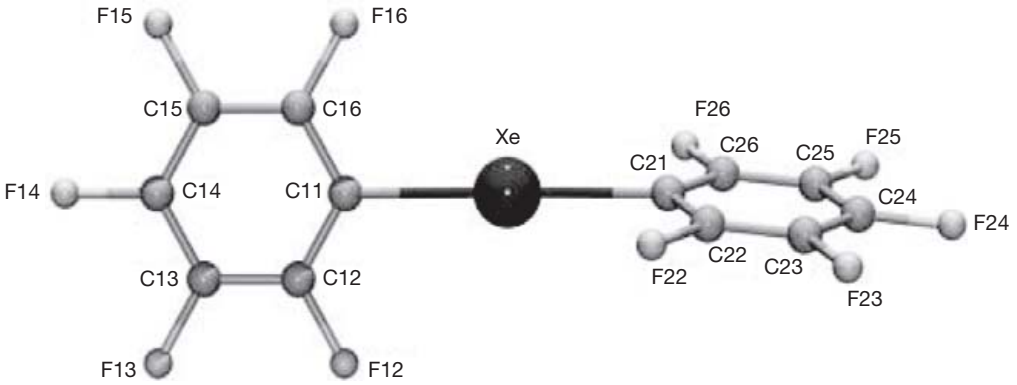

Figure 26 The structure of $Xe(C_6F_5)_2$ obtained by powder diffraction using the Rietveld method. Reproduced with permission from Bock, H.; Hinz-Hubner, D.; Ruschewitz, V.; Naumann, D. *Angew. Chem. Int. Ed.* **2002**, *41*, 448–450.

Copyright © 2013. Elsevier. All rights reserved.

Comprehensive Inorganic Chemistry II : From Elements to Applications, Elsevier, 2013. ProQuest Ebook Central, http://ebookcentral.proquest.com/lib/inflibnet-ebooks/detail.action?docID=1330977.
Created from inflibnet-ebooks on 2021-02-09 22:27:13.

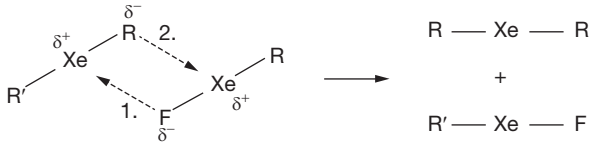

Scheme 8 Proposed rearrangement to form Xe(2,4,6-$C_6H_2F_3$)$_2$. Reproduced with permission from Frohn, H. J.; Theissen, M. *J. Fluorine Chem.* **2004**, *125*, 981–988.

Initial attempts to synthesize a 4-C_5F_4N derivative of xenon explored the reactions of XeF_2 with (4-C_5F_4N)BF_2 and with (4-C_5F_4N)Si$(CH_3)_3$ basified with $[N(CH_3)_4]F$.[81] In the case of (4-C_5F_4N)BF_2, an XeF_2 adduct was formed and the absence of a 4-C_5F_4N derivative of Xe(II) was attributed to the high acidity of (4-C_5F_4N)BF_2 and lower C-nucleophilicity of the 4-C_5F_4N group relative to the fluorinated aryl groups. In the case of (4-C_5F_4N)Si$(CH_3)_3$, only (4-C_5F_4N)$_2$, with traces of (4-C_5F_4N)H, was formed.

A synthetic approach, analogous to eqn [42], was employed that yielded the desired compound, C_6F_5Xe(4-C_5F_4N).[81] The decomposition products, C_6F_5H, (4-C_5F_4N)H, C_6F_5(4-C_5F_4N), $(C_6F_5)_2$, and (4-C_5F_4N)$_2$, were analogous to those of other bisaryl xenon compounds (*vide supra*). The C_6F_5Xe(4-C_5F_4N) compound was characterized by ^{19}F and ^{129}Xe NMR spectroscopy in CH_2Cl_2 solvent at −80 °C and displayed all the expected features and trends associated with C_6F_5Xe derivatives. Solvolysis of C_6F_5Xe(4-C_5F_4N) for 1 h in aHF at −78 °C gave (4-C_5F_4N)H and $[C_6F_5Xe][F(HF)_n]$, consistent with the greater anionic character of the 4-C_5F_4N group.

Many of the difficulties associated with the syntheses of C–Xe–C bonded compounds stem from the syntheses of the R–Xe–F precursors. The [2,6-$F_2C_6H_3Xe$][BF_4] salt was quantitatively converted to 2,6-$F_2C_6H_3XeF$ when reacted with $[N(CH_3)_4][F]$ in CH_2Cl_2 at −78 °C.[162] The reaction is driven by the low solubility of $[N(CH_3)_4][BF_4]$ in CH_2Cl_2. The product decomposed to 1,2,3-trifluorobenzene and xenon over 30 min at ambient temperature but was marginally stable in CH_2Cl_2 with an estimated half-life of 1 h. Reaction of 2,6-$F_2C_6H_3XeF$ and $(CH_3)_3SiAr$ (Ar = C_6F_5, 2,6-$F_2C_6H_3$) in the presence of catalytic amounts of $[N(CH_3)_4][F]$ gave the corresponding diarylxenon compounds Xe(2,6-$F_2C_6H_3)_2$ and 2,6-$F_2C_6H_3XeC_6F_5$, respectively. However, both preparations contained significant amounts of the starting materials. The reaction of 2,6-$F_2C_6H_3XeF$ and $(CH_3)_3SiC_6F_5$ in the absence of $[N(CH_3)_4][F]$ showed no evidence for 2,6-$F_2C_6H_3XeC_6F_5$ formation in the ^{19}F NMR spectrum, but a pure product was obtained by the reaction of 2,6-$F_2C_6H_3XeF$ with $C_6F_5SiF_3$ in CH_2Cl_2. The ^{13}C, ^{19}F, and ^{129}Xe chemical shifts were similar to other diaryl xenon compounds.[157–159] There was a large difference in the magnitudes of the $^1J(^{129}Xe-^{13}C)$ coupling constants, with a coupling of 105 Hz for the 2,6-F_2C_6H group and a coupling of 530 Hz for the C_6F_5 group.[162]

The reactivity of 2,6-$F_2C_6H_3XeF$ with elemental mercury was also examined and shown to form Hg(2,6-$F_2C_6H_3$)F. Reaction with $(CH_3)_3SiX$ (X = Cl, Br, CN, NCO, $OCOCF_3$, OSO_2CF_3) in CH_2Cl_2 resulted in the corresponding substitution products, 2,6-$F_2C_6H_3XeX$ and $(CH_3)_3SiF$.[162] The analogous reaction of 2,6-$F_2C_6H_3XeF$ with $(CH_3)_3SiI$ gave only 1-I-2,6-$F_2C_6H_3$, $(CH_3)_3SiF$, and xenon gas.[162]

The synthesis of 2,6-$F_2C_6H_3XeBr$ is of particular interest because it represents the first Xe–Br bonded compound to be isolated in macroscopic amounts. An early Mössbauer study reported the formation of $^{129}XeBr_2$ from β-decay of $^{129}IBr^-$.[163]

Attempts to synthesize the alkenyl and alkyl derivatives by reacting CF_2=$CFSiMe_3/F^-$, CF_3SiMe_3/F^-, and $Cd(CF_3)_2$, with C_6F_5XeF resulted in the consumption of the perfluoroalkenyl or alkyl transfer reagents without the observation of C_6F_5XeCF=CF_2 or $C_6F_5XeCF_3$.[158] Formation of the dismutation product, $Xe(C_6F_5)_2$, and, in the latter case, the coupling product, $C_6F_5CF_3$, suggested that C_6F_5XeCF=CF_2 and $C_6F_5XeCF_3$ were intermediates.

1.25.3.2.1.3 p-$C_6F_5XeO(O)CC_6F_4C(O)OXeC_6F_5$

Bis(pentafluorophenylxenonium) tetrafluoroterephthalate was obtained by metathesis reactions of pentafluorophenylxenonium and tetrafluoroterephthalate salts.[164] When CH_3CN was used as a solvent, two molecules of CH_3CN co-crystallized (eqn [43]).

$$2[C_6F_5Xe][BF_4] + [N(n\text{-}Bu_4]_2[p\text{-}(O_2C)_2C_6F_4] \xrightarrow[-40\ ^\circ C]{CH_3CN} p\text{-}C_6F_5XeO(O)CC_6F_4C(O)OXeC_6F_5\cdot 2CH_3CN\downarrow + 2[N(n\text{-}Bu)_4][BF_4] \quad [43]$$

Acetonitrile could not be removed under vacuum at 20 °C without product decomposition, but was removed by repeated washings with CH_2Cl_2 at −78 °C. Pure *p*-$C_6F_5XeO(O)CC_6F_4C(O)OXeC_6F_5$ was also isolated free of solvent using CH_2Cl_2 (eqn [44]) or by reaction of $[C_6F_5Xe][BF_4]$ and $Cs_2[p\text{-}(O_2C)_2C_6F_4]$ in CF_3CH_2OH at −40 °C (eqn [45]). The latter synthesis was less favorable because the mechanical separation of $Cs[BF_4]$ proved to be difficult.

$$2[C_6F_5Xe][B(CF_3)_4] + [N(n\text{-}Bu_4]_2[p\text{-}(O_2C)_2C_6F_4] \xrightarrow[-78\ ^\circ C]{CH_2Cl_2} p\text{-}C_6F_5XeO(O)CC_6F_4C(O)OXeC_6F_5\downarrow + 2[N(n\text{-}Bu)_4][B(CF_3)_4] \quad [44]$$

$$2[C_6F_5Xe][BF_4] + Cs_2[p\text{-}(O_2C)_2C_6F_4] \xrightarrow[-40\ ^\circ C]{CF_3CH_2OH} p\text{-}C_6F_5XeO(O)CC_6F_4C(O)OXeC_6F_5 + 2Cs[BF_4]\downarrow \quad [45]$$

Both *p*-$C_6F_5XeO(O)CC_6F_4C(O)OXeC_6F_5\cdot 2CH_3CN$ and unsolvated *p*-$C_6F_5XeO(O)CC_6F_4C(O)OXeC_6F_5$ are unstable, but the CH_3CN solvate is the less stable of the two compounds.[164] Although stable for 30 min at 20 °C, the solvate is completely decomposed to xenon and *p*-$(C_6F_5O(O)C)_2C_6F_4$ after 2 weeks at 20 °C. The onset of decomposition for both compounds was determined by differential scanning calorimetry (DSC) measurements and was found to occur at temperatures of 89 and 118 °C for the CH_3CN solvate and the unsolvated compound, respectively.

Only two types of solvents proved to be suitable for *p*-$C_6F_5XeO(O)CC_6F_4C(O)OXeC_6F_5$, nitriles such as CH_3CN, where there was poor solubility, and acidic alcohols such as CF_3CH_2OH (mp −44 °C) and $(CF_3)_2CHOH$ (mp −4 °C), which gave satisfactory solubilities.[164] However, the thermal stability of *p*-$C_6F_5XeO(O)CC_6F_4C(O)OXeC_6F_5$ in both alcohol solutions was lower than in the CH_3CN solution.

A $(CF_3)_2CHOH/CH_3CN$ mixture (1:1, v/v) was used to obtain the ^{13}C and ^{129}Xe NMR spectra, but the ^{129}Xe NMR

Copyright © 2013. Elsevier. All rights reserved.

Comprehensive Inorganic Chemistry II : From Elements to Applications, Elsevier, 2013. ProQuest Ebook Central, http://ebookcentral.proquest.com/lib/inflibnet-ebooks/detail.action?docID=1330977.
Created from inflibnet-ebooks on 2021-02-09 22:27:13.

spectra were also recorded in CH_3CN and $(CF_3)_2CHOH$. The *m*- and *p*-F resonances of the C_6F_5Xe moieties of *p*-$C_6F_5XeO(O)CC_6F_4C(O)OXeC_6F_5$ are indicative of a strong arylxenonium tetrafluoroterephthalate interaction which is further supported by large $^3J(^{19}F-^{129}Xe)$ couplings of 81 Hz, which are 11 Hz greater than in $[C_6F_5Xe][BF_4]$ and have a magnitude that is similar to that of C_6F_5XeF (82 Hz). The ^{129}Xe NMR resonance of *p*-$C_6F_5XeO(O)CC_6F_4C(O)OXeC_6F_5$ is more shielded (−3857 ppm) than that of $[C_6F_5Xe][BF_4]$[67] (−3825 ppm). All ^{19}F NMR resonances of *p*-$C_6F_5XeO(O)CC_6F_4C(O)OXeC_6F_5$ in CH_3CN solution at −40 °C are more shielded relative to those in $(CF_3)_2CHOH$ solutions because hydrogen bonding in $(CF_3)_2CHOH$ lowers the nucleophilicity of the carboxylate groups.

The most intense band in the solid-state Raman spectrum of *p*-$C_6F_5XeO(O)CC_6F_4C(O)OXeC_6F_5$ occurs at 180 cm^{-1} and is assigned to the Xe–C stretching mode. This band is at lower frequency relative to that of $[C_6F_5Xe][BF_4]$ (205 cm^{-1})[67] but is essentially unaffected in the CH_3CN solvate (181 cm^{-1}).[164]

The crystal structure has been determined for *p*-$C_6F_5XeO(O)CC_6F_4C(O)OXeC_6F_5$ which crystallized from a $(CF_3)_2CHOH/CH_3CN$ solvent mixture (**Figure 27**).[164] Each *p*-$C_6F_5XeO(O)CC_6F_4C(O)OXeC_6F_5$ molecule is solvated through hydrogen bridges with four alcohol molecules and the four oxygen atoms of the $C_6F_4(C(O)O)_2$ group. The Xe−C (2.101(4), 2.105(5) Å), and Xe−O (2.495(3), 2.511(4) Å) bond lengths are indicative of significant covalent character and the Xe−C bond lengths are comparable to those of $C_6F_5XeO(O)CC_6F_5$ (2.122(4) Å) and the $C_6F_5Xe^+$ cation in $[C_6F_5Xe][AsF_6]$ (2.081(6) Å, average).[165] The Xe atoms are anchored by additional short contacts to a second oxygen atom (3.156(5), 3.120(5) Å) where the longer Xe–O bond is likely a result of hydrogen bonding of four $(CF_3)_2CHOH$ moleculeswith each oxygen atom of $C_6F_4(C(O)O)_2$, thereby lowering their nucleophilicities. The average dihedral angle between the carboxylate groups is 15° and those between the aromatic rings are 42° and 58°.

1.25.3.2.1.4 Alkynyl xenon(II) fluorides

The reactions of trimethyl(alkynyl)silanes $(CH_3)_3SiC{\equiv}CR$ (R = CH_3, *n*-C_4H_9, C_6H_5) with XeF_2 and $[N(CH_3)_4][F]$ in CH_2Cl_2 or in a CH_2Cl_2/CH_3CH_2CN mixture were investigated between −78 and −30 °C by multi-NMR spectroscopy (eqn [46]).[166]

$$(CH_3)_3SiC{\equiv}CR + XeF_2 \xrightarrow[-78\ ^\circ C]{F^-,\ CH_2Cl_2\ \text{or}\ CH_2Cl_2/CH_3CH_2CN} RC{\equiv}CXeF + (CH_3)_3SiF \quad [46]$$

The reaction of the ethynyl silane with XeF_2 in CH_2Cl_2 at −78 °C led to products that could not be identified, and neither an alkynylxenon(II) fluoride nor XeF_2 was detected. Propynylxenon(II) fluoride, $CH_3C{\equiv}CXeF$, was detected in the ^{19}F spectrum with a chemical shift of −24.9 ppm and $^1J(^{19}F-^{129}Xe)$ coupling of 4241 Hz. Poor yields prevented further characterization. Better yields were obtained for *n*-$C_4H_9C{\equiv}CXeF$ and the ^{19}F and ^{129}Xe chemical shifts and $^1J(^{19}F-^{129}Xe)$ coupling constants were observed (−24.0 and −3765 ppm, and 4231 Hz, respectively). The most stable of the neutral compounds, $C_6H_5C{\equiv}CXeF$, displayed similar NMR parameters in CH_2Cl_2 (^{19}F, −23.1 ppm; ^{129}Xe, −3709 ppm; $^1J(^{19}F-^{129}Xe)$, 4301 Hz) and in a CH_2Cl_2/CH_3CH_2CN mixture (^{19}F, −21.9 ppm; ^{129}Xe, −3707 ppm; $^1J(^{19}F-^{129}Xe)$, 4331 Hz) at −78 °C. The compound, $C_6H_5C{\equiv}CXeF$, was the most stable among the series of alkynyl xenon(II) fluorides and could be stored in solution at −78 °C for several weeks, with the onset of decomposition occurring at −60 °C. A concentrated solution of $C_6H_5C{\equiv}CXeF$ was investigated by 1D ^{129}Xe, ^{19}F, and ^{13}C NMR spectroscopy, and by $^{19}F-^{13}C$ HMBC NMR correlation

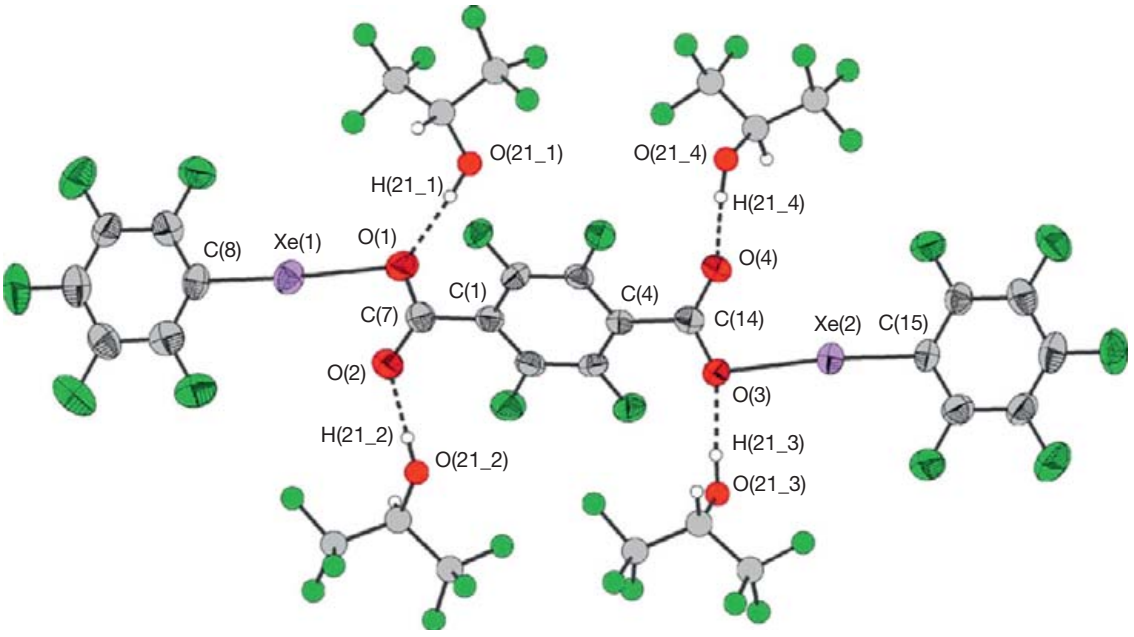

Figure 27 The X-ray crystal structure of *p*-$C_6F_5XeO(O)CC_6F_4C(O)OXeC_6F_5 \cdot 4(CF_3)_2CHOH$. Reproduced with permission from Bilir, V.; Bälser, D.; Boese, R.; Frohn, H.-J. *J. Fluorine Chem.* **2009**, *130*, 824–829.

Copyright © 2013. Elsevier. All rights reserved.

Comprehensive Inorganic Chemistry II : From Elements to Applications, Elsevier, 2013. ProQuest Ebook Central, http://ebookcentral.proquest.com/lib/inflibnet-ebooks/detail.action?docID=1330977.
Created from inflibnet-ebooks on 2021-02-09 22:27:13.

spectroscopy which supported the covalent nature of the three-center–four-electron C–Xe–F moiety.

1.25.3.2.2 $FXeONO_2$ and $XeF_2 \cdot HNO_3$

Three studies dealing with the formation of xenon(II) nitrates have been published. Two early studies have investigated the reaction of HNO_3 with XeF_2. The reactions between XeF_2 and anhydrous HNO_3 containing 20% NO_2 by weight at 20 °C resulted in red–brown solids that rapidly decomposed at 23 °C, forming an intense, transient blue color (the physical state was not specified in the original reference)[167] that likely resulted from N_2O_3.[168] The two colored species were formulated as $FXeONO_2$ and $Xe(ONO_2)_2$, but no structural characterizations were provided. The red–brown solids were not observed when the analogous reactions were carried out at −20 °C.[167] A subsequent study reported the *in situ* formation of $FXeONO_2$ by reaction of XeF_2 and HNO_3 in CH_2Cl_2 at −30 °C. It was shown that these solutions reacted with cyclohexene and 1-hexene to give 1,2-disubstituted fluoro-nitrato alkanes (1 = F, 2 = ONO_2).[169] It was proposed that $FXeONO_2$ was the fluoronitration agent, although it was neither characterized in solution nor isolated.[169]

Subsequent attempts to synthesize $FXeONO_2$ and $Xe(ONO_2)_2$ by reaction of XeF_2 with HNO_3 and HF elimination in SO_2ClF solution below −30 °C led to $XeF_2 \cdot HNO_3$.[168] The crystal structure of $XeF_2 \cdot HNO_3$ (**Figure 28**) revealed a hydrogen bond between HNO_3 and a fluorine atom of XeF_2 (1.86(2) Å), as well as an interaction between the oxygen atom of HNO_3 and the xenon atom of XeF_2 (3.317(1) Å), leading to a crystal lattice comprised of layered sheets.[168] The Xe–F bond length distortions (terminal (F_t), 1.9737(8) Å; bridge (F_b), 2.0506(8) Å) are similar to those found in compounds where XeF_2 is coordinated to a metal ion through a single fluorine bridge (see **Section 1.25.3.2.3**). The geometrical parameters of HNO_3 (N–O_H, 1.368(2) Å; N–O_S, 1.216(2) Å; N–O_A, 1.206(2) Å; O_S–N–O_A, 128.2(1)°, where S denotes syn and A denotes anti with respect to the O–H---F linkage) are of higher precision than those obtained from the structure of anhydrous HNO_3.[170] The Raman spectrum also displayed intense bands to lower frequency (458, 468 cm^{-1}) and to higher frequency (529 cm^{-1}) of free XeF_2, similar to other terminally coordinated XeF_2 compounds (see **Section 1.25.3.2.3**). The remaining bands assigned to HNO_3 modes were shifted somewhat relative to matrix-isolated HNO_3 but were otherwise in good agreement.[168]

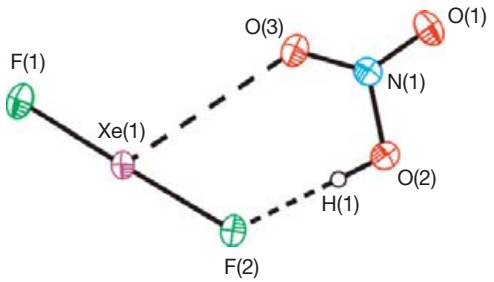

Figure 28 The structural unit in the X-ray crystal structure of $XeF_2 \cdot HNO_3$ showing the H···F and Xe···O contacts. Thermal ellipsoids are shown at the 70% probability level. Reproduced with permission from Moran, M. D.; Brock, D. S.; Mercier, H. P. A.; Schrobilgen, G. J. *J. Am. Chem. Soc.* **2010**, *132*, 13823–13839.

Xenon fluoride nitrate was successfully synthesized by the reaction of NO_2F with $[FXeOXeFXeF][AsF_6]$ at −50 °C (eqn [47]) and isolated.

$$[Xe_3OF_3][AsF_6] + 2NO_2F \rightarrow FXeONO_2 + 2XeF_2 + [NO_2][AsF_6] \quad [47]$$

Characterization was carried out in SO_2ClF and CH_3CN solutions by low-temperature ^{14}N, ^{19}F, and ^{129}Xe NMR spectroscopy (**Table 3**) and in the solid state by low-temperature Raman spectroscopy (−160 °C) and single-crystal X-ray diffraction (−173 °C).[168] Isotopic enrichment using $[FXe^{18}OXeFXeF][AsF_6]$ and $^{15}NO_2F$ aided in the assignment of the Raman spectra of $FXeONO_2$ and in establishing a likely reaction pathway. Raman spectroscopy indicated that $FXe^{16}ON(^{16}O^{18}O)$ formed, along with XeF_2 and $[N^{16}O^{18}O][AsF_6]$, when an excess of $N^{16}O_2F$ reacted with $[FXe^{18}OXeFXeF][AsF_6]$. A reaction mechanism consistent with these findings was proposed that included formation of FXeOXeF as an intermediate. The crystal structure of $FXeONO_2$ (**Figure 29**) shows that there are no significant intermolecular interactions and provides geometric parameters that are in good agreement with gas-phase values determined from quantum-chemical calculations. The Xe–O (2.126(4) Å) and Xe–F (1.992(4) Å) bond lengths and O–Xe–F angle (177.6(2)°) are similar to those determined for $FXeOSO_2F$ (2.155(8) Å, 1.940(8) Å, 177.4(3)°).[98] The N–O bond lengths of the -ONO_2 groups in $XONO_2$ (X = Cl,[171] Br[172]) differ in that the N–O_S bond is shorter than the N–O_A bond in the halogen nitrates, whereas the opposite trend is observed for $FXeONO_2$. Several decomposition

Table 3 NMR parameters of $FXeONO_2$ and related species

Solute	*Solvent*	*Temp (°C)*	*Species*	*δ(19F), ppm*	*δ(129Xe), ppm*	*δ(14N), ppm*	*1J(19F–129Xe), Hz*
$FXeONO_2$	SO_2ClF	−70	$FXeONO_2$	−131.9	−1974		5456
			XeF_2	−177.3	−1864		5603
$FXeONO_2$	SO_2ClF	−50	$FXeONO_2$			−65.8[a]	
$FXeONO_2$	CH_3CN	−40	$FXeONO_2$	−135.1	−1870		5503
			XeF_2	−179.2	−1775		5697
XeF_2	N_2O_4	30	$FXeONO_2$	−130.1	−1989		5408
			XeF_2	−179.4	−1841		5642
			NO_2F	397.8			
			Xe		−5243		

[a]Attempts to acquire the ^{15}N NMR spectrum of ^{15}N-enriched (98 + %) $FXeONO_2$ (SO_2ClF solvent, −70 °C) failed because the T_1-relaxation time was too long (relaxation delays as high as 180 s were used). Reproduced with permission from Moran, M. D.; Brock, D. S.; Mercier, H. P. A.; Schrobilgen, G. J. *J. Am. Chem. Soc.* **2010**, *132*, 13823–13839.

Copyright © 2013. Elsevier. All rights reserved.

Comprehensive Inorganic Chemistry II : From Elements to Applications, Elsevier, 2013. ProQuest Ebook Central, http://ebookcentral.proquest.com/lib/inflibnet-ebooks/detail.action?docID=1330977.
Created from inflibnet-ebooks on 2021-02-09 22:27:13.

pathways were proposed for solid $FXeONO_2$ to account for the decomposition products. Raman spectroscopy of solid $FXeONO_2$ in admixture with XeF_2 and $[NO_2][AsF_6]$ showed that $FXeONO_2$ had partially decomposed to N_2O_4 and $XeF_2 \cdot N_2O_4$ at −78 °C after 7 days and to N_2O_5 and XeF_2 at −50 °C after 5 h.[168]

The attempted synthesis of $[XeONO_2][AsF_6]$ by the reaction of $FXeONO_2$ with excess liquid AsF_5 between −78 and −50 °C resulted in slow formation of $[NO_2][AsF_6]$, Xe, and O_2 with no evidence for $[XeONO_2][AsF_6]$. Thermodynamic calculations indicated that the pathways to $[XeONO_2][AsF_6]$ formation and decomposition are exothermic and spontaneous under standard conditions and at −78 °C.[168]

When XeF_2 was dissolved in liquid N_2O_4 at 35 °C, a small steady-state concentration of $FXeONO_2$ was observed, but the predominant product was $XeF_2 \cdot N_2O_4$, which crystallized at 0 to −3 °C.[168] The X-ray crystal structure of $XeF_2 \cdot N_2O_4$ (**Figure 30**) shows that weak interactions occur between the xenon atom of XeF_2 and the oxygen atoms of N_2O_4 (3.435(4)–4.180(4) Å). The Xe–F (1.985(3) Å), N–O (1.194 (6), 1.182(6) Å), and N–N (1.378(8) Å) bond lengths of $XeF_2 \cdot N_2O_4$ are within $\pm 3\sigma$ of free XeF_2 and N_2O_4. In addition, the vibrational modes of $XeF_2 \cdot N_2O_4$ are essentially the same as those of free XeF_2 and N_2O_4 and therefore $XeF_2 \cdot N_2O_4$ can be classified as a molecular addition compound.

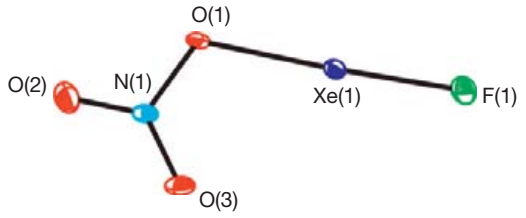

Figure 29 The structural unit in the X-ray crystal structure of $FXeONO_2$. Thermal ellipsoids are shown at the 50% probability level. Reproduced with permission from Moran, M. D.; Brock, D. S.; Mercier, H. P. A.; Schrobilgen, G. J. *J. Am. Chem. Soc.* **2010**, *132*, 13823–13839.

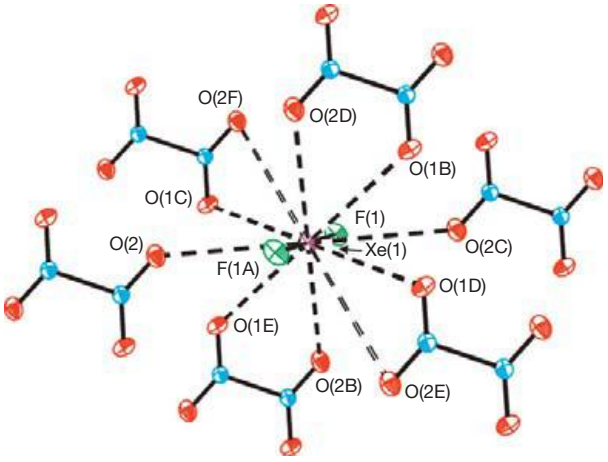

Figure 30 The local environment of the XeF_2 molecule in the crystal structure of $XeF_2 \cdot N_2O_4$, showing the weak interactions between the xenon atom and N_2O_4. Thermal ellipsoids are shown at the 50% probability level. Reproduced with permission from Moran, M. D.; Brock, D. S.; Mercier, H. P. A.; Schrobilgen, G. J. *J. Am. Chem. Soc.* **2010**, *132*, 13823–13839.

1.25.3.2.3 XeF_2 as a ligand

1.25.3.2.3.1 Introduction

The first compound in which a noble-gas fluoride, namely XeF_2, was shown to coordinate to a metal cation was $[Ag(XeF_2)_2][AsF_6]$.[173] Over the past decade, numerous coordination compounds in which XeF_2 functions as a ligand towards metal cations have been isolated and the majority of their structures have been determined by single-crystal X-ray diffraction.

Salts of the type $M^n[AF_6]_n$, where n is the net charge of the metal cation, M is an alkaline earth metal, and A is P, As, Sb, Bi, etc., have rather low lattice energies as a consequence of the anion volume (>100 Å^3).[174] Most of these anions are also poor Lewis bases, especially AF_6^-, where A is As, Sb, or Bi. Even the weak Lewis base solvent, aHF, can provide sufficient solvation energy to bring about the dissolution of $M^n[AF_6]_n$ salts. The high solubilities of $M^n[AF_6]_n$ salts in aHF and the isolation of compounds of the type $[M(HF)_m][AF_6]_2$ [175] show that the cations are extensively solvated (eqn [48]):

$$M^n[AF_6]_n + mHF \rightarrow M[HF]_m^{n+} + nAF_6^- \qquad [48]$$

Addition of XeF_2 to such solutions introduces a Lewis (fluoro) base that is stronger than HF, leading to HF displacement and the formation of compounds of the type $[M^n(XeF_2)_p][AF_6]_n$ (eqn [49]). Xenon difluoride, with its semi-ionic character and its relatively small formula volume (65 Å^3), competes effectively with AF_6^- in providing Coulomb energy. This is because the charges on the F atoms of XeF_2 are close to −0.5 and the charge on Xe is approximately +1, while the charge on each F ligand of AF_6^- is ca.–0.167.

$$M[HF]_m^{n+} + nAF_6^- + zXeF_2 \rightarrow M[XeF_2]_p^{n+} + nAF_6^- + (z-p)XeF_2 + mHF \qquad [49]$$

1.25.3.2.3.2 Syntheses

In order for the syntheses of $[M^n(XeF_2)_p][AF_6]_n$ to proceed, two requirements must be met (eqn [49]): (1) The Lewis acidities of the metal cations should not be strong enough to withdraw F^- from XeF_2, which would result in $[Xe_2F_3][AF_6]$ and/or $[XeF][AF_6]$ salts, and (2) because XeF_2 dissolved in aHF is a relatively strong oxidizing agent, it is essential that the metal cation be resistant to further oxidation.[176] Should the metal cation be oxidized, it would be converted to an even stronger Lewis acid, presenting the increased possibility that it will withdraw F^- from XeF_2.

The number of XeF_2 molecules coordinated to the metal cation (p) generally increases as aHF is removed under vacuum at low temperatures. In such cases, the coordination compound is mixed and also contains an excess of XeF_2. The weight-loss versus time-of-pumping curves reveal that free XeF_2 is no longer present at $p=6$ in the Raman spectrum, that is, ν_1 of XeF_2 at 496 cm^{-1} is absent in the product.[177] Coordination compounds having high p-values are usually unstable under dynamic vacuum, slowly losing XeF_2 to give white solids within the range, $5 \geq p \geq 2$. In the case of Mg^{2+}, the compounds $[Mg(XeF_2)_p][AsF_6]_2$ were detected for $p=2$, 4, 6.

Copyright © 2013. Elsevier. All rights reserved.

Comprehensive Inorganic Chemistry II : From Elements to Applications, Elsevier, 2013. ProQuest Ebook Central, http://ebookcentral.proquest.com/lib/inflibnet-ebooks/detail.action?docID=1330977.
Created from inflibnet-ebooks on 2021-02-09 22:27:13.

The compound corresponding to $p=6$ loses XeF_2 under dynamic vacuum at room temperature, yielding $[Mg(XeF_2)_4][AsF_6]_2$. This compound is also unstable, and slowly loses XeF_2 under dynamic vacuum at room temperature to give $[Mg(XeF_2)_2][AsF_6]_2$. The preparation of a pure compound corresponding to $p=2$ has only been possible when stoichiometric amounts of $Mg[AsF_6]_2$ and XeF_2 were allowed to react in aHF.[177] Occasionally, compounds having low p-values have been obtained by pumping under dynamic vacuum at higher temperatures. The compound, $[Ca(XeF_2)_{2.5}][AsF_6]_2$,[178] was obtained by pumping $[Ca(XeF_2)_4][AsF_6]_2$ to constant weight under dynamic vacuum at 60 °C.

In the case of PF_5, which does not form stable $[XeF][PF_6]$ or $[Xe_2F_3][PF_6]$ salts,[93] syntheses were carried out by direct reaction between XeF_2 and gaseous PF_5 in aHF. Because the solubility of PF_5 in aHF is low, a high pressure of PF_5 was employed, forming $M[PF_6]_2$ *in situ* which reacts further with XeF_2, yielding, for example, $[Ba(XeF_2)_4][PF_6]_2$.[179] Again, because BF_3 does not form stable $[XeF][BF_4]$ or $[Xe_2F_3][BF_4]$ salts, the compound $[Cd(XeF_2)][BF_4]_2$ has been synthesized using an analogous approach and by direct reaction of $Cd[BF_4]_2$ with XeF_2 in aHF.[180]

A special synthetic approach is also required in the case of lanthanide complexes. When the unsolvated $Ln[AsF_6]_3$ salts are prepared, they lose AsF_5, yielding compounds of the type $[LnF_x][AsF_6]_{3-x}$ ($x=1$, 1.5). In order to form $Ln[AsF_6]_3$ in solution, a 3:1 molar ratio of AsF_5:LnF_3 must be used. An excess of AsF_5 would only yield $[Xe_2F_3][AsF_6]$ upon addition of XeF_2 to the HF solution.[181,182]

1.25.3.2.3.3 *The structures of $[M^n(XeF_2)_p][AF_6]_n$, $[Cd(XeF_2)][BF_4]_2$, and $[Ba(XeF_2)][V_2O_2F_8]$ (A = As, Sb, Bi, P, Ta, Ru, Nb, V)*

In general, the coordination spheres of the metal centers in these systems consist of XeF_2 molecules only, XeF_2 molecules and AF_6^- anions, or AF_6^- anions only. The XeF_2 ligand in $[M^n(XeF_2)_p][AF_6]_n$ acts either as a bridging ligand, connecting two metal centers, or as a nonbridging ligand, interacting with only one metal center. The number of XeF_2 molecules (bridging and nonbridging) coordinated to a given metal cation ranges from one nonbridging XeF_2 molecule, as in $[Cd(XeF_2)][BF_4]_2$,[180] to nine XeF_2 molecules (five nonbridging and four bridging), as in the case of the Ca^{2+} cation in $[Ca_2(XeF_2)_9][AsF_6]_4$.[183] Cases where seven XeF_2 molecules are either bridging or nonbridging around one metal cation are presently unknown.

The structural types displayed by $[M^n(XeF_2)_p][AF_6]_n$ coordination compounds are diverse. The influence of the central metal cation on structural diversity is related to a number of cation properties including electron affinity, electronegativity, effective nuclear charge, effective volume, Lewis acidity, covalency of the M–F bond, and coordination number. The influence of the AF_6^- anion on structural diversity is also important but is less influential than the cation. Among the factors that should be considered in the case of the AF_6^- anion series are the fluorobasicities and the magnitudes of the negative charges on the fluorine ligands of the anions.

The following examples illustrate the general structural types that have been encountered among coordination compounds containing the XeF_2 ligand:

- *Molecular structure of $[Mg(XeF_2)_4][AsF_6]_2$.* The Mg^{2+} cation of $[Mg(XeF_2)_4][AsF_6]_2$ [177] is octahedrally coordinated to six F atoms. Four F atoms originate from four XeF_2 molecules, two are cis-coordinated to one another, and two are trans-coordinated. The remaining F atoms of the metal coordination sphere are from two monodentate AsF_6^- anions and are coordinated cis to one another (**Figure 31**). Each of the four XeF_2 molecules and the two AsF_6^- anions is crystallographically distinct. The octahedron of F atoms around the central Mg^{2+} cation is distorted. The Xe---F bridging distances range from 2.059(9) to 2.087(8) Å, while the Xe–F terminal distances range from 1.940(8) to 1.963(10) Å. The bridging As–F distances are 1.773(9) and 1.786(9) Å, while terminal As–F distances range from 1.701(12) to 1.726(10) Å. Several close intra- and intermolecular electrostatic interactions occur between the positively charged Xe atoms and the negatively charged F atoms of XeF_2 and AsF_6^-. The $[Mg(XeF_2)_4][AsF_6]_2$ structural units in the unit cell only interact by means of electrostatic forces, resulting in long Xe···F contact distances ranging from 3.180 to 3.698 Å (the sum of the respective van der Waals radii is 3.63 Å).[34]
- *The dimeric structure of $[Cd_2(XeF_2)_{10}][SbF_6]_4$.* The structural unit of $[Cd_2(XeF_2)_{10}][SbF_6]_4$ consists of two crystallographically distinct Cd atoms, ten Xe atoms, and four SbF_6^- anions.[176] The coordination numbers around Cd1 and Cd2 are seven and eight, respectively, with average Cd1–F and Cd2–F distances of 2.266(9) and 2.336(9) Å, respectively. The longer Cd2–F bond length is in accordance with the higher coordination number of Cd2. There is no significant difference between the Cd–F(Xe) and Cd–F(Sb) distances. This is likely because the negative charges on the F ligands of SbF_6^- do not differ significantly from the negative charges on the F ligands of the XeF_2 molecules. The Cd atoms are connected by means of a single bridging $Xe1F_2$ molecule having asymmetric Xe1–F (F6, 1.976(8); F1, 2.022(9) Å) bond lengths. While the Xe1–F6 bond

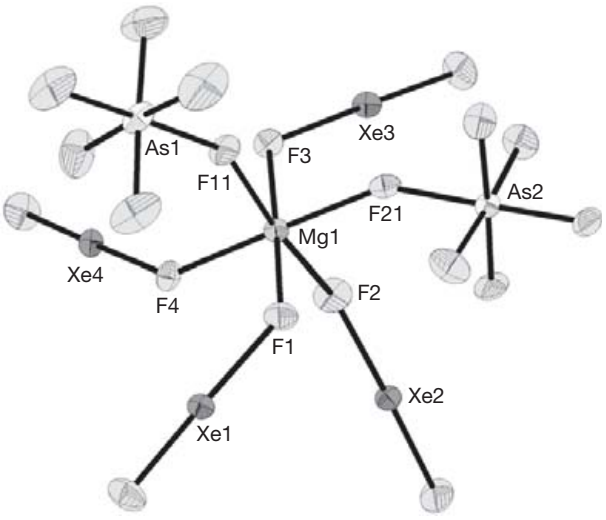

Figure 31 The molecular structure of $[Mg(XeF_2)_4][AsF_6]_2$. Reproduced with permission from Tramšek, M.; Benkič, P.; Žemva, B. *Inorg. Chem.* **2004**, *43*, 699–703.

Copyright © 2013. Elsevier. All rights reserved.

Comprehensive Inorganic Chemistry II : From Elements to Applications, Elsevier, 2013. ProQuest Ebook Central, http://ebookcentral.proquest.com/lib/inflibnet-ebooks/detail.action?docID=1330977.
Created from inflibnet-ebooks on 2021-02-09 22:27:13.

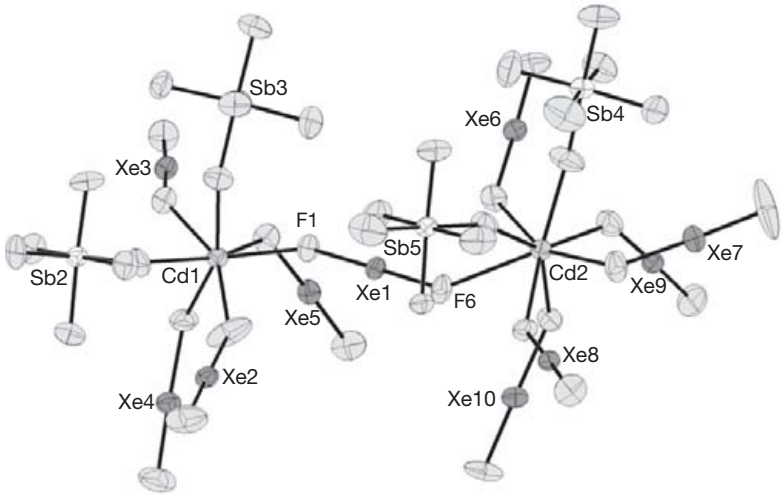

Figure 32 The X-ray crystal structure of dimeric $[Cd_2(XeF_2)_{10}][SbF_6]_4$. Reproduced with permission from Tavčar, G.; Tramšek, M.; Bunič, T.; Benkič, P.; Žemva, B. *J. Fluorine Chem.* **2004**, *125*, 1579–1584.

length is the shortest, the Cd2−F6 distance is the longest (2.646(9) Å) (Figure 32).

- *The chain structure of* $[Ca(XeF_2)_5][PF_6]_2$. The coordination sphere of Ca^{2+} consists of nine F atoms contributed by the two nonbridging PF_6^- anions and six XeF_2 molecules (Figure 33).[184] The $P1F_6^-$ anion is coordinated to the Ca^{2+} cation by two cis-F atoms that define an edge of the $P1F_6^-$ octahedron, while the $P2F_6^-$ anion only contributes one F ligand to the coordination sphere of Ca^{2+}. The Ca−F21 distance resulting from coordination to $P2F_6^-$ (2.363(7) Å) is shorter than both contact distances with the bidentate $P1F_6^-$ anion (Ca−F11, 2.570(8) Å; Ca−F12, 2.759(8) Å). There are four nonbridging XeF_2 molecules, with the Ca−F(Xe) distances ranging from 2.270(8) to 2.334(8) Å, and there are two bridging XeF_2 molecules, with longer Ca−F(Xe) distances (2.403(7) and 2.548(6) Å). Each Ca^{2+} cation is only connected to neighboring Ca^{2+} cations through two bridging $Xe1F_2$ molecules, forming infinite chains that run parallel to the *b*-axis of the unit cell. There are also long-range electrostatic interactions between the positively charged Xe atoms and the negatively charged F atoms of the XeF_2 molecules and the PF_6^- anions inside the chain as well as between adjacent chains.
- *The double-chain structure of* $[Nd(XeF_2)_{2.5}][AsF_6]_3$. Regular trigonal prismatic arrangements around Nd^{3+} are formed by the F atoms of six different edge-bridged AsF_6 octahedra which connect the Nd^{3+} cations to form infinite chains.[182] Each of the three rectangular faces of the trigonal prisms is occupied by a F ligand of a XeF_2 molecule. Two of these XeF_2 molecules are nonbridging ligands, whereas the third XeF_2 molecule bridges two Nd^{3+} cations forming a double chain (Figure 34). The Xe−F distance in the bridging XeF_2 molecule (1.991(6) Å) is not significantly different from the Xe−F distance in free XeF_2.[93] The nonbridging XeF_2 molecules are strongly distorted, with the bridging Xe−F bonds elongated to 2.073(6)–2.079(6) Å and the terminal Xe−F bonds contracted to 1.918(6)–1.936(6) Å. The Nd−F(As) distances range from 2.402(5) to 2.424(5) Å, while the Nd−F(Xe) distances range from 2.300(6) to 2.435(6) Å.

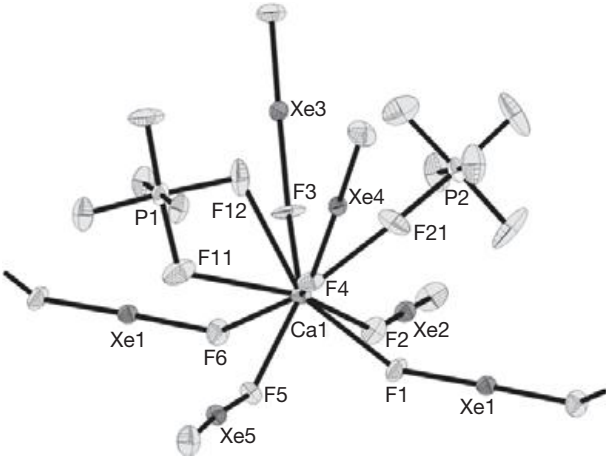

Figure 33 The X-ray crystal structure of $[Ca(XeF_2)_5][PF_6]_2$. Reproduced with permission from Bunič, T.; Tavčar, G.; Tramšek, M.; Žemva, B. *Inorg. Chem.* **2006**, *45*, 1038–1042.

The shortest distances occur for the nonbridging XeF_2 molecules, whereas the longest distance (2.435(6) Å) occurs for the bridging XeF_2 molecule. Electrostatic forces between the positively charged Xe atoms and negatively charged F ligands of XeF_2 and/or AsF_6^- anions result in contacts which range from 3.260 to 3.745 Å and serve to hold neighboring chains together.

- *The layered structure of* $[Ca(XeF_2)_4][AsF_6]_2$. The Ca^{2+} cations in this heteroleptic structure are coordinated to eight F atoms which provide a square antiprismatic Ca^{2+} coordination sphere.[178] One rectangular face of the antiprism is comprised of two F ligands from two terminal AsF_6^- anions and two F ligands from two bridging XeF_2 molecules. The opposite rectangular face is formed by two F ligands of two bridging XeF_2 molecules and two F ligands of two nonbridging XeF_2 molecules. The Ca−F(As) distances are 2.326(1) and 2.400(1) Å and the Ca−F(Xe) distances range from 2.274(9) to 2.391(9) Å, indicating that the F ligands from

Copyright © 2013. Elsevier. All rights reserved.

Comprehensive Inorganic Chemistry II : From Elements to Applications, Elsevier, 2013. ProQuest Ebook Central, http://ebookcentral.proquest.com/lib/inflibnet-ebooks/detail.action?docID=1330977.
Created from inflibnet-ebooks on 2021-02-09 22:27:13.

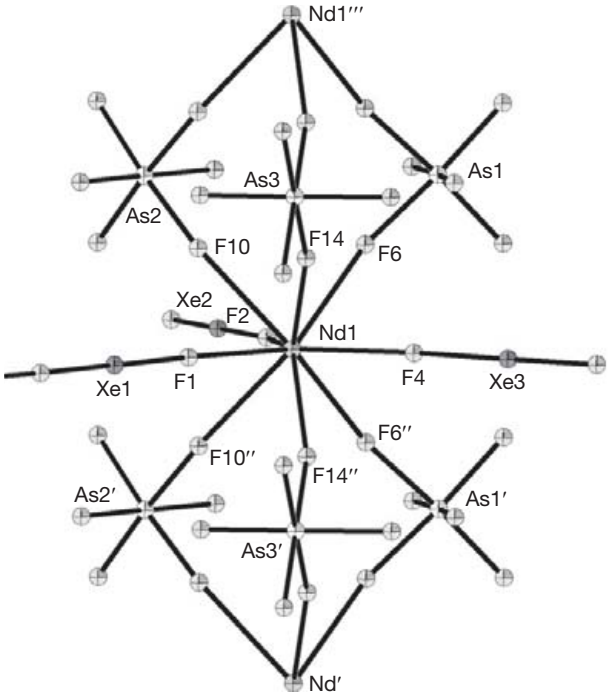

Figure 34 The X-ray structure of $[Nd(XeF_2)_{2.5}][AsF_6]_3$. Reproduced with permission from Tramšek, M.; Lork, E.; Mews, R.; Žemva, B. *J. Solid State Chem.* **2001**, *162*, 243–249.

AsF_6^- and XeF_2 effectively compete for coordination to the Ca^{2+} ion. Significant elongations of the bridging As–F bonds of both nonbridging AsF_6 units (1.756(9) and 1.781(9) Å) also indicate accumulation of the negative charge on these F ligands relative to the nonbridging ones. The Ca^{2+} cations are linked through bridging XeF_2 molecules forming layers perpendicular to the *c*-axis of the unit cell (**Figure 35**). Neighboring layers are staggered so that the terminal AsF_6^- anions of one layer alternate with the terminal XeF_2 molecules of its neighboring layer, giving rise to more efficient packing. In this way, the layers are interconnected by Coulomb forces between negatively charged F ligands of AsF_6^- anions and positively charged Xe centers of the neighboring layer.

- *$[M(XeF_2)_3][AsF_6]_2$ (M = Pb, Sr), a higher interconnected double-layer structure*. The metal cations of the title compound are coordinated to nine F atoms forming irregular tricapped trigonal prisms.[185] Six F atoms of the coordination sphere are contributed by six bridging XeF_2 molecules (Xe1, Xe2, and Xe3), two F atoms are contributed by two bridging AsF_6 units (As1), and the remaining F atom is contributed by a nonbridging AsF_6^- anion (As2) (**Figure 36**). The M^{2+} cations and the $Xe3F_2$ bridging molecules form layers where four M^{2+} cations and four $Xe3F_2$ bridging molecules form interconnecting rings, each M^{2+} cation being connected to four $Xe3F_2$ molecules. These layers are connected to each other through the bridging $Xe1F_2$ and $Xe2F_2$ molecules and through two bridging AsF_6^- anions per M^{2+} cation. The terminal AsF_6^- anions are positioned in such a way that they line up with the centers of the rings mentioned above. It is also noteworthy that the coordination polyhedron of Pb^{2+} does not show steric activity of the lone electron pair of Pb(II) atom, consistent with the structure of PbO.[185]
- *$[Ca(XeF_2)_{2.5}][AsF_6]_2$, a three-dimensional network structure*. The coordination sphere of the Ca^{2+} cation in $[Ca(XeF_2)_{2.5}][AsF_6]_2$ consists of nine F atoms which give a monocapped Archimedean antiprism. Five F ligands are from bridging XeF_2 molecules, one F ligand is from a nonbridging AsF_6^- anion (As1), and two F ligands are from two cis-bridged AsF_6^- anions (As2).[178] Additionally, one of the bridging AsF_6^- anions has a close contact with Ca^{2+} through F22 from above one rectangular face of the square antiprism, to give a nine-coordinate Ca^{2+} cation (**Figure 37**). The Ca–F distances do not differ by much, whether the F atoms are donated by the XeF_2 molecules or by the AsF_6^- anions. The Ca–F(Xe) distances range from 2.357(6) to 2.457(6) Å, the Ca–F(As2) distances are 2.335(6) to 2.432(7) Å, and the Ca–F(As1) distance is 2.315(6) Å. The Ca–F22 distance is significantly longer (2.813(8) Å) than the other Ca–F distances. This is in accordance with the observation that removal of XeF_2 from solid $[Ca(XeF_2)_4][AsF_6]_2$ at 333 K results in $[Ca(XeF_2)_{2.5}][AsF_6]_2$. The loss of 1.5 XeF_2 molecules per $[Ca(XeF_2)_4][AsF_6]_2$ formula unit is compensated for by cis-bridging interactions of AsF_6^- with Ca^{2+}, while the remaining XeF_2 molecules function as bridging ligands.[178]
- *Homoleptically coordinated XeF_2 in $[Ca_2(XeF_2)_9][AsF_6]_4$, $[Pb_3(XeF_2)_{11}][PF_6]_6$, and $[M(XeF_2)_6][SbF_6]_2$ (M = Cu, Zn)*. There are two crystallographically distinct Ca^{2+} cations in the crystal structure of $[Ca_2(XeF_2)_9][AsF_6]_4$ (**Figure 38**).[183] The Ca1 atom is in a homoleptic environment of nine XeF_2 molecules. Eight of the XeF_2 molecules donate F atoms to Ca^{2+} to form the apices of an Archimedean antiprism, while the ninth F atom from $Xe3F_2$ caps one square face of the antiprism. The four XeF_2 molecules that form the open square face of the antiprism bridge the $Ca1^{2+}$ and $Ca2^{2+}$ cations. The coordination sphere of Ca2 is also square antiprismatic and is comprised of F atoms from four monodentate AsF_6^- anions and four bridging XeF_2 molecules. Two $Ca1^{2+}$ cations and two $Ca2^{2+}$ cations are bridged by four XeF_2 molecules to form 16-membered rings, which are further connected, forming puckered layers. There are several electrostatic interactions between negatively charged fluorine atoms from AsF_6^- units and positively charged Xe atoms from nonbridging $Xe2F_2$ and $Xe3F_2$ molecules which occur between the layers stacked along the *c*-axis of the unit cell. Based on the different Ca^{2+} cation environments, the chemical formula can be written as a double salt $[(Ca(XeF_2)_5(XeF_2)_{4/2})][(Ca(AsF_6)_4(XeF_2)_{4/2})]$. This formulation suggests that in an aHF solution of $Ca(AsF_6)_2$ having a large amount of XeF_2, the Ca^{2+} cations are fully surrounded by XeF_2 molecules. Because the AsF_6^- anions are bulky, the grouping of only linear XeF_2 molecules around a single Ca^{2+} cation achieves an energetically and sterically preferred arrangement.[183] The crystal structure of $[Pb_3(XeF_2)_{11}][PF_6]_6$ contains two crystallographically independent Pb atoms (**Figure 39**).[186] Eight F atoms, belonging to eight bridging XeF_2 molecules, form a unique homoleptic cubic environment for the Pb1 atom. The arrangement of the Pb2

Copyright © 2013. Elsevier. All rights reserved.

Comprehensive Inorganic Chemistry II : From Elements to Applications, Elsevier, 2013. ProQuest Ebook Central, http://ebookcentral.proquest.com/lib/inflibnet-ebooks/detail.action?docID=1330977.
Created from inflibnet-ebooks on 2021-02-09 22:27:13.

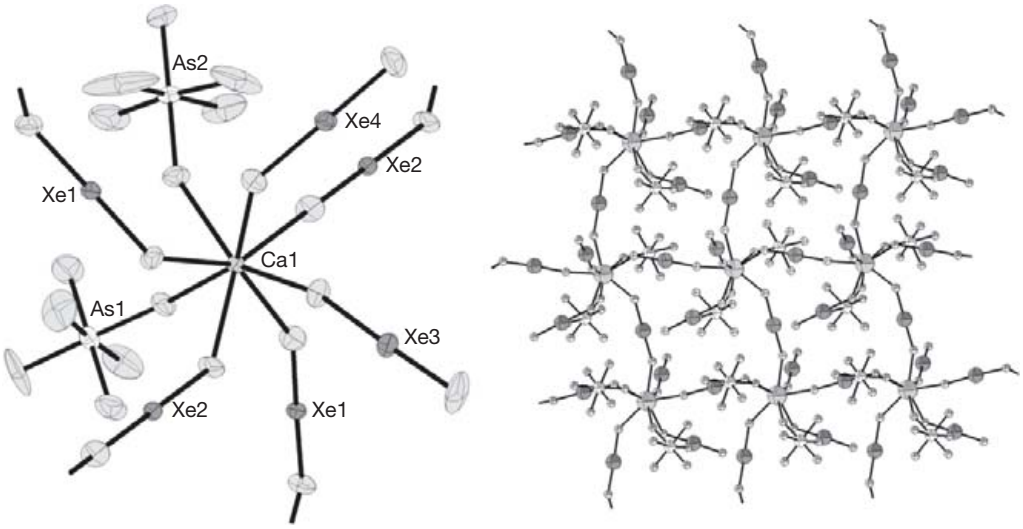

Figure 35 The X-ray crystal structure showing part of the layered $[Ca(XeF_2)_4][AsF_6]_2$ structure. Reproduced with permission from Benkič, P.; Tramšek, M.; Žemva, B. *Solid State Sci.* **2002**, *4*, 1425–1434.

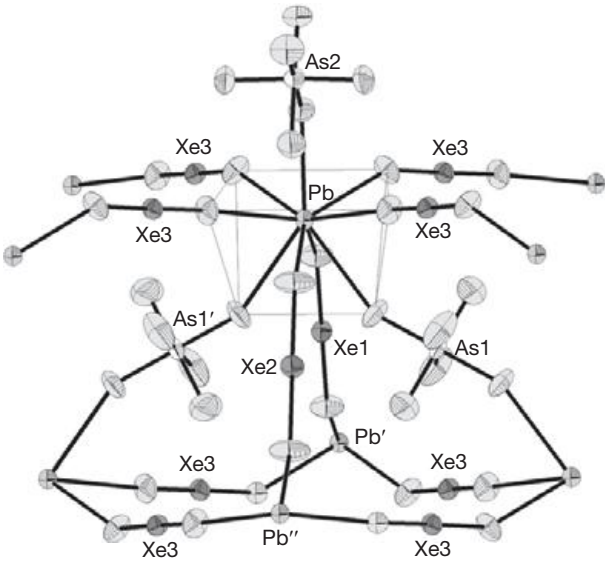

Figure 36 The X-ray crystal structure of $[Pb(XeF_2)_3][AsF_6]_2$, showing the highly interconnected double layers. Reproduced with permission from Tramšek, M.; Benkič, P.; Žemva, B. *Solid State Sci.* **2002**, *4*, 9–14.

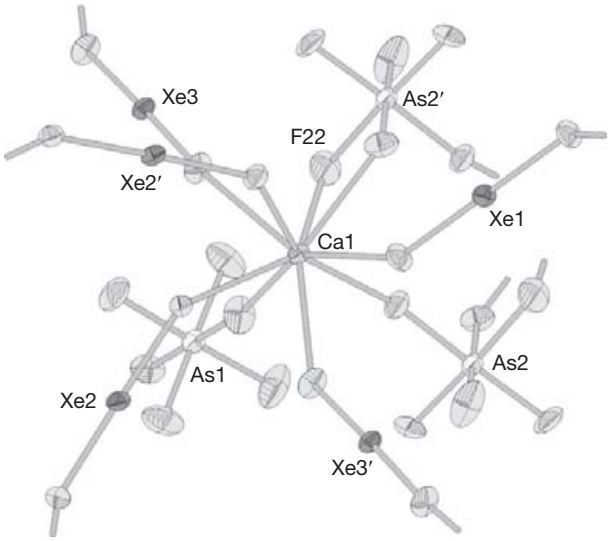

Figure 37 The three-dimensional network in the X-ray crystal structure of $[Ca(XeF_2)_{2.5}][AsF_6]_2$. Reproduced with permission from Benkič, P.; Tramšek, M.; Žemva, B. *Solid State Sci.* **2002**, *4*, 1425–1434.

coordination sphere is common to lead compounds, that is, a tricapped trigonal prism comprised of six F atoms from six bridging XeF_2 molecules and three F atoms from three non-bridging PF_6^- anions.[186] The bridging XeF_2 molecules form a 3D network. The remaining XeF_2 molecule (Xe1) does not participate in metal coordination; rather, it is fixed in the crystal lattice by weak Xe1···F interactions with PF_6^- anions which range from 3.35 to 3.37 Å. Uncoordinated XeF_2 (Xe–F, 1.99(1) Å) was also found in the crystal structure of $[Ba(XeF_2)_5][SbF_6]_2$.[187] The compounds, $[M(XeF_2)_6][SbF_6]_2$ (M = Cu, Zn), are isostructural and represent the first examples in which the M^{2+} cation is homoleptically coordinated to only terminal XeF_2 molecules (Figure 40).[188] The bridging and terminal Xe–F distances are very similar in both the copper and the zinc compounds (Cu: 2.083(3) Å and 1.934 (4) Å; Zn: 2.078(5) Å and 1.931(5) Å, respectively), whereas the SbF_6^- anions are well isolated and are not distorted.

- *$[Cd(XeF_2)][BF_4]_2$: the first XeF_2 coordination compound containing the BF_4^- anion.* The tetrahedral BF_4^- anion has a much smaller volume than any AF_6^- anion discussed previously.[180] Furthermore, the charge on each F ligand of BF_4^- is greater than on the F ligands of the AF_6^- anions cited above, which is mainly a consequence of the smaller number of F ligands, causing the F ligands of BF_4^- to be more strongly fluorobasic than the F ligands of AF_6^- and more competitive with the F ligands of XeF_2 when donating their valence electron pair density to a metal cation. It was further shown that in order to obtain pure $[Cd(XeF_2)][BF_4]_2$ in aHF at room temperature,

Copyright © 2013. Elsevier. All rights reserved.

Comprehensive Inorganic Chemistry II : From Elements to Applications, Elsevier, 2013. ProQuest Ebook Central, http://ebookcentral.proquest.com/lib/inflibnet-ebooks/detail.action?docID=1330977.
Created from inflibnet-ebooks on 2021-02-09 22:27:13.

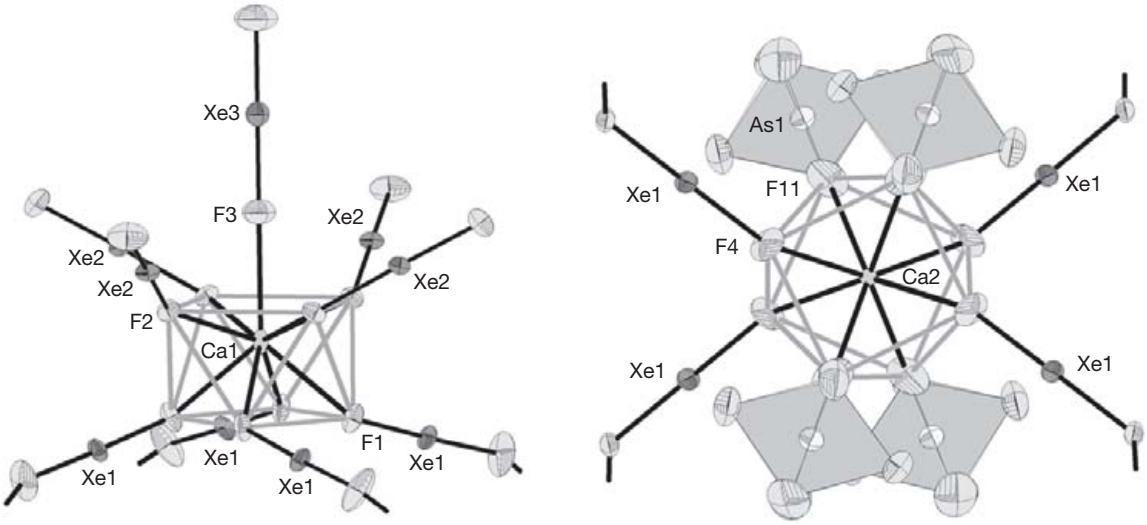

Figure 38 The structural units in the X-ray crystal structure of $[Ca_2(XeF_2)_9][AsF_6]_4$, showing the coordination geometries at the homoleptic Ca1 and the heteroleptic Ca2 centers. Reproduced with permission from Tramšek, M.; Benkič, P.; Žemva, B. *Angew. Chem., Int. Ed.* **2004**, *43*, 3456–3458.

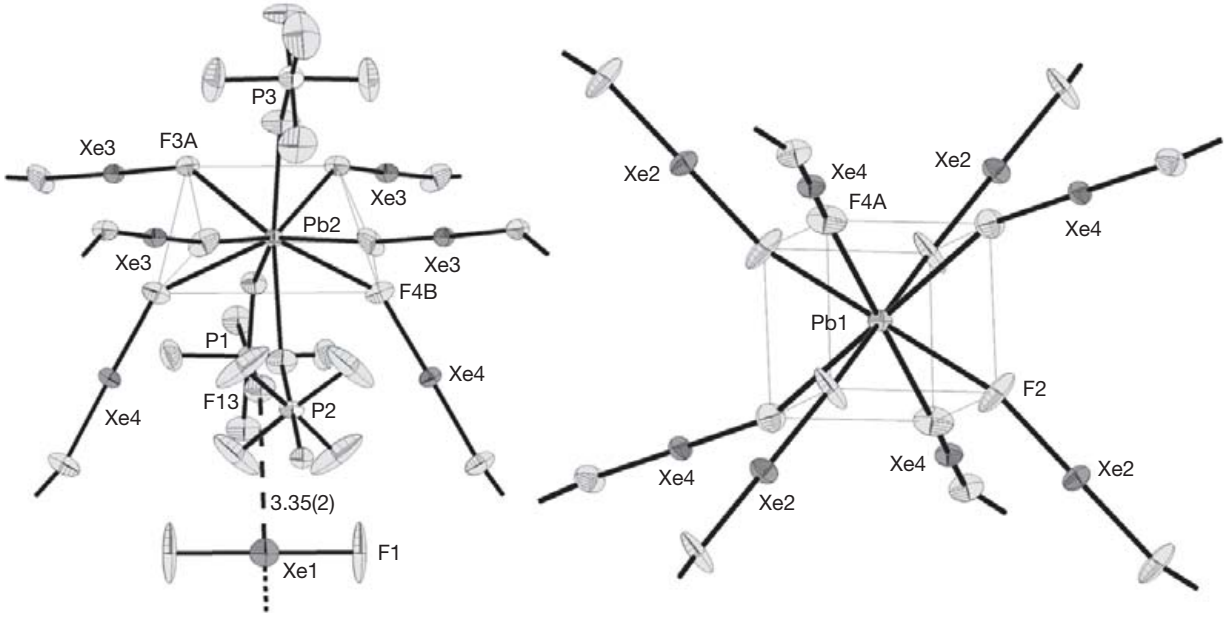

Figure 39 The homoleptic Pb1 center and the Pb2 environments in the X-ray crystal structure of $[Pb_3(XeF_2)_{11}][PF_6]_6$. Reproduced with permission from Bunič, T.; Tramšek, M.; Goreshnik, E.; Tavčar, G.; Žemva, B. *Inorg. Chem.* **2007**, *46*, 5276–5282.

the molar ratio, $Cd(XeF_2)^{2+}$: $(BF_4^-)_2$, should be at least 1:5 or higher. When aHF is removed under vacuum, the concentrations of BF_4^- and XeF_2 gradually increase and both slowly displace HF molecules that are coordinated to Cd^{2+}. Despite the relatively high fluorobasicity of XeF_2, it is essential that the XeF_2 concentration be sufficiently high to prevent $Cd[BF_4]_2$ formation. The coordination sphere of Cd^{2+} consists of eight F ligands, which form a square antiprismatic coordination sphere around Cd^{2+}. This is in accordance with eight-coordinate Cd^{2+} in CdF_2, although in that instance, the fluorite structure requires cubic symmetry. The main difference between the two fluoroborate structures is that one BF_4^- anion is replaced by a XeF_2 molecule, thus transforming a 3D structure into a layered structure (Figure 41). There are two crystallographically distinct BF_4^- anions; four $B1F_4$ anions bridge four Cd^{2+} cations and three $B2F_4^-$ anions bridge only three Cd^{2+} cations. The $B1F_4^-$ anions are nearly regular tetrahedra, whereas the $B2F_4^-$ anions are distorted. The XeF_2 molecule is nonbridging with $Xe-F_b$ and $Xe-F_t$ bond lengths equal to 2.065(3) Å and 1.943(4) Å, respectively.

- *$[Ba(XeF_2)][V_2O_2F_8]$; the first XeF_2 coordination compound containing an oxofluoro anion*. The reaction of BaF_2 and VOF_3 in a 1:2 molar ratio at room temperature in HF yielded $[Ba(HF)][V_2O_2F_8]$ which was isolated at room temperature as a white powder.[189] Further reaction with excess

Copyright © 2013. Elsevier. All rights reserved.

Comprehensive Inorganic Chemistry II : From Elements to Applications, Elsevier, 2013. ProQuest Ebook Central, http://ebookcentral.proquest.com/lib/inflibnet-ebooks/detail.action?docID=1330977.
Created from inflibnet-ebooks on 2021-02-09 22:27:13.

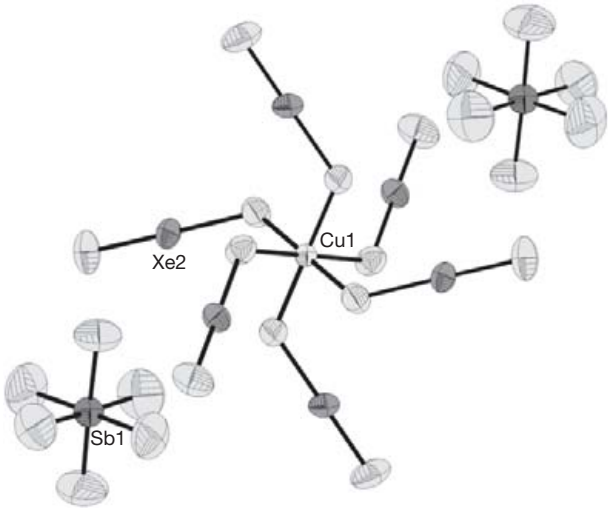

Figure 40 The structural unit in the X-ray crystal structure of the homoleptic compounds, $[M(XeF_2)_6][SbF_6]_2$ (M = Cu, Zn). Reproduced with permission from Tavčar, G.; Goreshnik, E.; Mazej, Z. *J. Fluorine Chem*. **2006**, *127*, 1368–1373.

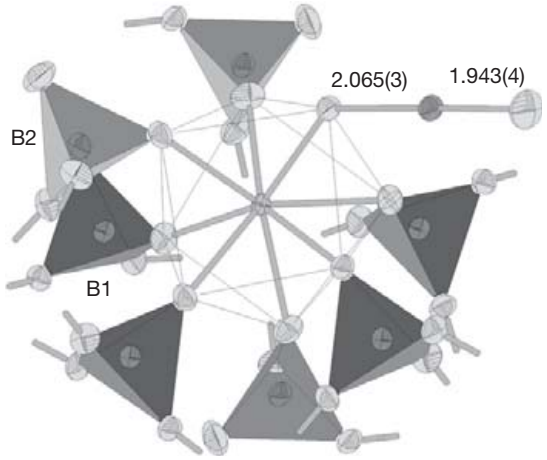

Figure 41 The X-ray crystal structure of $[Cd(XeF_2)][BF_4]_2$ showing the basic building block in the layered structure. Reproduced with permission from Tavčar, G.; Žemva, B. *Inorg. Chem*. **2005**, *44*, 1525–1529.

XeF_2 resulted in HF displacement, forming $[Ba(XeF_2)][V_2O_2F_8]$, the first coordination compound of XeF_2 having an oxofluoro anion. Suitable crystals of $[Ba(XeF_2)][V_2O_2F_8]$ were isolated from a saturated aHF solution at room temperature. The coordination sphere of Ba^{2+} is comprised of 12 F atoms (Figure 42). Ten F atoms are from four $V_2O_2F_8^{2-}$ anions, where two anions coordinate to the central Ba^{2+} cation through three F atoms and the other two anions coordinate through two F atoms. In addition, two fluorine atoms are from the XeF_2 molecules that lie along the *b*-axis and bridge the $Ba[V_2O_2F_8]$ layers that are stacked along the *a*-axis (Figure 43). It is generally noted that when the Xe–F bridging distance is long (1.993(7) Å), the Ba–F distance is short (2.773(7) Å) and when the Xe–F bridging distance is short (1.974(7) Å), the Ba–F distance is long (3.076(7) Å).

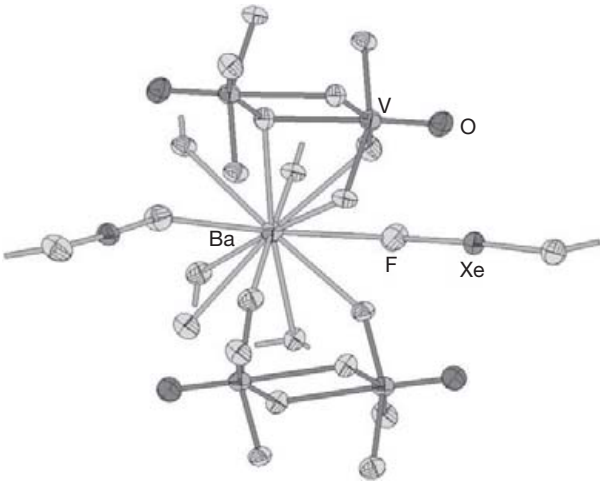

Figure 42 The coordination sphere of the Ba atom in the X-ray crystal structure of $[Ba(XeF_2)][V_2O_2F_8]$.[189]

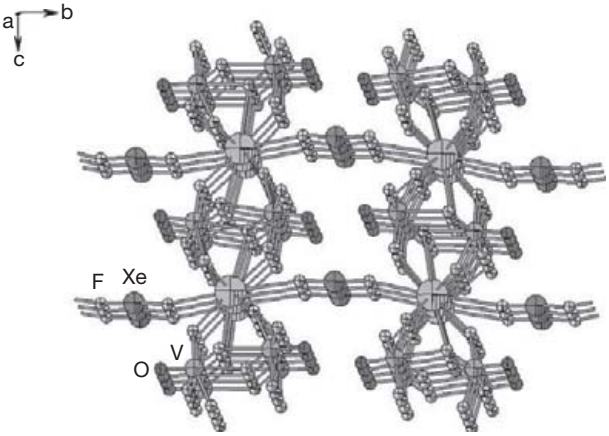

Figure 43 Coordination of XeF_2 to $Ba[V_2O_2F_8]$ layers in $[Ba(XeF_2)][V_2O_2F_8]$.[189]

1.25.3.2.3.4 The structural influence of the metal center

Table 4 lists all isolated metal coordination compounds in which XeF_2 serves as a ligand to a metal ion.

The influence of the metal center is demonstrated by the series of compounds, $[M(XeF_2)_4][AsF_6]_2$ (M = Mg,[177] Ca,[178] Cd[190]). The crystal structure of the Mg compound represents the first molecular structure found in the $M^n[AF_6]_n/XeF_2/aHF$ system. This structure type is a consequence of the small Mg^{2+} ion and its low coordination number (CN = 6) as well as the covalencies of the Mg–F bonds. The Mg–F(Xe) and Mg–F(As) distances in $[Mg(XeF_2)_4][AsF_6]_2$ are essentially the same (average Mg–F(Xe), 1.98(1) Å; average Mg–F(As), 1.99(1) Å), indicating that the F ligands of monodentate AsF_6^- can, in terms of relative fluorobasicity, compete effectively with the F ligands of the XeF_2 molecules when coordinating to the Mg^{2+} ion. The charge transfer from the XeF_2 molecule to the cation that results from the covalent character of the Mg–F bond renders the XeF_2 molecules less capable of bridging two Mg^{2+} cations.

In accordance with the much higher electron affinity of Cd^{2+} (16.91 eV)[191] compared to that of Ca^{2+} (11.87 eV),[191] a greater

Copyright © 2013. Elsevier. All rights reserved.

Comprehensive Inorganic Chemistry II : From Elements to Applications, Elsevier, 2013. ProQuest Ebook Central, http://ebookcentral.proquest.com/lib/inflibnet-ebooks/detail.action?docID=1330977.
Created from inflibnet-ebooks on 2021-02-09 22:27:13.

Table 4 A list of compounds, $[M^n(XeF_2)_p][AF_6]_n$,[a] $[Cd(XeF_2)][BF_4]_2$ and $[Ba(XeF_2)][V_2O_2F_8]$, in which the XeF_2 ligand coordinates to metal ions[b]

	p									
M	AsF_6^-	SbF_6^-	BiF_6^-	PF_6^-	TaF_6^-	RuF_6^-	NbF_6^-	VF_6^-	BF_4^-	$V_2O_2F_8^{2-}$
Li^+	*3*			3		3				
Ag^+	*2*			*2*						
Mg^{2+}	6, *4*, *2*	6, *2*	6		*2*					
Ca^{2+}	*4.5*, *4*, *2.5*	3.5	3	*5*		3				
Sr^{2+}	*3*		3	*3*, *10/3*	0.5	3				
Ba^{2+}	*5*, 3	*5*	2	*4*	0.5	*5*	*5*	*5*		*1*
Pb^{2+}	*3*	3		*3*, *11/3*						
Cd^{2+}	*4*	*8*, *5*, *3*, *2.5*, *4/3*	*4.5*	*5*	*1*		*1*		*1*	
Zn^{2+}		*2*, *6*								
Cu^{2+}		*2*, *4*, *6*								
Hg^{2+}	*5*, *2*	7, *3*								
La^{3+}	3, *2.5*									
Pr^{3+}	3									
Nd^{3+}	3, *2.5*	*3*	3							

[a] *n* is the net charge on the metal cation and ***p*** is the number of XeF_2 ligands per M^n cation.
[b] The X-ray crystal structures have been determined for the compounds where the index number, ***p***, is in italic script.

degree of charge is transferred from the XeF_2 molecule to the Cd^{2+} ion and, therefore, a higher degree of covalency in the M–F bonds is expected for the Cd^{2+} compound relative to the Ca^{2+} compound, making bridging interactions in the Cd structure less favorable. In the structure of $[Cd(XeF_2)_4][AsF_6]_2$,[190] there are only two bridging XeF_2 molecules which result in chain formation, while in the structure of $[Ca(XeF_2)_4][AsF_6]_2$,[178] there are four bridging XeF_2 molecules which yield a layered structure.

By only changing the cation, three different crystal structures were obtained: molecular (Mg^{2+}), chain (Cd^{2+}), and layered (Ca^{2+}) structures in which only XeF_2 molecules coordinate to the metal centers.

1.25.3.2.3.5 The influence of the AF_6^- anion

Overall, the effect of the anion is less significant. This can be seen in the series of isostructural $[Mg(XeF_2)_2][AF_6]_2$ (A = As[177] and Sb[192]) salts. In $[Nd(XeF_2)_{2.5}][AsF_6]_3$ [182] and $[Nd(XeF_2)_3][SbF_6]_3$,[192] the AsF_6^- anion is a stronger Lewis base than SbF_6^- which means that the interactions of six AsF_6^- anions with the Nd^{3+} cation are stronger than the corresponding interactions with the SbF_6^- anions (**Figure 34**). As a consequence, the interactions of the negatively charged F ligands of the XeF_2 molecules are stronger in the case of the SbF_6^- compound. This results in a shift of the negative charges on the F ligands of the XeF_2 molecules toward the metal center. Therefore, the ability of XeF_2 ligands in the SbF_6^- compound to act as bridging ligands is reduced. The interactions of the XeF_2 molecules with the metal center are weaker in the AsF_6^- compound, allowing one XeF_2 molecule to serve as a bridging ligand. Thus, the double-chain structure (**Figure 34**) was obtained. The Raman spectra are in accordance with the above interpretation and show that the M–F(Xe) bond is stronger in the case of SbF_6^- (ν(Xe–F) is 576 cm^{-1}) than in the case of AsF_6^- (ν(Xe–F) is 568 cm^{-1}).

Another example is the series of isostructural compounds, $[Ba(XeF_2)_5][AF_6]_2$ with A = Sb,[187] As,[193] Nb,[194] and Ru,[194] where the effect of the fluorobasicity of the AF_6^- anion on the structures of these compounds is insignificant.

1.25.3.2.3.6 Raman spectra

Raman spectroscopy of $[M^n(XeF_2)_p][AF_6]_n$ coordination compounds is an important and versatile tool for their characterization (**Table 5**). The high polarizability of xenon usually results in intense Raman-active Xe–F stretching bands for XeF_2 and its coordination compounds, whereas bands arising from A–F and M–F stretching modes are usually much less intense. The symmetric stretching mode of uncoordinated XeF_2[130] and the symmetric stretching mode of coordinated XeF_2 in compounds such as $XeF_2{\cdot}([XeF_5][AsF_6])_2$ [195] appear at or are slightly above 497 cm^{-1}. When XeF_2 is distorted, it may be regarded as being on the ionization pathway $XeF_2 \rightarrow XeF^+ + F^-$, so that the band at 497 cm^{-1} is replaced by two bands in the Raman spectrum. The higher frequency band is associated with the short Xe–F bond (ν(Xe–F_t)) and the lower frequency one is associated with the longer Xe–F bond of the fluorine bridge (ν(Xe–F_b)). In the extreme case where XeF_2 is completely ionized to XeF^+, the stretching frequency for XeF^+ should occur at 600 cm^{-1} or higher.[139]

The interaction strengths of the terminally coordinated XeF_2 molecules with the metal centers are indicated by the Xe–F_t stretching frequency, which ranges from 544 to 585 cm^{-1} (**Table 5**). The XeF_2 stretching frequencies of bridging XeF_2 molecules are in the range 510–534 cm^{-1} and are, as expected, closer to the symmetric stretching vibration of free XeF_2 (497 cm^{-1}). Shifts of the bridging XeF_2 stretching frequencies to higher values than free XeF_2 most likely result from the high Coulomb fields that these semi-ionic XeF_2 molecules experience when coordinated between two M^{n+} cations.

The AF_6^- octahedra are usually deformed by strong fluorine bridge interactions between the M atoms and AF_6^- anions as well as by interactions of the F atoms of the AF_6^- units with the positive Xe atoms of the XeF_2 molecules. As a consequence, the O_h symmetry of AF_6^- is lowered and, instead of three Raman-active vibrational modes, more bands appear that are assigned to AF_6^- vibrations because the doubly and triply degenerate bands are split, and bands that are formally Raman inactive under O_h symmetry are active under lower symmetries.[71,93,105,106,126,154,196,197]

Copyright © 2013. Elsevier. All rights reserved.

Comprehensive Inorganic Chemistry II : From Elements to Applications, Elsevier, 2013. ProQuest Ebook Central, http://ebookcentral.proquest.com/lib/inflibnet-ebooks/detail.action?docID=1330977.
Created from inflibnet-ebooks on 2021-02-09 22:27:13.

Table 5 Stretching modes of XeF_2 as a terminal and a bridging ligand[a]

Metal ion	*Anion*	***p***[b]	*ν(XeF$_2$)$_t$ (cm^{-1})*	*ν(XeF$_2$)$_b$ (cm^{-1})*	*Ref.*
Mg^{2+}	AsF_6^-	4	565(10)		177
Mg^{2+}	AsF_6^-	2	578(10), 585(sh)		177
Mg^{2+}	SbF_6^-	2	572(10), 582(sh)		192
Ca^{2+}	AsF_6^-	4	546(7.1)	533(10)	178
Ca^{2+}	AsF_6^-	2.5		519(10), 528(sh)	178
Ca^{2+}	PF_6^-	5	545(10)	522(4.0)	184
Sr^{2+}	AsF_6^-	3		531(10)	185
Pb^{2+}	AsF_6^-	3		514(10)	185
Ba^{2+}	NbF_6^-	5		510(10)	194
Ba^{2+}	PF_6^-	4		525(10)	179
Ba^{2+}	RuF_6^-	5		512(9.5), 525(sh)	194
Ba^{2+}	SbF_6^-	5		510(10), 521(5.8)	187
Cd^{2+}	AsF_6^-	4	547(10)	521(5.1)	190
Cd^{2+}	PF_6^-	5	546(10)	521(sh)	184
Cd^{2+}	SbF_6^-	5	544(10)		176
Nd^{3+}	AsF_6^-	2.5	575(10), 584(8.9)	534(1.5)	182
Nd^{3+}	AsF_6^-	3	568(10)		182
Nd^{3+}	SbF_6^-	3	566(9.1), 576(10)		192

[a]Frequencies are from the Raman spectra and relative intensities are given in parentheses.
[b]***p*** is the number of XeF_2 ligands per M^n cation and n is the net charge on the metal cation.

1.25.3.2.3.7 Solid-state NMR spectra

Solid-state ^{19}F and ^{129}Xe magic-angle spinning (MAS) NMR spectroscopy has been applied to the structural characterization of $[Mg(XeF_2)_2][AsF_6]_2$, $[Mg(XeF_2)_4][AsF_6]_2$, $[Ca(XeF_2)_{2.5}][AsF_6]_2$, $[Ba(XeF_2)_3][AsF_6]_2$, and $[Ba(XeF_2)_5][AsF_6]_2$.[193] The spectra were recorded for compounds having known and unknown crystal structures. The study has shown that bridging and terminal ^{19}F environments of coordinated XeF_2 can be distinguished. Fluorine-19 is the preferred nucleus for such studies because the ^{19}F chemical shifts are primarily dependent on their bridging and terminal natures, whereas the ^{129}Xe chemical shift is largely dependent on nonbonded interactions in the solid state. In addition, the extremely large shielding anisotropy of ^{129}Xe renders ^{129}Xe NMR spectroscopy very insensitive, causing difficulties in measuring $^1J(^{129}Xe-^{19}F)$ coupling constants. Each crystallographically distinct F atom bonded to Xe gave rise to a separate ^{19}F resonance. Furthermore, it was shown that the AsF_6^- anions of $[Mg(XeF_2)_4][AsF_6]_2$, $[Ca(XeF_2)_{2.5}][AsF_6]_2$, $[Ba(XeF_2)_3][AsF_6]_2$, and $[Ba(XeF_2)_5][AsF_6]_2$ rapidly reoriented on the NMR timescale, rendering the fluorines on arsenic equivalent on the NMR timescale, thereby emulating a perfectly octahedral environment. Thus, the static picture of fixed AsF_6^- anions, suggested by X-ray crystallography, has to be revised.

1.25.3.2.3.8 XeF_2 coordinated to main-group centers

Xenon difluoride behaves as a strong Lewis base toward Lewis acids of varying strengths such as AsF_5, SbF_5, BiF_5, NbF_5, TaF_5, RuF_5, VF_5, AuF_5, TiF_4, MnF_4, SnF_4, PdF_4, PtF_4, and CrF_4, forming XeF^+ and $Xe_2F_3^+$ salts.[121,122,139,198,199] Fewer cases exist where XeF_2 only functions as a ligand coordinated to the metal ion (see Section 1.25.3.2.1). In the former cases, a fluorine atom of XeF_2 is essentially transferred to the acid to form a XeF^+ salt. In the latter cases, the interaction of the XeF_2 molecule with a metal center is manifested by extension of the Xe–F bond to the coordinated fluorine atom and by shortening of the terminal Xe–F bond. A number of molecular addition compounds of XeF_2 are also known in which XeF_2 exhibits no tendency to coordinate. These are exemplified by $IF_5 \cdot XeF_2$,[200] $XeF_4 \cdot XeF_2$,[201] and $XeOF_4 \cdot XeF_2$,[202,203] which show that the XeF_2 vibrational frequencies and the Xe–F bond lengths are not significantly affected relative to those of XeF_2.

The α- and β-phases of $XeOF_4 \cdot XeF_2$ have been isolated and the crystal structure of the more stable α-phase was determined.[203] Each XeF_2 molecule is symmetrically coordinated through its fluorine ligands to four Xe(VI) atoms of the $XeOF_4$ molecules, which, in turn, are weakly coordinated to four XeF_2 molecules. The high-temperature phase, β-$XeOF_4 \cdot XeF_2$, was only characterized by low-temperature Raman spectroscopy. The geometric parameters and vibrational frequencies of both phases are essentially unaltered when compared with those of pure XeF_2 and $XeOF_4$.

The only examples presently known in which XeF_2 coordinates to nonmetal centers are $2XeF_2 \cdot [XeF_5][AsF_6]$, $XeF_2 \cdot [XeF_5][AsF_6]$, and $XeF_2 \cdot 2[XeF_5][AsF_6]$,[195] where XeF_2 coordinates to the Xe(VI) atom of the XeF_5^+ cation, and $[BrOF_2][AsF_6] \cdot XeF_2$[91,196] and $[BrOF_2][AsF_6] \cdot 2XeF_2$, where XeF_2 coordinates to Br(V) of the $BrOF_2^+$ cation.[196]

In the cases of the $BrOF_2^+$ adducts, the low-temperature solvolysis of $[XeOTeF_5][AsF_6]$ in liquid BrF_5 yielded an XeF_2 adduct of $BrOF_2^+$ according to eqn [50].

$$[XeOTeF_5][AsF_6] + (n+1)BrF_5 \xrightarrow[20\ ^\circ C]{BrF_5} [BrOF_2][AsF_6] \cdot XeF_2 \cdot nBrF_5 + TeF_6 \quad [50]$$

Slow cooling of this solution resulted in crystals of $[BrOF_2][AsF_6]$ in which the oxygen and fluorine atoms were positionally disordered. Alternatively, removal of the bulk solvent under dynamic vacuum at ca. −50 °C yielded pale yellow, polycrystalline $[BrOF_2][AsF_6] \cdot XeF_2 \cdot nBrF_5$. Continued pumping on $[BrOF_2][AsF_6] \cdot XeF_2 \cdot nBrF_5$ at −50 °C for several hours yielded $[BrOF_2][AsF_6] \cdot XeF_2$ as a white powder. Pumping at 0 °C for several more hours resulted in XeF_2 loss and the formation of $[BrOF_2][AsF_6]$.

Copyright © 2013. Elsevier. All rights reserved.

Comprehensive Inorganic Chemistry II : From Elements to Applications, Elsevier, 2013. ProQuest Ebook Central, http://ebookcentral.proquest.com/lib/inflibnet-ebooks/detail.action?docID=1330977.
Created from inflibnet-ebooks on 2021-02-09 22:27:13.

Dissolution of $[BrOF_2][AsF_6]\cdot XeF_2$ in aHF at −20 °C gave a clear, colorless solution which, when cooled to −78 °C, yielded a white precipitate consisting of a mixture of $[BrOF_2][AsF_6]\cdot 2XeF_2$ and $[BrOF_2][AsF_6]$ (eqn [51]). Slow cooling of the aforementioned solution resulted in the formation of crystalline $[BrOF_2][AsF_6]\cdot 2XeF_2$ between −28 and −32 °C. Pure $[BrOF_2][AsF_6]\cdot 2XeF_2$ was also synthesized by the reaction of $[BrOF_2][AsF_6]\cdot XeF_2$ or $[BrOF_2][AsF_6]$ with one and two equivalents, respectively, of XeF_2 in aHF (eqns [52] and [53]).

$$2[BrOF_2][AsF_6]\cdot XeF_2 \rightarrow [BrOF_2][AsF_6]\cdot 2XeF_2 + [BrOF_2][AsF_6] \quad [51]$$

$$[BrOF_2][AsF_6]\cdot XeF_2 + XeF_2 \rightarrow [BrOF_2][AsF_6]\cdot 2XeF_2 \quad [52]$$

$$[BrOF_2][AsF_6] + 2XeF_2 \rightarrow [BrOF_2][AsF_6]\cdot 2XeF_2 \quad [53]$$

The compound $[BrOF_2][AsF_6]\cdot 2XeF_2$ is isostructural and isomorphous with its krypton analog (see **Section 1.25.7.1**).[197] The primary coordination sphere around $BrOF_2^+$ is trigonal pyramidal where the weighted average of the Br–O (1.549(5) Å) and Br–F (1.734(4), 1.736(4) Å) bond lengths (1.673(4) Å) is slightly longer than the Br–O/F bond length in the disordered $[BrOF_2][AsF_6]$ (1.647(1) Å) structure. The F ligand of the AsF_6^- anion is coordinated trans to the O atom, whereas the F ligands of the XeF_2 molecules are coordinated trans to the F atoms of $BrOF_2^+$ so that the bromine coordination sphere is a distorted octahedron (**Figure 44**).

Coordination of XeF_2 molecules to $BrOF_2^+$ results in asymmetric Xe–F bond lengths, with bridging Xe–F bonds (2.052(4) and 2.053(4) Å) that are longer than the terminal Xe–F bonds (1.960(4) and 1.956(5) Å).[196] Such asymmetries have been observed for XeF_2 terminally coordinated to metal centers (see **Section 1.25.3.2.3**).[18,177]

The most intense vibrational bands in the Raman spectra of $[BrOF_2][AsF_6]\cdot 2XeF_2$ and $[BrOF_2][AsF_6]\cdot XeF_2$ are associated with the XeF_2 ligand stretching modes. Relative to the stretching bands of coordinated $BrOF_2^+$, they are less intense than the analogous KrF_2 stretching bands in $[BrOF_2][AsF_6]\cdot 2KrF_2$.[197] The assignments of the XeF_2 bands are in accordance with the assignments reported for XeF_2 molecules coordinated to metal centers.[18,177] The XeF_2 molecules of the complex were shown by calculations to exhibit strong couplings of their terminal $\nu(Xe–F_t)$ modes, whereas the bridging $\nu(Xe–F_b)$ stretching modes only weakly couple to one another. The opposite behavior was observed for $[BrOF_2][AsF_6]\cdot 2KrF_2$.[197]

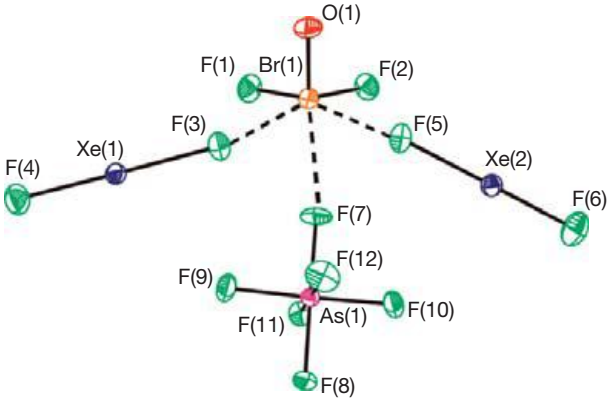

Figure 44 The structural unit in the X-ray crystal structure of $[BrOF_2][AsF_6]\cdot 2XeF_2$. Reproduced with permission from Brock, D. S.; Casalis de Pury, J. J.; Mercier, H. P. A.; Schrobilgen, G. J.; Silvi, B. *Inorg. Chem.* **2010**, *49*, 6673–6689.

An ELF (Electron Localization Function) and quantum theory of atoms in molecules (QTAIM) study revealed the localization domain associated with the valence electron lone pair of bromine decreased in size across the series $BrOF_2^+ > [BrOF_2][AsF_6]_3^{2-} > [BrOF_2][AsF_6]\cdot 2XeF_2 \approx [BrOF_2][AsF_6]\cdot 2KrF_2$,[197] as the Br(V) valence shell became more crowded.

Both $[BrOF_2][AsF_6]\cdot 2XeF_2$ and $[BrOF_2][AsF_6]\cdot XeF_2$ are kinetically stable for indefinite periods of time under anhydrous conditions at −78 °C.[196] An attempt to synthesize a XeF_4 adduct of $[BrOF_2][AsF_6]$ failed, in accordance with the lower fluoride ion donor ability of XeF_4 relative to that of XeF_2. The analogous chlorine systems, $[ClOF_2][AsF_6]/XeF_2$ and $[ClOF_2][AsF_6]/XeF_4$, were also investigated in the hope that $ClOF_2^+$, by virtue of the greater electronegativity of Cl(V), would prove to be a stronger Lewis acid. However, these attempts were unsuccessful. Warming of a mixture of $[ClOF_2][AsF_6]$ and XeF_2 in aHF to room temperature resulted in fluoride ion abstraction from XeF_2 by $ClOF_2^+$ to form $[Xe_2F_3][AsF_6]$ and $ClOF_3$. The latter result is indicative of the greater Lewis acid strength of $ClOF_2^+$ relative to that of $BrOF_2^+$.

1.25.3.2.3.9 *Quantum-chemical studies of krypton and xenon-fluoro species*

Atomization energies at 0 K, heats of formation at 0 and 298 K, and vibrational zero-point energies were calculated for XeF^+, XeF^-, XeF_2, XeF_4, XeF_5^-, and XeF_6,[204] for XeF_3^+, XeF_3^-, XeF_5^+, XeF_7^+, XeF_7^-, and XeF_8,[205] and for KrF^+, KrF^-, KrF_2, KrF_3^+, KrF_4, KrF_5^+, and KrF_6 [206] at the coupled-cluster level of theory. Evidence was presented for the fluxionality of XeF_6 caused by the presence of a sterically active free valence electron pair on Xe. The C_{3v} and O_h structures were shown to have essentially the same energy.[204] The geometries of XeF_6 and other AF_6E molecules have been studied by means of their ELFs.[207] The stabilities of noble-gas fluorides with respect to F_2 loss were studied and it was shown that XeF_8 and XeF_7^+ [205] and the krypton fluorides[206] are expected to be thermodynamically unstable, whereas XeF_3^+, XeF_5^+, XeF_3^-, XeF_5^-, and XeF_7^- are stable with respect to F_2 loss.[205] The F^+ and F^- affinities of Xe, XeF_2, XeF_4, and XeF_6 were also examined.[205] An analysis of the energetics of KrF_6 and KrF_4 indicates that KrF_6 could exist only at very low temperatures and the preparation of KrF_4 would be extremely difficult because the energy barriers toward fluorine atom loss are only 0.9 and 10 kcal mol^{-1}, respectively. Similar conclusions were arrived at for KrF_3^+ and KrF_5^+ which have calculated stabilities comparable to KrF_4.[206]

1.25.3.3 The XeF_3^- Anion

Of the binary xenon fluorides, only XeF_4 and XeF_6 form isolable anionic salts with fluoride ion donors. Xenon tetrafluoride behaves as a fluoride ion acceptor (calculated gas-phase FIA, fluonide ion affinity, 247.3 kJ mol^{-1})[205] toward alkali metal fluorides and the 'naked' fluoride ion source $[N(CH_3)_4][F]$ to give salts of the pentagonal planar XeF_5^- anion.[208] Xenon hexafluoride is a considerably stronger fluoride ion acceptor forming the XeF_7^- (FIA, 313.8 kJ mol^{-1})[204] and XeF_8^{2-} anions

Copyright © 2013. Elsevier. All rights reserved.

Comprehensive Inorganic Chemistry II : From Elements to Applications, Elsevier, 2013. ProQuest Ebook Central, http://ebookcentral.proquest.com/lib/inflibnet-ebooks/detail.action?docID=1330977.
Created from inflibnet-ebooks on 2021-02-09 22:27:13.

with alkali metal (Na, K, Rb, and Cs) fluorides.[209,210] Additionally, the NO^+ and NO_2^+ salts have been prepared by direct reaction of XeF_6 with NOF or NO_2F, namely, $[NO_2][XeF_7]$,[211] $[NO]_2[XeF_8]$,[212,213] and $[NO_2][Xe_2F_{13}]$.[211] The $[NO]_2[XeF_8]$ salt has been characterized by single-crystal X-ray diffraction.[212,213] Xenon hexafluoride also reacts with $[NF_4][HF_2]$ in aHF to give $[NF_4][XeF_7]$, which was converted to $[NF_4]_2[XeF_8]$ by selective laser photolysis.[214] The XeF_7^- and $Xe_2F_{13}^-$ anions have also been characterized by X-ray crystallography as their Cs^+ and NO_2^+ salts.[211]

Experimental evidence for the fluoride ion acceptor properties of XeF_2 in solution or in the solid state (FIA, 83.3 kJ mol^{-1})[205] has not been readily forthcoming.[205] Evidence for the XeF_3^- anion was obtained in the gas phase from the negative ion mass spectra of XeF_2 [215] and $XeOF_4$,[216] and from energy-resolved collision-induced dissociation studies of XeF_2.[217] The related $XeF_3\cdot$ radical has been stabilized in an argon matrix and characterized by IR spectroscopy and explored by kinetic measurements (see **Section 1.25.4.1.1**).[218] Although radiochemical experiments using ^{18}F (half-life = 109.7 min) have failed to confirm $^{18}F^-$ exchange with XeF_2 in water,[219] CH_2Cl_2,[220] and CH_3CN,[220] $^{18}F^-$ exchanges between $[^{18}F]$-HF, $[^{18}F]$-SiF_4, or $[^{18}F]$-AsF_5 and XeF_2 (through XeF^+ and $Xe_2F_3^+$ as intermediates) have been used for the synthesis of $[^{18}F]$-XeF_2,[221] which, in turn, was used for the preparation of $[^{18}F]$-2-fluoro-2-deoxy-D-glucose[222] and $[^{18}F]$-6-fluoro-L-3,4-dihydroxyphenylalanine.[223]

Chemical exchange between F^- and XeF_2 in CH_3CN solvent under rigorously anhydrous conditions was initially established by 2D ^{19}F–^{19}F exchange spectroscopy (EXSY) experiments.[220] Fluorine-19 exchange occurred between $[N(CH_3)_4][F]$ and XeF_2 in CH_3CN solvent at 15 °C, providing the first evidence for XeF_2/F^- exchange on the NMR timescale.[220] The ^{19}F exchange was postulated to proceed through XeF_3^- (eqn [54]).

$$XeF_2 + F^- \rightleftharpoons XeF_3^- \qquad [54]$$

The enthalpy of activation for this exchange, $\Delta H^{\ddagger}$, was subsequently investigated by single-selective inversion ^{19}F NMR spectroscopy and was determined to be 74.1 ± 5.0 kJ mol^{-1} (0.18 M) and 56.9 ± 6.7 kJ mol^{-1} (0.36 M) for equimolar amounts of $[N(CH_3)_4][F]$ and XeF_2 in CH_3CN solvent.[224]

Attempts have been made to synthesize $[N(CH_3)_4][XeF_3]$ by reaction of stoichiometric amounts of XeF_2 and $[N(CH_3)_4][F]$ in CH_3CN (1 h at −30 °C) and CHF_3 (0 °C for 12 h under autogenous pressure) solvents; however, only Raman bands arising from unreacted starting materials were observed.[224] The inability to form a XeF_3^- salt in either CHF_3 or CH_3CN solvents was attributed to the high solvation energies of fluoride ion in these polar solvents and to the low FIA of XeF_2. The syntheses of the Cs^+ and $N(CH_3)_4^+$ salts of XeF_3^- were also attempted in the absence of a solvent. Fusion of a fourfold molar excess of XeF_2 with CsF resulted in no reaction up to 170 °C. When a sixfold molar excess of XeF_2 with respect to $[N(CH_3)_4][F]$ was slowly heated to the melting point of XeF_2 (129 °C), rapid oxidative fluorination of the $N(CH_3)_4^+$ cation ensued, resulting in sample detonation. The inability to form XeF_3^- salts was supported by thermochemical calculations which indicated that XeF_3^- salt formation (eqn [55] is disfavored ($\Delta G°_{rxn}$ ($[Cs][XeF_3]$, s) = 114 kJ mol^{-1} and $\Delta G°_{rxn}$ ($[N(CH_3)_4][XeF_3]$, s) = 31 kJ mol^{-1}).[224]

$$[M][F](s) + XeF_2(s) \rightarrow [M][XeF_3](s) \quad (M = Cs^+, N(CH_3)_4^+) \qquad [55]$$

Computational studies have been used to investigate XeF_3^- in the gas phase,[205,217] and in CH_3CN solution.[224] The XeF_3^- anion represents the first example of an AX_3E_3 VSEPR arrangement of three electron lone-pair and three bond-pair domains, resulting in a highly crowded xenon valence shell for this species. The effect this crowding has on the molecular geometry of XeF_3^- is therefore of considerable interest. DFT calculations with the B3LYP functional indicated that the XeF_3^- anion (C_{2v}) is the energy-minimized structure (all frequencies real) when either an all-electron Maroulis basis set or an ECP basis set (SDB-cc-pVTZ) was used for xenon.[217] The $F_2Xe\cdots F^-$ adduct (C_{2v}) was higher in energy than the XeF_3^- anion by 2.1–15.1 kJ mol^{-1} [217] and was a transition state (one imaginary frequency). However, this work overlooked a lower-energy, ground-state conformation of the $F_2Xe\cdots F^-$ adduct possessing a lower symmetry (C_s), as found in a later study (4.85 kJ mol^{-1} lower than the C_{2v} structure at the CCSD(T)/aVTZ level of theory).[205] The existence of the XeF_3^- anion as a transition state was not explored.[205]

The transition state (XeF_3^-) was shown to be more strongly covalently bound than the ground-state F_2Xe---F^- adduct. Using DFT methods, the Y-shaped XeF_3^- anion (C_{2v} symmetry; **Figure 45(a)**) possesses three similar Xe−F bond lengths.[224] The two large angles and one small angle allow for the retention of the torus, comprised of three electron lone pairs, around the xenon atom as shown by the ELF analysis (**Figure 46**). The structure was also computed at the CCSD/aVTZ level of theory and found to possess similar geometric parameters to that of the DFT structure. The energy-minimized geometry of the ground-state F_2Xe---F^- anion (C_s symmetry) is a distorted Y-shaped geometry having two shorter, nearly equal Xe−F bonds and a third longer Xe−F bond (**Figure 45(b)**). The F^- anion is only weakly bound to XeF_2, while the XeF_3^- anion exists as a first-order transition state in the fluoride ion-exchange mechanism.

Quantum-chemical calculations at the CCSD/aVTZ level of theory,[224] using a continuum solvent model (CH_3CN), accurately reproduced the transition-state enthalpy observed by ^{19}F NMR spectroscopy and showed a negative but negligible enthalpy for the formation of the F_2Xe---F^- adduct in this solvent.

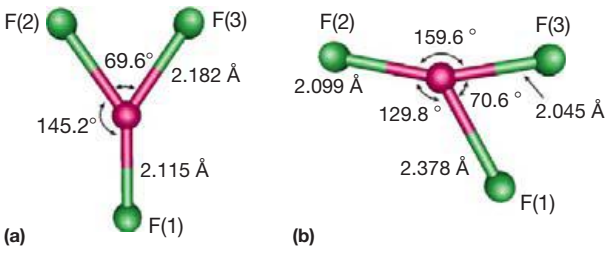

Figure 45 Calculated gas-phase geometries (PBE1PBE/aVTZ) of (a) the XeF_3^- anion (transition state, C_{2v} symmetry), and (b) the F_2Xe---F^- adduct (ground state, C_s symmetry). Reproduced with permission from Vasdev, N.; Moran, M. D.; Tuononen, H. M.; Chirakal, R.; Suontamo, R. J.; Bain, A. D.; Schrobilgen, G. J. *Inorg. Chem.* **2010**, *49*, 8997–9004.

Copyright © 2013. Elsevier. All rights reserved.

Comprehensive Inorganic Chemistry II : From Elements to Applications, Elsevier, 2013. ProQuest Ebook Central, http://ebookcentral.proquest.com/lib/inflibnet-ebooks/detail.action?docID=1330977.
Created from inflibnet-ebooks on 2021-02-09 22:27:13.

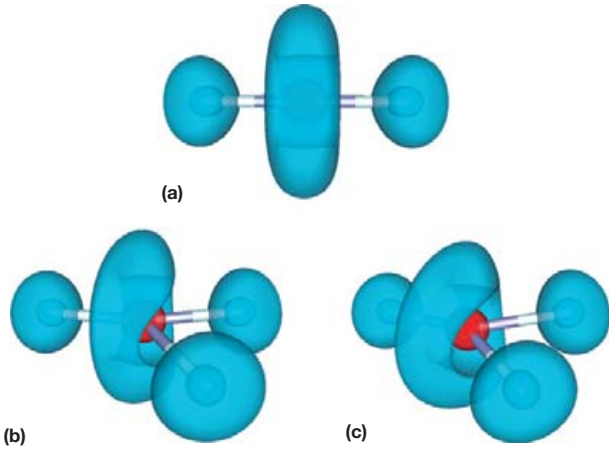

Figure 46 Electron localization function isosurfaces (contour level 0.7) of (a) XeF_2, (b) the $F_2Xe{\cdots}F^-$ adduct, and (c) the XeF_3^- anion (calculated at the PBE1PBE/aVTZ level of theory). Color scheme: blue, lone-pair (monosynaptic) basin; red, core basin. Reproduced with permission from Vasdev, N.; Moran, M. D.; Tuononen, H. M.; Chirakal, R.; Suontamo, R. J.; Bain, A. D.; Schrobilgen, G. J. *Inorg. Chem.* **2010**, *49*, 8997–9004.

1.25.4 Xe(IV) Compounds

Among the principal formal oxidation numbers of xenon, +4 has been the least studied. Prior to 2000, the chemistry of Xe(IV) was limited to two XeF_3^+ salts,[225–227] XeF_5^-,[208] XeF_4,[228–230] $Xe(OTeF_5)_4$,[229,231,232] $Xe(OTeF_5)_{4-x}F_x$ ($x=0$–3),[229] $C_6F_5XeF_2^+$,[233] $F_3XeOIOF_4$,[234] and $F_xXe(OTeF_5)_{3-x}^+$ ($x=0$–2),[235] and to preliminary reports of $XeOF_2$[236–238] and $XeOF_3^-$.[238]

1.25.4.1 Neutral Xe(IV) Species

1.25.4.1.1 $[Mg(XeF_2)(XeF_4)][AsF_6]_2$

A number of compounds have been synthesized in which XeF_2 and KrF_2 function as ligands (see Sections 1.25.3.2.3 and Section 1.25.7.1); however, only one compound, $[Mg(XeF_2)(XeF_4)][AsF_6]_2$, is presently known in which XeF_4 serves as a ligand. The difficulties encountered in forming XeF_4 adducts are attributable to the lower fluorobasicity of XeF_4 relative to those of XeF_2 and KrF_2. Reaction of a 1:1 or a higher molar ratio of XeF_4:XeF_2 with $Mg(AsF_6)_2$ in aHF yielded only $[Mg(XeF_2)(XeF_4)][AsF_6]_2$. In reactions involving the use of excess XeF_4, unreacted XeF_4 was removed under dynamic vacuum at room temperature. When a 2:1 or higher molar ratio of XeF_2:Mg was used, the only product was $[Mg(XeF_2)_2][AsF_6]_2$, which is again in accordance with the higher basicity of XeF_2 relative to that of XeF_4.[239]

The coordination around Mg^{2+} in the crystal structure of $[Mg(XeF_2)(XeF_4)][AsF_6]_2$ is pseudo-octahedral with four equatorial fluorine bridge contacts to four independent AsF_6^- anions and single fluorine bridge contacts to XeF_2 and XeF_4 that are trans to one another (Figure 47). The Mg^{2+} cations and AsF_6^- anions form chains with the trans-coordinated XeF_2 and XeF_4 molecules alternating positions (Figure 48).[239]

The Xe---F bridge bonds are elongated for both XeF_2 (2.059(7) Å) and XeF_4 (2.083(6) Å) relative to the Xe–F bond trans to it (1.936(7) Å and 1.871(7) Å, respectively).

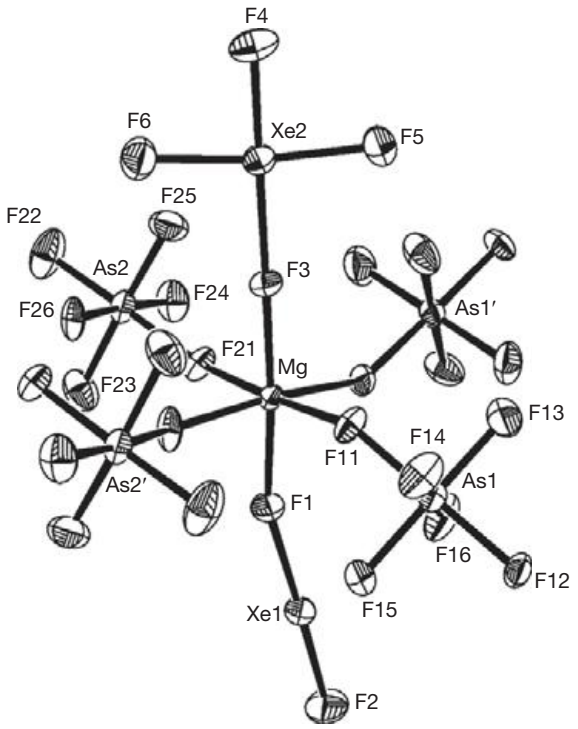

Figure 47 The coordination environment of Mg^{2+} in the crystal structure of $[Mg(XeF_2)(XeF_4)][AsF_6]_2$. Reproduced with permission from Tavčar; G.; Žemva, B. *Angew. Chem., Int. Ed.* **2009**, *48*, 1432–1434.

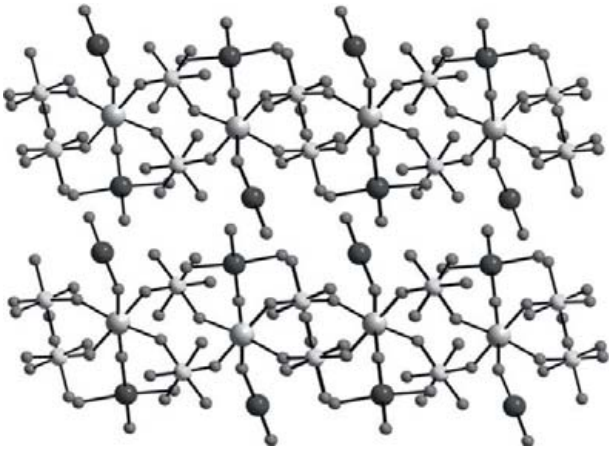

Figure 48 View of the structure of $[Mg(XeF_2)(XeF_4)][AsF_6]_2$ along the *b*-axis. Reproduced with permission from Tavčar; G.; Žemva, B. *Angew. Chem., Int. Ed.* **2009**, *48*, 1432–1434.

The Xe–F bonds cis to the bridge bond of XeF_4 (1.916(7) and 1.906(7) Å) are also somewhat shorter than those in free XeF_4 (1.953(2) Å).[230] The greater fluoride ion basicity of XeF_2 relative to that of XeF_4 is not clearly reflected in the Mg–F bond distances where the distance for XeF_2 (1.935(7) Å) appears to be slightly shorter than that of XeF_4 (1.956(7) Å), but the bond length difference is within $\pm 3\sigma$ and is not statistically significant. There is a secondary contact (3.103(8) Å) between a fluorine of XeF_2 in one layer with the xenon atom of XeF_4 in the next layer which helps stabilize the lattice.[239]

Copyright © 2013. Elsevier. All rights reserved.

Comprehensive Inorganic Chemistry II : From Elements to Applications, Elsevier, 2013. ProQuest Ebook Central, http://ebookcentral.proquest.com/lib/inflibnet-ebooks/detail.action?docID=1330977.
Created from inflibnet-ebooks on 2021-02-09 22:27:13.

The Raman spectrum of $[Mg(XeF_2)(XeF_4)][AsF_6]_2$ was also compared with the Raman spectra of XeF_4 and $[XeF_3][SbF_6]$.[239] The bands attributed to XeF_4 in the complex were intermediate with respect to those of XeF_4 and $[XeF_3][SbF_6]$ and therefore are consistent with XeF_4 coordination. The bands at 605, 596 (sh), and 552 cm^{-1} were assigned to the XeF_4 ligand, coordinated to Mg^{2+}, and the intense band at 575 cm^{-1} was assigned to the stretching mode of the terminal Xe−F bond of coordinated XeF_2. A weak band at 460 cm^{-1} was attributed to coupling between XeF_2 and XeF_4 vibrations but has not been explicitly assigned.

1.25.4.1.2 $XeOF_2$, $F_2OXeN{\equiv}CCH_3$, $XeOF_2 \cdot nHF$, and XeO_2

Although vibrational spectroscopic evidence for $XeOF_2$ had been communicated on three prior occasions,[236,237,240] these studies have not provided unambiguous characterizations or the isolation of $XeOF_2$ as a pure phase. Co-condensation of H_2O and XeF_4 vapors at low temperatures reportedly produced $XeOF_2$.[236,237] In both studies, the IR spectra of the co-deposited thin films were in good agreement. Bulk co-condensed samples were also prepared and characterized by Raman spectroscopy.[237] Both the bulk co-condensation product[237] and the IR spectra obtained from thin films[236,237] were subsequently shown to be mixtures of $XeOF_2$ and $XeOF_2 \cdot n$HF.[240] Shortly after these first reports, one of the components, $XeOF_2 \cdot n$HF, was synthesized in pure form by the hydrolysis of finely divided XeF_4 in HF at −63 °C, characterized by Raman spectroscopy, and assigned to $XeOF_2$.[238] These long-standing ambiguities among the published vibrational assignments ascribed to $XeOF_2$ were clarified when bulk syntheses of pure $XeOF_2$, as well as its HF and CH_3CN adducts, $XeOF_2 \cdot n$HF and $F_2OXeN{\equiv}CCH_3$, were achieved.[240]

The low-temperature hydrolysis of XeF_4 in a CH_3CN solution containing 2.00 M H_2O resulted in the isolation of $F_2OXeN{\equiv}CCH_3$ (eqn [56]), which crystallized as pale yellow blades at −35 to −45 °C. Pure $XeOF_2$ was obtained by pumping on polycrystalline $F_2OXeN{\equiv}CCH_3$ for several hours at −45 to −42 °C, which resulted in removal of adducted CH_3CN, and yielded bright yellow $XeOF_2$ (eqn [57]). Solvolysis of $XeOF_2$ in aHF at −78 °C resulted in a pale yellow and insoluble powder attributable to $XeOF_2 \cdot n$HF (eqn [58]). Removal of bound HF by pumping at −78 °C gave $XeOF_2$. In the case of $XeOF_2 \cdot n$HF, it has been shown by calculation of the energy-minimized structures for $XeOF_2 \cdot$HF and $XeOF_2 \cdot 2$HF, and by comparison of the calculated and experimental vibrational frequencies resulting from $^{16/18}O$ and $^{1/2}H$ isotopic substitution, that n is most likely one, and that HF is coordinated to $XeOF_2$ by means of weak O---H and Xe---F bonds (**Figure 49**).[240]

$$XeF_4 + H_2O + CH_3CN \xrightarrow[-45 \text{ to } -42\,^{\circ}C]{CH_3CN} F_2OXeN{\equiv}CCH_3 + 2HF \quad [56]$$

$$F_2OXeN{\equiv}CCH_3 \xrightarrow[-45 \text{ to } -42\,^{\circ}C]{\text{dynamic vac.}} XeOF_2 + CH_3CN \quad [57]$$

$$XeOF_{2\,(s)} + nHF \xrightarrow[12\text{ h, } -78\,^{\circ}C]{HF} XeOF_2 \cdot nHF \quad [58]$$

All three compounds, $F_2OXeN{\equiv}CCH_3$, $XeOF_2$, and $XeOF_2 \cdot n$HF, were kinetically stable at −78 °C for indefinite periods of time, but decomposed rapidly to explosively with emission of blue light upon warming to 0 °C.[240] Two decomposition pathways were proposed based on controlled

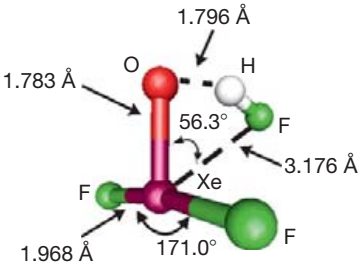

Figure 49 The geometry of $XeOF_2 \cdot$HF calculated at the MP2/(SDB-)cc-pVTZ level. Reproduced with permission from Brock, D. S.; Bilir, V.; Mercier, H. P. A.; Schrobilgen, G. J. *J. Am. Chem. Soc.* **2007**, *129*, 3598–3611.

low-temperature decompositions of solid $XeOF_2$ and $XeOF_2$ in CH_3CN solutions monitored by Raman and ^{19}F NMR spectroscopy, respectively. The major gas-phase decomposition pathway was O_2 elimination to produce XeF_2, whereas the minor pathway was disproportionation to XeF_2 and XeO_2F_2. Both pathways are supported by large negative ΔH^{o}_{rxn} and ΔG^{o}_{rxn} values (eqns [59] and [60]).

$$XeOF_{2(g)} \rightarrow XeF_{2(g)} + \tfrac{1}{2}O_{2(g)} \quad [59]$$

$\Delta H^{o}_{rxn} = -245.8$ kJ mol^{-1}

$\Delta G^{o}_{rxn} = -259.3$ kJ mol^{-1} MP2/(SDB−)cc–pVTZ

$$2XeOF_{2(g)} \rightarrow XeF_{2(g)} + XeO_2F_{2(g)} \quad [60]$$

$\Delta H^{o}_{rxn} = -98.8$ kJ mol^{-1}

$\Delta G^{o}_{rxn} = -86.9$ kJ mol^{-1} MP2/(SDB−)cc−pVTZ

By contrast with aHF solvent, $XeOF_2$ has an appreciable solubility in CH_3CN, allowing the characterization of $F_2OXeN{\equiv}CCH_3$ by ^{19}F, ^{17}O, and ^{129}NMR spectroscopy.[240] The ^{19}F NMR spectrum of $F_2OXeN{\equiv}CCH_3$ consisted of a singlet (−48.8 ppm) with accompanying ^{129}Xe satellites corresponding to $^1J(^{19}F-^{129}Xe) = 3446$ Hz. A triplet ($\delta(^{129}Xe)$, 242.3 ppm) arising from $^1J(^{129}Xe-^{19}F) = 3447$ Hz was observed in the ^{129}Xe NMR spectrum. Separate resonances for bound and free CH_3CN were not observed, suggesting that the interaction(s) were labile under the conditions used to obtain their spectra.

Oxygen-17 enriched water (35.4%, ^{16}O; 21.9%, ^{17}O; 42.77%, ^{18}O) dissolved in CH_3CN was used to synthesize $Xe^{17}OF_2$.[240] The central line and its ^{129}Xe satellites in the ^{19}F NMR spectrum were split as a result of the secondary isotope effect of ^{16}O and ^{18}O on the ^{19}F chemical shift [$^2\Delta^{19}F(^{18/16}O) = -0.0136$ ppm] and is the only two-bond isotope shift that has been observed for a xenon compound. A broad resonance at $\delta(^{17}O) = 209$ ppm ($\Delta\nu_{1/2} = 1300$ Hz) in the ^{17}O NMR spectrum was assigned to $XeOF_2$ and a weak, but very sharp resonance at $\delta(^{17}O) = 77.7$ ppm ($\Delta\nu_{1/2} = 10$ Hz) was tentatively assigned to acetonitrile *N*-oxide, $CH_3C{\equiv}N^+-O^-$. The latter was presumed to have formed by $XeOF_2$ attack of CH_3CN.[240]

The solid-state ^{16}O- and ^{18}O-enriched vibrational spectra of $XeOF_2$ and the calculated energy-minimized dimer and trimer geometries, and their vibrational frequencies, point to an extended structure in which neighboring $XeOF_2$ molecules

Copyright © 2013. Elsevier. All rights reserved.

Comprehensive Inorganic Chemistry II : From Elements to Applications, Elsevier, 2013. ProQuest Ebook Central, http://ebookcentral.proquest.com/lib/inflibnet-ebooks/detail.action?docID=1330977.
Created from inflibnet-ebooks on 2021-02-09 22:27:13.

weakly interact by means of asymmetric –O---Xe–O--- bridges and weaker Xe---F contacts.[240] The solid-state ^{16}O- and ^{18}O-enriched vibrational spectra of $F_2OXeN{\equiv}CCH_3$ and the calculated energy-minimized geometries and their vibrational frequencies show that ν(Xe–O) decreases across the series $F_2OXeN{\equiv}CCH_3$ (754.7, 762.4, 766.8 cm^{-1}), $XeOF_2$ (749.9 cm^{-1}), and $XeOF_2{\cdot}n$HF (733.5 cm^{-1}). This is in accordance with the decreased double-bond character that accompanies oxygen coordination in $XeOF_2$ and $XeOF_2{\cdot}$ n HF.[240]

Although considerably weaker than any of the presently known Xe(II)–N bonds, the crystal structure of $F_2OXeN{\equiv}CCH_3$ provides the only example of a Xe(IV)–N bond.[240] Two adduct conformations were observed where the coordinated CH_3CN molecule lies in the $XeOF_2$ plane, or is bent out of the $XeOF_2$ plane as a consequence of crystal packing (**Figure 50**). The primary xenon coordination sphere is a T-shaped arrangement of two valence electron lone pairs and an oxygen double-bond domain in the equatorial plane and two mutually trans-fluorine atoms perpendicular to that plane. The Xe–O bond lengths were equal for both conformers (1.778(4), 1.782(4) Å) while the Xe–F bond lengths of the out-of-plane conformation (1.975(3), 1.981 (3) Å) were slightly elongated relative to the Xe–F bond lengths of the in-plane conformation (1.952(3), 1.958(3) Å). These elongations correspond to a shorter Xe–N bond length for the out-of-plane conformation (2.752(5) Å) relative to that of the in-plane conformation (2.808(5) Å).

Shortly after the discovery of noble-gas reactivity, it was shown that hydrolysis of XeF_6 gave XeO_3 which was isolated as a white solid.[241,242] Soon thereafter, the pale yellow, volatile solid, XeO_4, was synthesized.[243,244] Both oxides are shock sensitive and highly endothermic (ΔH_f XeO_3, 402 kJ mol^{-1};[245] XeO_4, 643 kJ mol^{-1} [246]). Monomeric XeO has not been synthesized, but it has been shown by gas-phase quantum-chemical calculations to have an unstable $^1\Pi$ ground state.[247] Studies of the hydrolysis of XeF_4 initially postulated that the product was $Xe(OH)_4$ or $XeO_2{\cdot}2H_2O$,[248] but subsequent studies showed the product to be XeO_3, which resulted from redox disproportionation (eqn [61]).[249,250] Another early hydrolysis study of XeF_4 in aqueous H_2SO_4 reported a transient yellow solid at 0 °C which was never isolated or characterized.[251]

$$4XeF_4 + 8H_2O \xrightarrow{H_2} 2XeO_3 + 2Xe + O_2 + 16HF \qquad [61]$$

Recently, the yellow solid was investigated by low-temperature Raman spectroscopy and shown to be the missing Xe(IV) oxide, XeO_2.[252] Xenon dioxide was synthesized at 0 °C by hydrolysis of XeF_4 in water and in 2.00 M H_2SO_4 (eqn [62]). Vibrational assignments were aided by $^{16/18}O$ isotopic enrichment.

$$nXeF_4 + 2nH_2O \rightarrow (XeO_2)_n + 4nHF \qquad [62]$$

The striking similarity between the Raman spectrum of XeO_2 and that of XeF_4 [253] (see **Table 6**) led to the conclusion that XeO_2 does not exist as a bent monomer (Structure I), but possesses an extended structure in which Xe(IV) is oxygen bridged to four neighboring oxygen atoms to give a local square-planar XeO_4 geometry based on an AX_4E_2 VSEPR (valence shell electron pair repulsion) arrangement of bond pairs and valence electron lone pairs (Structure II).[252]

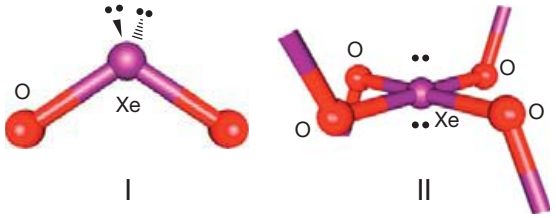

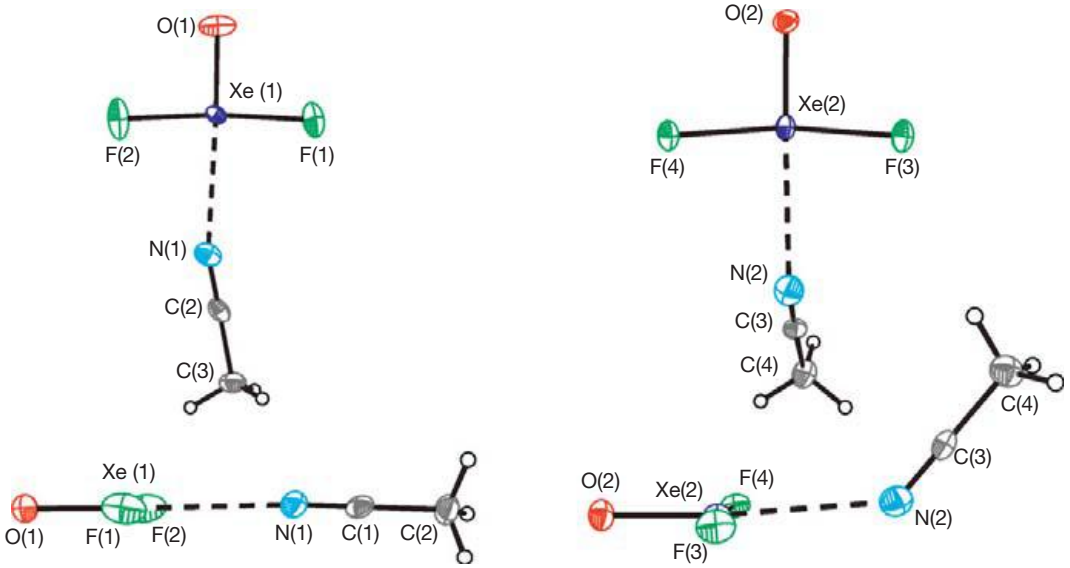

Figure 50 The X-ray crystal structure of $F_2OXeN{\equiv}CCH_3$ showing two independent structural units with thermal ellipsoids shown at the 50% probability level. Reproduced with permission from Brock, D. S.; Bilir, V.; Mercier, H. P. A.; Schrobilgen, G. J. *J. Am. Chem. Soc.* **2007**, *129*, 3598–3611.

Copyright © 2013. Elsevier. All rights reserved.

Comprehensive Inorganic Chemistry II : From Elements to Applications, Elsevier, 2013. ProQuest Ebook Central, http://ebookcentral.proquest.com/lib/inflibnet-ebooks/detail.action?docID=1330977.
Created from inflibnet-ebooks on 2021-02-09 22:27:13.

Table 6 Vibrational frequencies for XeF_4, $Xe^{16}O_2$, $Xe^{16/18}O_2$, and $Xe^{18}O_2$ [a]

XeF_4 [b]	$Xe^{16}O_2$ [c]	$Xe^{16/18}O_2$ [c,d]	$Xe^{18}O_2$ [c]	D_{2d} [e]	Assgnts ($L = F, O$) [f]
586 $\nu_6,\nu(E_u)$	632.3(1)	626.5sh	625.8(1)	$\nu(E)$	$\nu_{as}(XeL_t–XeL_t)$
554 $\nu_1,\nu(A_{1g})$ } 524 $\nu_4,\nu(B_{2g})$ }	570.3(100)	550.9(100)	542.6(100)	$\nu(A_1)$ / $\nu(B_2)$	$\nu_s(XeL_4)$ / $\nu_{as}(XeL_{2t}–XeL_{2t})$
291 $\nu_3,\nu(A_{2u})$	283.9(3)	276.9(2)	270.0(3)	$\nu(B_2)$	$\delta(XeL_4)$ o.o.p., umbrella mode
218 $\nu_2,\nu(B_{1g})$	239.1(2) / 227.9(4)	231sh / 221.3(4)	226.6(2) } 216.9(6) }	$\nu(B_1)$	$\delta(XeL_{2c}+XeL_{2c})$
n.o. $\nu_5,\nu(B_{2u})$	n.o.	n.o.	n.o.	$\nu(A_2)$	$\delta(XeL_{2t})$ o.o.p. – $\delta(XeL_{2t})$ o.o.p.
161 $\nu_7,\nu(E_u)$ [g]	168.9(13)	165.0(19)	161.1(13)	$\nu(E)$	$\delta(XeL_{2t})$ i.p.
	99.5(14)	99.3(17)	99.5(15)		lattice mode

[a] Frequencies are given in cm^{-1}.
[b] From Ref. 253. The symmetries refer to the D_{4h} point symmetry of XeF_4.
[c] Values in parentheses denote Raman intensities.
[d] The sample was prepared by hydrolysis of XeF_4 in an equimolar mixture of $H_2{}^{16}O$ and $H_2{}^{18}O$.
[e] The symmetries refer to the local D_{2d} point symmetry of the XeO_4 units in the extended structure of XeO_2.
[f] The abbreviations denote trans (t), cis (c), symmetric (s), asymmetric (as), stretch (ν), bend (δ), in-plane bend (i.p.), and out-of-plane bend (o.o.p.). The in-plane and out-of-plane mode descriptions are relative to the molecular planes of XeF_4 and the XeO_4-unit.
[g] This mode was not directly observed. The frequency was obtained from the $2\nu_7$ overtone at 322 cm^{-1}.
Source: Reproduced with permission from Brock, D. S.; Schrobilgen, G. J. *J. Am. Chem. Soc.* **2011**, *133*, 6265–6269.

Xenon dioxide also has implications for understanding xenon depletion from the atmospheres of Earth and Mars. Both atmospheres are depleted by a factor of approximately 20 relative to the lighter noble gases based on comparisons with chondrites.[254] A number of explanations have been advanced to account for atmospheric xenon depletion; however, the majority have been shown to be untenable,[255] including a recent explanation[256] which proposed that reaction between xenon and iron may occur at high pressures and high temperatures. Xenon has been shown to undergo metallization at high pressures and high temperatures, forming an *hcp* lattice, similar to that of iron. It was shown, however, that no compounds and no detectable dissolution of xenon into crystalline *hcp* iron occur even above the metallization pressure of xenon and that the ratio of *hcp* xenon and iron actually varies in opposite directions with increasing pressure.[256]

A proposal that xenon may be covalently bonded within SiO_2 [255] gained credibility when the most intense band in the Raman spectrum of XeO_2[252] was shown to agree closely with a vibrational band observed in xenon-doped SiO_2.[255] The former study proposed that xenon displaces silicon from quartz (SiO_2) at the high pressures (0.7–5 GPa) and temperatures (500–1500 K) that are encountered in the continental crust, with the implication that xenon may be retained within silicate minerals and SiO_2 as XeO_2.[255] The high abundance of SiO_2 would serve as a readily available reservoir for xenon and the experimental results indicated that xenon is covalently bound to oxygen in the SiO_2 lattice (~2.2 wt.% at 10 GPa and 2273 K).

A related ab initio study also proposed incorporation of xenon into SiO_2 as a covalently bound Xe–O species.[257] The energies associated with the incorporation of Xe into interstitial sites, along with the valencies of Si and O in SiO_2, were calculated. The study showed that while there was a barrier to insertion at all sites at $T = 0$ K, at the temperatures and pressures encountered in the Earth's crust, incorporation of Xe into interstitial spaces was energetically favorable. Under the aforementioned experimental conditions,[255] xenon could be incorporated at the Si site if the process occurred in two stages, namely, the elimination of Si to produce peroxide linkages, followed by the incorporation of xenon.[257]

1.25.4.2 Xe(IV) Cations

As noted in **Sections 1.25.3.1.1** and **1.25.3.2**, organoxenon(II) compounds have been prepared in the form of cationic xenonium compounds, [RXe][X], and neutral species having the general formulae, RXeF and RXeR′. In most cases, Xe(II)–C bond formation occurs through nucleophilic substitution with organoboranes, also referred to as xenodeborylation (eqn [63]), and, in some specific cases, through electrophilic substitution on electron-poor aromatic compounds, also referred to as xenonylation (eqn [64]).

$$XeF_2 + RBX_2 \rightarrow [RXe][BF_2X_2] \quad [63]$$

$$X{-}Xe{-}Y + C_6H_x(CF_3,F)_{6-x} \rightarrow \left[\left(C_6H_{x-1}(CF_3,F)_{5-x}\right)Xe\right][X] + HY \quad [64]$$

The former method was successfully used with XeF_4 to synthesize the first organoxenon(IV) compound.[233] The increased oxidation potential of XeF_4 relative to XeF_2 requires oxidatively resistant reactants and products having electron-poor organic groups. These criteria were achieved by the use of $C_6F_5BF_2$, which yields BF_4^- as the counteranion. In addition, the Lewis acidity of $C_6F_5BF_2$ is sufficient to polarize the hypervalent F–Xe–F bond, allowing transfer of the C_6F_5 group without initial complete fluoride ion abstraction.

Dichloromethane proved to be a suitable solvent, having the added advantage of facilitating the isolation of the insoluble product salt. As a result, $[C_6F_5XeF_2][BF_4]$ could be obtained in nearly quantitative yield by the reaction of $C_6F_5BF_2$ with a suspension of XeF_4 in CH_2Cl_2 at −55 °C (eqn [65]):[233]

$$C_6F_5BF_2 + XeF_4 \xrightarrow[-55\ ^\circ C]{CH_2Cl_2} [C_6F_5XeF_2][BF_4] \quad [65]$$

Other solvents were ineffective because solvents that were too acidic resulted in oxidation of the aromatic system and basic

Copyright © 2013. Elsevier. All rights reserved.

Comprehensive Inorganic Chemistry II : From Elements to Applications, Elsevier, 2013. ProQuest Ebook Central, http://ebookcentral.proquest.com/lib/inflibnet-ebooks/detail.action?docID=1330977.
Created from inflibnet-ebooks on 2021-02-09 22:27:13.

solvents, such as CH_3CN, hindered nucleophilic substitution to an extent that the desired product was not observed. The salt, $[C_6F_5XeF_2][BF_4]$, was a yellow solid that decomposed above −2 °C and was insoluble in CH_2Cl_2, but soluble in CH_3CN, forming a bright yellow solution which was characterized by ^{19}F, ^{129}Xe, ^{13}C, and ^{11}B NMR spectroscopy at −40 °C. The $C_6F_5XeF_2^+$ cation and the neutral isoelectronic $C_6F_5IF_2$ molecule are predicted to have T-shaped geometries based on AX_2YE_2 VSEPR arrangements.[233]

The ^{19}F NMR chemical shifts of the *p*-F and *m*-F substituents of the C_6F_5 ring in $C_6F_5XeF_2^+$ were significantly shifted to high frequency relative to those of $C_6F_5IF_2$. The ^{19}F resonances (−40 °C) of the axial fluorine atoms bound to Xe(IV) of the cation occurred at −29.54 ppm with $^1J(^{19}F-^{129}Xe) = 3893$ Hz. The *o*-F, *p*-F, and *m*-F environments of the C_6F_5 group occurred at −125.5, −134.97, and −153.44 ppm, respectively, and BF_4^- occurred at −149.01 ppm. The ^{129}Xe NMR spectrum consisted of a triplet centered at −1706.5 ppm, which is significantly more shielded with respect to XeF_4 (316.9 ppm),[208] displaying the same trend that was observed when going from XeF_2 (−1784.5 ppm) to $C_6F_5Xe^+$ (−3807.8 ppm). The ^{13}C chemical shift of carbon bound to Xe appeared at 121.86 ppm.[233]

The strong oxidative fluorinating ability of the XeF_2 moiety in $C_6F_5XeF_2^+$ is indicated by the oxidation of $P(C_6F_5)_3$ to $(C_6F_5)_3PF_2$, I_2 to IF_5, and C_6F_5I to $C_6F_5IF_2$ with the formation of the reduction product, $C_6F_5Xe^+$. The latter reactions have been achieved with other typically strong oxidizing agents such as F_2,[258] XeF_2,[259] ClF, $ClOCF_3$, Cl_2O,[260] and $HNO_3/(CF_3CO)_2O$.[233,261]

The crystal structure of $[XeF_3][Sb_2F_{11}]$, which has previously been reported,[46] has been redetermined at −173 °C, yielding a higher precision structure.[93] In an early attempt to synthesize $[XeF_3][As_2F_{11}]$ from XeF_4 and excess liquid AsF_5 at −100 °C, only $[XeF_3][AsF_6]$ was obtained with no evidence for $[XeF_3][As_2F_{11}]$.[262] More recent estimates of the corresponding gas-phase free energies of $[XeF_3][AsF_6]$ and $[XeF_3][As_2F_{11}]$ using volume-based thermodynamics (VBT) suggest instability or marginal stability for $[XeF_3][AsF_6]$ ($\Delta G = 14 \pm 15$ kJ mol^{-1}) and $[XeF_3][As_2F_{11}]$ ($\Delta G = 20 \pm 26$ kJ mol^{-1}) when the calculated errors are taken into account.[93]

1.25.4.3 The $XeOF_3^-$ Anion

Although the $XeOF_3^-$ anion was reported previously,[238] there were several ambiguities with regard to vibrational band assignments. With a high-yield synthesis of $XeOF_2$ in hand (see Section 1.25.4.2.1), the fluoride ion acceptor properties of $XeOF_2$ were investigated by the syntheses of the endothermic salts, $[M][XeOF_3]$ (M = $N(CH_3)_4$, Cs), in high yields and purities.[263] The salts were synthesized by the reaction of $XeOF_2$ with [M][F] in CH_3CN solvent (eqn [66]) and are kinetically stable at −78 °C, slowly decomposing at 10–25 °C (eqns [67] and [68]).

$$XeOF_2 + [M][F] \xrightarrow[-45\ ^\circ C]{CH_3CN} [M][XeOF_3] \quad [66]$$

$$[M][XeOF_3] \rightarrow XeF_2 + \tfrac{1}{2}O_2 + [M][F] \quad [67]$$

$$[M][XeOF_3] \rightarrow \tfrac{1}{2}XeF_2 + \tfrac{1}{2}[M][XeO_2F_3] + \tfrac{1}{2}[M][F] \quad [68]$$

The decomposition pathways were inferred by monitoring the salt decompositions by Raman spectroscopy. The decomposition pathways were supported by their calculated thermochemical cycles at 25 °C which showed that the proposed reduction and disproportionation pathways are mainly driven by lattice energy contributions, with entropy playing a significant role in the pathways that led to reduction of Xe(IV) to Xe(II) and O_2 evolution. The thermochemical cycles also revealed that disproportionation of Xe(IV) to Xe(II) and Xe(VI) is favored for $[Cs][XeOF_3]$ but not for $[N(CH_3)_4][XeOF_3]$, in accordance with the experimental findings.[263]

The $XeOF_3^-$ anion is presently the only known example of an AX_3YE_2 VSEPR arrangement in which a double-bond domain (Xe=O) subtends angles of ∼90° with two valence electron lone-pair domains (Figure 51).[263] When the solid-state ^{16}O- and ^{18}O-enriched vibrational spectra of $[N(CH_3)_4][XeOF_3]$ were compared with those of the calculated gas-phase $Xe^{16/18}OF_3^-$ anions, little interaction between the anion and cation was indicated. The highest frequency band associated with the anion (730.1 cm^{-1}) was attributed to the Xe–O stretch, with the bands at 447.6, 457.3, and 471.3 cm^{-1} assigned to the Xe–F stretching modes. Comparison of the Raman spectra of the Cs^+ and $N(CH_3)_4^+$ salts of $XeOF_3^-$ also showed that significant interactions occur between the Cs^+ cation and the oxygen atom of the $XeOF_3^-$ anion. The Xe–O stretching band of $[Cs][XeOF_3]$ appeared as two bands that were shifted to high frequency relative to those of the $N(CH_3)_4^+$ salt by as much as 30 cm^{-1} (748.9 and 759.6 cm^{-1}). The Xe–F stretching modes, which were likely factor-group split, were also shifted to slightly higher frequencies, occurring at 470.2, 474.5, 483.8, and 487.7 cm^{-1}. In contrast with the $N(CH_3)_4^+$ salt, additional bands were observed between 223.4 and 276.4 cm^{-1} in the spectrum of $[Cs][XeOF_3]$, indicating that the anions interact with one another through F---Xe fluorine bridges.

When the experimental frequencies of $[Cs][XeOF_3]$[263] were compared with those previously reported for $[Cs][XeOF_3]$,[238] it was clear that the product obtained in the earlier study was a mixture of XeF_2, $XeOF_2$, $[Cs][XeF_5]$, and $[Cs][XeO_3F]$. Thus, the latter work represents the first authentic synthesis and characterization of the $XeOF_3^-$ anion.[263]

Quantum-chemical calculations were used to examine the structural effects of fluoride addition to $XeOF_2$ and to compare and confirm vibrational frequency assignments and isotopic shifts. NBO analyses and natural population analysis (NPA) for the atomic charges were also carried out.[263]

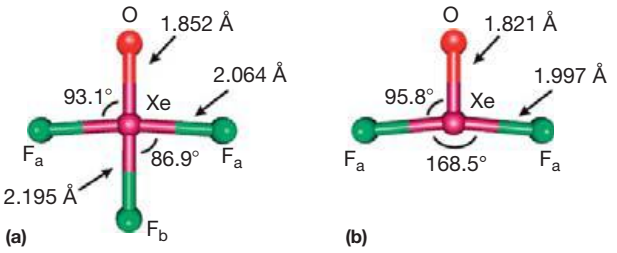

Figure 51 Calculated geometries [B3LYP/aug-cc-pVTZ(−PP)] for (a) $XeOF_3^-$ and (b) $XeOF_2$. Reproduced with permission from Brock, D. S.; Mercier, H. P. A.; Schrobilgen, G. J. *J. Am. Chem. Soc.* **2010**, *132*, 10935–10943.

Copyright © 2013. Elsevier. All rights reserved.

Comprehensive Inorganic Chemistry II : From Elements to Applications, Elsevier, 2013. ProQuest Ebook Central, http://ebookcentral.proquest.com/lib/inflibnet-ebooks/detail.action?docID=1330977.
Created from inflibnet-ebooks on 2021-02-09 22:27:13.

1.25.5 Xe(VI) Compounds

1.25.5.1 X-ray Crystal Structures of XeF_6

A comprehensive study of the crystallographic modifications of XeF_6 has revealed, based on single-crystal X-ray diffraction, neutron powder diffraction, solid-state MAS NMR, and DSC, that XeF_6 exists in at least seven different modifications.[264] Three modifications form at temperatures above room temperature, one exists at room temperature, while two have been identified at low temperatures.[264] Four of these phases corresponding to *mP*8 (phase I), *oP*16 (phase II), *mA*64 (phase III), and *cF*144 (phase IV) had been previously studied by diffraction methods.[265–269] In the early work, only the lattice constants, possible space groups, and approximate xenon positions were given[268] and only the structure having the cubic space group (IV) was subjected to further refinement.[269]

More recently, marginal improvements in the structural data for the four known modifications were achieved.[264] The latter study also showed that two high-temperature modifications (*mP*32 and *mC*32) of XeF_6 form which are comprised of asymmetric tetramers. These structures are closely related, only differing by the ordering imposed by the *C*-centered unit cell. The asymmetric tetramers consist of cyclic XeF_6 trimers that are weakly associated with a monomer, that is, $(XeF_5^+F^-)_3 \cdot XeF_6$ (**Figure 52**). The normal room-temperature modification, previously described as the cubic (*cF*144) phase IV, has disordered tetrameric and hexameric $XeF_5^+F^-$ units in its unit cell.[264] Crystallization of a tetrameric phase of XeF_6 (*mP*16) from inert solvents such as *n*-C_6F_{14}, *n*-$C_4F_9SO_2F$, CF_2Cl_2, or by maintaining neat XeF_6 for greater than 1 week at −40 °C provided an ordered low-temperature modification (*mP*16).[264] The structure consists of regular $(XeF_5^+F^-)_4$ units (**Figure 53**) and represents the best example of a regular XeF_6 tetramer. Crystallization of XeF_6 from HF yielded symmetric dimers that may be formulated as $(XeF_5^+)_2(HF_2)^-$ (**Figure 54**).[264]

1.25.5.2 Cationic Species

1.25.5.2.1 $[XeF_5][\mu\text{-}F(OsO_3F_2)_2]$, $[XeF_5][OsO_3F_3]$, and $[Xe_2F_{11}][OsO_3F_3]$

The title series of Xe(IV) salts has provided the first examples of noble-gas cations that are stabilized by metal oxide fluoride anions, with $[XeF_5][\mu\text{-}F(OsO_3F_2)_2]$ providing the first example of a salt of the fluorine-bridged $\mu\text{-}F(OsO_3F_2)_2^-$ anion.[270]

Fusion of stoichiometric mixtures of XeF_6 and $(OsO_3F_2)_\infty$ at 25–50 °C resulted in the formation of $[XeF_5][\mu\text{-}F(OsO_3F_2)_2]$, $[XeF_5][OsO_3F_3]$, and $[Xe_2F_{11}][OsO_3F_3]$.[270] Fluoride/oxide metathesis with the formation of $XeOF_4$ was not observed in fusion reactions with $(OsO_3F_2)_\infty$, even though XeF_6 is very oxophilic toward a number of transition metal and main-group oxides and oxide fluorides. Both $[XeF_5][\mu\text{-}F(OsO_3F_2)_2]$ and $[Xe_2F_{11}][OsO_3F_3]$ are orange solids at room temperature and $[XeF_5][OsO_3F_3]$ is an orange liquid at room temperature that solidifies at 5–0 °C. All three salts are room-temperature stable but significant dissociation to the starting materials occurs when they are heated at 50 °C under 1 atm of N_2 for more than 2 h. The X-ray crystal structures (−173 °C, **Figure 55**) show that the salts exist as discrete ion pairs and that the osmium coordination spheres in $OsO_3F_3^-$ and $\mu\text{-}F(OsO_3F_2)_2^-$ are pseudo-octahedral OsO_3F_3-units having facial arrangements of oxygen and fluorine atoms. The geometries of the XeF_5^+ and $Xe_2F_{11}^+$ cations, which have been previously well established by X-ray crystallography, are in close agreement with other salts of these cations.[132,141,271–277] The $\mu\text{-}F(OsO_3F_2)_2^-$ anion is comprised of two symmetry-related OsO_3F_2 groups that are fluorine-bridged to one another. Ion pairing results from secondary bonds between the F/O atoms of the anions and xenon of the cation, with the Xe···F/O contacts occurring opposite the axial fluorine and from beneath the equatorial XeF_4 planes of the XeF_5^+ and $Xe_2F_{11}^+$ cations. These interactions avoid the free valence electron lone pairs of the xenon atoms and have been observed in other XeF_5^+ and $Xe_2F_{11}^+$ salts.[132,141,271–277] The

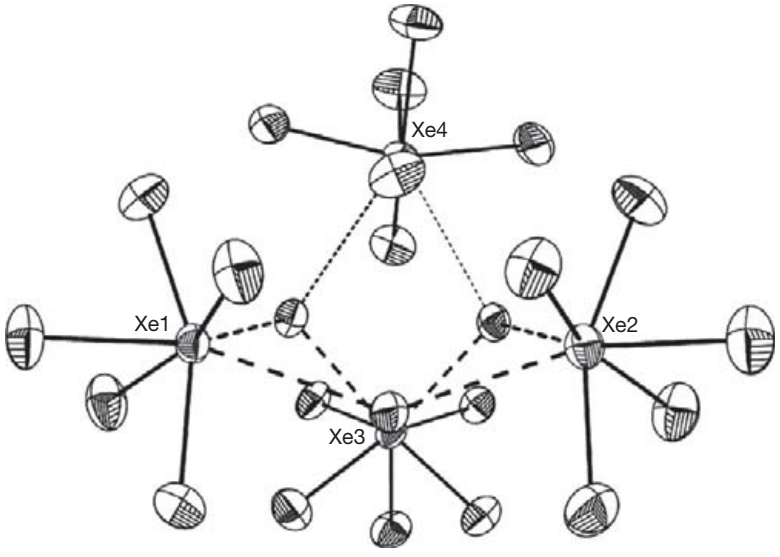

Figure 52 The trimer and monomer units in the crystal structure of XeF_6 (mP32), with thermal ellipsoids drawn at the 50% probability level. Reproduced with permission from Hoyer, S.; Emmler, T.; Seppelt, K. *J. Fluorine Chem.* **2006**, *127*, 1415–1422.

Copyright © 2013. Elsevier. All rights reserved.

Comprehensive Inorganic Chemistry II : From Elements to Applications, Elsevier, 2013. ProQuest Ebook Central, http://ebookcentral.proquest.com/lib/inflibnet-ebooks/detail.action?docID=1330977.
Created from inflibnet-ebooks on 2021-02-09 22:27:13.

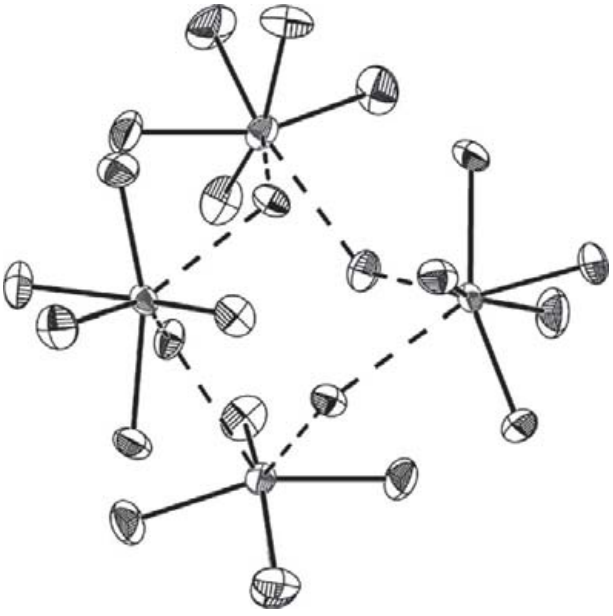

Figure 53 The tetramer unit $(XeF_6)_4$ of the low-temperature phase, XeF_6 (mP16), with thermal ellipsoids drawn at the 50% probability level. Reproduced with permission from Hoyer, S.; Emmler, T.; Seppelt, K. *J. Fluorine Chem.* **2006**, *127*, 1415–1422.

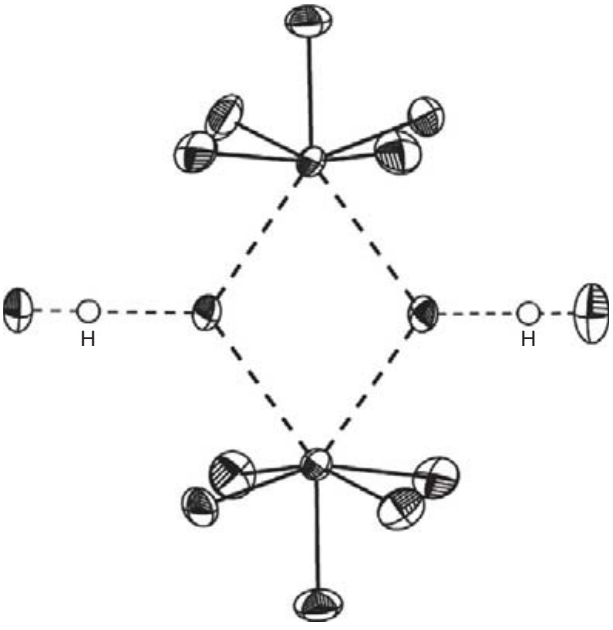

Figure 54 The dimer unit $(XeF_5^+)_2$ (HF_2^-) in $XeF_6 \cdot 1.5HF$ with thermal ellipsoids drawn at the 50% probability level. Reproduced with permission from Hoyer, S.; Emmler, T.; Seppelt, K. *J. Fluorine Chem.* **2006**, *127*, 1415–1422.

xenon atoms of $[XeF_5][\mu\text{-}F(OsO_3F_2)_2]$ and $[Xe_2F_{11}][OsO_3F_3]$ are nine-coordinate and that of $[XeF_5][OsO_3F_3]$ is eight-coordinate. The geometrical parameters of the $OsO_3F_3^-$ anions are closer to those of neutral trioxo Os(VIII) species,[278] indicating that XeF_5^+ and $Xe_2F_{11}^+$ withdraw significant electron density from the anion by means of their secondary bonding interactions with the anion. Quantum-chemical calculations have been successfully used to model the ion pairs and their component ions, providing energy-minimized geometries that are in very good agreement with the experimental structures. The Raman spectra of these salts have been fully assigned based on the calculated vibrational modes.[270]

1.25.5.2.2 $(OsO_3F_2)_2 \cdot 2XeOF_4$ and $[XeF_5][SbF_6] \cdot XeOF_4$

The $(OsO_3F_2)_2 \cdot 2XeOF_4$ adduct has been synthesized by dissolution of $(OsO_3F_2)_\infty$, in liquid $XeOF_4$ at room temperature followed by removal of excess liquid $XeOF_4$ under dynamic vacuum at 0 °C.[278] As in the case of the dissolution of $(OsO_3F_2)_\infty$ in molten XeF_6, $XeOF_4$ did not undergo F/O metathesis with the formation of *cis*-OsO_2F_4 and XeO_2F_2. The adduct is stable at room temperature for up to 5 h, slowly dissociating to $(OsO_3F_2)_\infty$ and $XeOF_4$. Continued pumping on $(OsO_3F_2)_2 \cdot 2XeOF_4$ at 0 °C resulted in the removal of associated $XeOF_4$, yielding $(OsO_3F_2)_2$, a new low-temperature phase of OsO_3F_2. Upon standing at 25 °C for 1½ h, $(OsO_3F_2)_2$ underwent an irreversible phase transition to the known monoclinic phase, $(OsO_3F_2)_\infty$, a polymeric chain structure. Crystallization of $(OsO_3F_2)_2 \cdot 2XeOF_4$ from $XeOF_4$ solution at 0 °C yielded light orange crystals suitable for X-ray structure determination. The structural unit (**Figure 56**) contains the $(OsO_3F_2)_2$ dimer in which the OsO_3F_3 units are joined by two Os---F---Os bridges. The dimer coordinates to two $XeOF_4$ molecules through Os−F---Xe bridges in which the Xe---F distances (2.757(5) Å) are significantly less than the sum of the Xe and F van der Waals radii (3.63 Å).[34] The $(OsO_3F_2)_2$ dimer has C_i symmetry in which the primary coordination spheres of the osmium atoms are *fac*-OsO_3F_3 arrangements in which the oxygen ligands are cis to one another and the bridging fluorine atoms are trans to an oxygen ligand. The $XeOF_4$ molecules are only slightly distorted from the gas-phase square pyramidal geometry of $XeOF_4$ obtained from previous microwave and electron diffraction structural studies.[279,280]

The reaction of $[H_3O][SbF_6]$ with XeF_6 at 0 °C in HF solvent (eqn [69]) has provided crystalline $[XeF_5][SbF_6] \cdot XeOF_4$.[273]

$$2XeF_6 + [H_3O][SbF_6] \rightarrow [XeF_5][SbF_6] \cdot XeOF_4 + 3HF \qquad [69]$$

An earlier study had shown that the reaction between liquid $XeOF_4$ and $[KrF][SbF_6]$ yielded a mixture of $[O_2][SbF_6]$ and $[XeF_5][SbF_6] \cdot XeOF_4$.[281] The solid mixture was characterized by Raman spectroscopy and in HF solution by ^{19}F NMR spectroscopy.

The crystal structure of $[XeF_5][SbF_6] \cdot XeOF_4$ is comprised of a well-separated $XeOF_4$ molecule and a fluorine-bridged $[XeF_5][SbF_6]$ ion pair (**Figure 57**).[273] The structure of $XeOF_4$ is a square-based pyramid of approximate C_{4v} symmetry corresponding to an AX_4YE VSEPR arrangement of bond-pair and lone-pair domains. The geometric parameters obtained for $XeOF_4$ are in good agreement with the gas-phase values.[279,280] The XeF_5^+ and SbF_6^- ions are well separated but interact through fluorine bridges with consequent distortion of the SbF_6^- anion from its regular octahedral geometry. The XeF_5^+ cation exhibits a distorted square-based pyramidal geometry corresponding to an AX_5E VSEPR arrangement, which has been well characterized in previous X-ray crystallographic studies.[132,141,271,274,275]

Copyright © 2013. Elsevier. All rights reserved.

Comprehensive Inorganic Chemistry II : From Elements to Applications, Elsevier, 2013. ProQuest Ebook Central, http://ebookcentral.proquest.com/lib/inflibnet-ebooks/detail.action?docID=1330977.
Created from inflibnet-ebooks on 2021-02-09 22:27:13.

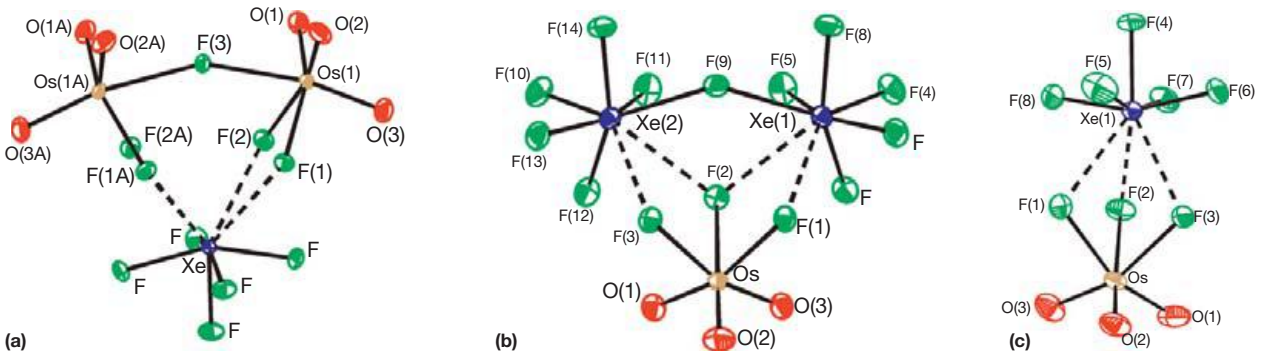

Figure 55 The structural units in the X-ray crystal structures of (a) $[XeF_5][\mu\text{-}F(OsO_3F_2)_2]$, (b) $[Xe_2F_{11}][OsO_3F_3]$, and (c) $[XeF_5][OsO_3F_3]$ with thermal ellipsoids drawn at the 70% probability level. Reproduced with permission from Hughes, M. J.; Mercier, H. P. A.; Schrobilgen, G. J. *Inorg. Chem.*, **2010**, *49*, 3501–3515.

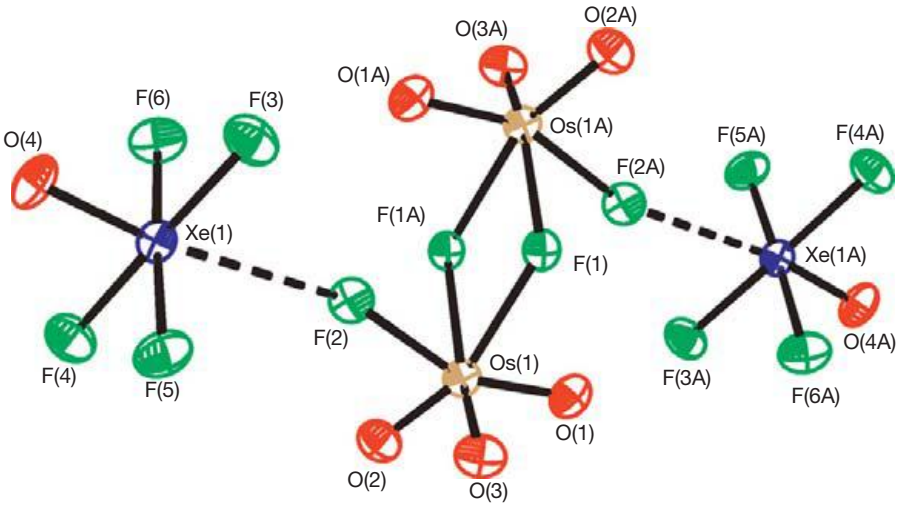

Figure 56 The structural unit in the X-ray crystal structure of $(OsO_3F_2)_2 \cdot 2XeOF_4$ with thermal ellipsoids drawn at the 70% probability level. Reproduced with permission from Hughes, M. J.; Mercier, H. P. A.; Schrobilgen, G. J. *Inorg. Chem.* **2009**, *48*, 4478–4490.

1.25.5.2.3 $[XeF_5]_3[Ti_4F_{19}]$

The reaction between TiF_4 and a stoichiometric excess of XeF_6 at ambient temperature has been shown to yield $(XeF_6)_4 \cdot TiF_4$.[282] The compound dissociates under dynamic vacuum at 40 °C to give XeF_6 and $XeF_6 \cdot TiF_4$, which, in turn, dissociates at 65 °C into XeF_6 and $XeF_6 \cdot 2TiF_4$.[282] Although the compositions of these phases have been determined by elemental analysis, and their IR spectra and magnetic susceptibilities have been reported,[282] no structural data for these or related TiF_4 complexes existed until a recent study.[283]

Reactions between different initial molar ratios of XeF_2 and TiF_4 were investigated [$n(XeF_2)/n(TiF_4) = 4{:}1$, 3:1, 2:1, 1:1, 1:2, 1:3]. Mixtures of XeF_2 and TiF_4 in aHF solvent were UV-irradiated under 6 bar of F_2 gas at room temperature to obtain the complex salts. Although several crystalline products were observed, only the crystal structure of $3XeF_6 \cdot 4TiF_4$ could be determined. The synthesis of $3XeF_6 \cdot 4TiF_4$ was later achieved by the photochemical fluorination of a XeF_2/TiF_4 mixture in aHF using a 3:4 molar ratio of XeF_2/TiF_4.[283]

The $[XeF_5]_3[Ti_4F_{19}]$ complex was prepared by the reaction of XeF_2, TiF_4, and UV-irradiated F_2 in aHF. The crystal structure (Figure 58) of $[XeF_5]_3[Ti_4F_{19}]$ consists of the previously known XeF_5^+ cations and $Ti_4F_{19}^{3-}$ anions. The XeF_5^+ cations have the usual distorted pseudo-octahedral symmetry where the equatorial Xe–F bonds are bent away from the axial electron lone pair toward the axial Xe–F bond.[132,141,270,271,274,275] Contrary to the previously reported $Ti_4F_{18}^{2-}$ anion,[284,285] where each TiF_6 octahedron shares three vertices with three other octahedra, only two μ_3-$[TiF_6]$ octahedra in $[Ti_4F_{19}]^{3-}$ share three vertices with three other $[TiF_6]^-$ anions. The remaining two μ_2-TiF_6^- octahedra share two vertices with two μ_3-TiF_6^- octahedra. The Raman spectrum of $[XeF_5]_3[Ti_4F_{19}]$ is in accordance with the presence of XeF_5^+ cations and $Ti_4F_{19}^{3-}$ anions.[283]

1.25.5.2.4 XeO_2F^+ and $FO_2XeFXeO_2F^+$

The salts, α-$[XeO_2F][SbF_6]$ and $[XeO_2F][AsF_6]$, have been synthesized in aHF by reaction of equimolar amounts of XeO_2F_2 and MF_5 (M = As and Sb) and were isolated as very pale yellow to white solids upon removal of the solvent, initially at −78 °C and finally at 0 °C (eqn [70]).[273] In the case of SbF_5, α-$[XeO_2F][SbF_6]$ was obtained.

$$XeO_2F_2 + MF_5 \rightarrow [XeO_2F][MF_6] \qquad [70]$$

Copyright © 2013. Elsevier. All rights reserved.

Comprehensive Inorganic Chemistry II : From Elements to Applications, Elsevier, 2013. ProQuest Ebook Central, http://ebookcentral.proquest.com/lib/inflibnet-ebooks/detail.action?docID=1330977.
Created from inflibnet-ebooks on 2021-02-09 22:27:13.

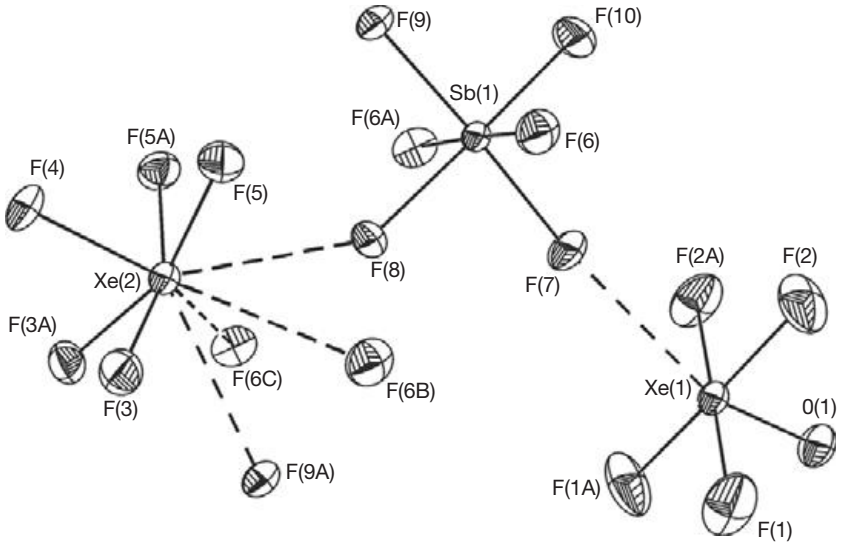

Figure 57 The structural unit in the X-ray crystal structure of $[XeF_5][SbF_6] \cdot XeOF_4$. Thermal ellipsoids are shown at the 50% probability level. Reproduced with permission from Pointner, B. E.; Suontamo, R. J.; Schrobilgen, G. J. *Inorg. Chem.* **2006**, *45*, 1517–1534.

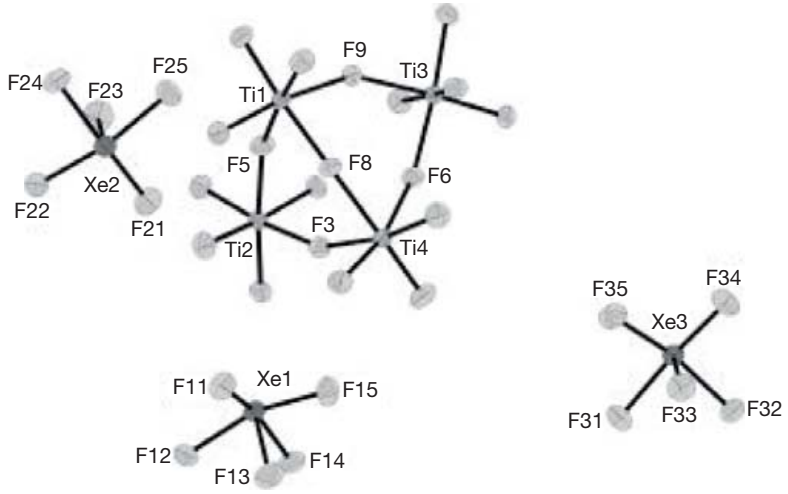

Figure 58 The X-ray crystal structure of $[XeF_5]_3[Ti_4F_{19}]$ showing the $Ti_4F_{19}^{3-}$ anion and three crystallographically independent XeF_5^+ cations. Thermal ellipsoids are drawn at the 40% probability level. Reproduced with permission from Mazej, Z.; Goreshnik, E. *Eur. J. Inorg. Chem.* **2009**, 4503–4506.

When XeO_2F_2 and SbF_5 were allowed to react in 1:2, 1:3, and 1:4 molar ratios in aHF at room temperature, tetrameric β-$[XeO_2F][SbF_6]$ consistently crystallized at −45 to −78 °C.

The salt, $[FO_2XeFXeO_2F][AsF_6]$, was formed by dynamically pumping on solid $[XeO_2F][AsF_6]$ at 0 °C. The high dissociation vapor pressure of $[XeO_2F][AsF_6]$ resulted in rapid AsF_5 loss (eqn [71]) and the formation of pale yellow $[FO_2XeFXeO_2F][AsF_6]$.

$$2[XeO_2F][AsF_6] \rightarrow [FO_2XeFXeO_2F][AsF_6] + AsF_5 \qquad [71]$$

Earlier studies had shown that SbF_5 solutions of $[XeO_2F][Sb_2F_{11}]$ rapidly decompose to XeF^+ and O_2 at room temperature[286] and that solid $[XeO_2F][Sb_2F_{11}]$ decomposes over a period of several months at room temperature.[262,287] The standard enthalpies and Gibbs free energies for reactions leading to $[XeO_2F][MF_6]$ and $[FO_2XeFXeO_2F][MF_6]$ salts from MF_5 (M = As, Sb) and XeO_2F_2 have been obtained from Born–Fajans–Haber cycles and are mildly exothermic and positive, respectively.[273] However, XeO_2F^+ and $FO_2XeFXeO_2F^+$ salts can be synthesized from XeO_2F_2 and MF_5 at low temperatures in aHF. The positive enthalpies of these reactions and their contributions to the Gibbs free energies are apparently diminished by HF solvation of the reactants and products. The degree to which XeO_2F^+ is stabilized and reaction spontaneity is promoted by HF solvation of XeO_2F^+ has been assessed by calculating the basis set superposition error (BSSE)-corrected enthalpies and Gibbs free energies for successive solvation steps leading to $XeO_2F^+ \cdot xHF$ ($x = 1$–5) at 298.15 and 195.15 K. While having considerable kinetic stabilities at room temperature, the enthalpies and Gibbs free energies for the decompositions of the MF_6^- and $Sb_2F_{11}^-$ salts of XeO_2F^+ to their corresponding XeF^+ salts and O_2 are predicted to be

Copyright © 2013. Elsevier. All rights reserved.

Comprehensive Inorganic Chemistry II : From Elements to Applications, Elsevier, 2013. ProQuest Ebook Central, http://ebookcentral.proquest.com/lib/inflibnet-ebooks/detail.action?docID=1330977.
Created from inflibnet-ebooks on 2021-02-09 22:27:13.

highly exothermic and spontaneous over a range of temperatures and are dominated by a large gas-phase enthalpy of decomposition for XeO_2F^+. With the exception of $[XeO_2F][AsF_6]$, the XeO_2F^+ and $FO_2XeFXeO_2F^+$ salts are kinetically stable toward dissociation to XeO_2F_2 and MF_5 at room temperature.

1.25.5.2.4.1 α-$[XeO_2F][SbF_6]$

The crystal structure of α-$[XeO_2F][SbF_6]$ consists of discrete XeO_2F^+ cations and SbF_6^- anions that interact by means of secondary fluorine bridge contacts (**Figure 59**). The primary coordination sphere of xenon in XeO_2F^+ is a trigonal pyramidal arrangement of the oxygen atoms and a fluorine atom. The isolated cation geometry is consistent with an AXY_2E VSEPR arrangement of a single-bond domain (X), two double-bond domains (Y), and a lone-pair domain (E). The Xe−F bond of XeO_2F^+ is shorter, within ±3σ, than in $XeOF_4$ (1.900(5);[279] 1.901(3)–1.9040;[280] 1.895(2), 1.890(2) Å[273]), and XeO_2F_2 (1.899(3);[288] 1.892(13), 1.925(13) Å[289]) and intermediate with respect to Xe−F_{ax} (1.879(12) Å), and Xe−F_{eq} (1.821(12) Å) in $XeOF_3^+$.[290] Although the net positive charge of the XeO_2F^+ cation leads to a shorter and less polar Xe−F bond, the Xe−O bond lengths in the XeO_2F^+ cation are similar to those of other xenon(VI) oxide fluorides ($XeOF_4$, 1.703(15),[279] 1.7053(9)–1.711(11),[280] 1.713(3) Å;[273] $XeOF_3^+$, 1.692(13) Å;[290] XeO_2F_2, 1.714(4),[288] 1.731(9) Å, [289] and XeO_3, 1.76(2) Å[242]). The O(1)−Xe(1)−O(2) (105.0(2)°), O(1)−Xe(1)−F(7) (95.7(1)°), and O(2)−Xe(1)−F(7) (98.2(1)°) bond angles of the XeO_2F^+ cation are considerably less than the ideal tetrahedral angle. The xenon atom of each XeO_2F^+ cation also has five nonequivalent secondary fluorine bridge contacts to five different SbF_6^- anions, which are significantly less than the sum of the xenon and fluorine van der Waals radii (3.63 Å),[34] indicating that these secondary contacts have substantial covalent character. The secondary contacts give rise to a distorted monocapped octahedral environment about the xenon atom that is consistent with an AXY_2Z_3E VSEPR arrangement of one primary single-bond domain (X), two primary double-bond pair domains (Y), three secondary bond (contact) domains (Z), and one electron lone-pair domain (E).

1.25.5.2.4.2 β-$[XeO_2F][SbF_6]$

The unit cell of β-$[XeO_2F][SbF_6]$ is comprised of three $([XeO_2F][SbF_6])_4$ units.[273] The xenon and antimony atoms of each tetrameric unit occupy alternate vertices of a cube (**Figure 60**). The compound crystallizes in the space group *R*3 with the threefold axis of the unit cell passing through Xe(2) and Sb(2), resulting in positional disorder of the fluorine and oxygen atoms bonded to xenon. The average Xe−O/F bond lengths in the tetramer bracket the weighted average of the Xe−O and Xe−F bond lengths obtained for the ordered α-phase (1.772 Å).[273] The Xe(1) atom has three secondary contacts to fluorine atoms of three SbF_6^- anions which are ∼1 Å less than the sum of the xenon and fluorine van der Waals radii.[34] The Xe(2) atom also has three similar contacts to fluorine atoms of the SbF_6^- anions that are equivalent by crystal symmetry.

Although the exterior O/F−Xe(1)−O/F and O/F−Xe(2)−O/F angles are significantly more open by 17–24° than the angles formed by the interior Xe---F contacts, they provide sufficient space to accommodate the xenon valence electron lone pairs between the Xe(1)---F(10)/F(11)/F(9B) and Xe(2)---F(8)/F(8A)/F(8B) contacts. These arrangements of primary bonds, long contacts, and the xenon valence electron lone pair are similar to the distorted octahedral AXY_2Z_3E VSEPR arrangement in the crystal structure of α-$[XeO_2F][SbF_6]$ (*vide supra*).

1.25.5.2.4.3 $[XeO_2F][AsF_6]$

The crystal structure of $[XeO_2F][AsF_6]$ was determined from a racemic twin crystal that also exhibited cubic twinning,

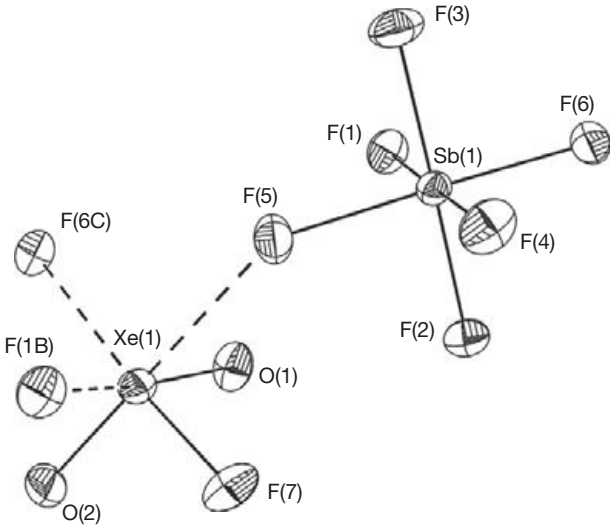

Figure 59 The structural unit in the X-ray crystal structure of α-$[XeO_2F][SbF_6]$. Thermal ellipsoids are shown at the 50% probability level. Reproduced with permission from Pointner, B. E.; Suontamo, R. J.; Schrobilgen, G. J. *Inorg. Chem.* **2006**, *45*, 1517–1534.

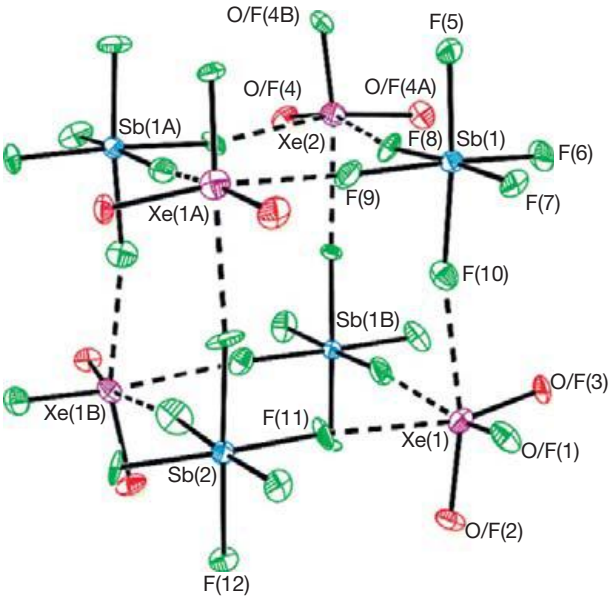

Figure 60 The tetrameric uint in the X-ray crystal structure of β-$[XeO_2F][SbF_6]$. Thermal ellipsoids are shown at the 50% probability level. Reproduced with permission from Pointner, B. E.; Suontamo, R. J.; Schrobilgen, G. J. *Inorg. Chem.* **2006**, *45*, 1517–1534.

Copyright © 2013. Elsevier. All rights reserved.

Comprehensive Inorganic Chemistry II : From Elements to Applications, Elsevier, 2013. ProQuest Ebook Central, http://ebookcentral.proquest.com/lib/inflibnet-ebooks/detail.action?docID=1330977.
Created from inflibnet-ebooks on 2021-02-09 22:27:13.

inducing a positional disorder between one oxygen and the fluorine atom of the XeO_2F^+ cation.[273] The disorder did not allow the extraction of discrete Xe–O and Xe–F bond lengths and angles for the oxygen and fluorine atoms that are involved in the disorder but did provide a reliable Xe(1)–O(1) bond length (1.740(10) Å). The disordered Xe–O/F bond lengths, however, are in good agreement with the weighted average of the Xe–O and Xe–F bond lengths obtained from the ordered α-$[XeO_2F][SbF_6]$ phase. The structural unit and secondary coordination spheres of xenon in $[XeO_2F][AsF_6]$ are also similar to those of α-$[XeO_2F][SbF_6]$.

1.25.5.2.4.4 $[FO_2XeFXeO_2F][AsF_6]$

The $[FO_2XeFXeO_2F][AsF_6]$ structural unit is comprised of well-separated $FO_2XeFXeO_2F^+$ cations and AsF_6^- anions (Figure 61).[273] The $FO_2XeFXeO_2F^+$ cation consists of two crystallographically independent XeO_2F units bridged by a fluorine atom to give a bent Xe---F---Xe arrangement. Each F---XeO_2F moiety approximates a disphenoidal AX_2Y_2E VSEPR arrangement of the electron lone-pair and four bond-pair domains in the xenon valence shell with terminal Xe–F and Xe–O bond lengths of 1.872(3) and 1.870(4) Å, and 1.715(4) and 1.721(4) Å, respectively. The terminal Xe–F bond lengths are intermediate with respect to those of the XeO_2F^+ cation in α-$[XeO_2F][SbF_6]$ and XeO_2F_2, corresponding to a charge decrease in xenon and increase in Xe–F bond polarity: $XeO_2F^+ > FO_2XeFXeO_2F^+ > XeO_2F_2$. The $FO_2XeFXeO_2F^+$ cation is asymmetric about the bridging fluorine atom with Xe---F bond lengths of 2.161(3) (Xe(1)---F(8)) and 2.230(3) (Xe(2)---F(8)) Å and has an average torsion angle, (O(1/2)–Xe(1)---Xe(2)–O(3/4), that is essentially 0°, resulting in a cation point symmetry of C_s. The xenon atom of each XeO_2F moiety has secondary fluorine bridge contacts from neighboring anions that approach their respective xenon centers, avoiding the xenon valence electron lone pair, that are trans to the equatorial oxygen atoms. The Xe---F---Xe bridge angle (166.4(2)°) and bond lengths of $FO_2XeFXeO_2F^+$ are very similar to those of $Xe_2F_{11}^+$ in its AuF_6^- salt (169.2(2)°; 2.21(1), 2.26(1) Å).[276] However, in $[Xe_2F_{11}][NiF_6]$ (140.3°; 2.35(1), 2.21(1) Å),[277] the Xe---F---Xe angle is much smaller and is likely a consequence of stronger cation–anion interactions that result from the higher negative charges on the fluorine ligands of the NiF_6^{2-} anion. The F(7)–Xe(1)---F(8) (169.7(2)°) and F(9)–Xe(2)---F(8) (170.8(2)°) bond angles of the F---XeO_2F moieties are bent toward the xenon lone pair and away from the equatorial Xe–O double-bond domains as in XeO_2F_2,[288] $TcO_2F_3 \cdot XeO_2F_2$,[289] and the O–XeO_2–O moiety of $XeO_2(OTeF_5)_2$.[232]

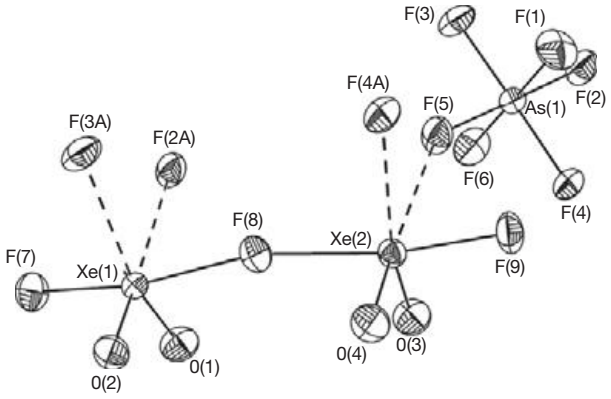

Figure 61 The structural unit in X-ray crystal structure of $[FO_2XeFXeO_2F][AsF_6]$. Thermal ellipsoids are shown at the 50% probability level. Reproduced with permission from Pointner, B. E.; Suontamo, R. J.; Schrobilgen, G. J. *Inorg. Chem.* **2006**, *45*, 1517–1534.

1.25.6 Xe(VIII) Compounds

1.25.6.1 NMR Studies of XeO_4 and $[Na_4][XeO_6]$

1.25.6.1.1 XeO_4

Like XeO_3 and XeO_2 (see Section 1.25.4.1.2), XeO_4 is thermodynamically and kinetically unstable, decomposing explosively in the gas phase and in the solid state to Xe and O_2 with the release of 642 kJ mol^{-1} of energy.[246] The treacherous nature of XeO_4 has, no doubt, impeded progress in Xe(VIII) chemistry. Consequently, there had been no prior information relating to the solution behavior of XeO_4. A modified and more detailed description of the original procedure[291] for the preparation of XeO_4 from Na_4XeO_6 and H_2SO_4 has been developed, along with a reliable procedure for forming its solutions which minimizes explosion risks.[291] Xenon tetroxide is soluble in the oxidatively resistant and synthetically useful solvents SO_2ClF, BrF_5, and aHF, giving solutions that are stable up to −30 °C. The work, which established protocols for safely creating synthetically useful XeO_4 solutions of sufficient stability, lays the groundwork for the solution chemistry of XeO_4 and for the extension of the presently limited chemistry of Xe(VIII). The ^{129}Xe, ^{131}Xe, and ^{17}O NMR spectra of XeO_4 were also recorded for the first time.[291]

The ^{129}Xe chemical shifts of XeO_4 in SO_2ClF (−78.5 °C), BrF_5 (−50 °C), and HF (−75 °C) solutions relative to liquid $XeOF_4$ are −92.9, −94.7, and −85.8 ppm, respectively.[291] The chemical shift differences are small when compared with those of other xenon species, for example, XeF_2 ($\delta(^{129}Xe) = -1905$ ppm in SO_2ClF, 25 °C; −1592 ppm in HF, 25 °C),[292] indicating that the tetrahedral molecule, and xenon in particular, interacts only weakly with its solvent environment. The temperature dependence of the ^{129}Xe chemical shift of XeO_4 was studied in SO_2ClF solvent up to 0 °C where decomposition became rapid.[291] Only XeO_4 was observed by ^{129}Xe NMR spectroscopy in HF and BrF_5 solutions, indicating that no fluorination or fluorine–oxygen exchange between XeO_4 and HF and BrF_5 had occurred, which is in agreement with the Raman spectroscopic characterization of XeO_4 in HF solvent carried out in the same study,[291] but contrasts with the solvolytic behavior of the isoelectronic IO_4^- anion (eqns [72] and [73]).[293]

$$IO_4^- + 8HF \rightarrow IO_2F_4^- + 2H_3O^+ + 2HF_2^- \quad [72]$$

$$IO_4^- + 2BrF_5 \rightarrow IO_2F_4^- + 2BrOF_3 \quad [73]$$

Besides ^{129}Xe, ^{131}Xe is the only other naturally occurring xenon isotope (21.18%) which is NMR active. Although the natural abundance of ^{131}Xe is similar to that of ^{129}Xe, the quadrupolar nature of ^{131}Xe ($I = {}^3/_2$) provides a very efficient relaxation pathway by means of interaction of the quadrupole moment with an electric field gradient. Thus, there has been no reported ^{131}Xe chemical shift for chemically bound xenon and

Copyright © 2013. Elsevier. All rights reserved.

Comprehensive Inorganic Chemistry II : From Elements to Applications, Elsevier, 2013. ProQuest Ebook Central, http://ebookcentral.proquest.com/lib/inflibnet-ebooks/detail.action?docID=1330977.
Created from inflibnet-ebooks on 2021-02-09 22:27:13.

solution ^{131}Xe NMR spectroscopy has been limited to studies of elemental xenon.[294] The high symmetry of XeO_4 (T_d point symmetry) affords a sufficiently long relaxation time to allow the observation of surprisingly sharp ^{131}Xe resonances and the first ^{131}Xe NMR studies of a xenon compound. The ^{131}Xe chemical shifts of XeO_4 in SO_2ClF (−78.5 °C), BrF_5 (−50 °C), and HF (−75 °C) solutions relative to liquid $XeOF_4$ are −92.8, −94.5, and −85.8 ppm, respectively. A variable temperature and variable field strength study of the spin–lattice relaxation times for ^{129}Xe and ^{131}Xe showed that the spin-rotation and the quadrupolar relaxation mechanisms, respectively, are dominant. A Raman spectroscopic study of XeO_4 in aHF solvent confirmed the point symmetry of XeO_4 and the absence of significant solvent–solute interactions.[291]

The ^{17}O NMR spectrum of natural abundance XeO_4 in SO_2ClF was recorded at −78 °C. The chemical shift was 509 ppm ($\Delta\nu_{1/2}$ = 46 Hz) but no $^1J(^{129}Xe-^{17}O)$ satellite coupling was observed because of the low satellite intensities and broadness of the ^{17}O resonance which is partially a consequence of the quadrupolar nature of the ^{17}O nucleus ($I = {}^5/_2$; 0.037% natural abundance).

1.25.6.1.2 $[Na_4][XeO_6]\cdot xH_2O$ (x = 0, 2)

Another first in ^{131}Xe NMR spectroscopy was achieved with the solid-state ^{131}Xe NMR studies of $[Na_4][XeO_6]\cdot xH_2O$ (x = 0, 2).[295] Xenon-129 and ^{131}Xe were selected to characterize the xenon magnetic shielding and quadrupolar interactions for both sodium perxenate salts at an applied magnetic field strength of 11.75 T. Solid-state $^{129/131}$Xe NMR line shapes indicate that the local Xe environment in anhydrous $[Na_4][XeO_6]$ adopts O_h symmetry and the Lorentzian ^{129}Xe NMR line shape suggests rapid reorientation of the XeO_6^{4-} anion in the solid state. Upon hydration, the XeO_6^{4-} anion becomes noticeably distorted from O_h symmetry. For stationary, anhydrous $[Na_4][XeO_6]$, the heteronuclear $^{129/131}$Xe, ^{23}Na dipolar interaction is the major contributor to the widths of the $^{129/131}$Xe NMR lines. For stationary and slow MAS of $[Na_4][XeO_6]\cdot 2H_2O$ samples, the anisotropic Xe shielding interaction dominates the ^{129}Xe NMR line shape, whereas the ^{131}Xe NMR line shape is completely dominated by the nuclear quadrupolar interaction. Distortions from O_h symmetry for the local xenon environment in $[Na_4][XeO_6]\cdot 2H_2O$ have been detected by measuring the xenon magnetic shielding tensor. The xenon shielding tensor is nearly axially symmetric, with a skew of -0.7 ± 0.3, an isotropic Xe chemical shift of -725.6 ± 1.0 ppm, and a span of 95 ± 5 ppm. The ^{131}Xe quadrupolar coupling constant (10.8 ± 0.5 MHz) is large for a nucleus at a site of approximate O_h symmetry and the quadrupolar asymmetry parameter indicates a lack of axial symmetry. The study demonstrated the high sensitivity of the ^{131}Xe nuclear quadrupolar interaction to changes in the local environment of xenon. This is a serious drawback in the study of chemically bound xenon species in the solid state, rendering acquisition of ^{131}Xe NMR spectra for species having low-symmetry xenon environments impractical. By contrast, solid-state ^{129}Xe NMR spectroscopic studies are considerably more promising in that both MAS and stationary samples can be studied with relative ease and in reasonable experimental time frames, and with no impractical restrictions on the external magnetic field strength.

1.25.7 Kr(II) Compounds

1.25.7.1 KrF_2 as a Ligand

Several KrF_2 adducts with transition metal centers have been previously reported[296–299] and a structurally unsubstantiated Raman study proposed the formation of $M[AuF_6]_2\cdot nKrF_2$ (M = Ca, Sr, Ba; n = 0–4).[300] However, only $[BrOF_2][AsF_6]\cdot 2KrF_2$ has been structurally characterized by X-ray crystallography.[197] The adduct was synthesized by the reaction of KrF_2 with $[BrOF_2][AsF_6]$ in a 2:1 molar ratio in aHF at −78 °C (eqn [74]).

$$[BrOF_2][AsF_6] + 2KrF_2 \xrightarrow[12\,h\,at\,-78\,^\circ C]{HF} [BrOF_2][AsF_6]\cdot 2KrF_2 \quad [74]$$

In contrast to $[BrOF_2][AsF_6]\cdot 2XeF_2$ (Section 1.25.3.2.3.8),[196] the krypton analog was stable in aHF solution up to 25 °C for at least 1 h, showing no discernible decomposition as a solid or under aHF solvent over 5 days at −78 °C.[197]

The X-ray crystal structure of $[BrOF_2][AsF_6]\cdot 2KrF_2$ (Figure 62) represents a rare example in which KrF_2 functions as a ligand[197] and is isostructural with the xenon analog,[196] with similar geometrical parameters (within $\pm 3\sigma$) for $BrOF_2^+$ and AsF_6^-. The KrF_2 molecules coordinate to the cation by means of Br---F(3) (2.318(4) Å) and Br---F(5) (2.356(4) Å) contacts. The Kr−F bridge bonds are elongated (1.943(4), 1.933(4) Å) and the terminal bonds are shortened by nearly equal amounts (1.840(5), 1.847(4) Å) relative to those of free KrF_2 (1.894(5) Å).[126] These distortions are significantly less than in KrF^+ and $Kr_2F_3^+$ salts (see Section 1.25.7.3), indicating that the Kr−F_b bonds of $[BrOF_2][AsF_6]\cdot 2KrF_2$ have considerably more covalent character than those of KrF^+ and $Kr_2F_3^+$ salts, and that the KrF_2 molecules behave as coordinating ligands rather than as fluoride ion donors.[197]

The solid-state Raman spectrum of $[BrOF_2][AsF_6]\cdot 2KrF_2$ has been assigned with the aid of quantum-chemical calculations.[197] The Raman spectrum is similar to that of $[BrOF_2][AsF_6]\cdot 2XeF_2$ [196] with the exception of more intense Kr–F stretching bands relative to their Xe–F counterparts in $[BrOF_2][AsF_6]\cdot 2XeF_2$. One notable difference that is apparent from quantum-chemical calculations is the weak vibrational

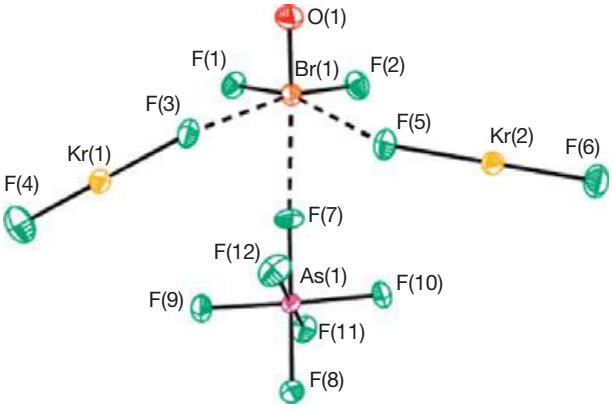

Figure 62 Structural unit in the X-ray crystal structure of $[BrOF_2][AsF_6]\cdot 2KrF_2$; thermal ellipsoids are shown at the 50% probability level. Reproduced with permission from Brock, D. S.; Casalis de Pury, J. J.; Mercier, H. P. A.; Schrobilgen, G. J.; Silvi, B. *J. Am. Chem. Soc.* **2010**, *132*, 3533–3542.

Copyright © 2013. Elsevier. All rights reserved.

Comprehensive Inorganic Chemistry II : From Elements to Applications, Elsevier, 2013. ProQuest Ebook Central, http://ebookcentral.proquest.com/lib/inflibnet-ebooks/detail.action?docID=1330977.
Created from inflibnet-ebooks on 2021-02-09 22:27:13.

coupling that occurs between the $\nu(Kr–F_t)$ modes of the coordinated KrF_2 molecules in contrast with the strong coupling that occurs between the $\nu(Kr–F_b)$ bridging modes. The opposite behavior was found for $[BrOF_2][AsF_6]\cdot 2XeF_2$.[196]

The QTAIM and ELF analyses were also carried out and indicated that $[BrOF_2][AsF_6]\cdot 2KrF_2$ is organized around $BrOF_2^+$ and its stabilization is due to its Coulomb interaction with the AsF_6^- anion and to electron delocalization and charge transfers involving the KrF_2 ligands.[197] A similar relationship between decreasing size of bromine electron lone pair and Br(V) coordination number also applies to $[BrOF_2][AsF_6]\cdot 2XeF_2$.

1.25.7.2 α-KrF_2

The crystal structure of the low-temperature phase, α-KrF_2 (**Figure 63**),[126] was determined in order to obtain more precise structural parameters for KrF_2, which are important for comparison with other Kr−F bond lengths, and to establish the structural basis for the dimorphism of KrF_2. Krypton difluoride was originally studied by Raman spectroscopy, in conjunction with a factor-group analysis[301] which indicated that α-KrF_2 is isomorphous with the room temperature XeF_2 phase (tetragonal space group $I4/mmm$).[130] The crystal structure of β-KrF_2 ($P4_2/mnm$) had been previously determined at −80 °C.[302] The more recent crystal structure determination of α-KrF_2 (−125 °C)[126] confirmed the dimorphism of KrF_2, the correctness of the earlier vibrational spectroscopic analysis, and the space group assignment based on the prior factor-group analysis.[301] The β→α-phase transition had been shown by variable-temperature Raman spectroscopy to occur below this temperature.[301] The fact that crystals of β-KrF_2 were initially grown by sublimation at −78 °C and then cooled to −125 °C for X-ray data collection on the α-phase indicates that the β→α-phase transition occurs without serious disruption of the crystal lattice. The Kr−F bond length in α-KrF_2 (1.894(5) Å) is of higher precision and in agreement with that determined for β-KrF_2 (1.89(2) Å, −80 °C) by X-ray diffraction[302] and for gaseous KrF_2 by electron diffraction (1.889(10) Å, −40 °C).[303] As observed for β-KrF_2, α-KrF_2 is linear by symmetry. The interatomic F···F distance between collinearly orientated KrF_2 molecules is 2.71 Å in both phases.

1.25.7.3 Fluoride Ion Donor Properties of KrF_2, and KrF^+ and $Kr_2F_3^+$ Salt Formation

Krypton difluoride has been shown to exhibit fluoride ion donor properties that are analogous to those of XeF_2.[87,121,124,132,299,304] The reactions of KrF_2 with strong fluoride ion acceptors have led to the formation of a number of KrF^+ and $Kr_2F_3^+$ salts, that is, $[KrF][MF_6]$ (M = As, Sb, Bi, Au, Pt, Ta),[125,305–309] $[KrF][M_2F_{11}]$ (M = Sb, Ta, Nb),[305,307–310] and $[Kr_2F_3][MF_6]$ (M = As, Sb, Ta).[305–309] All have been characterized by Raman spectroscopy. In related studies of $[BrO_2F][AsF_6]\cdot 2NgF_2$ (Ng = Kr,[197] Xe[196]), KrF_2 was shown to be less fluorobasic than XeF_2. Unlike their Xe(II) analogs, the Kr(II) salts are thermodynamically unstable. However, the kinetic stabilities of the krypton salts show considerable variance,[125,282,305–309] and salts, such as $[KrF][SbF_6]$,[306,307,309] $[KrF][Sb_2F_{11}]$,[308–310] $[Kr_2F_3][SbF_6]$,[307–309] and $[KrF][AuF_6]$,[281] can be handled and stored at room temperature for appreciable amounts of time without significant decomposition. Structural characterization of KrF^+ and $Kr_2F_3^+$ salts in the solid state has, in large measure, relied upon Raman spectroscopy.[125,281,305–309] The Raman spectra of KrF^+ salts indicate that the KrF^+ cation, like XeF^+, has considerable Lewis acidity and strongly interacts with the anion by formation of a fluorine bridge between krypton and a fluorine ligand of the anion. Vibrational modes associated with the fluorine bridge and vibrational modes resulting from symmetry lowering of the octahedral anion have been assigned.[125,281,308,309] The Raman spectra of $Kr_2F_3^+$ salts have been assigned on the basis of a V-shaped fluorine-bridged geometry for the cation,[126,307,309] analogous to that established by X-ray crystallography for $Xe_2F_3^+$.[140,141] In contrast with the KrF^+ salts, Raman spectroscopy has shown that the cation–anion interactions in the $Kr_2F_3^+$ salts are weak, as indicated by retention of the octahedral symmetry of the anion. Fluorine-19 NMR spectroscopy has also been used to study the KrF^+ cation in aHF solvent and the $Kr_2F_3^+$ cation in BrF_5 solvent, providing the first unambiguous characterization of the structure of the fluorine-bridged $Kr_2F_3^+$ cation.[307,309] The strong oxidant characters of KrF_2, KrF^+, and $Kr_2F_3^+$ have not only provided low-temperature synthetic routes to BrF_6^+,[307,311] ClF_6^+,[311,312] OsO_2F_4,[313] AuF_5,[281] and $TcOF_5$,[314] but also served as a significant impediment to their detailed structural characterization by single-crystal X-ray diffraction.

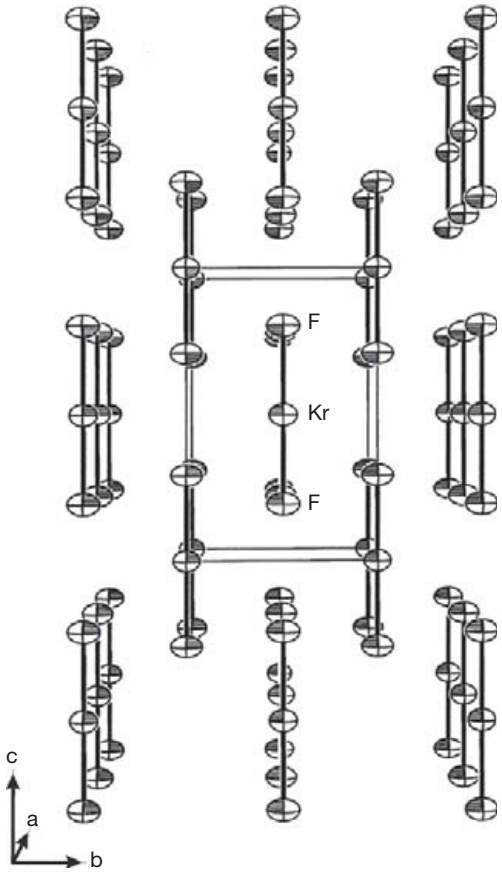

Figure 63 Packing diagram of α-KrF_2 (−125 °C) viewed along the *a*-axis. Reproduced with permission from Lehmann, J. F.; Dixon, D. A.; Schrobilgen, G. J. *Inorg. Chem.* **2001**, *40*, 3002–3017.

Copyright © 2013. Elsevier. All rights reserved.

Comprehensive Inorganic Chemistry II : From Elements to Applications, Elsevier, 2013. ProQuest Ebook Central, http://ebookcentral.proquest.com/lib/inflibnet-ebooks/detail.action?docID=1330977.
Created from inflibnet-ebooks on 2021-02-09 22:27:13.

Colorless, crystalline [KrF][MF_6] (M = As, Sb, Bi), [Kr_2F_3][SbF_6]·KrF_2, [Kr_2F_3]$_2$[SbF_6]$_2$·KrF_2, and [Kr_2F_3][AsF_6]·[KrF][AsF_6] salts were synthesized by reaction of KrF_2 with MF_5 in 1:1, 1:1, 2:1, 3.5: 1, and 2:1 molar ratios, respectively, in aHF solvent and were crystallized between −10 and −80 °C to minimize decomposition.[126] The [KrF][MF_6] salts crystallized as discrete colorless needles while [Kr_2F_3][SbF_6]·KrF_2 and [Kr_2F_3]$_2$[SbF_6]$_2$·KrF_2 crystallized as intergrown pale yellow plates. The stoichiometric mixture, $2KrF_2$:SbF_5, was found to decompose rapidly in aHF at temperatures as low as −40 °C, resulting in crystal growth of the less soluble [KrF][SbF_6] salt. The attempted crystallization of [Kr_2F_3][SbF_6] using excess KrF_2 to compensate for the decomposition resulted in a mixture of crystalline [KrF][SbF_6] and [Kr_2F_3]$_2$[SbF_6]$_2$·KrF_2 or [Kr_2F_3][SbF_6]·KrF_2. Crystallization of [Kr_2F_3][AsF_6] was also unsuccessful, but resulted in the crystalline double salt, [Kr_2F_3][AsF_6]·[KrF][AsF_6]. Samples of [KrF][AuF_6] were prepared as previously described[281] by the oxidation of gold powder by KrF_2 in aHF at 20 °C (eqn [75]), and pale yellow, needle-shaped [KrF][AuF_6] crystals were obtained by slowly cooling an aHF solution from −10 to −80 °C.[127]

$$Au + {}^{7}/_{2}KrF_2 \rightarrow [KrF][AuF_6] + {}^{5}/_{2}Kr \qquad [75]$$

Experimental trends in bond lengths and bond angles among [NgF][MF_6] ion pairs and NgF_2 and $Ng_2F_3^+$ salts are, for the most part, analogous for krypton and xenon. For this reason, few explicit comparisons are mentioned. The sections that explicitly deal with XeF^+ and $Xe_2F_3^+$ salts should be consulted (see **Sections 1.25.3.1.4.1** and **1.25.3.1.4.3**).

1.25.7.3.1 [KrF][MF_6] (M = As, Sb, Bi, Au)

The β-[KrF][AsF_6], [KrF][SbF_6], and [KrF][BiF_6] salts form an isomorphous and isostructural series (**Figure 64**) in which the KrF^+ cation strongly interacts with the anion by means of an asymmetric fluorine bridge that is bent at F_b, the fluorine bridge atom, which is more closely associated with the M atom of the hexafluoropnictate(V) anion.[126] The point group symmetries of the [KrF][MF_6] ion pairs are C_1 symmetry because the F_b---Kr−F_t groups are staggered, with F_e−M---F_b---Kr dihedral angles of 22.1°, 22.2°, 19.7°, and 28.1° for β-[KrF][AsF_6], [KrF][SbF_6], [KrF][BiF_6], and [Kr_2F_3][AsF_6]·[KrF][AsF_6], respectively. The geometry of the [KrF][AsF_6] ion pair in [Kr_2F_3][AsF_6]·[KrF][AsF_6] differs from that of β-[KrF][AsF_6] in that the dihedral F_e–M---F_b---Kr angle (28.1°) of the double salt is larger than that of β-[KrF][AsF_6] (22.1°), suggesting that the ion pair geometry is significantly influenced by the crystal packing. The Kr---F_b bond length is significantly shorter (2.106(6) Å) than in β-[KrF][AsF_6] (2.131(2)Å), whereas the Kr−F_t bond length (1.783 (6) Å) shows no significant change.

The Kr–F_t bond lengths (1.765(3)–1.774(6) Å) in these salts are significantly shorter and the Kr---F_b bridge bond lengths are significantly longer than the Kr−F bonds of α-KrF_2 (1.894(5) Å).[126] The bond length differences are also manifested in the Raman spectra by two bands, one shifted to high frequency, ν(Kr–F_t) and the other shifted to low frequency, ν(Kr–F_b), with respect to $\nu_s(KrF_2)$ of α-KrF_2.[126] The MF_6^- octahedra are distorted and may be regarded, in a first approximation, as having local C_{4v} or lower symmetries that result from bridge bond formation with the cation, giving rise to elongated M---F_b bonds. There is no clear distinction between the M−F_e and the M−F_a bond lengths in these compounds. Despite the strong fluorine bridge interactions and variations in the fluoride ion acceptor strengths of AsF_5, SbF_5, and BiF_5, the Kr−F_t bond lengths in all three salts and the Kr---F_b bond lengths in β-[KrF][AsF_6] (2.131(2) Å) and [KrF][SbF_6] (2.140(3) Å) exhibit no significant variation within ±3σ. The Kr---F_b bridge bond is, however, significantly shorter in the BiF_6^- salt (2.089(6) Å) than in the arsenic and antimony analogs, which is consistent with the weaker fluoride ion acceptor strength of BiF_5 when compared with those of AsF_5 and SbF_5. The Kr---F_b bond lengths of all three salts are significantly less than the sum of the fluorine (1.47 Å)[34] and krypton (2.02 Å)[34] van der Waals radii and are indicative of significant covalent bond character that is also reflected in the nonlinearity of the Kr---F_b–M angles (*vide infra*).

In contrast with the [KrF][MF_6] (M = As, Sb, Bi) salts, which all crystallize in the $P2_1/c$ space group, the isostructural [KrF][AuF_6] salt (**Figure 65**) crystallizes in the noncentrosymmetric space group, *Cc*.[127] Similar to the [KrF][MF_6] (M = As, Sb, Bi) series, [KrF][AuF_6] consists of a KrF^+ cation that interacts strongly with the AuF_6^- anion by means of a fluorine bridge (F_b). The Kr–F_t terminal bond length in [KrF][AuF_6] (1.76(1) Å)[127] cannot be differentiated (within ±3σ) from those of [KrF][MF_6] (M = As, Sb, Bi).[126] The Kr---F_b bridge bond length (2.16(1) Å) in [KrF][AuF_6] is similar to those

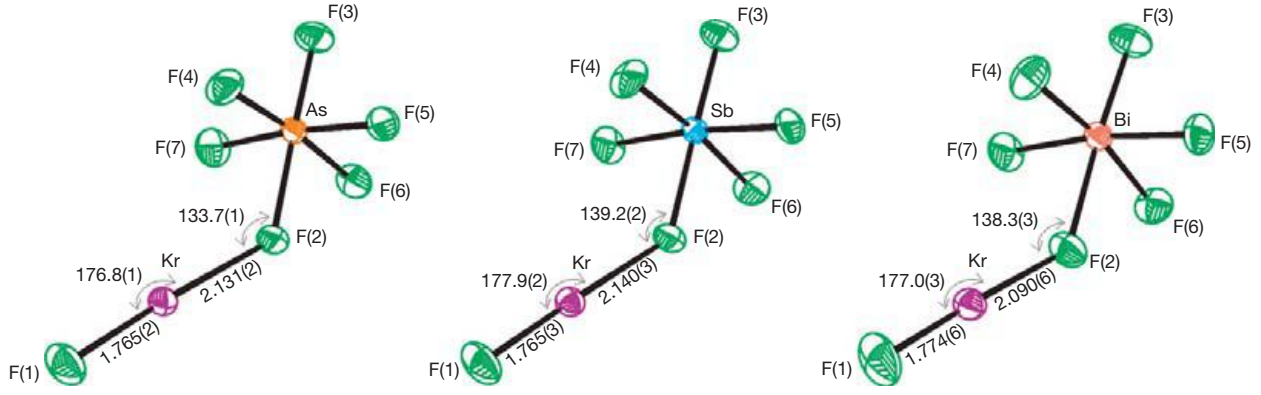

Figure 64 The structural units in the X-ray crystal structures of (a) [KrF][AsF_6], (b) [KrF][SbF_6], and (c) [KrF][BiF_6]. Thermal ellipsoids are shown at the 50% probability level. Reproduced with permission from Lehmann, J. F.; Dixon, D. A.; Schrobilgen, G. J. *Inorg. Chem.* **2001**, *40*, 3002–3017.

Copyright © 2013. Elsevier. All rights reserved.

Comprehensive Inorganic Chemistry II : From Elements to Applications, Elsevier, 2013. ProQuest Ebook Central, http://ebookcentral.proquest.com/lib/inflibnet-ebooks/detail.action?docID=1330977.
Created from inflibnet-ebooks on 2021-02-09 22:27:13.

reported for $[KrF][AsF_6]$ and $[KrF][SbF_6]$, but significantly longer than that of $[KrF][BiF_6]$.[126] Comparison of these Kr---F_b bond lengths, which are all significantly shorter than the sum of the krypton and fluorine van der Waals radii (3.49 Å),[34] supports the high FIA of AuF_5, but cannot be used to reliably establish the relative fluoride ion acceptor strengths of AuF_5, SbF_5, and AsF_5.[127]

Although a trans-effect resulting from the long Au---F_b bond (1.96(1) Å) may be expected to contract the Au−F(3) bond, this effect was not observed because the bond length uncertainties prevent discrimination among the nonbridging Au−F bonds (range, 1.89(1)–1.92(1) Å).[127] Failure to observe a trans-effect in $[KrF][AuF_6]$ is not surprising because there is no significant contraction of the M−F bond trans to the M---F_b bond in the MF_6^- (M = As, Sb, Bi) analogs, where the bond length uncertainties are more precise.[126] The fluorine bridges in $[KrF][MF_6]$ salts can be thought of in terms of a competition between the Lewis acids KrF^+ and MF_5 for F_b (Structures I–III).

$$\underset{\text{I}}{F^- Kr{-}F^+ MF_5} \leftrightarrow \underset{\text{II}}{F{-}Kr^+ F^- MF_5} \leftrightarrow \underset{\text{III}}{F{-}Kr^+ F{-}MF_5^-}$$

Thus, the ion pair has a significant amount of covalent character, which is reflected in the near-linear (AX_2E_3) F_t−Kr---F_b and bent (AX_2E_2) Kr---F_b---M bond angles. The F(1)−Kr−F(2) bond angle of the $[KrF][AuF_6]$ ion pair (175.4(7)°) deviates from the expected linear geometry which is consistent with the pnictogen analogs where this bond angle ranges from 176.8(1) (M = As) to 177.9(2)° (M = Sb).[126] Of the $[KrF][MF_6]$ species investigated by single-crystal X-ray diffraction, the $[KrF][AuF_6]$ ion pair most closely resembles an eclipsed C_s conformation in which the F(4)–Au–F(2)–Kr torsion angle is 13.6°, compared to those of $[KrF][AsF_6]$ (22.1°), $[Kr_2F_3][AsF_6]\cdot[KrF][AsF_6]$ (28.1°), $[KrF][SbF_6]$ (22.0°), and $[KrF][BiF_6]$ (19.7°).[126] The variations in the Kr---F_b---M bond angles and torsion angles may have some anion dependence; however, these values are also likely to be influenced by long interionic contacts in the solid state as inferred from the differences observed between the ion pairs in $[KrF][AsF_6]$ and $[Kr_2F_3][AsF_6]\cdot[KrF][AsF_6]$.[126]

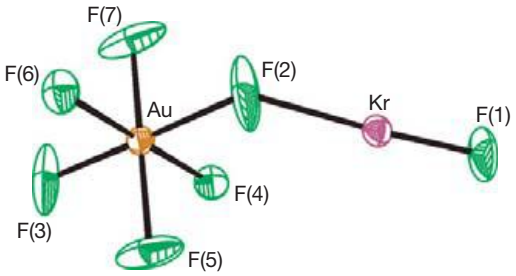

Figure 65 The structural unit in X-ray crystal structure of $[KrF][AuF_6]$. Thermal ellipsoids are shown at the 50% probability level. Reproduced with permission from Lehmann, J. F.; Schrobilgen,G. J. *J. Fluorine Chem.* **2003**, *119*, 109–124.

1.25.7.3.2 $[Kr_2F_3][SbF_6]\cdot KrF_2$, $([Kr_2F_3][SbF_6])_2\cdot KrF_2$, $[Kr_2F_3][AsF_6]\cdot[KrF][AsF_6]$, and $[Kr_2F_3][PF_6]\cdot nKrF_2$

The Kr−F_t bond lengths of the $Kr_2F_3^+$ cations exhibit no crystallographically significant variation among the structures of $([Kr_2F_3][SbF_6])_2\cdot KrF_2$ (**Figure 66**), $[Kr_2F_3][SbF_6]\cdot KrF_2$ (**Figure 67**), and $[Kr_2F_3][AsF_6]\cdot[KrF][AsF_6]$ (**Figure 68**), ranging from 1.780(7) to 1.805(5) Å with an average value of 1.796(9) Å.[126] The longer, more polar Kr---F_b bridge bonds are somewhat more sensitive to their environments, ranging from 2.027(5) to 2.065(4) Å with an average value of 2.048(14) Å. Long Kr···F interionic contacts are likely responsible for the variability of Kr---F_b bond lengths and Kr---F_b---Kr bond angles. Half of the $Kr_2F_3^+$ cations in $([Kr_2F_3][SbF_6])_2\cdot KrF_2$ are asymmetric and exhibit a small, but significant, bond length difference between Kr(1)−F_b(3) (2.041(4) Å) and Kr(2)−F_b(3) (2.065(4) Å). This is the first example of an asymmetric $Ng_2F_3^+$ (Ng = Kr, Xe) cation that has been documented crystallographically, although the possibility of an asymmetric $Kr_2F_3^+$ cation in $[Kr_2F_3][SbF_6]$ had been proposed based on Raman spectroscopic evidence.[307–309] In all other cases, $Ng_2F_3^+$ cations had been described as symmetrical (C_{2v} point symmetry).

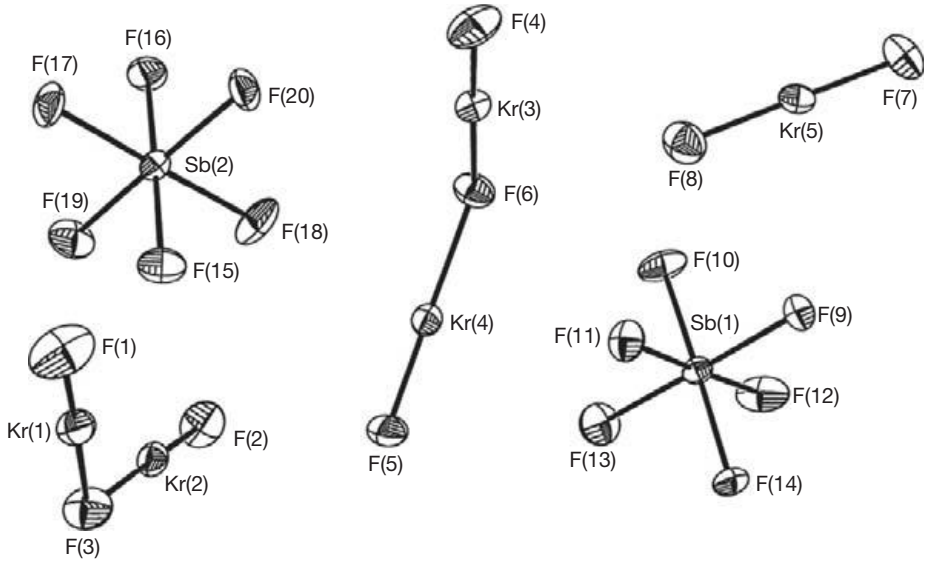

Figure 66 The structural unit in the X-ray crystal structure of $([Kr_2F_3][SbF_6])_2\cdot KrF_2$; thermal ellipsoids are shown at the 50% probability level. Reproduced with permission from Lehmann, J. F.; Dixon, D. A.; Schrobilgen, G. J. *Inorg. Chem.* **2001**, *40*, 3002–3017.

Copyright © 2013. Elsevier. All rights reserved.

Comprehensive Inorganic Chemistry II : From Elements to Applications, Elsevier, 2013. ProQuest Ebook Central, http://ebookcentral.proquest.com/lib/inflibnet-ebooks/detail.action?docID=1330977.
Created from inflibnet-ebooks on 2021-02-09 22:27:13.

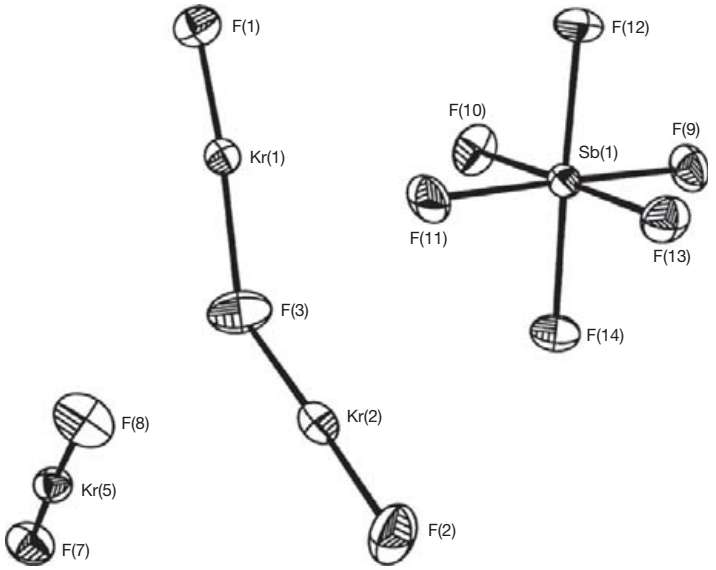

Figure 67 The structural unit in the X-ray crystal structure of $[Kr_2F_3][SbF_6]\cdot KrF_2$; thermal ellipsoids are shown at the 50% probability level. Reproduced with permission from Lehmann, J. F.; Dixon, D. A.; Schrobilgen, G. J. *Inorg. Chem.* **2001**, *40*, 3002–3017.

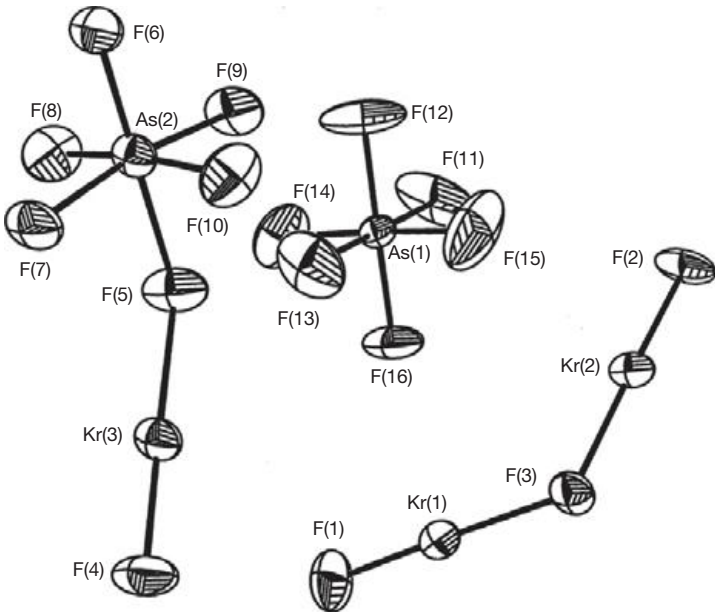

Figure 68 The structural unit in the X-ray crystal structure of $[Kr_2F_3][AsF_6]\cdot[KrF][AsF_6]$; thermal ellipsoids are shown at the 50% probability level. Reproduced with permission from Lehmann, J. F.; Dixon, D. A.; Schrobilgen, G. J. *Inorg. Chem.* **2001**, *40*, 3002–3017.

The F_t—Kr---F_b bond angles of the $Kr_2F_3^+$ cation structures investigated exhibit small, but significant, distortions from the expected linear AX_2E_3 VSEPR arrangements, ranging from 177.8(2) to 178.7(2)° in $([Kr_2F_3][SbF_6])_2\cdot KrF_2$, 175.1(2) to 176.8(2)° in $[Kr_2F_3][SbF_6]\cdot KrF_2$ and 178.2(3) to 178.6(3)° in $[Kr_2F_3][AsF_6]\cdot[KrF][AsF_6]$. The most significant bond angle variations occur for the Kr---F_b---Kr bridge, which is 126.0(2) to 128.0(2)° in $([Kr_2F_3][SbF_6])_2\cdot KrF_2$, 127.5(3)° in $[Kr_2F_3][AsF_6]\cdot[KrF][AsF_6]$, with the largest occurring in $[Kr_2F_3][SbF_6]\cdot KrF_2$ (142.5(3)°). The variability of the Kr---F_b---Kr bond angles can be attributed to long interionic/intermolecular Kr···F contacts[126] and to the effects of crystal packing on these highly deformable angles. Small F_t—Kr---F_b angle distortions result in W-shaped $Kr_2F_3^+$ cations in these salts. Although these angle distortions may also be attributed to secondary Kr···F contacts and crystal packing, they persist in the calculated gas-phase energy-minimized geometry.[126] The X-ray crystal structures and energy-minimized structures derived from theory for the $Xe_2F_3^+$ cation[140] also show that $Xe_2F_3^+$ is W-shaped. The F_t—Xe---F_b angles are distorted from linearity by similar amounts (expt., 2.4(3)° [As] and 1.4(4)° [Sb]; theor., 2.3°) when compared with those of $Kr_2F_3^+$ (expt., 3.2(1)–2.1(2)°; theor., 2.6°).

Copyright © 2013. Elsevier. All rights reserved.

Comprehensive Inorganic Chemistry II : From Elements to Applications, Elsevier, 2013. ProQuest Ebook Central, http://ebookcentral.proquest.com/lib/inflibnet-ebooks/detail.action?docID=1330977.
Created from inflibnet-ebooks on 2021-02-09 22:27:13.

Unlike the KrF_2 molecules in α-KrF_2 and β-KrF_2, which are linear by symmetry, the KrF_2 molecules in $[Kr_2F_3][SbF_6]\cdot KrF_2$ and $\{[Kr_2F_3][SbF_6]\}_2\cdot KrF_2$ are slightly bent (178.0(2) and 179.1 (2)°) with Kr−F bond lengths of 1.868(4), 1.888(4) Å, 1.881(4), and 1.887(4) Å, respectively.[126] The X-ray structure determinations of $[Kr_2F_3]_2[SbF_6]_2\cdot KrF_2$ and $[Kr_2F_3][SbF_6]\cdot KrF_2$ confirm earlier Raman spectroscopic studies of the KrF_2/SbF_5 and KrF_2/AsF_5 systems in which an undetermined excess of KrF_2 was found to associate with $[Kr_2F_3][SbF_6]$ and $[Kr_2F_3][AsF_6]$.[307–309] The symmetric KrF_2 stretch of associated KrF_2 was shifted by $\sim 10\ cm^{-1}$ to high frequency of that of free KrF_2.

1.25.7.4 KrF_2 and the Synthesis of $TcOF_5$

The last member of the series of technetium(VII) oxide fluorides, $TcOF_5$, has been prepared from TcO_2F_3 by taking advantage of the strong oxidative fluorination properties of KrF_2.[314] Technetium dioxide trifluoride, TcO_2F_3, was previously synthesized for the first time by reaction of XeF_6 with TcO_3F in aHF solvent[315] (eqn [76]).

$$XeF_6 + TcO_3F \xrightarrow[RT]{aHF} TcO_2F_3 + XeOF_4 \qquad [76]$$

No evidence was found for the fluorination of TcO_2F_3 to $TcOF_5$ when a stoichiometric excess of XeF_6 was used. Instead, excess XeF_6 present in these systems acts as a fluoride ion donor, solubilizing TcO_2F_3 to form $[XeF_5][TcO_2F_4]$.[315] In an attempt to produce a stronger fluorinating medium, TcO_2F_3 was dissolved in an eightfold molar excess of molten XeF_6 at 35 °C, forming a yellow solution which gave no indication of $TcOF_5$ formation after 5 h.[314] Upon fractionation, the components were examined by Raman spectroscopy; the volatile fraction was found to contain only XeF_6, and the involatile fraction was shown to be $[Xe_2F_{11}][TcO_2F_4]$ (eqn [77]).

$$TcO_2F_3 + 2XeF_6 \xrightarrow{XeF_6,\ 35\ ^\circ C} [Xe_2F_{11}][TcO_2F_4] \qquad [77]$$

Krypton difluoride has been shown to be a sufficiently strong fluorinating agent to fluorinate TcO_2F_3 to $TcOF_5$ in aHF. A tenfold molar excess of KrF_2 was initially used because of the competing decomposition of the KrF_2 to Kr and F_2 at room temperature over the 48-h period required for complete reaction (eqn [78]):[314]

$$TcO_2F_3 + KrF_2 \xrightarrow{HF} TcOF_5 + Kr + \tfrac{1}{2}O_2 \qquad [78]$$

The unfavorable kinetics likely result from the strong Tc–O double bonds of TcO_2F_3 and its insolubility in aHF. The reaction was repeated using the HF-soluble $[Cs][TcO_2F_4]$ salt with the view that the negative charge of $TcO_2F_4^-$ would render the Tc–O bonds more polar and the oxygen more susceptible to electrophilic attack and oxidation by KrF_2 (eqn [79].

$$[Cs][TcO_2F_4] + KrF_2 + xHF \xrightarrow{HF} TcOF_5 + Kr + \tfrac{1}{2}O_2 + [Cs]\left[(HF)_xF\right] \qquad [79]$$

However, the reaction rate did not increase significantly. Periodic sonication of a mixture of TcO_2F_3 and a fivefold molar excess of KrF_2 in aHF at room temperature for 24 h followed by solvent removal under vacuum at −78 °C proved to be the most efficient method for the synthesis of $TcOF_5$.

Technetium oxide pentafluoride is a volatile orange solid that melts reversibly and without decomposition at 57–58 °C and is deep red–orange in color in the liquid state. When maintained under anhydrous conditions, the solid is stable for at least 2 weeks at room temperature and is stable indefinitely when stored at −78 °C. The pseudo-octahedral (C_{4v}) structure of $TcOF_5$ has been determined by ^{19}F and ^{99}Tc NMR spectroscopy, Raman and IR spectroscopies, and by single-crystal X-ray diffraction.

1.25.8 Thermochemistries of Known and Unknown Ionic Noble-Gas Compounds

Studies of the thermochemistries of noble-gas compounds have been limited by the general paucity of available thermochemical data. For this reason, the VBT approach[174,316–319] has been used to confirm and predict the stabilities of a variety of known and unknown noble-gas salts.[93] The VBT approach provides a link between structural (crystal) features, through volume and lattice energy, and the corresponding thermochemistry of the crystalline material. In the few situations where thermochemical facts are known, VBT tends to validate and confirm these, giving some confidence that the predicted results should provide a guide to thermodynamic possibilities.

The VBT lattice energies, U_{POT}, enthalpies of formation, ΔH_f^o, VBT standard entropies, S_{298}^o, standard entropies of formation, ΔS_f^o, and Gibbs free energies of formation, ΔG_f^o, for XeF^+, XeF_3^+, $XeOF_3^+$, XeF_5^+, Xe_2^+, $Xe_2F_3^+$, $Xe_2F_{11}^+$, $FXeOS(F)OXeF^+$, $XeN(SO_2F_2)_2^+$, $XeOSeF_5^+$, $XeOTeF_5^+$, $XeCl^+$, KrF^+, and $Kr_2F_3^+$ salts, as well as for hypothetical ArF^+ salts have been determined.[93] The stabilities of $[XeF_n][Sb_2F_{11}]$ ($n = 2, 3$) and $[XeF][AsF_6]$ were confirmed with respect to dissociation to the xenon fluoride and pnictogen pentafluoride, whereas the stabilities of $[XeF_3][AsF_6]$ and $[XeF_3][As_2F_{11}]$ were shown to be marginal under standard conditions. The VBT method confirmed that the known XeF^+ salts are thermodynamically stable with respect to redox decomposition and that KrF^+ salts and all (hypothetical) ArF^+ salts (MF_6^-, M = P, As, Sb, Au, and $Sb_2F_{11}^-$) considered are unstable with respect to redox decomposition to Ng(g), F_2(g), and MF_5(g) (Ng = Ar, Kr).

1.25.9 Noble-Gas Molecules Characterized by Mass Spectrometry and Matrix Isolation

Noble-gas containing molecules that lie at the fringes of stability and have been formed/characterized by use of matrix isolation, laser ablation, and mass spectrometric techniques have attracted considerable attention since 1994 when Ar was shown to interact with BeO in a solid Ar matrix.[320] While these molecules have been formed, spectroscopically characterized, and modeled computationally using ab initio methods (DFT methods were not always reliable),[321] they have not been synthesized in bulk amounts and cannot be used as synthetic precursors for further chemistry; however, in a number of cases, it may be possible to isolate macroscopic quantities by other means. Over the past decade, a significant body of work has been carried out in this area to warrant two reviews summarizing experimental and computational findings

Copyright © 2013. Elsevier. All rights reserved.

Comprehensive Inorganic Chemistry II : From Elements to Applications, Elsevier, 2013. ProQuest Ebook Central, http://ebookcentral.proquest.com/lib/inflibnet-ebooks/detail.action?docID=1330977.
Created from inflibnet-ebooks on 2021-02-09 22:27:13.

relating to the HNgY family of molecules (Ng = Ar, Kr, Xe; Y = electronegative fragments).[322,323] In general, matrix-isolated species are formed by photolysis of a precursor having the general formula HY in a solid noble-gas matrix at approximately 10–30 K followed by annealing between 30 and 40 K with temperatures depending on the noble-gas matrix used and the stability of the product.

1.25.9.1 Matrix-Isolated Noble Gases Bonded to Non-metals

The argon-containing molecule, HArF, was formed by the photolysis of HF in a solid argon matrix below 27 K and was identified by IR spectroscopy and by isotopic substitution using HF/^{40}Ar, HF/^{36}Ar, and DF/^{40}Ar matrices.[324] Three bands appeared at 1969.5, 687.0, and 435.7 cm^{-1} in the HF/^{40}Ar spectrum, while two bands in the DF/^{40}Ar spectrum were shifted to lower frequency: 1466.3 (H–Ar stretch), 513.0 (bending), and 435.3 cm^{-1} (Ar–F stretch). When HF/^{36}Ar was used, the three IR absorptions were shifted to higher frequencies (2, 2, and 7 cm^{-1}, respectively) relative to their values in HF/^{40}Ar matrices. The vibrational assignments and energy-minimized geometries of these isotopomeric molecules were calculated using ab initio methods.[324] A second, more stable form of HArF was obtained by preparing samples as described above and annealing them at 30 K. The new solid-state configuration of HArF showed bands at 2020.8 and 697.0 cm^{-1}.[325] The effects of the precursor concentration, deuteration, IR radiation, and deposition temperature as well as thermal activation of this reaction were also studied experimentally,[326] while the bonding in gas-phase HArF was studied computationally.[327] The two forms of HArF have been referred to as 'unstable' and 'stable' forms, respectively, and their interconversions were investigated experimentally and computationally.[328] Two conversion mechanisms were proposed. One involved the local mobility of a neighboring vacancy. The second involved formation of stable HArF by rotation of the trapped molecule inside the matrix cavity without vacancy assistance. The latter pathway was energetically improbable at the experimental temperatures that were used.

The method used for generating HArF was also applied to form HKrF. The fundamental vibrations were observed by IR spectroscopy at ~1950 cm^{-1} (H–Kr stretch), ~650 cm^{-1} (bending), and ~415 cm^{-1} (Kr–F stretch).[329] Two distinct sites were observed for HKrF with a significant (~26 cm^{-1}) energy difference between the H–Kr stretching vibrations of HKrF in the two sites.

A variety of noble-gas species bonded to the halogens have been formed in low-temperature Ng matrices having the general formula, $^{1/2}$HNgY (Ng = Xe, Y = Cl, Br, I; Ng = Kr, Y = Cl).[330] An interesting property of HXeI is its ability to orientate in a weak static electric field allowing for its detection in the gas phase by time-of-flight mass spectrometry.[331] Matrix-isolated $^{1/2}$HNgY was characterized by IR spectroscopy and by quantum-chemical calculations. Of the three bands that are predicted for linear HNgY molecules, only the intense Ng–$^{1/2}$H stretch was observed, in most cases, in the IR spectrum and was used to identify $^{1/2}$HNgY.[330] The Ng–$^{1/2}$H stretch decreased across the halogen series for Xe [Cl: 1648 cm^{-1} (^{1}H), 1198 (^{2}H); Br: 1504 cm^{-1} (^{1}H), 1100 cm^{-1} (^{2}H); I: 1193 cm^{-1} (^{1}H), 893 cm^{-1} (^{2}H)] and also decreased from $^{1/2}$HXeCl [1648 cm^{-1} (^{1}H), 1198 cm^{-1} (^{2}H)] to $^{1/2}$HKrCl [1476 cm^{-1} (^{1}H), 1106 cm^{-1} (^{2}H)].

The HNgY molecules generally exhibited closely spaced sets of bands in the H–Ng stretching region. The most intense band was attributed to matrix sites where embedded HNgY molecules interacted with noble-gas matrix atoms, whereas the weaker band was attributed to hindered rotation of the embedded molecules in the lattice with the latter band shifting to higher frequency.[332] In an effort to better understand the site geometries, annealing behaviors, and band splittings observed in the IR spectra, several of the new noble-gas compounds characterized in matrix environments were studied computationally and the findings were in good agreement with the experimental results.[333] Comparison with the experimental findings indicated that the matrix shifts were considerably greater than typically found for neutral strongly bonded molecules and that the effects of the matrix site for HXeCl and HXeI, which are more restrictive, are significantly different from the matrix sites of HArF and HKrF, where there is more space around the F atoms.

UV-absorption spectroscopy of HXeY (Y = Cl, Br, I, CN) in a solid xenon matrix at 12 K in conjunction with multireference configuration interaction (MRCI) calculations indicated the single absorption band observed for each species resulted from A $^1\Sigma \leftarrow$ X $^1\Sigma$ transitions.[334] In addition, the absorption bandwidth was indicative of a transition from a bound ground state to a repulsive excited state.

Although it has not been possible to examine the subsequent chemistry and reactivities of these matrix-isolated molecules, N_2 complexes with HArF,[335] HKrF,[335] HKrCl,[335] HXeCl,[336] and HXeBr[336] have been formed by introducing small amounts (0–1:500, N_2:Ng) of nitrogen into the noble-gas matrix prior to photolysis. Two complex configurations were observed where N_2 coordinated linearly to the H atom (Figure 69, Structure 1) and where N_2 coordinated in a bent fashion to the Ng atom (Figure 69, Structure 2) of HArF, HKrF, and HKrCl.[335] Electrostatic forces are the dominant interaction in the linear complex and electrostatic and dispersion forces are almost equally dominant for the bent complexes. Complexation also resulted in exceptionally large high-frequency shifts, especially for the linearly coordinated structures (>100 cm^{-1} for ν(H–Kr) of HKrF).

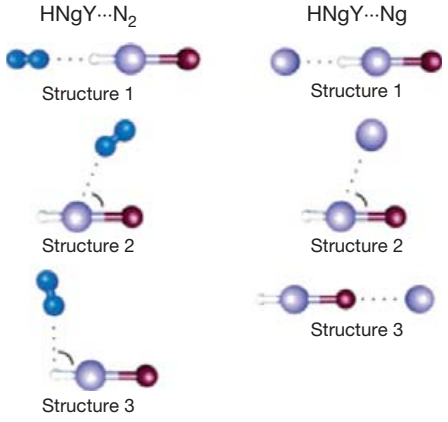

Figure 69 The proposed coordination geometries for HNgY···N_2 and HNgY···Ng. Reproduced in modified form from Khriachtchev, L.; Tapio, S.; Räsänen, M.; Domanskaya, A.; Lignell, A. *J. Chem. Phys.* **2010**, *133*, 084309/1–084309/13.

Copyright © 2013. Elsevier. All rights reserved.

Comprehensive Inorganic Chemistry II : From Elements to Applications, Elsevier, 2013. ProQuest Ebook Central, http://ebookcentral.proquest.com/lib/inflibnet-ebooks/detail.action?docID=1330977.
Created from inflibnet-ebooks on 2021-02-09 22:27:13.

By contrast, the complexation shifts of HXeCl and HXeBr were much smaller (~10 cm^{-1}), ruling out the possibility of a linearly coordinated nitrogen molecule, suggesting both molecules are bent and exist in one of two configurations (Figure 69, Structures 2 and 3).[336]

A number of matrix-isolated molecules having the general formula $^{1/2}$HNgY (Ng=Xe, Y=CN, NC, NCO, O$^{1/2}$H, S$^{1/2}$H, $^{1/2}$H; Ng=Kr, Y=CN) have been identified on the basis of their ν(H–Ng) stretching bands by IR spectroscopy. The ν(H–Ng) bands occurred at highest frequency for the nitrogen-bound ligands, –NC and –NCO, and at lowest frequency for the –S$^{1/2}$H and –$^{1/2}$H ligands.[330] The HNgCN, HNgNC (Ng=Kr, Xe), HXeSH, and HXeOH molecules were also investigated by topological analyses of their ELFs, which models the bonding and delocalization of electron density. In all cases, the calculations revealed that the species are best described as charge-transfer systems.[337]

Ultra-violet photolysis of H_2S, HI, and H_2CO in solid xenon has led to the formation and characterization of HXeSH, HXeI, and HXeH.[338] The absorption maxima of HXeSH and HXeH are near 290 and 230 nm, respectively, whereas HXeI has two maxima at 310 and 410 nm.

The identification of HXeOXeH, which seems to be the smallest known neutral matrix-isolated molecule with two noble-gas atoms, was confirmed by IR spectroscopy and was supported by quantum-chemical calculations.[339] Preliminary evidence for the fluorine analog, FXeOXeF, has also been reported (see Section 1.25.3.2.2). The HXeOXeH molecule was formed by UV photolysis of water in a xenon matrix and subsequent annealing at 40–45 K. The HXeOXeH molecule was formed by the reaction, HXeO·+Xe+H, where the HXeO· radical (see Section 1.25.9.1.1) is an intermediate precursor formed by H+Xe+O. It has been suggested that HXeOXeH may represent a first step toward the possible formation of $(Xe–O)_n$ chains and that it may be relevant to depletion of xenon from the Earth's atmosphere.[252,254–256] The kinetic stabilities of HXeOH and HXeOXeH have also been studied computationally and have intrinsic half-lives of 1 h at 170 and 120 K, respectively.[340]

Interest in the aforementioned matrix-isolated molecules has prompted numerous computational studies including an examination of HNgF (Ng=He, Ar, Kr) hyperpolarizabilities,[341] suppression of the decomposition of HNgY to HY and Ng,[342] and reexamination of the HXeY (Y=F, Cl, Br, I, CCH, CN, NC)[343] and HNgF (Ng=Ar–Rn)[344] families of molecules. Other studies have probed interactions of HArF or HKrF with CO[345] and of BO^+ with He[346] and have postulated the possible formation of other noble-gas species including HArCl,[347] HNgNgF (Ng=Ar–Xe),[348,349] $HNgFNgH^+$ (Ng=He–Xe),[350] XeI,[351] XeI^+,[351] XeI^-,[351] NgH^+ (Ng=He–Xe),[352] and the first Ng–Se-bonded species, $FNgSe^-$ (Ng=Kr and Xe).[353]

With the existence of the aforementioned molecules/ions, it is not surprising that xenon incorporation into unsaturated hydrocarbons, including acetylene, benzene, and phenol, has also been considered. Calculations showed these compounds to be stable[354] and the predictions were confirmed when HXeCCH,[355–357] HXeCCXeH,[355] and HXeCC[355] were formed by photolysis of HC≡CH in a xenon matrix. Alternatively, HXeCCH has been formed by irradiation of HC≡CH with fast electrons (~1 MeV) in a xenon matrix.[356] Three IR bands were observed for HXeCCH.[355] The H–C stretching and HCC bending modes were assigned to bands at 3273 and 626 cm^{-1}, respectively, with a band at 1486 cm^{-1} assigned to the H–Xe stretching mode. Two stretching bands were observed for HXeCC, with the H–Xe stretch assigned at 1478 cm^{-1} and the C≡C stretch assigned at 1748 cm^{-1}. Only a single band at 1301 cm^{-1}, assigned to the H–Xe stretch, was observed for HXeCCXeH. In addition to the more polarizable Xe matrix, Ar and Kr matrices were used to form HXeCCH where the H–Xe stretching bands are shifted to higher frequency (44.9 and 32.3 cm^{-1}, respectively) with respect to the values measured in a Xe matrix.[357] The assignments of the HXeCCH and HXeCC spectra, as well as that of HXeH, were confirmed by ^{129}Xe and ^{136}Xe enrichment studies.[358] Although the isotopic shifts for the H–Xe stretching absorptions were small (0.17–0.38 cm^{-1}), they were reproducible and are in agreement with those predicted by quantum-chemical calculations. The ^{129}Xe and ^{136}Xe spectra of HXeH were also calculated.

The photolysis of propriolic acid (HCCCOOH) in a xenon matrix was shown to form HXeCCH and CO_2, which, in turn, interacted to form a complex (Figure 70).[359] Coordination of CO_2 to HXeCCH resulted in two H–Xe stretching bands which are shifted to higher frequency relative to HXeCCH monomer by 5.8 and 31.9 cm^{-1}. Of the three stable models for the complex (Figure 70), it was proposed that the band which shifted by 5.8 cm^{-1} is the parallel structure and that the band shifted by 31.9 cm^{-1} is the same structure in another matrix site or the linear structure.

The krypton analog, HKrCCH, was also formed in a krypton matrix in a manner analogous to the formation of HXeCCH.[360] The formation of HArCCH was, however, unsuccessful using the analogous method. The H–Kr stretching absorption appears as closely spaced bands at 1241.5, 1249.5, and 1257 cm^{-1} which are attributed to different matrix sites. The H–C stretching and C–C–H bending modes were observed at 3290 and 608/610 cm^{-1}, respectively. All three vibrational frequencies are shifted to lower frequency than in the xenon analog, in accordance with the calculated frequencies.

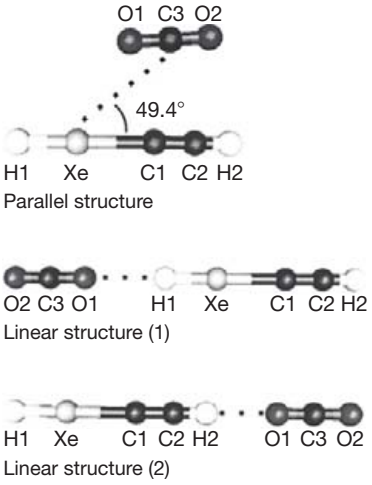

Figure 70 The proposed geometries for the complex formed by HXeCCH and CO_2 in a xenon matrix. Reproduced with permission from Tanskanen, H.; Johansson, S.; Lignell, A.; Khriachtchev, L.; Räsänen, M. *J. Chem. Phys.* **2007**, *127*, 154313/1–154313/7.

Copyright © 2013. Elsevier. All rights reserved.

Comprehensive Inorganic Chemistry II : From Elements to Applications, Elsevier, 2013. ProQuest Ebook Central, http://ebookcentral.proquest.com/lib/inflibnet-ebooks/detail.action?docID=1330977.
Created from inflibnet-ebooks on 2021-02-09 22:27:13.

In a related computational study, it was shown that the same experimental approach could plausibly be extended to yield radon species, HRnCCH and HRnOH,[361] the disubstituted compounds HCCNgCCH (Ng = Kr, Xe),[362] and the tetra- and hexa-substituted compounds, $Ng(CCH)_4$ and $Ng(CCH)_6$ (Ng = Kr, Xe),[363] which are predicted to be stable in the gas phase.

The fluorine analogs, HNgCCF and HCCNgF (Ng = Kr, Xe), were also observed when HCCF was photolyzed in xenon or krypton matrices.[364] The HNgCCF molecules displayed greater stabilities than the corresponding HNgCCH compounds. However, no conclusive evidence for the existence of the Ar analog was obtained. The possibility of forming the related hydrogen-free molecules, XNgCCX and XNgCCNgX (Ng = Kr, Ar; X = F, Cl), has also been investigated computationally, showing them to be stable.[365]

The formation of noble-gas hydrides having longer carbon chains was successful when diacetylene was photolyzed at 193–250 nm in krypton and xenon matrices and followed by annealing.[366] The $HNgC_4H$ (Ng = Kr, Xe) molecules are the highest molecular weight noble-gas hydrides presently known and are predicted to be more stable than their lighter $HNgC_2H$ analogs[366] which have led to the prediction that the argon analog, $HArC_4H$, may also be formed under matrix-isolation conditions.[367] It has also been suggested that the larger, as yet unknown, $HNgC_6H$ and $HNgC_8H$ molecules might be good candidates for bulk syntheses.[366]

1.25.9.1.1 The ·XeF_3 and HXeO· Radicals

Matrix isolation has also provided the discovery of the Xe(IV) radical, ·XeF_3, which possesses a T-shaped geometry.[218] The XeF_3^+ cation also has a T-shaped geometry that results from a trigonal bipyramidal AX_3E_2 VSEPR arrangement with the equatorial plane occupied by a fluorine atom and two lone electron pairs and the axial positions occupied by two fluorine atoms. The trans-axial fluorine atoms are bent toward the equatorial fluorine atom. This contrasts with XeF_3· where the axial fluorine atoms are bent away from the equatorial fluorine atom, implying that two lone electron pairs occupy positions trans to one another and 90° from the trans-axial fluorine atoms and that the lone electron is positioned trans to the equatorial fluorine atom. Dilute mixtures (1:2:3000) of XeF_2 and F_2 in an Ar matrix were photolyzed at 12 K using 337 nm radiation followed by annealing at 20 K. The ·XeF_3 radical was stable up to 27 K and revealed a new, intense IR band at 568 cm^{-1} and a very weak band at 523 cm^{-1} assigned to the asymmetric and symmetric XeF_2 stretching modes of the trans-axial Xe–F bonds, respectively. The Xe–F stretch of the equatorial Xe–F bond was not observed.

The HXeO· radical was observed as an intermediate during the annealing process leading to HXeOH formation.[368] When annealing was carried out at 35 K, significant amounts of the radical were indicated by the appearance of the ν(H–Xe) band at 1466.1 cm^{-1} (1070.3 cm^{-1} for ^{2}H-enriched samples). Upon annealing at 45 K, this band decreased in intensity with the appearance of a band at 1578 cm^{-1} assigned to ν(H–Xe) of HXeOH. The potential energy surface and vibrational energy levels of HXeO· have also been calculated and show that a three-body dissociation channel is the dominant dissociation channel for HXeO·.[369]

1.25.9.2 Coordination of Noble Gases to Transition Metal Oxides

Laser ablation of an uranium target produces uranium atoms that, when co-condensed with carbon monoxide, argon, and xenon, yield $CUO(Ar)_{4-n}(Xe)_n$ ($n = 1–4$).[370,371] Four noble-gas atoms are coordinated to uranium, representing the first neutral compound involving four noble-gas atoms around a single metal center. This chemistry has been extended to krypton, resulting in species of the type $CUO(Ar)_{4-n}(Kr)_n$.[371,372] In solid argon, triplet states are formed for the different compounds but linear, singlet states are formed in neon. When uranium atoms were isolated in inert and CO-doped matrices using dilute Ar, Kr, or Xe in an excess of neon, CUO(Ar), CUO(Kr), and CUO(Xe) were identified which also contained neon atoms in the uranium coordination sphere.[373] A singlet ground state was observed for $CUO(Ne)_x(Ng)_y$ complexes for $y = 0–2$, and a triplet spin state was observed for $y = 3$, 4, or when neon was absent.

Laser ablation of uranium in the presence of O_2 resulted in UO_2, which was co-condensed with argon.[374] The electronic ground state of UO_2 in solid argon was determined by near-UV spectroscopy. It was anticipated that, as for CUO (see above), the presence of argon atoms may result in reordering of the low-lying electronic states of UO_2. While the results did not support this interpretation, it was concluded that UO_2 exhibits 'unusually strong interactions with argon.' Coupled-cluster and DFT calculations suggested that the most likely complex observed under the conditions described above was $UO_2(Ar_5)$.[375] Additionally, the very large difference in vibrational frequencies observed on changing the matrix from argon to neon suggested that a reordering of the electronic states had occurred. A related study indicated a significantly stronger interaction between the uranium atom and the noble-gas atom for UO_2^+ than between the uranium atom and the noble-gas for neutral UO_2.[376]

Laser ablation of various metal oxides (Cr_2O_3, MnO_2, Fe_2O_3, Co_2O_3, and Ni_2O_3) in noble-gas (Ar, Kr, and Xe) matrices resulted in the 1:1 complexes, NgMO (Ng = Ar, Kr, Xe).[377] When Sc_2O_3 or Y_2O_3 was used, computational studies indicated that the transition metal monoxide cations, ScO^+ and YO^+, coordinate five and six noble-gas atoms, respectively, to form $[ScO(Ng)_5]^+$ (Ng = Ar, Kr, Xe)[378] and $[YO(Ng)_6]^+$ (Ng = Ar, Kr).[379] When mixed noble-gas matrices were used, the new species $[ScO(Ar)_{5-n}(Kr)_n]^+$, $[ScO(Kr)_{5-n}(Xe)_n]^+$ ($n = 1–5$), $[YO(Ar)_{6-n}(Kr)_n]^+$ ($n = 1–6$), and $[YO(Ar)_{6-n}(Xe)_n]^+$ ($n = 1–4$) were formed.[378,379] The VO_2 and VO_4 species were formed by analogous procedures and coordinated two Ar or Xe atoms and one Ar or Xe atom, respectively.[380] The binding of Be_2O_2 to noble-gas atoms and the stabilities of the resulting complexes were also studied computationally and indicated that Be_2O_2 can bind two noble-gas atoms, with the calculated binding energy increasing from He to Xe.[381]

Xenon compounds of gold have been characterized by X-ray crystallography (see **Section 1.25.2.2**); so it is not surprising that the matrix isolation of noble-gas species of the coinage metals has been undertaken. Laser ablation of a gold surface in gaseous chlorine and noble-gas mixtures resulted in ArAuCl and KrAuCl in the gas phase, which were characterized by microwave rotational spectroscopy.[53] Laser-ablated gold and

Copyright © 2013. Elsevier. All rights reserved.

Comprehensive Inorganic Chemistry II : From Elements to Applications, Elsevier, 2013. ProQuest Ebook Central, http://ebookcentral.proquest.com/lib/inflibnet-ebooks/detail.action?docID=1330977.
Created from inflibnet-ebooks on 2021-02-09 22:27:13.

silver have been reacted with SF_6 or Br_2 in the presence of krypton to give KrAuF, KrAgF, and KrAgBr.[382] Using similar methodology, XeAuF was produced from laser-ablated gold, SF_6, and xenon.[383] Microwave rotational spectroscopy of the krypton complexes showed that they are linear, rigid, and possess relatively short krypton–metal bonds [r_o(Kr–Au) = 2.463253(15) Å, r_o(Kr–Ag) = 2.6681(39) Å]. The ^{83}Kr and ^{197}Au nuclear quadrupole coupling constants allowed the electronic distribution to be obtained, and suggested that weak chemical bonding existed, especially for NgAuF.[382] The XeAuF complex was also shown to be linear and to possess an Au–Xe bond length of 2.54 Å.[383] The analogous copper complexes have also been investigated and evidence has been found for both KrCuF and KrCuCl as weakly bound molecules.[384] The complexes lie at the limit between van der Waals interactions and weak covalent bonds (Kr–Cu bond lengths: KrCuF, 2.32 Å; KrCuCl, 2.36 Å). By contrast, XeCuF and XeCuCl possess rather short Xe–Cu bonds (2.43 and 2.47 Å, respectively).[385] A number of computational papers have also examined coinage metal complexes[386–390] and have postulated the existence of HePtF.[391]

Laser ablated metals such as Ti, V, Nb, and Ta react with O_2 and xenon mixtures in argon matrices to form $XeOO^+$ which was characterized by ^{18}O-isotopic enrichment, using IR spectroscopy, and by ab initio and DFT calculations.[392]

1.25.9.3 Noble-Gas Species Observed by Mass Spectrometry

Noble-gas species that form in the gas phase may suggest molecules or ions that are likely to be stable in electron-poor environments such as those encountered in noble-gas matrices and superacid media.

Although HXeCCH has been characterized in the solid state by matrix isolation (see **Section 1.25.9.1**), its observation in a time-of-flight mass spectrometer was achieved by photolysis of acetylene in the presence of Xe_n ($n = 390$) clusters.[393] Other new noble-gas species, including $HCCNg^{2+}$ (Ng = Ar, Kr), have also been observed by mass spectrometry.[394] Hyperthermal collisions of neutral argon and krypton gases with mass-selected acetylene dications yielded organo-noble-gas dications. Although the yields were low, the use of multiply charged ions as reagents may prove successful for the formation of other noble-gas compounds that have been predicted by theory.

The reaction of argon with mass-selected CH_3Br^{2+}/CH_2BrH^{2+} dications led to a noble-gas carbene cation, $ArCH_2^+$,[395] while reaction of argon with the CF_3^{2+} dication yielded $ArCF_2^{2+}$.[396] An analogous procedure was used in which argon was allowed to react with the superelectrophilic SiF_3^{2+} dication, produced by dissociative double ionization of SiF_4, to form the $ArSiF_2^{2+}$ dication and, presumably, a fluorine atom as the major products.[397] The calculated Ar–Si bond is relatively strong (2.78 eV) and covalent in character. In a similar reaction, small amounts of $^{20}NeSiF_2^{2+}$ and $^{22}NeSiF_2^{2+}$ have also been observed which possess much weaker Ne–Si bonds (0.80 eV).

Interactions of germanium or barium with the noble gases have also been observed by mass spectrometry. The Ba^{2+} cation has been shown to interact with He, Ar, Kr, and Xe to form $BaHe^{2+}$, $BaAr^{2+}$, $BaKr^{2+}$, $BaXe^{2+}$, $Ba(Ar)_2^{2+}$, $Ba(Kr)_2^{2+}$, and $Ba(Xe)_2^{2+}$ with the increasing polarizability of the noble-gas atom resulting in stronger Ba–Ng bonding interactions.[398] Nucleophilic displacement of HF from protonated GeF_4 by Xe forms F_3GeXe^+, a stable cation in the gas phase.[399] This class of cations has also led to the proposal, based on quantum-chemical calculations, that $AlNg^+$,[400] $BeNg^{n+}$,[401] and $MgNg^{n+}$[402] ($n = 1, 2$; Ng = He, Ne, Ar, Kr, Xe, Rn) may also be formed in the gas phase.

1.25.10 Synthetic Applications of XeF_2

1.25.10.1 XeF_2 as an Oxidizing and Fluorinating Agent

Xenon difluoride has considerable potential as an oxidative fluorinating agent because of its low average Xe–F bond energy (133.9 kJ mol^{-1}) and the inertness of its reduction product, xenon. Furthermore, it has been shown that XeF_2 has considerable kinetic stability, for example, it can be recovered from aqueous solution, in which it is thermodynamically unstable toward hydrolysis, by extraction with CCl_4 or by fractional distillation.[402] The formation of cationic Xe(II) species such as XeF^+ and $Xe_2F_3^+$ in aHF solvent and in the presence of Lewis acids provides even stronger oxidative fluorinating reagents. The electron affinities of XeF^+ and $Xe_2F_3^+$ salts are greater than that of XeF_2. Electron transfer to either of these cations generates the FXe· radical, which is an effective fluorine atom source.[403]

Elements, lower fluorides, halides, halo-complexes, and oxides and carbonyls of several elements can be oxidized with XeF_2 in aHF. This section provides the reader with an overview of the extent to which XeF_2 has been utilized as an oxidative fluorinator in inorganic and organic chemistry.

1.25.10.2 Inorganic Syntheses

1.25.10.2.1 XeF_2 as a fluorinating agent in the preparation of fluorofullerenes

Fluorofullerenes having low fluorine contents have been synthesized by the fluorination of bromofullerenes or chlorofullerenes. It is known that the halogen atom can act as a blocking agent to prevent the formation of reaction products having high fluorine content.[404] The fluorination of $C_{60}Br_{24}$ with elemental fluorine at room temperature yielded a mixture of $C_{60}F_n$ fluorofullerenes ($n \leq 44$) which contained predominantly $C_{60}F_{36}$. The reaction of $C_{60}Br_{24}$ bromofullerene with XeF_2 in aHF yielded $C_{60}F_{24}$ which was characterized by X-ray photoelectron spectroscopy.[405] When BrF_5 was used instead of aHF under the same reaction conditions, $C_{60}Br_4F_{20}$ was the major product.[406]

The solid-phase fluorination of $C_{60}Br_{24}$ with XeF_2 was carried out over a wide range of temperatures.[407] The degree of substrate fluorination was primarily determined by the duration of reactant contact. It was shown that T_h-$C_{60}Br_{24}$ reacts with XeF_2 dissolved in aHF to form T_h-$C_{60}F_{24}$ in ~80% compositional purity.[408] This kinetically stable isomer represents the first example of a new family of fluorofullerenes having a noncontiguous addition pattern.

1.25.10.2.2 The role of XeF_2 in the synthesis of Ni_2F_5 and its oxidation by KrF_2

The compound, Ni_2F_5, is stable at room temperature when kept in a dry atmosphere.[409] It slowly decomposes in aHF to

Copyright © 2013. Elsevier. All rights reserved.

Comprehensive Inorganic Chemistry II : From Elements to Applications, Elsevier, 2013. ProQuest Ebook Central, http://ebookcentral.proquest.com/lib/inflibnet-ebooks/detail.action?docID=1330977.
Created from inflibnet-ebooks on 2021-02-09 22:27:13.

NiF_2 and fluorine. Among the higher nickel fluorides, it is the most stable and has been prepared from rhombohedral NiF_3 (R-NiF_3) by thermal decomposition, which is the best method for its preparation, or by reduction with an excess of xenon (eqn [80]) or XeF_2 (eqn [81]).

$$4R\text{-}NiF_3 + nXe \xrightarrow{22\,^\circ C} 2Ni_2F_5 + XeF_2 + (n-1)Xe \qquad [80]$$

$$4R\text{-}NiF_3 + nXeF_2 \longrightarrow 2Ni_2F_5 + XeF_4 + (n-1)XeF_2 \qquad [81]$$

Mass balances indicate that R-NiF_3 oxidizes XeF_2 to XeF_6. In the presence of XeF_6, a fluorobase, the remaining R-NiF_3 disproportionates to Ni(II) and Ni(IV). Nickel(IV) presumably forms salts with XeF_6 of the type $(XeF_5)(Ni_xF_{4x+1})$ ($x = 1, 2, 3, \ldots$), which have no vapor pressure and cannot be removed from the sample by pumping on a vacuum line. There is no further characterization of these minor byproducts.

Reaction of Ni_2F_5 with excess Xe in aHF at room temperature yields XeF_2 (eqn [82]). The oxidation of Ni_2F_5 by excess KrF_2 in aHF yields R-NiF_3 (eqn [83] where n is excess KrF_2 and z is the amount of KrF_2 which decomposes in aHF). The reaction was carried out over 4 days at 0 °C to minimize decomposition of R-NiF_3 in aHF.

$$2Ni_2F_5 + nXe \xrightarrow[\text{aHF}]{22\,^\circ C} 4NiF_2 + XeF_2 + (n-1)Xe \qquad [82]$$

$$2Ni_2F_5 + nKrF_2 \xrightarrow[\text{aHF}]{0\,^\circ C} 4R\text{-}NiF_3 + (1+z)Kr + zF_2 + (n-1-z)KrF_2 \qquad [83]$$

1.25.10.2.3 Reactions of tri(9-anthryl) derivatives of phosphorus and bismuth

Recently, π-electron systems containing main-group elements have attracted attention because of their unusual photophysical and electrical properties. The approach involves changing the coordination number of the central element or its valence state and represents a powerful new way to control the properties of the π-electron systems through the intrinsic electronic effect as well as through structural changes.

A series of tri(9-anthryl)phosphorus derivatives have been synthesized from tri(9-anthryl)phosphane. The synthesis of tri(9-anthryl)difluorophosphorane was achieved by use of XeF_2 as the oxidative fluorinating agent.[410] Pentacoordinate tri(9-anthryl)difluorophosphorane exhibits intense fluorescence which is comparable to that of the parent anthracene. Xenon difluoride was also used to oxidatively fluorinate tri(9-anthryl)-bismutine derivatives to the corresponding tri(9-anthryl)-difluorobismuth derivatives.[411] The goal of the investigation was to study the influence of the heaviest main-group element, having the largest atomic radius, on through-space interactions among the three anthryl groups.

1.25.10.2.4 Syntheses of organotellurium(IV) diazides and triazides

Xenon difluoride has been used as an oxidative fluorinating agent in the syntheses of organotellurium(IV) diazides and triazides.[412] Diorganotellurides and diorganoditellurides were oxidized by XeF_2 to give the corresponding diorganotellurium difluorides and organotellurium trifluorides. The trifluorides, which were not isolated, were treated with a slight excess of trimethylsilyl azide to form alkyl/aryltellurium(IV) triazides.

1.25.10.2.5 Syntheses of Pd(II), Pd(IV), Pt(II), and Pt(IV) fluoride complexes

Transition metal fluoride complexes are important intermediates in selective C–F bond activation processes and in catalysis. Because the nucleophilic fluoride anion is known to cause reductive decomposition of several Pd(II) phosphane complexes,[413] an alternative approach to their fluorinations was investigated.[414] When the dimethyl $L_2Pd(CH_3)_2$ complexes were treated with an equivalent amount of XeF_2 in dry CH_2Cl_2, the quantitative formation of the difluoro complex, L_2PdF_2, resulted (eqn [84]). The reaction was carried out in the temperature range −30 °C to room temperature using di(*i*-propylphosphino)propane (dippp) and di(cyclohexylphosphino)propane (dcpp) as ligands.

$$L_2Pd(CH_3)_2 + XeF_2 \rightarrow L_2PdF_2 + Xe + C_2H_6 \qquad [84]$$

The compounds, L_2PdF_2, are white solids which decompose in solution at room temperature and as solids in an inert atmosphere. The exact stoichiometry in eqn [84] must be adhered to because a stoichiometric excess of XeF_2 results in partial decomposition, and the formation of fluorinated phosphorus(V) products, palladium black, and HF adducts of L_2PdF_2.[415]

No change in oxidation state occurs because the addition of two fluorine atoms is coupled with the reductive elimination process. This method was also applied in the synthesis of the Pt(II) fluoro-complexes. When $(R_3P)_2Pt(Ph)_2$ was allowed to react with XeF_2 in CH_2Cl_2 solvent in the temperature range, −30 °C to room temperature, the complexes, L_2PtF_2, L_2 = dippp, dppp, $2Ph_3P$, were obtained in quantitative yields. Biphenyl was identified as a side product (eqn [85][415]):

$$L_2Pt(C_6H_5)_2 + XeF_2 \rightarrow L_2PtF_2 + Xe + C_{12}H_{10} \qquad [85]$$

Stable Pd(II) complexes of the type $(R_3P)_2PtF_2$ are strictly limited to alkylphosphane ligands that can adopt mutual cis orientations. The platinum analogs are more stable, yielding isolable difluoride complexes with both alkyl and aryl phosphane ligands.

The Pt(IV) difluoro complexes, $(R_3P)_2Ar_2PtF_2$, were synthesized by the reaction of Pt(II) diaryl precursors with XeF_2. The fluoro ligands are located in *trans*-positions relative to the aryl groups in the distorted octahedral coordination sphere of the metal.[416]

The reaction of a series of chelating Pd(II) aryl iodide complexes with XeF_2 results in remarkably mild and selective reductive elimination of the iodoarene and the formation of the rare Pd(II) difluorodiphosphane complexes.[417] Although Ar–X (X = halogen atom) reductive elimination can be influenced by chelate size, no such effect was observed in the cases of five- and six-membered chelates which underwent clean Ar–I reductive eliminations.

Aryl fluoride groups are important components of many biologically active molecules. While a variety of synthetic approaches are available for generating sp^3 C–F bonds, there are relatively few general and practical methods for the formation of aryl fluorides. The reaction of the Pd(II) precursor, (*t*-Bu-bpy)Pd^{II}(*p*-FC_6H_4)(F), with the electrophilic fluorinating

Copyright © 2013. Elsevier. All rights reserved.

Comprehensive Inorganic Chemistry II : From Elements to Applications, Elsevier, 2013. ProQuest Ebook Central, http://ebookcentral.proquest.com/lib/inflibnet-ebooks/detail.action?docID=1330977.
Created from inflibnet-ebooks on 2021-02-09 22:27:13.

agent, XeF_2, in nitrobenzene at 90 °C for 1 h yielded 1, 4-difluorobenzene (57%) and the biaryl species (7%).[418] During the fluorination of (*t*-Bu-bpy)Pd^{II}(*p*-FC_6H_4)(F) with XeF_2 at 70 °C for 2.5 min, the new organometallic species, (*t*-Bu-bpy)Pd^{IV}(Ar)$(F)_2$(FHF), was formed. This is the first reported example of a Pd^{IV} difluoride. The stable compound, (*t*-Bu-bpy)Pd^{IV}(Ar)$(F)_2$(FHF), undergoes Ar—F bond formation in the presence of an 'F^{+}' source, for example, XeF_2, $(PhSO_2)_2NF$, 1-fluoro-2,4,6-trimethylpyridinium tetrafluoridoborate.[418]

1.25.10.2.6 Oxidative carbonylation of $Fe(CO)_5$ in HF/SbF_5 and HF/BF_3

It has been shown that XeF_2 is a better reagent for oxidative carbonylation of $Fe(CO)_5$ than Cl_2[419] or AsF_5.[419] The $Fe(CO)_6^{2+}$ cation was synthesized according to eqn [86].[420] The reaction was carried out in HF/SbF_5 under 1 atm of CO at 50 °C for 2 days (yield ~50%).

$$Fe(CO)_5 + XeF_2 + CO + 4SbF_5 \rightarrow (Fe(CO)_6)(Sb_2F_{11})_2 + Xe \quad [86]$$

By analogy with the generation of $Fe(CO)_6^{2+}$ in HF/SbF_5, the oxidation of $Fe(CO)_5$ by XeF_2 in HF/BF_3 proceeds according to eqn [87].[421] The reaction was carried out in HF/BF_3 at 25 °C for 3 days (yield ~73%).

$$Fe(CO)_5 + XeF_2 + CO + 2BF_3 \rightarrow (Fe(CO)_6)(BF_4)_2 + Xe \quad [87]$$

1.25.10.2.7 Syntheses of polyfluoroorganoiodine(V) tetrafluorides

Xenon difluoride solutions of 1,1,1,3,3-pentafluorobutane (PFB) acidified with BF_3 fluorinates perfluoroorganyliodides and perfluoroorganoiodine difluorides to give perfluoroorganoiodine tetrafluorides.[422] When iodopentafluorobenzene was used as the starting compound, fluorine addition to the pentafluorophenyl group occurred, yielding cyclohexadienyliodine and cyclohexenyliodine tetrafluorides in addition to fluorination of the iodine center. Perfluorocyclohexyliodine tetrafluoride was not obtained even when a stronger Lewis acid such as NbF_5 was used in aHF solvent.

Xenon difluoride acidified with BF_3 or NbF_5 does not add fluorine across the C=C bond in molecules containing the CF=CIF_4 group. Furthermore, fluorine addition to the IF_4 group also did not occur.

Fluorination of perfluoroalkenyl and perfluoroaryl iodides, $C_6F_5IF_n$ ($n = 0, 2, 4$), with XeF_2 acidified by HF, BF_3, or NbF_5 yields alk-1-enyliodine tetrafluorides and cycloalk-1-enyliodine tetrafluorides, respectively. The formation of organoiodine(VII) or perfluorocyclohexyliodine tetrafluoride was not detected even when XeF_2/NbF_5/HF was used.

The electrophilic oxygenation of pentafluorophenyl iodo compounds, $C_6F_5IF_n$ ($n = 0, 2, 4$), with XeF_2/H_2O in aHF yields isomeric mixtures of oxopentafluoro-cyclohexadien-1-yliodine tetrafluorides, $C_6(O)F_5IF_4$.[423]

1.25.10.2.8 Syntheses of Ir(III) fluoride complexes

Although the coordination chemistry of *N*-heterocyclic carbenes (NHCs) has been extensively studied, reports of late transition metal fluoride-*N*-heterocyclic carbene complexes had been restricted to monofluorides. The oxidative fluorination of a series of neutral and cationic iridium(I) NHC complexes (NHC = IMes = *N*,*N*′-bis(2,4,6-trimethylphenyl)imidazole-2-ylidene); (NHC = IPr = *N*,*N*′-bis(2,6-diisopropylphenyl)imidazole-2-ylidene) with XeF_2 in solution generates difluoroiridium(III) complexes, [$IrClF_2$(NHC)(COD)], [$IrClF_2(CO)_2$(NHC)] (NHC = IMes, IPr; COD = 1,5-cyclooctadiene), [IrF_2py(IMes)(COD)][BF_4], [IrF_2L$(CO)_2$(NHC)][BF_4] (NHC = IMes; L = PPh_2Et, PPh_2CCPh, py; NHC = IPr, L = py), stabilized by the NHC ligands.[424]

1.25.10.2.9 Fluorination of dibenzoselenophene and dibenzo(1,2)diselenine

The syntheses of the selenium-containing heterocycles dibenzoselenophene (biphenSe) and dibenzo(1,2)-diselenine (biphenSe_2) were optimized and their fluorinations with XeF_2 in CH_2Cl_2 were investigated.[425] The reaction of biphenSe with XeF_2 yielded the expected organoselenium(IV) difluoride, biphenSeF_2, and the reaction between biphenSe_2 and XeF_2 yielded biphen$(SeF_3)_2$.

1.25.10.3 Organic Syntheses

Xenon difluoride reacts with selenides of the type RSe−EMe_3 (R = CH_3, CH_2CH_3, C_6H_5; E = Si, Ge, Sn, Pb) by cleavage of the Se–E bond yielding RSe–F as an intermediate and Me_3EF.[426] By contrast, the Se−C bond in PhSe-*t*-Bu is stable to attack by XeF_2. The intermediacy of RSe−F was confirmed by addition to acetylenes. Thus, the fluoroselenenylation of acetylenes gives fluoro-(organylseleno)olefins. In the cases of E = Si, Ge, Sn, and Pb, the aryl and *n*-alkyl groups are suitable as R substituents.

The XeF_2–CF_3SO_3H–Me_3SiNCO system makes it possible to conveniently perform electrophilic, one-step aminations of aromatic compounds leading to the formation of anilines in moderate yields.[427] In the case of the XeF_2–CF_3SO_3H–Me_3SiNCO system, $OCNXeOSO_2CF_3$ is postulated to be an intermediate, which readily oxidizes iodobenzene to [PhI−NCO][OTf].

The compound, 3-*trans*-bromo-5-*cis*-fluoro-2,6,6-trimethyl-2-phenyl-tetrahydropyran, has been prepared by the treatment of racemic 5-bromo-2,2,6-trimethyl-6-phenyltetrahydropyrancarboxylic acid with XeF_2 in anhydrous CH_2Cl_2.[428]

For the first time, *ipso*-amidation of boronic acids by XeF_2 has been achieved under mild reaction conditions.[429] The method provides a simple, one-pot procedure for the direct synthesis of a series of anilides from the corresponding arylboronic acids and alkyl/aryl nitriles. Arylboronic acids, which have electron-donating groups, give anilides in high yield, while moderate yields are obtained for arylboronic acids which have electron-withdrawing groups.

The reaction of carboxylic acids with XeF_2 in CH_2Cl_2 was studied in polytetrafluoroethylene (PTFE) and in Pyrex® vessels.[430] Fluorodecarboxylation to HF, CO_2, Xe, and R–F consistently occurred in PTFE, whereas the use of a Pyrex® vessel was reported to be a very effective heterogeneous catalyst for alternative reaction channels, including rearrangement and cyclization, which are consistent with the formation of intermediate fluoroxenon esters, RC(O)OXeF.[430] The use of CH_2Cl_2 as a solvent and a Pyrex® surface appears

Copyright © 2013. Elsevier. All rights reserved.

Comprehensive Inorganic Chemistry II : From Elements to Applications, Elsevier, 2013. ProQuest Ebook Central, http://ebookcentral.proquest.com/lib/inflibnet-ebooks/detail.action?docID=1330977.
Created from inflibnet-ebooks on 2021-02-09 22:27:13.

to be superior for achieving rapid electrophilic reactions with XeF_2.

Treatment of *cis*-5-norbornene-2,3-*endo*-dicarboxylic acid or its monomethyl and dimethyl esters with [F-TEDA][BF_4] (TEDA = triethylenediamine) or XeF_2 resulted in selective fluorolactonization. The reactions of 5-norbornene-*endo*-2-carboxylic acid and its monomethyl ester with [F-TEDA][BF_4] or XeF_2 proceed in a nonselective manner to give fluorolactonization as well as addition and rearrangement products.[431] The factor primarily responsible for selectivity of the fluorolactonization is the presence of two endo-oriented carboxyl groups in the substrate molecule. It was found that the electrophilicity and the type of the fluorinating agent are of secondary importance in this sense.

The reaction of (4*E*)-4-[(dimethylamino)methylidene]-1,8,8-trimethyl-2-oxabicyclo[3.2.1] octan-3-one with XeF_2 in CH_3CN in a 1:1.24 molar ratio formed the α-fluoro aldehyde, 4-fluoro-1,8,8-trimethyl-3-oxo-2-oxabicyclo[3.2.1]octane-4-carbaldehyde, as a single diastereoisomer in 20% yield.[432] The formation of this product was anticipated because similar enol acetates and silyl enol ethers also yield α-fluoro carbonyl products upon reaction with XeF_2.[433–440]

The formation of 4-fluoro-1,8,8-trimethyl-3-oxo-2-oxabicyclo[3.2.1]octane-4-carbaldehyde can account for the initial attack of electrophilic XeF_2 from the less hindered endo-face of the nucleophilic enamine C=C double bond of (4*E*)-4-[(dimethylamino)methylidene]-1,8,8-trimethyl-2-oxabicyclo-[3.2.1]octan-3-one to form the 4-fluoro-1,8,8-trimethyl-3-oxo-2-oxabicyclo[3.2.1]oct-4-yl)-*N*,*N*-dimethylmethaniminium intermediate. The product was subsequently hydrolyzed by water present in the solvents used for product purification to give the final α-fluoro aldehyde.

The first synthesis of 1′-fluoronucleosides, which have been long-standing synthetic targets as potential antimetabolites, was achieved[441] by fluorination of 2′,3′,5′-tri-*O*-acetyl-1′-phenylselenouridine with electrophilic and nucleophilic fluorinating agents. Treatment of 2′,3′,5′-tri-*O*-acetyl-1′-phenylselenouridine with XeF_2 gave the desired β-nucleoside 1′-fluorouridine triacetate as the major product in 29% yield.

Complexes of the type (NHC)AuMe have been oxidatively fluorinated by XeF_2 to yield *cis*-(NHC)$AuMeF_2$ products and were found to be in equilibrium with their fluoride-dissociated, dimeric [(NHC)AuMe(μ-F)]$_2$[F]$_2$ forms.[442]

1.25.10.4 Applications of [^{18}F]XeF_2 to the Syntheses of ^{18}F-Labeled Radiopharmaceuticals for Positron Emission Tomography

The chemistry of [^{18}F]F^- and [^{18}F]F_2, and related fluorinating agents derived from these compounds, is well known[443–445] and continues to be an active research area with recent interest in transition metal-catalyzed fluorination creating electrophilic ^{18}F-labeled fluorination sources from [^{18}F]F^-.[446,447] Of particular interest is ^{18}F-labeled xenon difluoride which has been used as a fluorinating agent for a wide variety of inorganic and organic compounds.[448] Fluorine-18 labeled XeF_2 has been used in the first regioselective fluorinations of the most commonly used ^{18}F-labeled radiopharmaceuticals for positron emission tomography (PET) such as [^{18}F]2-fluoro-2-deoxy-D-glucose and [^{18}F]6-fluoro-L-DOPA. The first preparation of fluorine-18-labeled XeF_2 was obtained by treatment of SO_2ClF solutions of XeF_2 with [^{18}F]HF, [^{18}F]SiF_4, or [^{18}F]AsF_5.[220] It was later shown that [^{18}F]XeF_2 could be synthesized by thermochemical reaction of [^{18}F]F_2 and xenon.[449] A more recent study[450] claimed catalytic behavior of 2,2,2-crypt-M^+ in the ionization of XeF_2 and in fluoride ion exchange with XeF_2 in a glass or a glassy carbon vial[449] and subsequently in a microfluidic reactor;[451] however, this exchange is attributable to [^{18}F]HF formation.[220] In these reactions, ^{18}F-labeled HF, generated by fluoride attack of organic solvents and/or a cryptand, undergoes fluorine exchange with XeF_2 by acting as a weak fluoride ion acceptor toward XeF_2.[221] The exchange of fluoride with XeF_2 has been demonstrated by NMR EXSY in CH_3CN solvent,[220] in conjunction with single-selective inversion NMR spectroscopy and most likely proceeds through the XeF_3^- intermediate.[224]

1.25.11 Conclusion

In the aftermath of Neil Bartlett's discovery of noble-gas reactivity[3] 50 years ago, the syntheses and structural characterization of noble-gas compounds have burgeoned to become an intriguing and highly challenging topic in contemporary inorganic chemistry. Although compounds having expanded valence octets were known for nearly two-thirds of the main-group nonmetals prior to Bartlett's discovery, the success of valency theory enforced the notion that filled octets are to be associated with stability. Neil Bartlett's momentous discovery of noble-gas reactivity on 23 March 1962 with the synthesis of '[Xe][PtF_6]' resulted in a flurry of synthetic and structural work in the field that quickly revealed the true nature of two of the group 18 elements, xenon and krypton, and laid waste to the octet myth then prevalent in chemistry textbooks.

This chapter summarizes only 11 years of progress in noble-gas chemistry and illustrates, beyond doubt, that noble-gas chemistry is a vibrant field rife with interesting new compounds, bonding modalities, rich structural chemistry, and intriguing synthetic applications. The recent record of research achievements in the field of noble-gas chemistry promises new and exciting developments in fundamental and applied chemistry that were not dreamed of by Neil Bartlett and his fellow researchers in the formative years of this field. The rapidity of continued developments in noble-gas chemistry is intimately tied to those who have the imagination and skills to confront its challenges and those who have the foresight to fund curiosity-driven research.

Acknowledgments

The authors are grateful to Dr. Hélène P.A. Mercier for her generous and tireless assistance in preparing, editing, and proof reading this chapter.

References

1. Thomas, J. M. *Angew. Chem. Int. Ed.* **2004**, *43*, 6418–6424.
2. Yost, D. M.; Kaye, A. L. *J. Am. Chem. Soc.* **1933**, *55*, 3890–3892.
3. Bartlett, N. *Proc. Chem. Soc.* **1962**, 218.
4. Bartlett, N. In *Fluorine Chemistry at the Millennium, Fascinated by Fluorine*, 1st ed.; Banks, R. E., Ed.; Elsevier: Oxford, 2000; p 37, Chapter 3.

Copyright © 2013. Elsevier. All rights reserved.

Comprehensive Inorganic Chemistry II : From Elements to Applications, Elsevier, 2013. ProQuest Ebook Central, http://ebookcentral.proquest.com/lib/inflibnet-ebooks/detail.action?docID=1330977.
Created from inflibnet-ebooks on 2021-02-09 22:27:13.

5. Bartlett, N.; Lohmann, D. H. *Proc. Chem. Soc.* **1962**, 115–116 and references therein.
6. Bartlett, N. In: Bartlett, N., Ed.; *World Scientific Series in 20th Century Chemistry*; World Scientific, 2005; Vol. 9, pp 47–50.
7. Ball, P. In *Elegant Solutions*. The Royal Society of Chemistry: Cambridge, 2005 pp 139–150.
8. Graham, L.; Graudejus, O.; Jha, N. K.; Bartlett, N. *Coord. Chem. Rev.* **2000**, *197*, 321–334.
9. Christe, K. O. *Angew. Chem. Int. Ed.* **2001**, *40*, 1419–1421.
10. Gerken, M.; Schrobilgen, G. J. *Coord. Chem. Rev.* **2000**, *197*, 335–395.
11. Tramšek, M.; Žemva, B. *Acta Chim. Slov.* **2006**, *53*, 105–116.
12. Frohn, H.-J.; Bardin, V. V. *Organometallics* **2001**, *20*, 4750–4762.
13. Smith, G. L.; Mercier, H. P. A.; Schrobilgen, G. J. *Inorg. Chem.* **2011**, *49*, 12359–12373.
14. Jacox, M. E. *Chem. Soc. Rev.* **2002**, *31*, 108–115.
15. Lehmann, J. F.; Mercier, H. P. A.; Schrobilgen, G. J. *Coord. Chem. Rev.* **2002**, *233*, 1–39.
16. Seppelt, K. *Z. Anorg. Allg. Chem.* **2003**, *629*, 2427–2430.
17. Lovallo, C. C.; Klobukowski, M. *Chem. Phys. Lett.* **2003**, *368*, 589–593.
18. Tramšek, M.; Žemva, B. *J. Fluorine Chem.* **2006**, *127*, 1275–1284.
19. Raftery, D. *Ann. Rep. NMR Spectrosc.* **2006**, *57*, 205–270.
20. Grochala, W. *Chem. Soc. Rev.* **2007**, *36*, 1632–1655.
21. Gerken, M.; Schrobilgen, G. J. In *Encyclopedia of Magnetic Resonance*; Harris, R. K., Wasylishen, R., Eds.; Wiley: Chichester, 2011.
22. Nabiev, Sh. Sh.; Sokolov, V. B.; Chaivanov, B. B. *Crystallogr. Rep.* **2011**, *56*, 774–791.
23. Hornbeck, J. A.; Molnar, J. P. *Phys. Rev.* **1951**, *84*, 621–625.
24. Samson, J. A. R.; Cairns, R. B. *J. Opt. Soc. Am.* **1966**, *56*, 1140–1141.
25. Miller, T. M.; Ling, J. H.; Saxon, R. P.; Moseley, J. T. *Phys. Rev. A* **1976**, *13*, 2171–2177.
26. Ng, C. Y.; Trevor, D. J.; Mahan, B. H.; Lee, Y. T. *J. Chem. Phys.* **1976**, *65*, 4327–4329.
27. Lorents, D. C.; Olson, R. E.; Conklin, G. M. *Chem. Phys. Lett.* **1973**, *20*, 589–591.
28. Jones, P. R.; Conklin, G. M.; Lorents, D. C.; Olson, R. E. *Phys. Rev. A* **1974**, *10*, 102–109.
29. Stein, L.; Norris, J. R.; Downs, A. J.; Minihan, A. R. *J. Chem. Soc. Chem. Commun.* **1978**, 502–504.
30. Stein, L. *Nature* **1973**, *243*, 30–32.
31. Brown, D. R.; Clegg, M. J.; Downs, A. J.; Fowler, R. C.; Minihan, A. R.; Norris, J. R.; Stein, L. *Inorg. Chem.* **1992**, *31*, 5041–5052.
32. Stein, L.; Henderson, W. W. *J. Am. Chem. Soc.* **1980**, *102*, 2856–2857.
33. Drews, T.; Seppelt, K. *Angew. Chem. Int. Ed Engl.* **1997**, *36*, 273–274.
34. Bondi, A. J. *Phys. Chem.* **1964**, *68*, 441–451.
35. Seidel, S.; Seppelt, K.; van Wüllen, C.; Sun, X. Y. *Angew. Chem. Int. Ed.* **2007**, *46*, 6717–6720.
36. Kalus, R.; Hrivňák, D. *Chem. Phys.* **2002**, *278*, 21–29.
37. Paška, P.; Hrivňák, D.; Kalus, R. *Chem. Phys.* **2003**, *286*, 237–248.
38. Kalus, R.; Hrivňák, D.; Paška, P. *Chem. Phys.* **2005**, *311*, 287–297.
39. von Issendorf, B.; Hofmann, A.; Haberland, H. *J. Chem. Phys.* **1999**, *111*, 2513–2518.
40. Gascón, J. A.; Hall, R. W.; Ludewigt, C.; Haberland, H. *J. Chem. Phys.* **2002**, *117*, 8391–8403.
41. Simpson, M. B.; Poliakoff, M.; Turner, J. J.; Maier, W. B.; McLaughlin, J. G. *J. Chem. Soc. Chem. Commun.* **1983**, 1355–1357.
42. Weiller, B. H. *J. Am. Chem. Soc.* **1992**, *114*, 10910–10915.
43. Fairhurst, S. A.; Morton, J. R.; Perutz, R. N.; Preston, K. F. *Organometallics* **1984**, *3*, 1389–1391.
44. Wells, J. R.; Weitz, E. *J. Am. Chem. Soc.* **1992**, *114*, 2783–2787.
45. Ehlers, A. W.; Frenking, G.; Baerends, E. J. *Organometallics* **1997**, *16*, 4896–4902.
46. Sun, X.-Z.; Grills, D. C.; Nikiforov, S. M.; Poliakoff, M.; George, M. W. *J. Am. Chem. Soc.* **1997**, *119*, 7521–7525.
47. Weiller, B. H.; Wasserman, E. P.; Bergman, R. G.; Moore, C. B.; Pimentel, G. C. *J. Am. Chem. Soc.* **1989**, *111*, 8288–8290.
48. Weiller, B. H.; Wasserman, E. P.; Moore, C. B.; Bergman, R. G. *J. Am. Chem. Soc.* **1993**, *115*, 4326–4330.
49. Bengali, A. A.; Schultz, R. H.; Moore, C. B.; Bergman, R. G. *J. Am. Chem. Soc.* **1994**, *116*, 9585–9589.
50. Bengali, A. A.; Bergman, R. G.; Moore, C. B. *J. Am. Chem. Soc.* **1995**, *117*, 3879–3880.
51. McNamara, B. K.; Yeston, J. S.; Bergman, R. G.; Moore, C. B. *J. Am. Chem. Soc.* **1999**, *121*, 6437–6443.
52. Schröder, D.; Schwarz, H.; Hrušák, J.; Pyykkö, P. *Inorg. Chem.* **1998**, *37*, 624–632.
53. Evans, C. J.; Lesarri, A.; Gerry, M. C. L. *J. Am. Chem. Soc.* **2000**, *122*, 6100–6105.
54. Seidel, S.; Seppelt, K. *Science* **2000**, *290*, 117–118.
55. Drews, T.; Seidel, S.; Seppelt, K. *Angew. Chem. Int. Ed.* **2002**, *41*, 454–456.
56. Einstein, F. W. B.; Rao, P. R.; Trotter, J.; Bartlett, N. *J. Chem. Soc. A* **1967**, 478–482.
57. Hwang, I. C.; Seidel, S.; Seppelt, K. *Angew. Chem. Int. Ed.* **2003**, *42*, 4392–4395.
58. Küster, R.; Seppelt, K. *Z. Anorg. Allg. Chem.* **2000**, *626*, 236–240.
59. Lucier, G.; Elder, L. H.; Chacon, L.; Bartlett, N. *Eur. J. Solid State Inorg. Chem.* **1996**, *33*, 809–820.
60. Berski, S.; Latajka, Z.; Andrés, J. *Chem. Phys. Lett.* **2002**, *356*, 483–489.
61. Tyrra, W.; Naumann, D. In *Inorganic Chemistry Highlights*; Meyer, G., Naumann, D., Wesemann, L., Eds.; Wiley-VCH: Weinheim, 2002; pp. 297–317.
62. Frohn, H.-J.; Jakobs, S. *J. Chem. Soc. Chem. Commun.* **1989**, *10*, 625–627.
63. Naumann, D.; Tyrra, W. *J. Chem. Soc. Chem. Commun.* **1989**, *10*, 47–50.
64. Frohn, H.-J.; Franke, H.; Bardin, V. V. *Z. Naturforsch.* **1999**, *54b*, 1495–1498.
65. Frohn, H.-J.; Bardin, V. V. *Z. Anorg. Allg. Chem.* **2002**, *628*, 1853–1856.
66. Koppe, K.; Bilir, V.; Frohn, H.-J.; Mercier, H. P. A.; Schrobilgen, G. J. *Inorg. Chem.* **2007**, *46*, 9425–9437.
67. Koppe, K.; Frohn, H.-J.; Mercier, H. P. A.; Schrobilgen, G. J. *Inorg. Chem.* **2008**, *47*, 3205–3217.
68. Emara, A. A. A.; Schrobilgen, G. J. *J. Chem. Soc. Chem. Commun.* **1987**, 1644–1646.
69. Emara, A. A. A.; Schrobilgen, G. J. *Inorg. Chem.* **1992**, *31*, 1323–1332.
70. Fir, B. A.; Mercier, H. P. A.; Schrobilgen, G. J.; Emara, A. A. A., unpublished results.
71. Smith, G. L.; Mercier, H. P. A.; Schrobilgen, G. J. *Inorg. Chem.* **2007**, *46*, 1369–1378.
72. Enjalbert, R.; Galy, J. *Acta Crystallogr. B* **2002**, *58*, 1005–1010.
73. Frohn, H.-J.; Bardin, V. V. *J. Chem. Soc. Chem. Commun.* **1999**, 919–920.
74. Frohn, H.-J.; Adonin, N. Yu.; Bardin, V. V. *Z. Anorg. Allg. Chem.* **2003**, *629*, 2499–2508.
75. Frohn, H.-J.; Bardin, V. V. *Z. Anorg. Allg. Chem.* **2003**, *629*, 2465–2469.
76. Zhdankin, V. V.; Stang, P. J.; Zefirov, N. S. *J. Chem. Soc. Chem. Commun.* **1992**, 578–579.
77. Frohn, H.-J.; Bardin, V. V. *Chem. Commun.* **2003**, 2352–2353.
78. Frohn, H.-J.; Bardin, V. V. *Eur. J. Inorg. Chem.* **2006**, 3948–3953.
79. Frohn, H. J.; Bardin, V. V. *Z. Anorg. Allg. Chem.* **2004**, *630*, 1022–1024.
80. Frohn, H.-J.; Bardin, V. V. *Z. Anorg. Allg. Chem.* **2007**, *633*, 1627–1632.
81. Abo-Amer, A.; Frohn, H.; Steinberg, C.; Westphal, U. *J. Fluorine Chem.* **2006**, *127*, 1311–1323.
82. Mercier, H. P. A.; Moran, M. D.; Sanders, J. C. P.; Schrobilgen, G. J.; Suontamo, R. J. *Inorg. Chem.* **2005**, *44*, 49–60.
83. Ulferts, P.; Seppelt, K. *Z. Anorg. Allg. Chem.* **2004**, *630*, 1589–1593.
84. Sladky, F. *Monatsh. Chem.* **1970**, *101*, 1578–1582.
85. Sladky, F. *Angew. Chem. Int. Ed Engl.* **1970**, *9*, 375–376.
86. Fir, B. A.; Mercier, H. P. A.; Sanders, J. C. P.; Dixon, D. A.; Schrobilgen, G. J. *J. Fluorine Chem.* **2001**, *110*, 89–107.
87. Selig, H.; Holloway, J. H. In *Topics in Current Chemistry*; Boschke, F. L., Ed.; Springer: Berlin, 1984; Vol. 124, pp 33–90.
88. Mercier, H. P. A.; Moran, M. D.; Schrobilgen, G. J.; Steinberg, C.; Suontamo, R. J. *J. Am. Chem. Soc.* **2004**, *126*, 5533–5548.
89. Mercier, H. P. A.; Moran, M. D.; Schrobilgen, G. J. In *Recent Developments in Carbocation and Onium Ion Chemistry*, ACS Symposium Book Series 965; Laali, K., Ed.; American Chemical Society: Washington, DC, 2007; pp 394–427, Chapter 19.
90. Mercier, H. P. A.; Moran, M. D.; Schrobilgen, G. J.; Suontamo, R. J. *J. Fluorine Chem.* **2004**, *125*, 1553–1807.
91. Keller, N.; Schrobilgen, G. J. *Inorg. Chem.* **1981**, *20*, 2118–2129.
92. Mercier, H. P. A.; Sanders, J. C. P.; Schrobilgen, G. J. *J. Am. Chem. Soc.* **1994**, *116*, 2921–2937.
93. Elliott, H. St. A.; Lehmann, J. F.; Mercier, H. P. A.; Jenkins, H. D. B.; Schrobilgen, G. J. *Inorg. Chem.* **2010**, *49*, 8504–8523.
94. Holloway, J. H.; Hope, E. G. *Adv. Inorg. Chem.* **1998**, *46*, 51–100.
95. Casteel, W. J., Jr.; Kolb, P.; LeBlond, N.; Mercier, H. P. A.; Schrobilgen, G. J. *Inorg. Chem.* **1996**, *35*, 929–942.
96. Gerken, M.; Kolb, P.; Wegner, A.; Mercier, H. P. A.; Borrmann, H.; Dixon, D. A.; Schrobilgen, G. J. *Inorg. Chem.* **2000**, *39*, 2813–2824.
97. Fir, B.; Whalen, J. M.; Mercier, H. P. A.; Dixon, D. A.; Schrobilgen, G. J. *Inorg. Chem.* **2006**, *45*, 1978–1996.

Copyright © 2013. Elsevier. All rights reserved.

Comprehensive Inorganic Chemistry II : From Elements to Applications, Elsevier, 2013. ProQuest Ebook Central, http://ebookcentral.proquest.com/lib/inflibnet-ebooks/detail.action?docID=1330977.
Created from inflibnet-ebooks on 2021-02-09 22:27:13.

98. Bartlett, N.; Wechsberg, M.; Jones, G. R.; Burbank, R. D. *Inorg. Chem.* **1972**, *11*, 1124–1127.
99. Templeton, L. K.; Templeton, D. H.; Seppelt, K.; Bartlett, N. *Inorg. Chem.* **1976**, *15*, 2718–2720.
100. Gillespie, R. J.; Hargittai, I. *The VSEPR Model of Molecular Geometry*. Allyn & Bacon: Boston, 1991.
101. Oberhammer, H.; Seppelt, K. *Inorg. Chem.* **1978**, *17*, 1435–1439.
102. Zylka, P.; Oberhammer, H.; Seppelt, K. *J. Mol. Struct.* **1991**, *243*, 411–418.
103. Mercier, H. P. A.; Sanders, J. C. P.; Schrobilgen, G. J. *Inorg. Chem.* **1995**, *34*, 5261–5273.
104. Casteel, W. J., Jr.; MacLeod, D. M.; Mercier, H. P. A.; Schrobilgen, G. J. *Inorg. Chem.* **1996**, *35*, 7279–7288.
105. Smith, G. L.; Mercier, H. P. A.; Schrobilgen, G. J. *J. Am. Chem. Soc.* **2009**, *131*, 7272–7286.
106. Smith, G. L.; Mercier, H. P. A.; Schrobilgen, G. J. *Inorg. Chem.* **2008**, *47*, 4173–4184.
107. Smith, G. L.; Schrobilgen, G. J. *Inorg. Chem.* **2009**, *48*, 7714–7728.
108. Schrobilgen, G. J. *J. Chem. Soc. Chem. Commun.* **1988**, 1506–1508.
109. Emara, A. A. A.; Schrobilgen, G. J. *J. Chem. Soc. Chem. Commun.* **1988**, 257–259.
110. Sanders, J. C. P.; Schrobilgen, G. J. In *A Methodological Approach to Multinuclear NMR in Liquids and Solids-Chemical Applications, NATO Advanced Study Institute, Magnetic Resonance*; Granger, P., Harris, R. K., Eds.; Kluwer Academic Publishers: Dordrecht, 1990; pp 157–186, Chapter 11.
111. LeBlond, R. D.; DesMarteau, D. D. *J. Chem. Soc. Chem. Commun.* **1974**, 555–556.
112. DesMarteau, D. D.; LeBlond, R. D.; Hossain, S. F.; Nothe, D. *J. Am. Chem. Soc.* **1981**, *103*, 7734–7739.
113. Sawyer, J. F.; Schrobilgen, G. J.; Sutherland, S. J. *Inorg. Chem.* **1982**, *21*, 4064–4072.
114. Schumacher, G. A.; Schrobilgen, G. J. *Inorg. Chem.* **1983**, *22*, 2178–2183.
115. Faggiani, R.; Kennepohl, D. K.; Lock, C. J. L.; Schrobilgen, G. J. *Inorg. Chem.* **1986**, *25*, 563–571.
116. Glemser, O.; Mews, R. *Angew. Chem. Int. Ed Engl.* **1980**, *19*, 883–899.
117. Kirchhoff, W. H.; Wilson, E. B., Jr. *J. Am. Chem. Soc.* **1962**, *84*, 334–336.
118. Borrmann, T.; Lork, E.; Mews, R.; Parsons, S.; Petersen, J.; Stohrer, W.-D.; Watson, P. G. *Inorg. Chim. Acta* **2008**, *361*, 479–486.
119. Buss, B.; Clegg, W.; Hartmann, G.; Jones, P. G.; Mews, R.; Noltemeyer, M.; Sheldrick, G. M. *J. Chem. Soc. Dalton Trans.* **1981**, 61–63.
120. Behrens, U.; Lork, E.; Petersen, J.; Waterfeld, A.; Mews, R. *Z. Anorg. Allg. Chem.* **1997**, *623*, 1518–1524.
121. Zalkin, A.; Ward, D. L.; Biagioni, R. N.; Templeton, D. H.; Bartlett, N. *Inorg. Chem.* **1978**, *17*, 1318–1322.
122. Gillespie, R. J.; Landa, B. *Inorg. Chem.* **1973**, *12*, 1383–1388.
123. McRae, V. M.; Peacock, R. D.; Russell, D. R. *Chem. Commun.* **1969**, 62–63.
124. Burgess, J.; Fraser, C. J. W.; McRae, V. M.; Peacock, R. D.; Russell, D. R. In *Inorganic Nuclear Chemistry*; Katz, J. J., Sheft, I., Eds.; Pergamon Press: New York, 1976; supplement to the *J. Inorg. Nucl. Chem.*; Herbert H. Hyman Memorial Volume, pp 183–188.
125. Gillespie, R. J.; Martin, D.; Schrobilgen, G. J. *J. Chem. Soc. Dalton Trans.* **1980**, 1898–1903.
126. Lehmann, J. F.; Dixon, D. A.; Schrobilgen, G. J. *Inorg. Chem.* **2001**, *40*, 3002–3017.
127. Lehmann, J. F.; Schrobilgen, G. J. *J. Fluorine Chem.* **2003**, *119*, 109–124.
128. Edwards, A. J.; Holloway, J. H.; Peacock, R. D. *Proc. Chem. Soc.* **1963**, 275–276.
129. Levy, H. A.; Agron, P. A. *J. Am. Chem. Soc.* **1963**, *85*, 241–242.
130. Agron, P. A.; Begun, G. M.; Levy, H. A.; Mason, A. A.; Jones, C. G.; Smith, D. F. *Science* **1963**, *139*, 842–844.
131. Siegel, S.; Gebert, E. *J. Am. Chem. Soc.* **1963**, *85*, 240.
132. Bartlett, N.; Gennis, M.; Gibler, D. D.; Morrell, B. K.; Zalkin, A. *Inorg. Chem.* **1973**, *12*, 1717–1721.
133. Brassington, N. J.; Edwards, H. G. M.; Long, D. A. *J. Chem. Soc., Faraday Trans. 2* **1978**, *74*, 1208–1213.
134. Bürger, H.; Kuna, R.; Ma, S.; Breidung, J.; Thiel, W. *J. Chem. Phys.* **1994**, *101*, 1–14.
135. Rundle, R. E. *J. Am. Chem. Soc.* **1963**, *85*, 112–113.
136. Christe, K. O.; Zhang, X.; Bau, R.; Hegge, J.; Olah, G. A.; Prakash, G. K. S.; Sheehy, J. A. *J. Am. Chem. Soc.* **2000**, *122*, 481–487.
137. Minkwitz, R.; Neikes, F. *Inorg. Chem.* **1999**, *38*, 5960–5963.
138. Minkwitz, R.; Dzyk, M. *Eur. J. Inorg. Chem.* **2002**, 569–572.
139. Sladky, F. O.; Bulliner, P. A.; Bartlett, N. *J. Chem. Soc. A* **1969**, 2179–2188.
140. Fir, B. A.; Gerken, M.; Pointer, B. E.; Mercier, H. P. A.; Dixon, D. A.; Schrobilgen, G. J. *J. Fluorine Chem.* **2000**, *105*, 159–167.
141. Bartlett, N.; DeBoer, B. G.; Hollander, F. J.; Sladky, F. O.; Templeton, D. H.; Zalkin, A. *Inorg. Chem.* **1974**, *13*, 780–785.
142. Nelson, L. Y.; Pimentel, G. C. *Inorg. Chem.* **1967**, *6*, 1758–1759.
143. Beattie, I. R.; German, A.; Blayden, H. E.; Brumbach, S. B. *J. Chem. Soc. Dalton Trans.* **1975**, 1659–1662.
144. Boal, D.; Ozin, G. A. *Spectrosc. Lett.* **1971**, *4*, 43–46.
145. Perlow, G. J.; Perlow, M. R. *J. Chem. Phys.* **1968**, *48*, 955–961.
146. Willet, R. D.; Peterson, S. W.; Coyle, B. A. *J. Am. Chem. Soc.* **1977**, *99*, 8202–8208.
147. Frohn, H.-J.; Schroer, T.; Henkel, G. *Angew. Chem. Int. Ed.* **1999**, *38*, 2554–2556.
148. Siedel, S.; Seppelt, K. *Angew. Chem. Int. Ed.* **2001**, *40*, 4225–4227.
149. Seidel, S.; Seppelt, K. *Angew. Chem. Int. Ed.* **2000**, *39*, 3923–3925.
150. Carpenter, G. B.; Richards, S. M. *Acta Crystallogr.* **1962**, *15*, 360–364 and references therein.
151. Boswijk, K. H.; van der Heide, J.; Vos, A.; Wiebenga, E. H. *Acta Crystallogr.* **1956**, *9*, 274–277.
152. Hughes, M.; Mercier, H. P. A.; Schrobilgen, G. J. *Inorg. Chem.* **2010**, *49*, 271–284.
153. Minkwitz, R.; Nowicki, G. *Angew. Chem. Int. Ed Engl.* **1990**, *29*, 688–689.
154. Gerken, M.; Moran, M. D.; Mercier, H. P. A.; Pointner, B. E.; Schrobilgen, G. J.; Hoge, B.; Christe, K. O.; Boatz, J. A. *J. Am. Chem. Soc.* **2009**, *131*, 13474–13489.
155. Frohn, H.-J.; Klose, A.; Henkel, G. *Angew. Chem. Int. Ed.* **1993**, *32*, 99–100.
156. Frohn, H.-J.; Theissen, M. *Angew. Chem. Int. Ed.* **2000**, *39*, 4591–4593.
157. Maggiarosa, N.; Naumann, D.; Tyrra, W. *Angew. Chem. Int. Ed.* **2000**, *39*, 4588–4591.
158. Frohn, H. J.; Theissen, M. *J. Fluorine Chem.* **2004**, *125*, 981–988.
159. Bock, H.; Hinz-Hübner, D.; Ruschewitz, U.; Naumann, D. *Angew. Chem. Int. Ed.* **2002**, *41*, 448–450.
160. Farnham, W. B.; Calabrese, J. C. *J. Am. Chem. Soc.* **1986**, *108*, 2449–2451.
161. Pauling, L. *Die Natur der Chemischen Bindung*, 3rd ed.; VCH Publishers: Weinheim, 1962; p. 223.
162. Bock, H.; Scherer, H.; Tyrra, W.; Naumann, D. *J. Fluorine Chem.* **2006**, *127*, 1440–1445.
163. Perlow, G. J.; Yoshida, H. *J. Chem. Phys.* **1968**, *49*, 1474–1478.
164. Bilir, V.; Bälser, D.; Boese, R.; Frohn, H.-J. *J. Fluorine Chem.* **2009**, *130*, 824–829.
165. Frohn, H.-J.; Klose, A.; Schroer, T.; Henkel, G.; Buss, V.; Opitz, D.; Vahrenhorst, R. *Inorg. Chem.* **1998**, *37*, 4884–4890.
166. Schmidt, H.; Scherer, H.; Tyrra, W.; Hahn, J.; Naumann, D. *Inorg. Chem.* **2004**, *43*, 1837–1839.
167. Eisenberg, M.; DesMarteau, D. D. *Inorg. Nucl. Chem. Lett.* **1970**, *6*, 29–34.
168. Moran, M. D.; Brock, D. S.; Mercier, H. P. A.; Schrobilgen, G. J. *J. Am. Chem. Soc.* **2010**, *132*, 13823–13839.
169. Zefirov, N. S.; Gakh, A. A.; Zhdankin, V. V.; Stang, P. J. *J. Org. Chem.* **1991**, *56*, 1416–1418.
170. Luzzati, V. *Acta Crystallogr.* **1951**, *4*, 120–131.
171. Obermeyer, A.; Borrmann, H.; Simon, A. *J. Am. Chem. Soc.* **1995**, *117*, 7887–7890.
172. Minkwitz, R.; Hertel, T. *Z. Naturforsch.* **1997**, *52b*, 1307–1310.
173. Hagiwara, R.; Hollander, F.; Maines, C.; Bartlett, N. *Eur. J. Solid State Inorg. Chem.* **1991**, *28*, 855–866.
174. Jenkins, H. D. B.; Roobottom, H. K.; Passmore, J.; Glasser, L. *Inorg. Chem.* **1999**, *38*, 3609–3620.
175. Tramšek, M.; Benkič, P.; Turičnik, A.; Tavčar, G.; Žemva, B. *J. Fluorine Chem.* **2002**, *114*, 143–148.
176. Tavčar, G.; Tramšek, M.; Bunič, T.; Benkič, P.; Žemva, B. *J. Fluorine Chem.* **2004**, *125*, 1579–1584.
177. Tramšek, M.; Benkič, P.; Žemva, B. *Inorg. Chem.* **2004**, *43*, 699–703.
178. Benkič, P.; Tramšek, M.; Žemva, B. *Solid State Sci.* **2002**, *4*, 1425–1434.
179. Bunič, T.; Tramšek, M.; Goreshnik, E.; Žemva, B. *Solid State Sci.* **2008**, *10*, 1511–1516.
180. Tavčar, G.; Žemva, B. *Inorg. Chem.* **2005**, *44*, 1525–1529.
181. Lutar, K.; Borrmann, H.; Mazej, Z.; Tramšek, M.; Benkič, P.; Žemva, B. *J. Fluorine Chem.* **2000**, *101*, 155–160.
182. Tramšek, M.; Lork, E.; Mews, R.; Žemva, B. *J. Solid State Chem.* **2001**, *162*, 243–249.
183. Tramšek, M.; Benkič, P.; Žemva, B. *Angew. Chem. Int. Ed.* **2004**, *43*, 3456–3458.
184. Bunič, T.; Tavčar, G.; Tramšek, M.; Žemva, B. *Inorg. Chem.* **2006**, *45*, 1038–1042.
185. Tramšek, M.; Benkič, P.; Žemva, B. *Solid State Sci.* **2002**, *4*, 9–14.
186. Bunič, T.; Tramšek, M.; Goreshnik, E.; Tavčar, G.; Žemva, B. *Inorg. Chem.* **2007**, *46*, 5276–5282.

Copyright © 2013. Elsevier. All rights reserved.

Comprehensive Inorganic Chemistry II : From Elements to Applications, Elsevier, 2013. ProQuest Ebook Central, http://ebookcentral.proquest.com/lib/inflibnet-ebooks/detail.action?docID=1330977.
Created from inflibnet-ebooks on 2021-02-09 22:27:13.

187. Turičnik, A.; Benkič, P.; Žemva, B. *Inorg. Chem.* **2002**, *41*, 5521–5524.
188. Tavčar, G.; Goreshnik, E.; Mazej, Z. *J. Fluorine Chem.* **2006**, *127*, 1368–1373.
189. Lozinšek, M.; Radan, K.; Goreshnik, E.; Žemva, B. 242nd ACS National Meeting & Exposition, Denver, CO_2 Aug 28-Sept 1, 2011, abstract # 42. Unpublished results.
190. Tavčar, G.; Benkič, P.; Žemva, B. *Inorg. Chem.* **2004**, *43*, 1452–1457.
191. Pearson, R. G. *Inorg. Chem.* **1988**, *27*, 734–740.
192. Turičnik A (2003) PhD Thesis, University of Ljubljana, Ljubljana, Slovenia.
193. Gerken, M.; Hazendonk, P.; Iuga, A.; Nieboer, J.; Tramšek, M.; Goreshnik, E.; Žemva, B.; Zheng, S.; Autschbach, J. *Inorg. Chem.* **2007**, *46*, 6069–6077.
194. Bunič, T.; Tramšek, M.; Goreshnik, E.; Žemva, B. *Collect. Czech. Chem. Commun.* **2008**, *73*, 1645–1654.
195. Žemva, B.; Jesih, A.; Templeton, D. H.; Zalkin, A.; Cheethman, A. K.; Bartlett, N. *J. Am. Chem. Soc.* **1987**, *109*, 7420–7427.
196. Brock, D. S.; Casalis de Pury, J. J.; Mercier, H. P. A.; Schrobilgen, G. J.; Silvi, B. *Inorg. Chem.* **2010**, *49*, 6673–6689.
197. Brock, D. S.; Casalis de Pury, J. J.; Mercier, H. P. A.; Schrobilgen, G. J.; Silvi, B. *J. Am. Chem. Soc.* **2010**, *132*, 3533–3542.
198. Frlec, B.; Holloway, J. H. *J. Chem. Soc., Dalton Trans.* **1975**, 535–540.
199. Holloway, J. H.; Knowles, J. G. *J. Chem. Soc. A.* **1969**, 756–761.
200. Jones, G. R.; Burbank, R. D.; Bartlett, N. *Inorg. Chem.* **1970**, *9*, 2264–2268.
201. Burns, J. H.; Ellison, R. D.; Levy, H. A. *Acta Crystallogr.* **1965**, *18*, 11–16.
202. Bartlett, N.; Wechsberg, M. *Z. Anorg. Allg. Chem.* **1971**, *385*, 5–17.
203. Hughes, M. J.; Brock, D. S.; Mercier, H. P. A.; Schrobilgen, G. J. *J. Fluorine Chem.* **2011**, *132*, 660–668.
204. Dixon, D. A.; deJong, W. A.; Peterson, K. A.; Christe, K. O.; Schrobilgen, G. J. *J. Am. Chem. Soc.* **2005**, *127*, 8627–8634.
205. Grant, D. J.; Wang, T.-H.; Dixon, D. A.; Christe, K. O. *Inorg. Chem.* **2010**, *49*, 261–270.
206. Dixon, D. A.; Wang, T.-H.; Grant, D. J.; Peterson, K. A.; Christe, K. O.; Schrobilgen, G. J. *Inorg. Chem.* **2007**, *46*, 10016–10021.
207. Pilmé, J.; Robinson, E. A.; Gillespie, R. J. *Inorg. Chem.* **2006**, *45*, 6198–6204.
208. Christe, K. O.; Curtis, E. C.; Dixon, D. A.; Mercier, H. P. A.; Sanders, J. C. P.; Schrobilgen, G. J. *J. Am. Chem. Soc.* **1991**, *113*, 3351–3361.
209. Peacock, R. D.; Selig, H.; Sheft, I. *Proc. Chem. Soc.* **1964**, 285.
210. Peacock, R. D.; Selig, H.; Sheft, I. *J. Inorg. Nucl. Chem.* **1966**, *28*, 2561–2567.
211. Ellern, A.; Mahjoub, A.-R.; Seppelt, K. *Angew. Chem. Int. Ed Engl.* **1996**, *35*, 1123–1125.
212. Peterson, S. W.; Holloway, J. H.; Coyle, B. A.; Williams, J. M. *Science* **1971**, *173*, 1238–1239.
213. Adam, S.; Ellern, A.; Seppelt, K. *Chem. Eur. J.* **1996**, *2*, 398–402.
214. Christe, K. O.; Wilson, W. W. *Inorg. Chem.* **1982**, *21*, 4113–4117.
215. Begun, G. M.; Compton, R. N. *Int. J. Mass Spectrom. Ion Phys.* **1979**, *30*, 379–382.
216. Studier, M. H.; Sloth, E. N. In *Noble Gas Compounds*; Hyman, H. H., Ed.; University of Chicago Press: Chicago, 1963; pp 47–49.
217. Krouse, I. H.; Hao, C.; Check, C. E.; Lobring, K. C.; Sunderlin, L. S.; Wenthold, P. G. *J. Am. Chem. Soc.* **2007**, *129*, 846–852.
218. Misochko, E. Y.; Akimov, A. V.; Belov, V. A.; Tyurin, D. A. *Inorg. Chem.* **2009**, *48*, 8723–8728.
219. Appelman, E. H. *Inorg. Chem.* **1967**, *6*, 1268–1269.
220. Vasdev, N.; Pointner, B. E.; Chirakal, R.; Schrobilgen, G. J. *J. Am. Chem. Soc.* **2002**, *124*, 12863–12868.
221. Schrobilgen, G.; Firnau, G.; Chirakal, R.; Garnett, E. S. *J. Chem. Soc. Chem. Commun.* **1981**, 198–199.
222. Sood, S.; Firnau, G.; Garnett, E. S. *Int. J. Appl. Radiat. Isot.* **1983**, *34*, 743–745.
223. Firnau, G.; Chirakal, R.; Sood, S.; Garnett, E. S. *J. Labelled Compd. Rad.* **1981**, *18*, 7–8.
224. Vasdev, N.; Moran, M. D.; Tuononen, H. M.; Chirakal, R.; Suontamo, R. J.; Bain, A. D.; Schrobilgen, G. J. *Inorg. Chem.* **2010**, *49*, 8997–9004.
225. Gillespie, R. J.; Landa, B.; Schrobilgen, G. J. *Chem. Commun.* **1971**, 1543–1544.
226. Boldrini, P.; Gillespie, R. J.; Ireland, P. R.; Schrobilgen, G. J. *Inorg. Chem.* **1974**, *13*, 1690–1694.
227. McKee, D. E.; Zalkin, A.; Bartlett, N. *Inorg. Chem.* **1973**, *12*, 1713–1717.
228. Claassen, H. H.; Chernick, C. L.; Malm, J. G. *J. Am. Chem. Soc.* **1963**, *85*, 1927–1928.
229. Schumacher, G. A.; Schrobilgen, G. J. *Inorg. Chem.* **1984**, *23*, 2923–2929.
230. Burns, J. H.; Agron, P. A.; Levy, H. A. *Science* **1963**, *139*, 1208–1209.
231. Jacob, E.; Lentz, D.; Seppelt, K.; Simon, A. *Z. Anorg. Allg. Chem.* **1981**, *472*, 7–25.
232. Turowsky, L.; Seppelt, K. *Z. Anorg. Allg. Chem.* **1992**, *609*, 153–156.
233. Frohn, H.-J.; Leblond, N.; Lutar, K.; Žemva, B. *Angew. Chem. Int. Ed.* **2000**, *39*, 391–393.
234. Syvret, R. G.; Schrobilgen, G. J. *J. Chem. Soc. Chem. Commun.* **1985**, 1529–1530.
235. Syvret, R. G.; Mitchell, K. M.; Sanders, J. C. P.; Schrobilgen, G. J. *Inorg. Chem.* **1992**, *31*, 3381–3385.
236. Ogden, J. S.; Turner, J. J. *Chem. Comm.* **1966**, *19*, 693–694.
237. Jacob, E.; Opferkuch, R. *Angew. Chem. Int. Ed Engl.* **1976**, *15*, 158–159.
238. Gillespie, R. J.; Schrobilgen, G. J. *Chem. Commun.* **1977**, 595–597.
239. Tavčar, G.; Žemva, B. *Angew. Chem. Int. Ed.* **2009**, *48*, 1432–1434.
240. Brock, D. S.; Bilir, V.; Mercier, H. P. A.; Schrobilgen, G. J. *J. Am. Chem. Soc.* **2007**, *129*, 3598–3611.
241. Smith, D. F. *J. Am. Chem. Soc.* **1963**, *85*, 816–817.
242. Templeton, D. H.; Zalkin, A.; Forrester, J. D.; Williamson, S. M. *J. Am. Chem. Soc.* **1963**, *85*, 817.
243. Selig, H.; Claassen, H. H.; Chernick, C. L.; Malm, J. G.; Huston, J. L. *Science* **1964**, *143*, 1322–1323.
244. Huston, J. L.; Studier, M. H.; Sloth, E. N. *Science* **1964**, *143*, 1161–1162.
245. Gunn, S. R. In *Noble Gas Compounds*; Hyman, H. H., Ed.; University of Chicago Press: Chicago, 1963; pp 149–151.
246. Gunn, S. R. *J. Am. Chem. Soc.* **1965**, *87*, 2290–2291.
247. Yamanishi, M.; Hirao, K.; Yamashita, K. *J. Chem. Phys.* **1998**, *108*, 1514–1521.
248. Bartlett, N.; Rao, P. R. *Science* **1963**, *139*, 506.
249. Williamson, S. M.; Koch, C. W. *Science* **1963**, *139*, 1046–1047.
250. Appelman, E. H.; Malm, J. G. *J. Am. Chem. Soc.* **1964**, *86*, 2141–2148.
251. Williamson, S. M.; Koch, C. W. In *Noble Gas Compounds*; Hyman, H. H., Ed.; University of Chicago Press: Chicago, 1963; pp 158–166.
252. Brock, D. S.; Schrobilgen, G. J. *J. Am. Chem. Soc.* **2011**, *133*, 6265–6269.
253. Tsao, P.; Cobb, C. C.; Claassen, H. H. *J. Chem. Phys.* **1971**, *54*, 5247–5253.
254. Anders, E.; Owen, T. *Science* **1977**, *198*, 453–465.
255. Sanloup, C.; Schmidt, B. C.; Chamorro Perez, E. M.; Jambon, A.; Gregoryanz, E.; Mezouar, M. *Science* **2005**, *310*, 1174–1177.
256. Nishio-Hamane, D.; Yagi, T.; Sata, N.; Fujita, T.; Okada, T. *Geophys. Res. Lett.* **2010**, *37 L04302/1–L04302/4*.
257. Probert, M. I. J. *J. Phys. Condens. Matter* **2010**, *22*, 025501/1–025501/10.
258. Schmeisser, M.; Dahmen, K.; Sartori, P. *Chem. Ber.* **1970**, *103*, 307–311.
259. Yagupol'skii, L. M.; Lyalin, V. V.; Orda, V. V.; Alekseeva, L. A. *Zh. Org. Khim.* **1970**, *6*, 329–332; *J. Org. Chem. USSR* **1970**, *6*, 317–319.
260. Frohn, H.-J.; Helber, J. *J. Fluorine Chem.* **1980**, *16*, 568.
261. Schmeisser, M.; Dahmen, K.; Sartori, P. *Chem. Ber.* **1967**, *100*, 1633–1637.
262. Gillespie, R. J.; Landa, B.; Schrobilgen, G. J. *Inorg. Chem.* **1976**, *15*, 1256–1263.
263. Brock, D. S.; Mercier, H. P. A.; Schrobilgen, G. J. *J. Am. Chem. Soc.* **2010**, *132*, 10935–10943.
264. Hoyer, S.; Emmler, T.; Seppelt, K. *J. Fluorine Chem.* **2006**, *127*, 1415–1422.
265. Agron, P. A.; Johnson, C. K.; Levy, H. A. *Inorg. Nucl. Chem. Lett.* **1965**, *1*, 145–148.
266. Jones, G. R.; Burbank, R. D.; Falconer, W. E. *J. Chem. Phys.* **1970**, *53*, 1605–1606.
267. Jones, G. R.; Burbank, R. D.; Falconer, W. E. *J. Chem. Phys.* **1970**, *52*, 6450–6451.
268. Burbank, R. D.; Jones, G. R. *Science* **1971**, 485–487.
269. Burbank, R. D.; Jones, G. R. *J. Am. Chem. Soc.* **1974**, *96*, 43–48.
270. Hughes, M. J.; Mercier, H. P. A.; Schrobilgen, G. J. *Inorg. Chem.* **2010**, *49*, 3501–3515.
271. Leary, K.; Templeton, D. H.; Zalkin, A.; Bartlett, N. *Inorg. Chem.* **1973**, *12*, 1726–1730.
272. Jesih, A.; Lutar, K.; Leban, I.; Zemva, B. *Eur. J. Solid State Inorg. Chem.* **1991**, *28*, 829–840.
273. Pointner, B. E.; Suontamo, R. J.; Schrobilgen, G. J. *Inorg. Chem.* **2006**, *45*, 1517–1534.
274. Bartlett, N.; Einstein, F.; Stewart, D. F.; Trotter, J. *J. Chem. Soc. A.* **1967**, 1190–1193.
275. Lutar, K.; Jesih, A.; Leban, I.; Žemva, B.; Bartlett, N. *Inorg. Chem.* **1989**, *28*, 3467–3471.
276. Leary, K.; Zalkin, A.; Bartlett, N. *Inorg. Chem.* **1974**, *13*, 775–779.
277. Jesih, A.; Lutar, K.; Leban, I.; Žemva, B. *Inorg. Chem.* **1989**, *28*, 2911–2914.
278. Hughes, M. J.; Mercier, H. P. A.; Schrobilgen, G. J. *Inorg. Chem.* **2009**, *48*, 4478–4490.
279. Martins, J. F.; Wilson, E. B., Jr. *J. Mol. Spectrosc.* **1968**, *26*, 410–417.
280. Jacob, E. J.; Thompson, H. B.; Bartell, L. S. *J. Mol. Struct.* **1971**, *8*, 383–394.
281. Holloway, J. H.; Schrobilgen, G. J. *J. Chem. Soc. Chem. Commun.* **1975**, 623–624.
282. Žemva, B.; Slivnik, J.; Bohinc, M. *J. Inorg. Nucl. Chem.* **1976**, *38*, 73–74.

Copyright © 2013. Elsevier. All rights reserved.

Comprehensive Inorganic Chemistry II : From Elements to Applications, Elsevier, 2013. ProQuest Ebook Central, http://ebookcentral.proquest.com/lib/inflibnet-ebooks/detail.action?docID=1330977.
Created from inflibnet-ebooks on 2021-02-09 22:27:13.

283. Mazej, Z.; Goreshnik, E. *Eur. J. Inorg. Chem.* **2009**, 4503–4506.
284. Decken, A.; Jenkins, H. D. B.; Knapp, C.; Nikiforov, G. B.; Passmore, J.; Rautiainen, J. M. *Angew. Chem. Int. Ed.* **2005**, *44*, 7958–7961.
285. Mazej, Z.; Goreshnik, E. *Inorg. Chem.* **2009**, *48*, 6918–6923.
286. Gillespie, R. J.; Landa, B.; Schrobilgen, G. J. *J. Chem. Soc. Chem. Commun.* **1972**, 607–609.
287. Gillespie, R. J.; Schrobilgen, G. J. *Inorg. Chem.* **1974**, *13*, 2370–2374.
288. Peterson, S. W.; Willett, R. D.; Huston, J. L. *J. Chem. Phys.* **1973**, *59*, 453–459.
289. LeBlond, N.; Dixon, D. A.; Schrobilgen, G. J. *Inorg. Chem.* **2000**, *39*, 2473–2487.
290. Mercier, H. P. A.; Sanders, J. C. P.; Schrobilgen, G. J.; Tsai, S. S. *Inorg. Chem.* **1993**, *32*, 386–393.
291. Gerken, M.; Schrobilgen, G. J. *Inorg. Chem.* **2002**, *41*, 198–204.
292. Schrobilgen, G. J.; Holloway, J. H.; Granger, P.; Brevard, C. *Inorg. Chem.* **1978**, *17*, 980–987.
293. Christe, K. O.; Wilson, R. D.; Schack, C. J. *Inorg. Chem.* **1981**, *20*, 2104–2114.
294. Luhmer, M.; Reisse, J. *Prog. Nucl. Magn. Reson. Spectrosc.* **1998**, *33*, 57–76.
295. Forgeron, M. A. M.; Wasylishen, R. E.; Gerken, M.; Schrobilgen, G. J. *Inorg. Chem.* **2007**, *46*, 3585–3592.
296. Žemva, B.; Slivnik, J.; Šmalc, A. *J. Fluorine Chem.* **1975**, *6*, 191–193.
297. Lutar, K.; Jesih, A.; Žemva, B. *Polyhedron* **1988**, *7*, 1217–1219.
298. Christe, K. O.; Wilson, W. W.; Bougon, R. A. *Inorg. Chem.* **1986**, *25*, 2163–2169.
299. Holloway, J. H.; Schrobilgen, G. J. *Inorg. Chem.* **1981**, *20*, 3363–3368.
300. Nabiev, S. S.; Sokolov, V. B.; Spirin, S. N.; Chaivanov, B. B. *Russ. J. Phys. Chem. A* **2011**, *85*, 1931–1941.
301. Al-Mukhtar, M.; Holloway, J. H.; Hope, E. G.; Schrobilgen, G. J. *J. Chem. Soc. Dalton Trans.* **1991**, 2831–2834.
302. Burbank, R. D.; Falconer, W. E.; Sunder, W. A. *Science* **1972**, *178*, 1285–1286.
303. Harshbarger, W.; Bohn, R. K.; Bauer, S. H. *J. Am. Chem. Soc.* **1967**, *89*, 6466–6469.
304. Holloway, J. H.; Schrobilgen, G. J. *Inorg. Chem.* **1980**, *19*, 2632–2640.
305. Frlec, B.; Holloway, J. H. *J. Chem. Soc. Chem. Commun.* **1973**, 370–371.
306. Frlec, B.; Holloway, J. H. *J. Chem. Soc. Chem. Commun.* **1974**, 89–90.
307. Gillespie, R. J.; Schrobilgen, G. J. *J. Chem. Soc. Chem. Commun.* **1974**, 90–92.
308. Frlec, B.; Holloway, J. H. *Inorg. Chem.* **1976**, *15*, 1263–1270.
309. Gillespie, R. J.; Schrobilgen, G. J. *Inorg. Chem.* **1976**, *15*, 22–31.
310. Selig, H.; Peacock, R. D. *J. Am. Chem. Soc.* **1964**, *86*, 3895.
311. Lehmann, J. F.; Schrobilgen, G. J.; Christe, K. O.; Kornath, A.; Suontamo, R. J. *Inorg. Chem.* **2004**, *43*, 6905–6921.
312. Christe, K. O.; Wilson, W. W.; Curtis, E. C. *Inorg. Chem.* **1983**, *22*, 3056–3060.
313. Christe, K. O.; Dixon, D. A.; Mack, H. G.; Oberhammer, H.; Pagelot, A.; Sanders, J. C. P.; Schrobilgen, G. J. *J. Am. Chem. Soc.* **1993**, *115*, 11279–11284.
314. LeBlond, N.; Mercier, H. P. A.; Dixon, D. A.; Schrobilgen, G. J. *Inorg. Chem.* **2000**, *39*, 4494–4509.
315. Mercier, H. P. A.; Schrobilgen, G. J. *Inorg. Chem.* **1993**, *32*, 145–151.
316. Mallouk, T. E.; Rosenthal, G. L.; Müller, G.; Brusasco, R.; Bartlett, N. *Inorg. Chem.* **1984**, *23*, 3167–3173.
317. Shen, C.; Hagiwara, R.; Mallouk, T.; Bartlett, N. In *Inorganic Fluorine Chemistry, Toward the 21st Century*, ACS Symposium Series 555; Thrasher, J. S., Strauss, S. H., Eds.; American Chemical Society: Washington, DC, 1994; pp 26–39, Chapter 2.
318. Jenkins, H. D. B.; Tudela, D. *J. Chem. Educ.* **2003**, *80*, 1482–1487.
319. Glasser, L.; Jenkins, H. D. B. *Chem. Soc. Rev.* **2005**, *34*, 866–874.
320. Thompson, C. A. T.; Andrews, L. *J. Am. Chem. Soc.* **1994**, *116*, 423–424.
321. Panek, J.; Latajka, Z.; Lundell, J. *Phys. Chem. Chem. Phys.* **2002**, *4*, 2504–2510.
322. Khriachtchev, L.; Räsänen, M.; Gerber, R. B. *Acc. Chem. Res.* **2009**, *42*, 183–191.
323. Grochala, W.; Khriachtchev, L.; Räsänen, M. In *Physics and Chemistry at Low Temperatures*; Khriachtchev, L., Ed.; Pan Stanford Publishing, 2011; pp 419–446.
324. Khriachtchev, L.; Pettersson, M.; Runeberg, N.; Lundell, J.; Räsänen, M. *Nature* **2000**, *406*, 874–876.
325. Khriachtchev, L.; Pettersson, M.; Lignell, A.; Räsänen, M. *J. Am. Chem. Soc.* **2001**, *123*, 8610–8611.
326. Lignell, H.; Khriachtchev, L.; Lignell, A.; Räsänen, M. *Low Temp. Phys.* **2010**, *36*, 400–406.
327. Runeberg, N.; Pettersson, M.; Khriachtchev, L.; Lundell, J.; Räsänen, M. *J. Chem. Phys.* **2001**, *114*, 836–841.
328. Bochenkova, A. V.; Bochenkov, V. E.; Khriachtchev, L. *J. Phys. Chem. A* **2009**, *113*, 7654–7659.
329. Pettersson, M.; Khriachtchev, L.; Lignell, A.; Räsänen, M.; Bihary, Z.; Gerber, R. B. *J. Chem. Phys.* **2002**, *116*, 2508–2515.
330. Lundell, J.; Khriachtchev, L.; Pettersson, H.; Räsänen, M. *Low Temp. Phys.* **2000**, *26*, 680–690.
331. Nahler, H. N.; Baumfalk, R.; Buck, V.; Bihary, Z.; Gerber, R. B. *J. Chem. Phys.* **2003**, *119*, 224–231.
332. KHriachtchev, L.; Lignell, A.; Juselius, J.; Räsänen, M.; Savchenko, E. *J. Chem. Phys.* **2005**, *122*, 014510/1–014510/9.
333. Bihary, Z.; Chaban, G. M.; Gerber, R. B. *J. Chem. Phys.* **2002**, *116*, 5521–5529.
334. Ahokas, J.; Vaskouen, K.; Eloranta, J.; Kunttu, H. *J. Phys. Chem. A* **2000**, *104*, 9506–9511.
335. Lignell, H.; Khriachtchev, L.; Pettersson, M.; Räsänen, M. *J. Chem. Phys.* **2003**, *118*, 11120–11128.
336. Khriachtchev, L.; Tapio, S.; Räsänen, M.; Domanskaya, A.; Lignell, A. *J. Chem. Phys.* **2010**, *133*, 084309/1–084309/13.
337. Berski, S.; Latajka, Z.; Silvi, B.; Lundell, J. *J. Chem. Phys.* **2001**, *114*, 4349–4358.
338. Ahokas, J.; Kunttu, H.; Khriachtchev, L.; Pettersson, M.; Rasanen, M. J. *J. Phys. Chem. A* **2002**, *106*, 7743–7747.
339. Khriachtchev, L.; Isokoski, K.; Cohen, A.; Räsänen, M.; Gerber, R. B. *J. Am. Chem. Soc.* **2008**, *130*, 6114–6118.
340. Tsivion, E.; Gerber, R. B. *Chem. Phys. Lett.* **2009**, *482*, 30–33.
341. Liu, Z.-B.; Li, Z.-R.; Zuo, M.-H.; Li, Q.-Z.; Ma, F.; Li, Z.-J.; Chen, G.; Sun, C.-C. *J. Chem. Phys.* **2009**, *131*, 044308/1–044308/12.
342. Mück, L. A.; Timoshkin, A. Y.; von Hopffgarten, M.; Frenking, G. *J. Am. Chem. Soc.* **2009**, *131*, 3942–3949.
343. Pérez-Peralta, N.; Juárez, R.; Cerpa, E.; Bickelhaupt, F. M.; Merino, G. *J. Phys. Chem. A* **2009**, *113*, 9700–9706.
344. Fitzsimmons, A.; Mori, H.; Miyoshi, E.; Klobukowski, M. *J. Phys. Chem. A* **2010**, *114*, 8786–8792.
345. McDowell, S. A. C. *J. Chem. Phys.* **2004**, *120*, 3630–3634.
346. Borocci, S.; Bronzolino, N.; Grandinetti, F. *Chem. Phys. Lett.* **2004**, *398*, 357–360.
347. McDowell, S. A. C. *J. Chem. Phys.* **2001**, *114*, 8395–8396.
348. Jiménez-Halla, C. O. C.; Fernández, I.; Frenking, G. *Angew. Chem. Int. Ed.* **2009**, *48*, 366–369.
349. Avramopoulos, A.; Serrano-Andrés, L.; Li, J.; Papadopoulos, M. G. *J. Chem. Theory Comput.* **2010**, *6*, 3365–3372.
350. Borocci, S.; Bronzolino, N.; Giordani, M.; Grandinetti, F. *J. Phys. Chem. A* **2010**, *114*, 7382–7390.
351. Hoffman, G. J. *Chem. Phys.* **2009**, *361*, 68–74.
352. Cukras, J.; Antušek, A.; Holka, F.; Sadlej, J. *Chem. Phys. Lett.* **2009**, *474*, 258–262.
353. Borocci, S.; Bronzolino, N.; Grandinetti, F. *Chem. Phys. Lett.* **2009**, *470*, 49–53.
354. Lundell, J.; Cohen, A.; Gerber, R. B. *J. Phys. Chem. A* **2002**, *106*, 11950–11955.
355. Khriatchchev, L.; Tanskanen, H.; Lundell, J.; Pettersson, M.; Kiljunen, H.; Räsänen, M. *J. Am. Chem. Soc.* **2003**, *125*, 4696–4697.
356. Feldman, V. I.; Sukhov, F. F.; Orlov, A. Y.; Tyulpina, I. V. *J. Am. Chem. Soc.* **2003**, *125*, 4698–4699.
357. Tanskanen, H.; Khriachtchev, L.; Lundell, J.; Räsänen, M. *J. Chem. Phys.* **2006**, *125*, 074501/1–074501/10.
358. Feldman, V. I.; Kobzarenko, A. V.; Baranova, I. A.; Danchenko, A. V.; Sukhov, F. F.; Tsivion, E.; Gerber, R. B. *J. Chem. Phys.* **2009**, *131*, 151101/1–151101/3.
359. Tanskanen, H.; Johansson, S.; Lignell, A.; Khriachtchev, L.; Räsänen, M. *J. Chem. Phys.* **2007**, *127*, 154313/1–154313/7.
360. Khriachtchev, L.; Tanskanen, H.; Cohen, A.; Gerber, R. B.; Lundell, J.; Pettersson, M.; Kiljunen, H.; Räsänen, M. *J. Am. Chem. Soc.* **2003**, *125*, 6876–6877.
361. Tsivion, E.; Gerber, R. B. *Phys. Chem. Chem. Phys.* **2010**, *12*, 11791–11794.
362. Ansbacher, T.; Gerber, R. B. *Phys. Chem. Chem. Phys.* **2006**, *8*, 4175–4181.
363. Sheng, L.; Gerber, R. B. *J. Chem. Phys.* **2006**, *124*, 231103/1–231103/3.
364. Khriachtchev, L.; Domanskaya, A.; Lundell, J.; Akimov, A.; Räsänen, M.; Misochko, E. *J. Phys. Chem. A* **2010**, *114*, 4181–4187.
365. Yockel, S.; Gawlik, E.; Wilson, A. K. *J. Phys. Chem. A* **2007**, *111*, 11261–11268.
366. Tanskanen, H.; Khriachtchev, L.; Lundell, J.; Kiljunen, H.; Räsänen, M. *J. Am. Chem. Soc.* **2003**, *125*, 16361–16366.
367. Sheng, L.; Cohen, A.; Gerber, R. B. *J. Am. Chem. Soc.* **2006**, *128*, 7156–7157.
368. Khriatchchev, L.; Pettersson, M.; Lundell, J.; Tanskanen, H.; Kivinjemi, T.; Runeberg, N.; Räsänen, M. *J. Am. Chem. Soc.* **2003**, *125*, 1454–1455.
369. Huang, Z. *Chem. Phys.* **2009**, *359*, 34–39.
370. Li, J.; Bursten, B. E.; Liang, B.; Andrews, L. *Science* **2002**, *295*, 2242–2245.
371. Liang, B.; Andrews, L.; Li, J.; Bursten, B. E. *J. Am. Chem. Soc.* **2002**, *124*, 9016–9017.
372. Andrews, L.; Liang, B.; Li, J.; Bursten, B. E. *J. Am. Chem. Soc.* **2003**, *125*, 3126–3139.
373. Liang, B.; Andrews, L.; Li, J.; Bursten, B. E. *Inorg. Chem.* **2004**, *43*, 882–894.
374. Lue, C. J.; Jin, J.; Ortiz, M. J.; Rienstra-Kiracofe, J. C.; Heaven, M. C. *J. Am. Chem. Soc.* **2004**, *126*, 1812–1815.

Copyright © 2013. Elsevier. All rights reserved.

Comprehensive Inorganic Chemistry II : From Elements to Applications, Elsevier, 2013. ProQuest Ebook Central, http://ebookcentral.proquest.com/lib/inflibnet-ebooks/detail.action?docID=1330977.
Created from inflibnet-ebooks on 2021-02-09 22:27:13.

375. Li, J.; Bursten, B. E.; Andrews, L.; Marsden, C. J. *J. Am. Chem. Soc.* **2004**, *126*, 3424–3425.
376. Wang, X.; Andrews, L.; Li, J.; Bursten, B. E. *Angew. Chem. Int. Ed.* **2004**, *43*, 2554–2557.
377. Zhao, Y.; Gong, Y.; Zhou, M. *J. Phys. Chem. A* **2006**, *110*, 10777–10782.
378. Zhao, Y.; Gong, Y.; Chen, M.; Ding, C.; Zhou, M. *J. Phys. Chem. A* **2005**, *109*, 11765–11770.
379. Zhao, Y.; Gong, L.; Chen, M.; Zhou, M. *J. Phys. Chem. A* **2005**, *109*, 6621–6623.
380. Zhao, Y.; Gong, Y.; Chen, M.; Zhou, M. *J. Phys. Chem. A* **2006**, *110*, 1845–1849.
381. Kobayashi, T.; Seki, K.; Takayanagi, T. *Chem. Phys. Lett.* **2010**, *498*, 235–239.
382. Thomas, J. M.; Walker, N. R.; Cooke, S. A.; Gerry, M. C. L. *J. Am. Chem. Soc.* **2004**, *126*, 1235–1246.
383. Cooke, S. A.; Gerry, M. C. L. *J. Am. Chem. Soc.* **2004**, *126*, 17000–17008.
384. Michaud, J. M.; Cooke, S. A.; Gerry, M. C. L. *Inorg. Chem.* **2004**, *43*, 3871–3881.
385. Michaud, J. M.; Gerry, M. C. L. *J. Am. Chem. Soc.* **2006**, *128*, 7613–7621.
386. Zou, W.; Liu, Y.; Boggs, J. E. *Chem. Phys. Lett.* **2009**, *482*, 207–210.
387. Holka, F.; Avramopoulos, A.; Loboda, O.; Kellö, V.; Papadopoulos, M. G. *Chem. Phys. Lett.* **2009**, *472*, 185–189.
388. Rodrigues, E. F. F.; de Sá, E. L.; Haiduke, R. L. A. *J. Phys. Chem. A* **2010**, *114*, 5222–5229.
389. Evans, C. J.; Wright, T. G.; Gardner, A. M. *J. Phys. Chem. A* **2010**, *114*, 4446–4454.
390. Beyhan, S. M.; Götz, A. W.; Jacob, C. R.; Visscher, L. *J. Chem. Phys.* **2010**, *132*, 044114/1–044114/9.
391. Zou, W.; Liu, Y.; Boggs, J. E. *Dalton Trans.* **2010**, *39*, 2023–2026.
392. Zhou, M.; Zhao, Y.; Gong, Y.; Li, J. *J. Am. Chem. Soc.* **2006**, *128*, 2504–2505.
393. Poterya, V.; Votava, O.; Fárník, M.; Ončák, M.; Slaviček, P.; Buck, U.; Friedrich, B. *J. Chem. Phys.* **2008**, *128*, 104313/1–104313/10.
394. Ascenzi, D.; Tosi, P.; Roithová, J.; Ricketts, C. L.; Schröder, D.; Lockyear, J. F.; Parkes, M. A.; Price, S. D. *Phys. Chem. Chem. Phys.* **2008**, *10*, 7121–7128.
395. Ascenzi, D.; Tosi, P.; Roithová, J.; Schröder, D. *Chem. Commun.* **2008**, 4055–4057.
396. Lockyear, J. F.; Douglas, K.; Price, S. D.; Karwowska, M.; Fijalkowski, K. J.; Grochala, W.; Remeš, M.; Roithová, J.; Schröder, D. *J. Phys. Chem. Lett.* **2010**, *1*, 358–362.
397. Roithová, J.; Schröder, D. *Angew. Chem. Int. Ed.* **2009**, *48*, 8788–8790.
398. Koyanagi, G. K.; Bohme, D. K. *J. Phys. Chem. Lett.* **2010**, *1*, 41–44.
399. Antoniotti, P.; Bottizzo, E.; Operti, L.; Rabezzana, R.; Borocci, S.; Grandinetti, F. *J. Phys. Chem. Lett.* **2010**, *1*, 2006–2010.
400. Gardner, A. M.; Gutsmiedl, K. A.; Wright, T. G.; Breckenridge, W. H.; Chapman, C. Y. N.; Viehland, L. A. *J. Chem. Phys.* **2010**, *133*, 164302/1–164302/6.
401. Gardner, A. M.; Withers, C. D.; Graneek, J. B.; Wright, T. G.; Viehland, L. A.; Breckenridge, W. H. *J. Phys. Chem. A* **2010**, *114*, 7631–7641.
402. Žemva, B. *Croat. Chem. Acta* **1988**, *61*, 163–187.
403. Bartlett, N.; Sladky, F. O. *Chem. Commun.* **1968**, 1046–1047.
404. Adamson, A. J.; Holloway, J. H.; Hope, E. G.; Taylor, R. *Fullerene Sci. Technol.* **1997**, *5*, 629–642.
405. Dementjev, A. P.; Bezmelnitsin, V. N.; Ryjkov, A. V.; Sokolov, V. N. In Proceedings of the 12th European Symposium on Fluorine Chemistry, Berlin, Germany, 1998; Abstract P–II.
406. Yudanov, N. F.; Ocotrub, A. V.; Bulusheva, L. G.; Asanov, I. P.; Shevtsov, Y. V. *Mol. Mater.* **1998**, *43*, 122–127.
407. Denisenko, N. I.; Streletskiĭ, A. V.; Boltalina, O. V. *Phys. Solid State* **2002**, *44*, 539–541.
408. Denisenko, N. I.; Troyanov, S. I.; Popov, A. A.; Kuvychko, I. V.; Žemva, B.; Kemnitz, E.; Strauss, S. H.; Boltalina, O. V. *J. Am. Chem. Soc.* **2004**, *126*, 1618–1619.
409. Tramšek, M.; Žemva, B. *Acta Chim. Slov.* **2002**, *49*, 209–220.
410. Yamaguchi, S.; Akiyama, S.; Tamao, K. *J. Organometallic Chem.* **2002**, *646*, 277–281.
411. Yamaguchi, S.; Shirasaka, T.; Tamao, K. *Organometallics* **2002**, *21*, 2555–2558.
412. Klapötke, T. M.; Krumm, B.; Mayer, P.; Piotrowski, H.; Ruscitti, O. P.; Schiller, A. *Inorg. Chem.* **2002**, *41*, 1184–1193.
413. Mason, M. R.; Verkade, J. G. *Organometallics* **1992**, *11*, 2212–2220; Mason, M. R.; Verkade, J. G. *Organometallics* **1990**, *9*, 864–865.
414. Yahav, A.; Goldberg, I.; Vigalok, A. *J. Am. Chem. Soc.* **2003**, *125*, 13634–13635.
415. Grushin, V. V. *Organometallics* **2000**, *19*, 1888–1900.
416. Yahav, A.; Goldberg, I.; Vigalok, A. *Inorg. Chem.* **2005**, *44*, 1547–1553.
417. Kaspi, A. W.; Yahav-Levi, A.; Goldberg, I.; Vigalok, A. *Inorg. Chem.* **2008**, *47*, 5–7.
418. Ball, N. D.; Sanford, M. S. *J. Am. Chem. Soc.* **2009**, *131*, 3796–3797.
419. Bley, B.; Willner, H.; Aubke, F. *Inorg. Chem.* **1997**, *36*, 158–160.
420. Bernhardt, E.; Bach, C.; Bley, B.; Wartchow, R.; Westphal, U.; Sham, I. H. T.; von Ahsen, B.; Wang, C.; Willner, H.; Thompson, R. C.; Aubke, F. *Inorg. Chem.* **2005**, *44*, 4189–4205.
421. Finze, M.; Bernhardt, E.; Willner, H.; Lehmann, C. W.; Aubke, F. *Inorg. Chem.* **2005**, *44*, 4206–4214.
422. Frohn, H. J.; Bardin, V. V. *J. Fluorine Chem.* **2005**, *126*, 1036–1043.
423. Frohn, H. J.; Bardin, V. V. *J. Fluorine Chem.* **2006**, *127*, 18–21.
424. Fawcett, J.; Harding, D. A. J.; Hope, E. G.; Singh, K.; Solan, G. A. *Dalton Trans.* **2010**, *39*, 10781–10789.
425. Klapötke, T. M.; Krumm, B.; Scherr, M. *Z. Anorg. Allg. Chem.* **2010**, *636*, 1955–1961.
426. Poleschner, H.; Heydenreich, M.; Schilde, U. *Eur. J. Inorg. Chem.* **2000**, 1307–1313.
427. Pirkuliev, N. Sh.; Brel, V. K.; Akhmedov, N. G.; Zefirov, N. S.; Stang, P. J. Electronic Version *Mendeleev Commun.* **2001**, *11*, 172–173.
428. Hartung, J.; Greb, M.; Svoboda, I.; Fuess, H. *Acta Crystallogr. E* **2005**, *61*, o2770–o2771.
429. Prakash, G. K. S.; Moran, M. D.; Mathew, T.; Olah, G. A. *J. Fluorine Chem.* **2009**, *130*, 806–809.
430. Ramsden, C. A.; Shaw, M. M. *Tetrahedron Lett.* **2009**, *50*, 3321–3324.
431. Lourie, L. F.; Serguchev, Y. A.; Shevchenko, G. V.; Ponomarenko, M. V.; Chernega, A. N.; Rusanov, E. B.; Howard, J. A. K. *J. Fluorine Chem.* **2006**, *127*, 377–385.
432. Grošelj, U.; Tavčar, G.; Bevk, D.; Meden, A.; Žemva, B.; Stanovnik, B.; Svete, J. *Tetrahedron: Asymmetr.* **2006**, *17*, 1715–1727.
433. Zupan, M. In *The Chemistry of Halides, Pseudo-Halides and Azides Part 1*; Saul, P., Zvi, R., Eds.; Wiley: Chichester, 1995; pp 821–860.
434. Zajc, B.; Zupan, M. *J. Chem. Soc. Chem. Commun.* **1980**, 759–760.
435. Zajc, B.; Zupan, M. *J. Org. Chem.* **1982**, *47*, 573–575.
436. Stavber, S.; Šket, B.; Zajc, B.; Zupan, M. *Tetrahedron* **1989**, *45*, 6003–6010.
437. Cantrell, G. L.; Filler, R. *J. Fluorine Chem.* **1985**, *27*, 35–45.
438. Patrick, T. B.; Mortezania, R. *J. Org. Chem.* **1988**, *53*, 5153–5155.
439. Tsushima, T.; Kawada, K.; Tsuji, T. *Tetrahedron Lett.* **1982**, *23*, 1165–1168.
440. Garrett, G. S.; Emge, T. J.; Lee, S. C.; Fischer, E. M.; Dyehouse, K.; McIver, J. M. *J. Org. Chem.* **1991**, *56*, 4823–4826.
441. Kodama, T.; Matsuda, A.; Shuto, S. *Tetrahedron* **2006**, *62*, 10011–10017.
442. Mankad, N. P.; Toste, F. D. *J. Am. Chem. Soc.* **2010**, *132*, 12859–12861.
443. Ametamey, S. M.; Honer, M.; Schubiger, P. A. *Chem. Rev.* **2008**, *108*, 1501–1516.
444. Cai, L. S.; Lu, S. Y.; Pike, V. W. *Eur. J. Org. Chem.* **2008**, 2853–2873.
445. Miller, P. W.; Long, N. J.; Vilar, R.; Gee, A. D. *Ang. Chem. Int. Engl.* **2008**, *47*, 8998–9033.
446. Hollingworth, C.; Gouverneur, V. *Chem. Commun.* **2012**, *48*, 2929–2942.
447. Gouverneur, V. *Nat. Chem.* **2012**, *4*, 152–154.
448. Brel, V. K.; Pirkuliev, N. Sh.; Zefirov, N. S. *Russ. Chem. Rev.* **2001**, *70*, 231–264.
449. Chirakal, R.; Firnau, G.; Schrobilgen, G. J.; Mckay, J.; Garnett, E. S. *Int. J. Appl. Radiat. Isot.* **1984**, *35*, 401–404.
450. Constantinou, M.; Aigbirhio, F. I.; Smith, R. G.; Ramsden, C. A.; Pike, V. W. *J. Am. Chem. Soc.* **2001**, *123*, 1780–1781.
451. Lu, S.; Pike, V. W. *J. Fluorine Chem.* **2010**, *131*, 1032–1038.

Copyright © 2013. Elsevier. All rights reserved.

Comprehensive Inorganic Chemistry II : From Elements to Applications, Elsevier, 2013. ProQuest Ebook Central, http://ebookcentral.proquest.com/lib/inflibnet-ebooks/detail.action?docID=1330977.
Created from inflibnet-ebooks on 2021-02-09 22:27:13.